université PARIS-SACLAY

Oleate: an atypical cellular stress inducer that stalls protein secretion

Thèse de doctorat de l'université Paris-Saclay

École doctorale n° 582 Cancérologie : biologie, médecine, santé (CBMS)
Spécialité de doctorat : Aspects moléculaires et cellulaires de la biologie
Unité de recherche : Metabolomics and Cell Biology Platforms, Gustave Roussy Comprehensive Cancer Institute, Villejuif, France
Référent : Faculté de Médecine

Thèse présentée et soutenue à Villejuif (Paris), le 26 mars 2021, par

Giulia CERRATO

Composition du Jury

José Manuel FUENTES RODRIGUEZ Pr, University of Extremadura, Cacéres	Président et rapporteur
Ilio VITALE Dr, University of Rome Tor Vergata, Rome	Rapporteur
Véronique BAUD DR2, Université Paris Descartes, Paris	Examinatrice
Ken André OLAUSSEN MCU, Université Paris-Saclay, Paris	Examinateur
Guido KROEMER Pr, Centre de recherche des Cordeliers, Paris	Directeur de thèse
Oliver KEPP Dr, Institut Gustave Roussy, Villejuif	Invité

Thèse de doctorat

NNT : 2021UPASL023

"The more I learn, the more I realize
how much I don't know"
A. Einstein

université PARIS-SACLAY | ÉCOLE DOCTORALE Cancérologie : biologie - médecine - santé (CBMS)

Titre : Oléate: un inducteur atypique de stress cellulaire qui bloque la sécrétion protéique

Mots clés : Acides gras, autophagie, sécrétion protéique, criblage à haut débit, oléate, stress du réticulum endoplasmique

Résumé : Les diverses classes d'acides gras (chaines carbonées saturées ou *cis*-/*trans*- insaturées) influencent la physiologie au niveau de la cellule et de l'organisme de façon différente. Curieusement, ces catégories distinctes ont un effet important (mais différent) sur l'autophagie, le mécanisme intracellulaire de dégradation qui maintient l'homéostasie énergétique et protège les cellules contre le stress. L'oléate, l'acide gras *cis*-insaturé endogène et alimentaire le plus abondant, possède la propriété atypique d'induire une redistribution de la protéine LC3 (signe particulier d'autophagie) de manière non-canonique et préférentiellement dans l'appareil de Golgi. Puisqu'il a été montré que, d'une part, les acides gras *cis*-insaturés présentent des effets bénéfiques pour la santé et que, d'autre part, les acides gras *trans*-insaturés et saturés induisent des effets toxiques, nous avons décidé d'explorer les mécanismes à la base de la redistribution de LC3 au niveau de l'appareil de Golgi induite par l'oléate. Cette analyse pourrait nous éclairer sur l'origine des différents effets des acides gras sur la santé. Pour cela, un criblage robotisé du génome entier par ARNs interférents a permis d'identifier plusieurs gènes impliqués dans le transport des protéines lié à l'appareil de Golgi, et également dans la réponse intégrée au stress.
Des expériences supplémentaires ont montré que l'oléate impacte la morphologie subcellulaire de l'appareil de Golgi, en corrélation avec le blocage de la sécrétion protéique conventionnelle (dépendante du Golgi) lorsque que la cargaison est bloquée au niveau du réseau trans-golgien. L'inhibition de la sécrétion protéique a été observée dans plusieurs systèmes expérimentaux, tant *in vitro* qu'*in vivo*. De plus, un criblage visant à rechercher des agents chimiques capables d'induire les mêmes effets cellulaires que l'oléate, a permis d'identifier plusieurs composés appartenant à diverses classes pharmacologiques. De la même manière que l'oléate ces composés induisent un blocage de la sécrétion protéique conventionnelle, renforçant l'idée que cette voie de perturbation du Golgi joue un rôle pharmacologique important. En conclusion, ces résultats montrent que l'oléate représente une classe de molécules agissant sur l'appareil de Golgi pour y induire l'agrégation de LC3, tout en bloquant en même temps la sécrétion protéique.

Title : Oleate: an atypical cellular stress inducer that stalls protein secretion

Keywords : Fatty acids, autophagy, protein secretion, high-throughput screening, oleate, endoplasmic reticulum stress

Abstract : Distinct classes of fatty acids (FAs) (saturated or *cis*-/*trans*-unsaturated carbon chains) impact on cellular and organismal physiology in a different manner. Interestingly, these diverse categories have a profound (but different) effect on autophagy, the conserved intracellular degradation mechanism that maintains energy homeostasis and protects cells against stress. Oleate, the most abundant endogenous and dietary *cis*-unsaturated FA, has the atypical property to induce the redistribution of the LC3 protein (peculiar sign of autophagy) in a non-canonical fashion and preferentially to the Golgi apparatus. Intrigued by these observations, which might be related to the health-improving effects of *cis*-unsaturated FAs (and the notorious toxicity of *trans*-unsaturated and saturated FAs), we decided to explore the mechanisms causing the oleate-induced relocation of LC3 to the Golgi apparatus. To achieve this goal, a robotized RNA interference genome-wide screen led to the identification of multiple genes involved in the Golgi-related protein transport, as well as in the integrated stress response. Follow-up experiments revealed that oleate affected the subcellular morphology of the Golgi apparatus, correlating with a blockade of conventional (Golgi-dependent) protein secretion that caused secretory cargo to be stalled at the level of the trans-Golgi network. The inhibition of protein secretion was observed using several experimental systems, both *in vitro* and *in vivo*. Moreover, a systematic screen searching for other chemical entities that mimic the oleate-induced cellular effects led to the identification of several compounds belonging to rather different pharmacological classes. These "oleate mimetics" also shared with oleate the capacity to block conventional protein secretion, supporting the notion that this pathway of Golgi perturbation is indeed of pharmacological relevance. In conclusion, this research work shows that oleate represents a class of molecules that act on the Golgi apparatus to cause the recruitment of LC3 and to stall protein secretion.

Acknowledgements

Comme j'adore voyager, j'aime imaginer mon parcours de thèse comme une expédition qui a débuté en étant errante et plutôt à zig-zag, mais qui au cours des années a fini par prendre la bonne direction jusqu'à sa destination finale. Chaque étape de ce voyage a été merveilleusement enrichissante et m'a permis d'apprendre beaucoup sur tous les plans. Ce manuscrit de thèse représente la plupart de ma vie scientifique et dans ces pages (car une seule n'aurait suffi !), je tiens à remercier tous les gens qui ont rendu ce voyage possible, qui m'ont accompagné tout au long de ce dernier et surtout, qui l'ont enrichi et enjolivé.

Je tiens tout d'abord à remercier tous les membres du jury pour leur disponibilité, José Manuel Fuentes Rodriguez et Ilio Vitale pour avoir accepté d'être rapporteurs de cette thèse et avoir consacré du temps a la correction du manuscrit, ainsi que mes examinateurs Véronique Baud et Ken Olaussen pour avoir accepté de participer à ma soutenance.

Aucun voyage ne peut être entrepris sans son étoile polaire, et mon directeur de thèse Guido a été un phare scientifique pendant ces 3.5 années. Un énorme merci à toi Guido, pour m'avoir accueilli dans le laboratoire, pour avoir cru en moi, pour m'avoir guidé et donné la chance d'évoluer dans un environnement très enrichissant. L'incroyable flamboiement d'inputs scientifiques que tu dispenses constamment est des plus inspirants, et très précieux.

Allan, je ne sais même pas par où commencer. Tu es tout simplement le meilleur, le plus fou et le plus encourageant compagnon de voyage que j'aurais pu avoir à mes côtés. Si tu n'existais pas, il faudrait vraiment te coder dans R ! Un merci du plus profond du cœur pour tout ce que tu représentes pour moi et tout ce que tu m'as appris. Tu as été une infatigable épaule et un brillant rayon de soleil pendant tout ce temps, me transmettant toute ton énergie positive, ton soutien et ta confiance. Nos longueurs d'ondes synchronisées, notre complémentarité ainsi que notre enthousiasme sont les principaux ingrédients du duo gagnant qu'on constitue et rien de ce voyage dans toutes les différentes aventures n'aurait été le même sans ta flamboyante présence. Pour résumer, « toi-même tu sais ».

Juliette, adorable guerrière, merci pour ton aide précieuse, ton soutien, ta sincère bienveillance et tout le temps délicieux passé ensemble, que ça soit à pipeter l'une à côté de l'autre ou à rire autour d'une raclette. J'ai trop hâte de venir te voir au Canada !

Marion, ta gentillesse et ton calme sont très réconfortants, merci d'avoir été toujours à l'écoute, attentionnée et disponible pour partager des moments sympas. Même nos chaises du bureau sont devenues proches !

Oliver, merci pour m'avoir introduite à GR et donné l'opportunité d'intégrer la plateforme de biologie cellulaire, merci aussi pour ton soutien et pour avoir été toujours et tout de suite prêt à m'aider.

Wei, merci pour ton amabilité et ouverture d'esprit, ainsi que pour tous nos échanges intéressants, les mots de réconfort qui m'ont souvent soulagée et ta disponibilité à aider. Ça a été sympa de partager ce chemin (et la nourriture aussi !) avec toi.

Sabrina (évidemment prononcé à l'italienne), merci pour toutes nos discussions et tes conseils bénéfiques, pour nos repas partagés et pour ton investissement pour que tout soit bien organisé. Ton énergie et ta « bam »-attitude sont utiles.

Giorgio, merci pour les moments sympas que nous avons passés ensemble. Lucillia, merci pour ta précision technique, tes conseils et ton rire sympa.

Sylvère, merci pour les très enrichissantes discussions culturelles, ta passion pour ma patrie m'a fait apprendre pas mal de choses et j'apprécie ton effort à parler italien avec moi.

Lorenzo et Aitzi, merci de m'avoir fait découvrir ce laboratoire et m'avoir inspiré pour en faire partie.

Taka-sama, merci pour ton infinie et réconfortante gentillesse, ton encouragement et pour Fuku, le petit chat porte-bonheur qui est toujours sur mon bureau et m'accompagne au jour le jour.

Léa, merci pour ta patience, ton affabilité et ton aide pour toute la partie bureaucratique, tu as toujours été souriante, même quand je débarquais dans ton bureau sans préavis.

Franci et Lelli, même si on s'est rapprochées tardivement, « fraichement » merci pour vos conseils et encouragements, ainsi que pour votre peps.

Chiara, merci pour ton soutien moral et ton inlassable énergie.

Lynda, merci pour ta gentillesse avec toutes les procédures administratives et, avec Sylvie, pour vos doux sourires dès que je mettais les pieds dans votre bureau.

Zeinaf, Ali et Awatef, merci pour vos sourires même au plus tardif des horaires et le bonheur que vous répandez dans les couloirs.

J'ai bien évidemment une pensée pour tous les membres présents et passés du laboratoire à l'Institut Gustave Roussy et Centre de Recherche des Cordeliers (vous êtes vraiment nombreux !) qui ont contribué à rendre cette expérience si belle et ces années si agréables.

Fréd, coloc' spécial et ami fidèle, vraiment merci de m'avoir soutenue et supportée (surtout !), tu as été un refuge en rentrant chaque jour et une inépuisable source de conseils. Et Flo, merci pour ton calme et tes courageuses (mais inutiles) tentatives pour améliorer l'esprit sportif à l'appart.

Je pense forcément à mes amis de toujours. Frenzy, qui n'a jamais arrêté de m'encourager et être présent en me transmettant plein de force et surtout de bonheur, Giuli, qui a été à mes côtés dans toutes mes expériences à l'étranger et jamais laissée seule, Marti, toujours attentionnée et source de profonds conseils, Nuccia, doux soutien et acolyte de petit-déjeuner, Lele et Albs, des compagnons si amusants. Merci pour votre présence et soutien nonobstant la distance qui a quand même démontré que les plus profondes amitiés sont toujours là. C'est incroyable comme en une si courte mais intense durée, on peut rattraper ce temps perdu que l'on n'a pas pu partager.

Enfin, j'ai une énorme pensée à ma famille, à laquelle je dois la plupart de mes réussites. Tout d'abord à mes parents sans qui je n'aurais jamais pu arriver jusque-là. Maman et papa, vous m'avez toujours inspirée en étant les guides dans les plus importants choix de ma vie. Il n'y aura jamais de mots assez forts pour vous remercier de tout ce que vous avez fait, faites et continuez à faire pour votre « petite » fille. Votre amour inconditionnel, votre soutien infini et votre présence sont les choses les plus chères dans mon cœur. Mon frère El et ma belle-sœur Sil, merci pour votre constant soutien et votre « cooLitude ». Mati, la petite crevette, et vous, êtes une source inestimable d'ondes positives et de détente. Ma tante et Carlo, merci d'être toujours là pour m'encourager et pour toujours croire en moi.

Enfin, merci à toi Simone, merci d'être le rocher auquel m'accrocher peu importe les travers. Merci d'être toujours à mes côtés, de m'encourager à déplier mes ailes pour prendre mon envol vers d'autres horizons, pour être si patient et avoir une âme si gentille. Ton soutien immense malgre la distance et ton amour au jour le jour sont parmi les plus précieux piliers que j'ai.

Ce chapitre de ma vie s'est terminé mais je suis plus que prête pour tourner la page et me plonger dans de nouvelles aventures! Grazie !

Preface

Fatty acids are important components of lipids in nature, food and organisms. They play a panoply of biological functions, as well as structural roles, facilitating homeostasis and performance of the organism. Nevertheless, their positive or negative impact on human health has been shown to be intimately linked with their specific chemical properties such as carbon length and saturation state. This type-mediated effect is also reflected in their ability to induce autophagy, the major intracellular degradation mechanism that maintains energy homeostasis and protects cells against stress. Indeed, our team showed that fatty acids have a profound effect on autophagy, although the underlying molecular machinery differs from saturated to unsaturated fatty acids. The present work aims to explore the genetic basis of this difference, with a special focus on oleate, the most intriguing and abundantly occurring *cis*-unsaturated fatty acid, shown here to be an unconventional cellular stress inducer that stalls protein secretion. Consequently, a description of autophagy and protein secretion pathways, detailed in their molecular machineries, as well as the most common techniques allowing the monitoring of these processes introduce the topic of this research. This is followed by a brief description of fatty acids, their impact on general health and their major biological effects. The last part of the introduction focuses on autophagy-related cellular effects of oleate and its clinical use. In agreement with the Doctoral School, the chapters "Material and methods" and "Results" are replaced by the scientific article "Cerrato G, Leduc M, Muller K, Liu P, Zhao L, Humeau J, Xie W, Zhang S, Kepp O, Sauvat A, Kroemer G. **Oleate-induced aggregation of LC3 at the trans-Golgi network is linked to a protein trafficking blockade**" published in *Cell Death and Differentiation*, the Autophagic Punctum "Cerrato G, Kepp O, Sauvat A, Kroemer G. **A genome-wide RNA interference screen disentangles the Golgi tropism of LC3**" published in *Autophagy*, and the method paper "Cerrato G, Sauvat A, Kepp O, Kroemer G. **Live cell imaging of LC3 dynamics**" accepted for publication in *Methods in Cell Biology,* copyright Elsevier.

Contents

Abbreviations

AcbA	acyl-coenzyme A-binding protein
AMBRA1	activating molecule in Beclin-1-regulated autophagy
AMPK	AMP-activated protein kinase
AP-1	adaptor protein complex-1
Arf1	ADP-ribosylation factor 1
ATF6	activating transcription factor-6
ATG	autophagy related proteins
BafA1	bafilomycin A1
Bcl-2	B-cell lymphoma/leukemia-2
BFA	brefeldin A
BiP	binding immunoglobulin protein
CALR	calreticulin
CCCP	carbonyl cyanide *m*-chlorophenylhydrazone
CFTR	cystic fibrosis transmembrane conductor
CMA	chaperone mediated autophagy
COPI	coat protein complex I
COPII	coat protein complex II
CVD	cardiovascular disease
DDIT3	DNA damage-inducible transcript 3
DEPTOR	DEP domain-containing mTOR-interacting protein
eIF2α	eukaryotic initiation factor 2α
ELISA	enzyme-linked immunosorbent assay
ELISPOT	enzyme-linked immunospot
ER	endoplasmic reticulum
ERES	ER-exit sites
ERGIC	ER-Golgi intermediate compartment
ESCRT	endosomal sorting complexes required for transport
EVOO	extra virgin olive oil
FA	fatty acid

FGF2	fibroblast growth factor 2
FIP200	focal adhesion kinase family interacting protein of 200 kDa
GCN2	general control non-derepressible-2
GFP	green-fluorescence protein
HMGB1	high mobility group box 1
HRI	heme regulated inhibitor
HSC70	heat shock cognate 70
HT	high throughput
i.p.	intraperitoneal
ICD	immunogenic cell death
IFN-γ	interferon-γ
IL	interleukin
IRE1	inositol-requiring enzyme 1
ISG	immature secretory granules
KO	knock out
LAMP2A	lysosome-associated membrane protein type 2A
LAP	LC3-associated phagocytosis
LDL	low-density lipoprotein
LIR	LC3-interacting region
LPS	lipopolysaccharide
MAP1LC3B	microtubule-associated proteins 1A/1B light chain 3B (also known as LC3)
MSG	mature secretory granules
mTOR	mammalian target of rapamycin
mTORC1	mTOR complex 1
mTORC2	mTOR complex 2
MUFA	monounsaturated fatty acid
MVB	multivesicular body
PE	phosphatidylethanolamine
PERK	PKR-like ER protein kinase
PI	phosphatidylinositol

PI3KC3	class III phosphatidylinositol 3-kinase
PI3P	PI-3-phosphate
PKR	protein kinase R
PM	plasma membrane
PUFA	polyunsaturated fatty acid
RAPTOR	regulatory-associated protein of mammalian target of rapamycin
RUSH	retention using selective hooks
Sar1	secretion-associated RAS-related 1
SBP	streptavidin-binding domain
SNARE	soluble N-ethylmaleimide-sensitive factor adaptor protein receptor
SQSTM1	sequestosome1
SR	signal receptor
SRP	signal recognition particle
STR	streptavidin
STX5	syntaxin-5
SV	secretory vesicles
TFEB	transcription factor EB
TGN	trans-Golgi network
TNF	tumor necrosis factor
TRAPP	transport protein particle
TSC	tuberous sclerosis complex
ULK	Unc-51-like kinase
UPR	unfolded protein response
UPS	unconventional protein secretion
UVR8	ultraviolet-B receptor
VPS34	vacuolar protein sorting 34
VSVG	vesicular stomatitis virus-G
WIPI	WD-repeat proteins interacting with phosphoinositide
WT	wild type
XBP1	x-box binding protein 1

1. Autophagy regulation

In 2016, the Nobel Prize in Physiology or Medicine was awarded to Yoshinori Ohsumi for his exceptional breakthrough in the discovery of autophagic molecular mechanisms, clearly recognizing the remarkable importance of autophagy. The term "autophagy" takes its origin from the Greek words eating *(phagein)* and oneself *(auto)*, denoting "self-eating", and this definition already contains the general principle of the autophagic mechanism, that is the degradation, hence "eating", of superfluous or potentially dangerous "self" cellular matter. Autophagy is an evolutionarily highly conserved pathway that has two fundamental features: i) it targets endogenous or exogenous cytoplasmic material and ii) it concludes with its degradation within the lysosome (Galluzzi et al, 2017). Autophagy plays a primary role in cellular and organismal homeostasis and it can be initiated by diverse cellular stresses, including but not limited to nutrient deprivation. Dysfunctional autophagy has been associated with pathologies such neurodegenerative disorders and cancer (Choi et al, 2013). In the next paragraphs, autophagy will be described with its canonical and non-canonical molecular machineries. In addition, the most commonly employed techniques to conveniently monitor these processes will be discussed.

1.1 Molecular mechanisms of autophagy

Depending on selectivity and the modality of autophagic cargo delivery, distinct forms of autophagy have been described including macroautophagy, microautophagy and chaperone-mediated autophagy (CMA) (Mizushima, 2007).

In microautophagy, the cellular contents are directly trapped by the lysosome itself via invaginations of its own membrane (in yeast and plants), giving rise to small vesicles that detach from the surface and reach the lumen, not only "in bulk" as originally believed, but also in a selective way, leading to the description of micromitophagy (for damaged mitochondria) (Lemasters, 2014) and microlipophagy (for lipid droplets) (Seo et al, 2017). In mammals, a similar process is occurring, commonly known as "endosomal microautophagy"

that involves multivesicular bodies (MVB) originating from the late endosomes and relies on various endosomal sorting complexes required for transport (ESCRT) (Uytterhoeven et al, 2015).

Another type of autophagy is the CMA mechanism, characterized by its selective cargo recognition and internalization. Thus, soluble proteins which constitute the only possible cargo of CMA, are targeted for degradation and this necessitates the presence of a specific targeting motif (the pentapeptide KFERQ-motif) in their amino acid sequence. This consensus motif is recognized by the cytosolic chaperon heat shock cognate 70 (HSC70) in coordination with a co-chaperon complex and initiates the internalization of the KFERQ-protein cargo across the membrane into the lysosomal lumen via a protein-translocation complex, interacting with the receptor lysosome-associated membrane protein type 2A (LAMP2A) (Cuervo & Dice, 1996). As a note, the autophagic substrate is required to be unfolded before its HSC70-mediated lysosomal translocation (Kaushik & Cuervo, 2018).

Macroautophagy, commonly and from here onward referred to as autophagy, is the most abundant type of autophagy occurring in cells. The delivery of sequestered cargo has a characteristic intermediate: a double-membraned vesicle, referred to as the autophagosome, which eventually fuses with lysosomes, culminating with the degradation and recycling of its content by lysosomal hydrolyses. Broadly, this essential stress-responsive intracellular mechanism facilitates constitutive cytoplasmic clearance and recycling of superfluous and potentially dangerous cellular material. It removes at basal rate long-lived, aggregated or misfolded proteins, clears damaged organelles and regulates growth with the aim of maintaining cellular homeostasis, in order to avoid the accumulation of detrimental cellular components. In addition, it promotes cellular adaptation upon a variety of cellular insults, such as fluctuation in external conditions, and it protects the cell from invading pathogens, hence supporting survival in response to multiple stressor (Yang & Klionsky, 2010a). Various physiological and pathological states can induce autophagy, and the process finally culminates with the compensation for nutrient shortage and with a conversion of targeted molecules into catabolic constituents to sustain metabolic reactions or repair processes.

1.1.1 Initiation of the autophagic signaling cascade

The autophagic process can be subdivided into five major distinct phases: initiation, nucleation, elongation, autophagosome-lysosome fusion and lysosomal degradation (**Figure 1**) all concerted by a set of autophagy related proteins (ATG) originally identified in yeast (Mizushima et al, 2011).

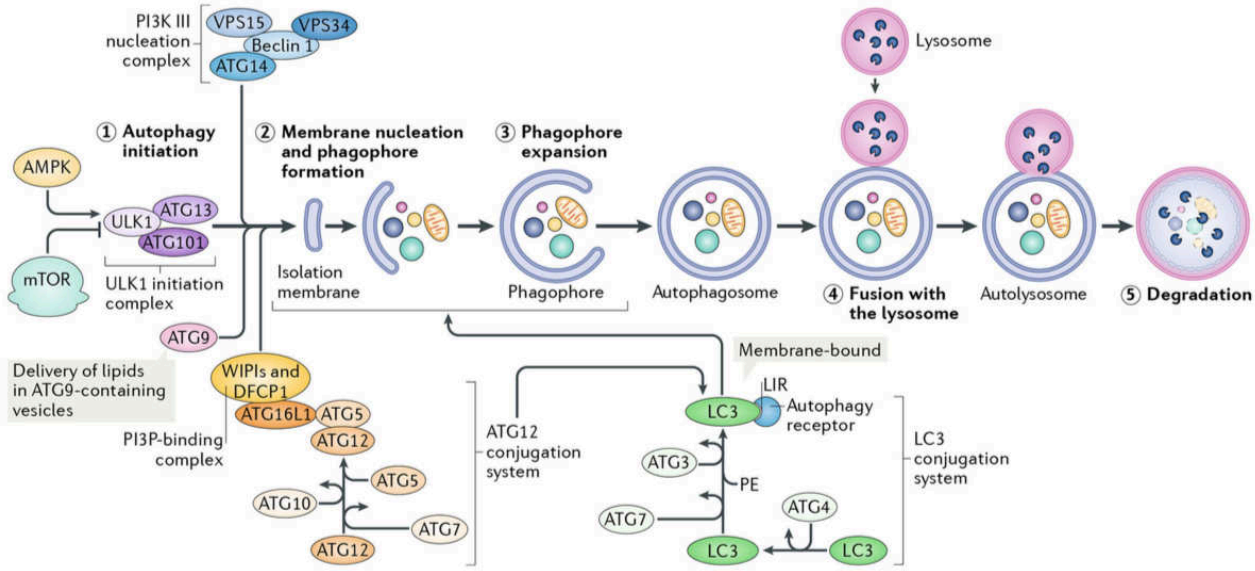

Figure 1. The autophagy process (Hansen et al, 2018). The main regulatory steps of autophagy, a multistep process finely tuned by a set of autophagy-related proteins (ATG), is depicted in the scheme: (1) initiation, (2) membrane nucleation and phagophore formation, (3) phagophore expansion, (4) fusion with the lysosome and (5) degradation. mTOR and AMPK are the main regulatory sensors of autophagy, acting as inhibitor and activator, respectively. Induction of autophagy leads to the sequestration of cytoplasmic material (cargo) in double-membraned autophagosome, originating from a cup-shaped phagophore, and subsequent fusion with acidic lysosomes forming the autolysosome where cargo is degraded. Several ATG-assembled complexes regulate the process: the ULK1 initiation complex, including ATG13 and ATG101, the PI3K III nucleation complex, including Beclin1, VPS34, VPS15 and ATG14, and the PI3P-binding complex, formed by WIPIs and DFCP1. The latter enables autophagosome formation and includes the ATG12-ATG5 conjugation system, where ATG12 is attached to ATG5 and subsequently to ATG16L1. It further interacts with PI3P-binding complex and promotes the action of the LC3 conjugation system. LC3 is cleaved by ATG4 to form LC3-I, which is then conjugated with PE to form LC3-II. This conjugate is incorporated into pre-autophagosomal and autophagosomal membranes, where LC3 can interact with cargo receptors harboring LIR motifs. ATG9-containing vesicles partially allow the delivery of membranes for phagophore expansion. Abbreviations: ATG, autophagy-related proteins; mTOR, mechanistic target of rapamycin; AMPK, AMP-activated protein kinase; ULK1, Unc-51-like kinase 1; PI3K III, phosphoinositide 3-kinase class III; PI3P, phosphatidylinositol 3-phosphate; VPS15, PI3K regulatory subunit 4 (also known as PIK3R4 in humans); VPS34, phosphatidylinositol 3-kinase catalytic subunit type 3 (also known as PIK3C3 in humans); LC3, microtubule-associated protein light chain 3; WIPIs, WD repeat domain phosphoinositide-interacting proteins; DFCP1, double FYVE-containing protein 1; LIR, LC3-interacting region; PE, phosphatidylethanolamine.

Autophagosomes arise from the elongation and closure of a membrane precursor, the phagophore, also called isolation membrane, a cup-shaped structure whose origin remains controversial, nonetheless multiple sources have been shown to likely contribute, such as the endoplasmic reticulum (ER) (Axe et al, 2008), the Golgi apparatus, the ER-Golgi intermediate compartment (ERGIC) (Ge et al, 2013) as well as the plasma membrane (Puri et al, 2013).

Among the various signaling cascades regulating autophagy, the coordination of the mammalian target of rapamycin (mTOR) and AMP-activated protein kinase (AMPK) exquisitely controls the process (**Figure 2**).

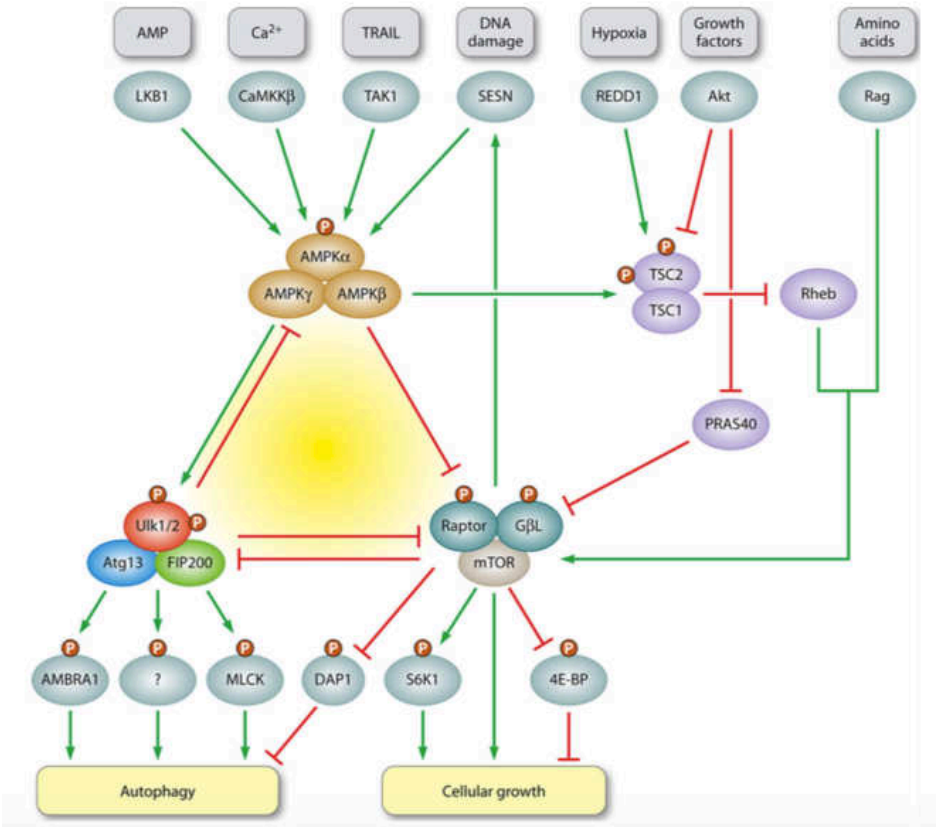

Figure 2. Fine adjustment of autophagy by AMPK and mTOR1. (Alers et al, 2012) AMPK and mTORC1 are the two main complexes oppositely regulating autophagy, predominantly interacting with the Ulk-1 complex. In nutrients/growth factors rich conditions, mTORC1 is active and stimulates processes such as protein translation by the phosphorylation of S6K1 and 4E-BP, while simultaneously inhibiting self-consuming processes such as autophagy. mTORC1 activity is positively regulated by growth factor signaling via the PI3K-Akt pathway. The Akt-mediated activation of mTORC1 inhibits two negative regulators of mTORC1 TSC1/2 or PRAS40, both antagonizing the Rheb-mediated activation. AMPK activity is mostly enhanced when the ATP/AMP ratio decreases. Under low-energy conditions, AMPK positively regulates autophagy induction through the inhibition of mTORC1, whose negative regulation on the Ulk-1-ATG13-FIP200 complex is released, especially on the Ulk1/2 kinase activity. mTORC1 inhibition by AMPK is mediated either via the TSC1/2-Rheb pathway or by direct phosphorylation of Raptor. However, AMPK can activate Ulk1/2 by direct binding and phosphorylation. In addition, mTORC1 inhibits DAP1, a negative regulator of autophagy. Abbreviations: AMPK: AMPK-activated protein kinase; mTORC1: mammalian target of rapamycin complex 1, 4E-BP, eukaryotic translation initiation factor 4E binding protein 1, S6K1, ribosomal protein S6 kinase.

Indeed, mTOR and AMPK serve as environmental sensors for levels of nutrients/energy-related molecules and a lack of thereof can initiate a cascade of (de)phosphorylation events yielding the initiation of the phagophore, that expands to surround portions of the cytoplasm, protein aggregates and dysfunctional organelles. mTOR and AMPK initate autophagy predominantly via the Unc-51-like kinases ULK1 and ULK2 that are part of the multiprotein ULK1 complex also comprising ATG13, ATG101 and FIP200 (focal adhesion kinase family interacting protein of 200 kDa) (Zachari & Ganley, 2017).

mTOR is a serine/threonine kinase playing a major role in the regulation of cellular metabolism and coordination of cell growth. Its binding with multiple proteins forms two structurally and functionally distinct signaling complexes: mTOR complex 1 (mTORC1) and mTOR complex 2 (mTORC2). In addition to mTOR, the multiprotein mTORC1 contains regulatory-associated protein of mammalian target of rapamycin (RAPTOR), a scaffold protein allowing the correct localization of mTORC1, DEP domain-containing mTOR-interacting protein (DEPTOR) and AKT1 substrate 1 (AKT1S1, best known as PRAS40) (Rabanal-Ruiz et al, 2017). mTORC2 shares some components of mTORC1 including mTOR and DEPTOR and contains distinctive components such as rapamycin-insensitive companion of mTOR (RIPTOR). These two complexes can be distinguished based on their sensitivity to rapamycin which only inhibits mTORC1 and on their functions, as mTORC2 regulates cytoskeleton organization and cell survival while mTORC1 mostly controls cell growth. In particular, mTORC1 acts as control point integrating a variety of extracellular and intracellular inputs, including oxygen levels, growth factors, amino acids and energy status. In conditions of nutrients rich status and energy sufficiency, mTORC1 is active and induces a shift in the metabolic program of the cells upregulating anabolic processes such as protein and lipid synthesis while inhibiting catabolic processes such as autophagy via different mechanisms, even if a low basal level of autophagy still occurs to prevent built-up of misfolded proteins or damaged organelles.

Indeed, the active state of mTORC1, and hence autophagy suppression, in response to growth factors, phosphorylates eukaryotic translation initiation factor 4E binding protein 1 (EIF4EBP1, best known as 4EBP1) and ribosomal protein S6 kinase (RPS6K, best known as p70S6K) promoting protein synthesis (Galluzzi et al, 2014). Moreover, the phosphorylation

of RAPTOR mediated by Akt can also activate mTORC1 (Neufeld, 2010). Similarly, amino acids can cause the activation of mTORC1 through the Rag family of GTPases by a direct interaction with RAPTOR (Efeyan & Sabatini, 2010). On the other hand, reduced growth factors availability, amino acids levels or more generally in conditions where AMPK is activated, dampened the activity of mTORC1, thus eliciting an autophagic response.

AMPK is a heterotrimeric protein complex and main energy sensor that coordinates with mTORC1 to regulate autophagy through multiple mechanisms. The energetic status of a cell is mainly reflected by the cellular concentration of ATP and AMP and the ratio of AMP:ATP governs the AMPK activity. A decrease in cellular energy value as result of a drastic increase in AMP levels, and the corresponding lowering in ATP concentrations, boost AMPK activity that leads to the induction of autophagy via a direct phosphorylation of ULK1, promoting the dissociation from mTORC1, or by phosphorylating Beclin-1, part of the core complex for autophagosomes elongation described in the following paragraph. ULK1 activation by AMPK leading to mTORC1 inhibition is also further amplified through several signaling mechanisms. Indeed, AMPK can inhibit mTORC1 directly by phosphorylating the regulatory protein RAPTOR that disrupts the mTORC1 signal transduction or indirectly by phosphorylating and thus activating tuberous sclerosis complex (TSC)1-TSC2, a negative regulator of mTORC1 (Kim & Guan, 2015). mTORC1 dissociation from the ULK1 complex, relieves the inhibitory effect and leads to the dephosphorylation of ULK1 and ATG13, activation of ULK1 and subsequent ULK1-mediated phosphorylation of ATG13 and FIP200 (Mizushima, 2010). Of note, this reversible phosphorylation of ULK1 is the central mechanism controlling the regulation of starvation-induced autophagy.

Inhibition of mTORC1 is chemically achieved by employing agents such as rapamycin, torin 1 or everolimus.

In addition, mTORC1 also controls autophagy through the family of transcriptional factors regulating autophagy and lysosomal-related genes. Indeed, the activation of the transcription factor EB (TFEB) leads to an increase in autophagosomes number, biogenesis of new lysosomes and clearance of storage material. Under nutrient-rich conditions, mTORC1 contributes to the phosphorylation of TFEB which retains, and thus inactivates, TFEB in the cytoplasm. Under amino acid deprivation, mTORC1 inactivation leads to

dephosphorylation and relocalization of TFEB to the nucleus, where it promotes autophagic and lysosomal gene expression (Settembre et al, 2012).

1.1.2 Autophagosomal assembling steps and cargo degradation

The second crucial step after the ULK1 activation that leads to the initial assembly of the phagophore membrane, requires the production of class III phosphatidylinositol 3-kinase (PI3KC3) (Russell et al, 2013). The complex which includes PI3KC3, also known as Vps34 (vacuolar protein sorting 34), beclin-1, p150 (Vps15 in yeast), ATG14, activating molecule in Beclin-1-regulated autophagy (AMBRA1) and UVRAG, forms the core of the nucleation system.

Beclin-1 plays a central role in the activity of this complex, regulated by the sequestration by B-cell lymphoma/leukemia-2 (Bcl-2), an antiapoptotic protein that inhibits autophagy. Bcl-2 needs to be dissociated from beclin-1 in order to switch to an initiate autophagy (He & Klionsky, 2009). A mediator role is played by AMBRA1, which is able to activate beclin-1-dependent autophagy and in addition, both AMBRA1 and beclin-1 get phosphorylated by activated ULK1, leading to the activation of the Vps34 complex. In this setting, Atg14 allows the redirection of the complex to the ER, initiating a dot-like accumulation at the initiation site of autophagosome formation (Matsunaga et al, 2010), where the Vps34 complex catalyzes the transformation of phosphatidylinositol (PI) into the lipid molecule PI-3-phosphate (PI3P). PI3P serves as substrate for phagosomal membrane growth, creating a platform that recruits PI3P-binding proteins, required for the successive recruitment of ATG9-containing vesicles, and the uptake of endomembranes (Shibutani & Yoshimori, 2014). In addition, PI3P serves as a critical recruitment signal for phagophore expansion, which triggers the partially overlapping action of two ubiquitin-like conjugation systems: ATG12-ATG5 complex and microtubule-associated proteins 1A/1B light chain 3B (MAP1LC3B), best known as LC3, and phosphatidylethanolamine (PE) complex (Mizushima, 2007). These systems are necessarily needed to conjugate ubiquintin-like LC3 (Atg8 in yeast) to PE, a process that is referred to as LC3 lipidation. In the first pathway, downstream of PIP3 generation, the E1-like enzyme ATG7 and the E2-like enzyme ATG10 operate sequentially to catalyze the conjugation of ATG12 to ATG5, forming a multimeric complex upon association

with ATG16. Of note, this complex serves as E3-like ligase for ATG3-LC3 conjugates, determining the sites of LC3 lipidation (Yang & Klionsky, 2010b). This lipid conjugation plays a central role for autophagosomal membrane extension and curvature, allowing the cleavage and lipidation of the cytosolic precursors LC3-like proteins into their mature forms. Indeed, the coordinated action of ATG4, an E1-like enzyme that mediates a proteolytic cleavage at the C-terminus to generate cytosolic LC3-I from pro-LC3, and of ATG7 and ATG3, E1- and E2-like enzymes respectively, that conclude with the conjugation with PE, leads to the conversion of LC3-I to the autophagosomal membrane-associated form, LC3-II (Yang & Klionsky, 2010b). The recruitment of the latter to the inner and outer surface of the autophagosome is mediated by the ATG5-ATG12 complex and is supported by WD-repeat proteins interacting with phosphoinositides (WIPI). The WIPI family, composed of four members (WIPI1 to WIPI4), is considered to bridge PI3P production and LC3 lipidation (Lamb et al, 2013; Proikas-Cezanne et al, 2015).

Notably, immunofluorescence microscopy and immunoblotting, two preferentially and widely implied techniques among others to follow the evolution of the autophagic machinery, are based on the detection of mature LC3, as detailed in **Paragraph 1.4**.

The selection of autophagic cargo is facilitated by several proteins such as p62, also known as sequestosome1 (SQSTM1) and NBR1 (neighbor of BRACA1) (Kirkin et al, 2009), that interact with LC3 via their LC3-interacting region (LIR), thus enabling cargo selectivity by serving as adaptors to target defined structures such as ubiquitinated proteins.

On closure, the canonical pathway of cellular vacuole membrane fusion involving LAMP2 and Rab7, a component of the late-endosome/trans-Golgi network, allows the fusion of autophagosomes with lysosomes, thus generating the so-called autolysosome (Jager et al, 2004). Autolysosome formation characterizes the last and degradative step of the autophagic process, where lysosomal hydrolases mediate the proteolytic cleavage of the autophagosomal content and the recycling of essential metabolites.

1.2 Non-canonical mechanisms of autophagy

Over the past decade, findings revealed that a variety of "autophagy-like" pathways exist, resulting in the formation of functional autophagosomes but without following the canonical

way of autophagy induction (Codogno et al, 2011). These alternative pathways underscore the molecular complexity of autophagy, raising the possibility of stimuli-related changes to the process. Although under debate, it is becoming apparent that the formation of functional autophagosomes can bypass key proteins of the core autophagy machinery in various settings (Mathur et al, 2018) and this bypass can occur at different steps of the process. Even if it is not yet clear how some ATG modules can be bypassed to form functional autophagosomes, there is evidence for several types of non-canonical autophagy, such as (i) ULK1-independent autophagy, (ii) Beclin-1- independent and VPS34-independent, (iii) VPS34-VPS15-independent autophagy and (iv) autophagy independent on ubiquitin-like conjugation actors.

A form of autophagy that bypasses the canonical ULK1 initiation step has been reported in response to ammonia or upon glucose deprivation in mouse embryonic fibroblasts knock out (KO) for ULK1 and ULK2 (Cheong et al, 2011). Since the observation that ULK1 complex is not an absolute requirement to initiate autophagy, multiple studies have shown that autophagosome formation does not always require the activity of AMPK and cannot always be inhibited by mTORC1 (Grotemeier et al, 2010; Yamamoto et al, 2006), suggesting a bypass of the canonical initiation and thus an autophagic sequestration employing other entry routes.

The first evidence the Beclin1-complex independency for the autophagic response was demonstrated in neurons treated with 1-methyl-4-phenylpyridinium (Zhu et al, 2007) where the beclin-1-independent autophagy induced by this neurotoxin was proposed to be the mechanism for cell death induction. Among similar lines, the polyphenol resveratrol, mostly found in grapes and other plants, was shown to elicit autophagy in human breast cancer cells without the requirement of beclin-1 and to use the activation of this pathway as a cell death mechanism (Scarlatti et al, 2008). Furthermore, Z18, a compound acting on Bcl-2 was shown to induce a beclin-1 independent-autophagy and consequent cell death in Hela cells (Tian et al, 2010), as well as some other proapoptotic compounds such as staurosporine, MK801 and etoposide were shown to induce beclin-1 independent autophagy in primary cortical neurons (Grishchuk et al, 2011). These findings underscore the possibility of using proapoptotic compounds inducing non-canonical autophagy for therapeutic purposes in

cancer when the functions of canonical autophagy proteins are compromised. Nevertheless, Beclin-1 independency was shown also in context unrelated to cell death, such as during viral infection (Berryman et al, 2012), differentiation (Arsov et al, 2011) or bacterial toxin uptake (Mestre et al, 2010). Of note, Beclin-1 independent autophagy does not necessarily exclude PdtIns3KC3-WIPI-ATG5-LC3 route. The same effect holds when ovarian cells and epithelial cells were exposed to arsenic trioxide or gossypol, respectively but dependent on PdtIns3KC3 and involving WIPI1 in certain circumstances (Gao et al, 2010; Smith et al, 2010). Interestingly, our team showed that, differently from saturated fatty acids that activate a canonical pathway of autophagy, *cis*-unsaturated fatty acids-induced autophagy in human osteosarcoma cells is independent on Beclin-1 and VPS34 and confirmed this finding in the yeast *Saccharomyces cerevisiae*, in the nematode *Caenorhabditis elegans* and in mice (Niso-Santano et al, 2015b).

VPS34-independent autophagy was shown to happen in sensory neurons (Zhou et al, 2010) and VPS15-deficient mouse skeletal muscle was demonstrated to form LC3-positive autophagosomes as well (Nemazanyy et al, 2013). Although the formation of LC3-II is inhibited in cells knock out for ATG5, electron microscopy of cells exposed to etoposide over a prolonged period, showed the formation of autophagosomes (Nishida et al, 2009). In this context, the unusual lamination of the membrane identifies the trans-Golgi network as the membrane source for this form of alternative autophagy, initiated by ULK1 and PtdIns3KC3 complexes. However, the initial autophagosomal elongation does not require ATG9 or ATG proteins of the ubiquitin-like conjugation systems, including ATG5, ATG7 and LC3, while RAB9, a GTPase involved in the vesicular traffic does. This form of autophagy independent on ATG5 and ATG7 was observed in various cell types and was shown to be related in the clearance during erythroid maturation (Nishida et al, 2009), even if in erythroblast this happens in a ATG5 and ATG7-dependent fashion, suggesting that both pathways contribute to mitochondria elimination and the physiological relevance of this non-canonical pathway remains to be elucidated.

Recently, one study claimed that certain lysosomotropic drugs, such as chloroquine initially believed to be autophagic flux inhibitors, were able to induce a non-canonical form of autophagy. Indeed, various autophagy-related proteins and LC3 lipidation are recruited to

single-membraned endolysosomal compartments, probably driven by osmotic imbalances (Florey et al, 2015). In this setting, LC3 lipidation was shown in non-autophagosome structures, independently of ATG13, ATG9 or VPS34 activity, conventionally required for autophagosomal biogenesis. This type of autophagy is characterized by single-membraned and low pH granules (Jacquin et al, 2017). In the same study, carbonyl cyanide *m*-chlorophenylhydrazone (CCCP), a common mitophagy inducer, was also shown to induce non-canonical autophagy in parallel to mitophagy at higher concentrations compared to the latter phenomenon, but still within levels commonly used in the study of autophagy (Jacquin et al, 2017) and in the absence of FIP200, ATG13 and ATG14 (Chen et al, 2013a). Furthermore, amiodarone, an FDA-approved antiarrhythmic drug, was shown to activate non-canonical autophagy and to induce endolysosomal LC3 lipidation (Jacquin et al, 2017).

Interestingly, a variety of autophagy-like pathways are characterized by the shared usage of the autophagy machinery and over the past decade these distinctive functions of autophagy proteins have been referred to as non-canonical autophagy, although technically these do not involve "self-eating". For this reason, a recent preference for referring to such processes as "non-canonical functions of autophagy proteins" has emerged. Indeed, accumulating evidence suggests that most (if not all) components of the molecular apparatus involved in autophagy mediate other effects that are independent of the lysosomal degradation of the autophagic cargo. Thus, the tendency of attributing unique functions to specific proteins may have led to confound autophagy-independent effects of single autophagy-regulatory factors to autophagy as a process. In particular, cellular functions in the context of vesicle uptake, trafficking and other processes involving membrane rearrangements, as well as mechanisms for innate and adaptive control of invading pathogens, have been shown to be mediated by autophagy relevant proteins while inducing non-autophagic effects (Galluzzi & Green, 2019).

One such form of these novel non-canonical functions of autophagy proteins is the pathway of LC3-associated phagocytosis (LAP) present in phagocytic cells including macrophages, epithelial and endothelial cells. This divergent pathway utilizes components of the canonical autophagy machinery, including a subset of ATG, to conjugate LC3 to phagosome membranes in order to clear pathogens or dead cells (Martinez et al, 2011; Romao et al,

2013). In contrast to canonical autophagy, LAP is not dependent on the AMPK-mTORC1-ULK1 and is not sensitive to nutrient status or intracellular stress sensing (Heckmann & Green, 2019), while toll-like receptors able to sense diverse pathogen-associated molecular patterns have been shown to stimulate LAP (Sanjuan et al, 2007). How the conjugation machinery is recruited to the phagosomal membrane remains unclear, but the two classical ubiquitin-like conjugation systems required for LC3 conjugation in LAP are known to facilitate phagosome maturation and cargo digestion. Another remarkable difference between canonical autophagy and LAP is the timing of LC3 lipidation, as it happens when the phagosome is fully sealed for the first, while it occurs during autophagosomal membrane elongation for the second. It is noteworthy to underline that the functions of LAP in inflammation and autoimmunity, together with the important role in mediating bacterial clearance and antifungal host defense, reinforce the broad importance of this divergent form of autophagy to cell and organismal homeostasis. Thus, it is clear that defective LAP mechanism can have a breadth of immunological consequences, as shown in LAP-deficient mice that tend to have a pro-inflammatory response when challenged with dead cells, leading to autoinflammation and lupus-like syndrome (Martinez et al, 2016).

Taken together, these pathways observed in various settings underline the complexity of what is defined as non-canonical autophagy and more detailed characterizations are needed, as the important question whether or not these non-canonical forms of autophagy have specific functions in cellular physiology and pathological conditions remains elusive. As a consequence, careful consideration of all available data should be taken before characterizing diverse biological processes as autophagy.

1.3 Phosphorylation of eukaryotic initiation factor-2α in autophagy

The ER is not only the organelle where synthesis, maturation and protein folding take place, as it will be detailed in **Paragraph 2.2.1**, but it also serves as a major source of the isolation membrane of the phagophore (Hayashi-Nishino et al, 2009). The unfolded protein response (UPR) is the canonical response to ER stress (Buchberger et al, 2010) and constitutes a potent stimulus of autophagy in certain contexts. Three ER-transmembrane proteins mediate the

canonical pathways of the UPR: protein kinase R (PKR)-like endoplasmic reticulum kinase (PERK, also known as EIF2AK3), inositol-requiring enzyme 1 (IRE1) and the activating transcription factor-6 (ATF6) (**Figure 3**) (Hetz, 2012). In normal conditions, these proteins are bound and inactivated by the chaperone binding immunoglobulin protein (BiP). The release of BiP during ER stress to bind unfolded or misfolded proteins results in the activation of the three UPR branches. Of note, only PERK and ATF6-mediated pathways have been shown to positively regulate autophagy (Kroemer et al, 2010), as for example PERK was shown to mediate the transcriptional activation of the essential autophagic proteins LC3 and Atg5 in hypoxic responses (Rouschop et al, 2010).

The transmembrane kinase IRE1 exists in two isoforms, IRE1α and IRE1β. IRE1α is present in all cell types and widely studied, upon ER stress-induced activation and autophosphorylation, it catalyzes the splicing of x-box binding protein 1 (XBP1) unleashing the transcription factor that upregulates UPR genes involved in ER-associated protein degradation and protein folding. The second arm of the UPR involves ATF6, which also has two isoforms, ATF6α and ATF6β. After dissociation from BiP, ATF6α transits from the ER membrane to the Golgi apparatus where it is cleaved and its N-terminal fragment is transported to the nucleus activating the expression of UPR genes like XBP1 and BiP to promote protein folding (Kato & Nishitoh, 2015). The third arm of the UPR depends on PERK, whose dissociation from BiP induces its oligomerization and autophosphorylation while promoting the phosphorylation of serine 51 on eukaryotic initiation factor 2α (eIF2α) thus initiating a cascade of events to alleviate ER stress by decreasing the overload of misfolded proteins (Harding et al, 2003). Indeed, eIF2α phosphorylation leads to a general attenuation of protein translation by preventing the formation of ribosomal initiation complexes, while promoting the selective translation of stress-responsive transcripts such as several autophagy genes and ATF4 (Hotamisligil, 2010). ATF4 is a transcription factor responsible for growth arrest and upregulation of genes coding for chaperones, antioxidants, XBP1, as well as DNA damage-inducible transcript 3 (DDIT3, also known as CHOP, CCAAT/enhancer-binding homologous protein).

Of note, multiple other stress signals beyond ER stress (where the phosphorylation is mediated by PERK) can induce the phosphorylation of eIF2α: eIF2AK1 (best known as heme

regulated inhibitor, HRI) mediates the phosphorylation of eIF2α in conditions of heme deprivation, PKR in response to viral infections and eIF2AK4 (best known as general control non-derepressible-2, GCN2) in the context of nutrient deprivation.

Increasing evidence proves that ER stress and autophagy exert a mutual-counterbalance to promote the maintenance of cellular viability (Bugliani et al, 2019; Demirtas et al, 2016). The phosphorylation of eIF2α plays a major role in autophagy regulation, as it was shown in cells carrying a non-phosphorylable mutant of eIF2α (S51A) where starvation failed to induce autophagy (Kouroku et al, 2007; Talloczy et al, 2002). Technically, the knockin mutation S51A used to render eIF2α non phosphorylable constitutes a convenient tool to deepen the mechanistic exploration of the implication of eIF2α, in the initiation of autophagy.

Biologically, the contribution of eIF2α phosphorylation in autophagy initiation still remains intriguing. Our team provided evidence that autophagy induction by multiple pharmacological agents generally requires the phosphorylation of eIF2α. Indeed, autophagy triggered by these compounds was accompanied by the phosphorylation of eIF2α and was partially inhibited in the S51A mutant as well as in cells lacking all four eIF2α kinases (Humeau et al, 2020). However, the mode of action of distinct autophagy inducers may depend on distinct eIF2α kinases, and further investigation is needed.

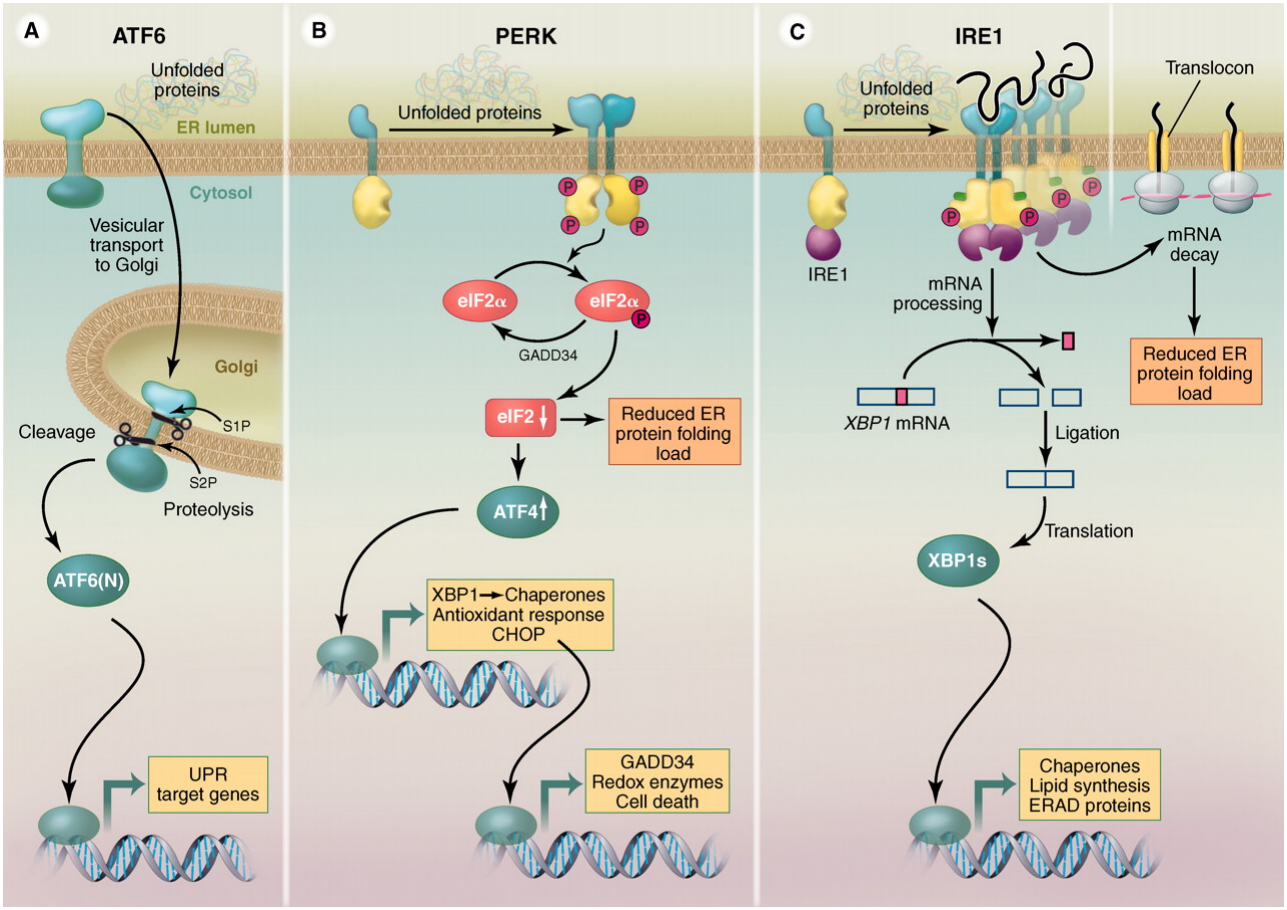

Figure 3. The unfolded protein response (UPR) is composed of three branches (Hetz, 2012). Protein-folding condition in the ER lumen is sensed by three families of signal transducers that activate three pathways: (A) ATF6 translocation to the Golgi apparatus, where it undergoes proteolytic cleavage followed by translocation to the nucleus of the N-terminal part, (B) PERK-mediated eIF2α phosphorylation leading to the activation of ATF4 and (C) IRE1 dimerization inducing the alternative splicing of XBP1. The activation of these three branches drives transcription of UPR target genes largely serving to increase the protein-folding capacity in the ER, as well as PERK- and IRE1-mediated responses reduce the ER folding load. Abbreviations: ATF6, activating transcription factor 6; ER, endoplasmic reticulum; S1P, site-1 protease; S2P, site-2 protease; PERK, PKR-like ER protein kinase; eIF2α, eukaryotic initiation factor 2α; ATF4, activating transcription factor-4; XBP1, x-box binding protein 1; CHOP, CCAAT/enhancer-binding homologous protein; IRE1, inositol-requiring enzyme 1.

1.4 Autophagy monitoring techniques

Unquestionably, LC3 is the most widely used autophagy-related protein for the assessment of the autophagic process and the characterization of its molecular details. A chimera of green-fluorescence protein (GFP) fused to the N-terminus of LC3 allows for monitoring the distinct subcellular localization of the lipidated form of the protein by fluorescence microscopy (Bravo-San Pedro et al, 2017). Of note, the generation of fluorescent reporter cell lines required the plasmid-drive expression of random genomic integration of transgenes and thus effects on cellular physiology cannot be entirely excluded.

In normal conditions, GFP-LC3 is rather homogeneously distributed in the cytoplasm and nucleus. Upon autophagy induction however, GFP-LC3 accumulates in forming autophagosomes and the signal manifests as transient bright dots that are quenched in the acidic environment of autolysosomes upon lysosomal fusion. GFP-LC3 aggregation can be conveniently monitored via fluorescence microscopy, in end-point assays but it is also possible to study the aggregation dynamics by time-lapse live cell imaging, as described in **"Live cell imaging of LC3 dynamics"**. It is thus possible to quantify the number and surface of so-called GFP-LC3 *puncta* as indicators for autophagic responses in a high throughput (HT) fashion. Of note, GFP-LC3 can be lipidated also to non-autophagosome membrane and for this reason results obtained with the protein chimera need additional secondary validations. Nevertheless, during the past decade, several novel autophagy activating and inhibiting drugs have been identified by LC3-based HT screens (Hale et al, 2016; Orvedahl et al, 2011; Zhang et al, 2007).

The maturation of endogenous LC3 can be readily assessed by immunoblotting. The latter is another frequently used technique to monitor autophagy, that relies on the detection of 2 kDa shift in the molecular weight of the cleaved form of LC3 (LC3-II) displaying a faster electrophoretic motility with respect to its immature counterpart (LC3-I). Nonetheless, although it constitutes a reliable approach to determine LC3 maturation *in vitro* and *ex vivo*, this technique is not prone to be automatized for HT screening campaigns as the method is time consuming and absolute quantification of the obtained results is difficult.

Tandem mRFP-GFP-LC3 constructs are commonly employed to measure autophagic flux thanks to distinct spectral properties of GFP and mRFP under acidic conditions: given the pH-dependent quenching of the GFP-LC3 fluorescence, exclusively mRFP-LC3 can be detected in autolysosomes, whereas autophagosomes are marked by a combination of the red and green signal, thus appearing yellow. An increase in the ratio of dual RFP and GFP over single RFP signal is thus assumed to be associated with a blockade of autophagosome-lysosome fusion (Kimura et al, 2007). Nevertheless, caution in the interpretation needs to be taken as LC3 associated with endolysosomal membranes will also retain both signals (Jacquin et al, 2017).

Of note, autophagy is active in basal conditions, as the cellular autophagic status is a balance between formation and degradation of autophagosomes. This is the reason why it is important to evaluate the process in terms of autophagic flux using chemical compounds that inhibit lysosomal fusion with autophagosomes such as bafilomycin A1 (BafA1) (Klionsky et al, 2016) or the tandem report described above, to discriminate among inhibitory agents. Hence, the inhibitory effect can be different in function of the point at which the pathway is disrupted and this constitutes another aspect that needs further consideration, as an increase in GFP-LC3 *puncta* and LC3-II levels can either reflect an increase in the number of autophagosomes or an accumulation of lipidated LC3 in early formation due to flux inhibition, respectively (Klionsky et al, 2016).

In addition, other peculiar markers of the autophagic responses are the degradation of the LC3 interacting protein p62/sequestrosome 1 (SQSTM1) and the degradation of radioactively-labelled long-lived protein. Transmission electron microscopy is the only tool that is able to reveal the morphology of autophagosomal structures at a resolution in the nm range. Furthermore, monitoring autophagic flux *in vivo* or in organs is one of the least developed areas at present, and it has to be noted that the level of basal autophagy, its time course and the bioavailability of autophagy stimulating and inhibiting drugs is likely tissue specific, thus requiring specific optimizations. LC3 lipidation can be simply assessed in harvested tissues by microscopy or western blot. In addition, transgenic mice expressing GFP-LC3 either on an organismal level or tissue-specific allow the monitoring of autophagy in organs such as skeletal muscle, liver, heart and brain (Mizushima et al, 2004). A multitude of additional techniques are available to study the process, just to cite a few examples: flow and multispectral imaging cytometry, immunohistochemistry or the monitoring of the activation/inhibition of mTOR, AMPK and Atg1/ULK1 proteins levels such as Atg12-Atg5 and Atg16L1 (Klionsky et al, 2016).

2. Trafficking machinery

2.1 Mechanisms of protein secretion

Protein secretion is an essential function in every living organism allowing for the precise delivery of soluble proteins to distinct acceptor compartments, mainly the extra-cellular space, and the characterization of its mechanism dates back to the 1950s. It plays an important role in the physiology of cells as it mediates a multitude of fundamental processes dealing with the expulsion of cargoes, such as cell-to-cell communication, homeostasis, growth, defense and structural maintenance among others. The fidelity of transport is ensured by elaborate molecular machineries composed of an integrated intracellular membrane system with multiple transport routes that functionally interconnect different organelles across the cytoplasm, each one related to specific functions. The intracellular trafficking among compartments is responsible for biogenesis and distribution of a wide collection of proteins and occurs via vesicular carriers, as well as sequential budding from a donor membrane that then fuses with an acceptor compartment (Bonifacino & Glick, 2004). Proteins can be secreted by the conventional protein secretion, that delivers proteins from the ER to the extracellular space passing through the different compartments of the Golgi apparatus, or via several unconventional protein secretion (UPS) mechanisms. Next, conventional and unconventional protein secretion are detailed in their molecular mechanisms together with classical and recent techniques that have been successfully applied for the analysis of protein secretion.

2.2. The conventional pathway

Constitutive secretion employs secretory vesicles and is constantly active in every eukaryotic cell, while regulated secretion can be additionally elicited by extracellular stimuli in special types of animal cells, such as endocrine cells, neurons and exocrine cells and makes use of secretory granules (Tooze et al, 2001). Neurotransmitter release at the synapses, insulin secretion of endocrine pancreatic β-cells or zymogen secretion during digestion from exocrine pancreatic cells are examples of regulated secretion. Both constitutive and regulated secretion follow the conventional secretory pathway.

Canonical protein secretion (**Figure 4**) originates from the ribosomes, where nascent polypeptides are equipped with signal sequences to be translocated to the ER, where they are chaperoned and glycosylated (Viotti, 2016). Then, proteins destined for secretion exit the ER via trafficking vesicles, that pass through the Golgi apparatus for additional processing and then transit in the trans-Golgi network (TGN), where cargo segregation takes place and proteins are sorted into secretory vesicles and granules (Kelly, 1985). Secretory vesicles and granules then travel along cytoskeletal filaments to reach and fuse with the plasma membrane (PM) in order to deliver their content to the extracellular space. Trafficking along this route is not restricted to secretory proteins but is utilized as well by integral proteins, targeting the PM.

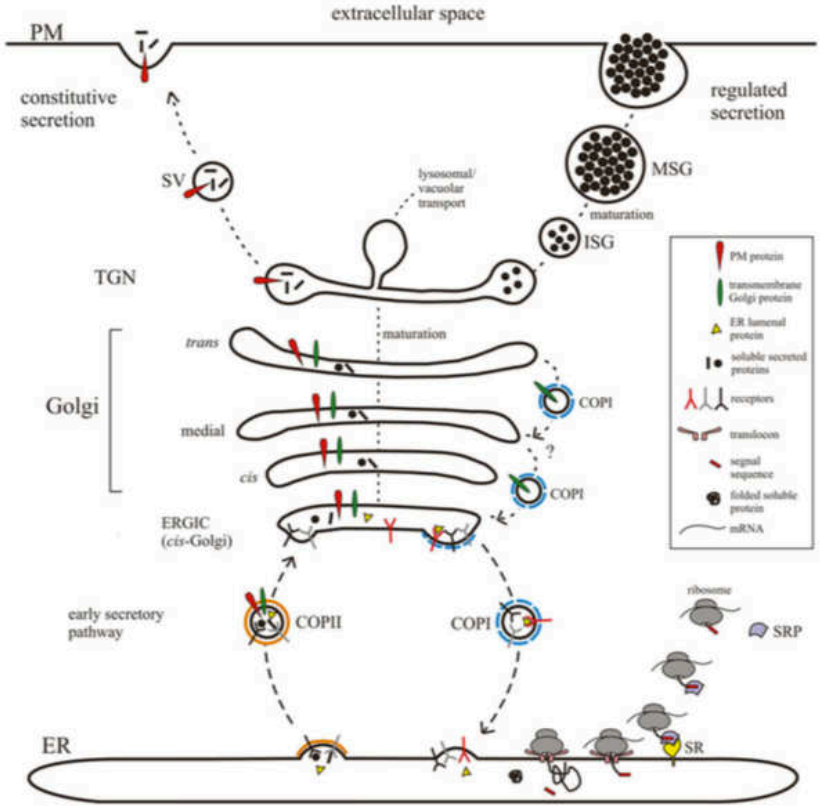

Figure 4. Conventional protein secretion in eukaryotes (Viotti, 2016). The signal recognition particle (SRP) recognizes the signal sequence in the ribosomes, and it interacts with the signal receptor (SR) residing in the ER to transport secretory proteins through the translocon and into the ER lumen. In the ER, the signal sequence is cleaved off and proteins are folded by molecular chaperons to be subsequently packed upon receptor-ligand interaction in COPII vesicles that are delivered to the ERGIC (in animals) or to the cis-Golgi (in yeasts and plants). Retro-transportation of escaped ER luminal proteins is mediated by COPI vesicles. Secretory proteins and plasma proteins are then transported to the TGN, whereas integral proteins are retrieved via intra-Golgi transportation mediated by COPI vesicles. At the TGN, proteins destined to be secreted are sorted in secretory vesicles (SV) that are constitutively delivered toward the plasma membrane, or immature secretory granules (ISG) that accumulate in the cytoplasm and upon the arrival of specific stimuli become mature secretory granules (MSG) and are transported to the plasma membrane. Abbreviations: ER, endoplasmic reticulum; SR, signal receptor; SRP, signal recognition particle; COPII, coat protein complex II; COPI, coat protein complex I; ERGIC, ER-Golgi intermediate compartment; TGN, trans-Golgi network; SV, secretory granule; PM, plasma membrane; ISG, immature secretory granules; MSG, mature secretory granules.

2.2.1. Translocation to the ER: the starting line of the protein *voyage*

The ER, an extensive network of interconnected membrane tubules and sheets forming closed polygons and enclosing an internal lumen, is the starting point for protein synthesis, folding and quality control. Indeed, newly synthesized proteins are promptly transported from the ribosomes across the ER-limiting membrane into its lumen. This process depends on the presence of a specific amino acid sequence at the N-terminal portion of the nascent polypeptide chain, that interacts with the cytosolic signal recognition particle (SRP). After recognition, SRP interacts with the SRP receptor, that resides in the ER and allows the transport through the translocon into the interior space of the ER. In mammals, the translocon is composed of the heterotrimeric Sec61 complex (Sec61α, Sec61γ highly conserved and essential for cellular viability and Sec61β, non-essential) (Gorlich & Rapoport, 1993). Inside the ER, the signal sequence is cleaved and the protein is folded by means of the action of a multitude of chaperons that creates its three-dimensional conformation. If protein folding rate is not sufficiently high, unfolded proteins can accumulate in the ER which triggers several signaling pathways aiming to reduce transcription and to increase folding capacity. Collectively this response to protein aggregation is named the unfolded protein response (UPR), as described in **Paragraph 1.3**. When stress is enduring the ER-associated degradation is elicited to dispose unfolded proteins (Walter & Ron, 2011).

2.2.2. ER-Golgi interface: COPI-COPII-mediated transportation

The ER-Golgi segment of the trafficking route is bidirectional and anterograde and retrograde vesicle transport is mediated by coat protein complex II (COPII) and I (COPI), respectively. The ER-Golgi interface exhibits an extensive plasticity that allows to adapt to cargo-dependent variations in carrier size and number (Brandizzi & Barlowe, 2013). Once chaperoned, non-ER-resident proteins are transferred to vesicles whose morphogenesis is mediated by COPII and its association with the secretion-associated RAS-related 1 protein (Sar1), that is composed of a Sec23 and Sec24 heterodimer and activated by the integral ER membrane protein Sec12 that catalyzes GDP/GTP exchange on Sar1 (Barlowe & Schekman, 1993; Nakano & Muramatsu, 1989). Then, the cytosolic Sec13/Sec31 heterodimer binds to

the Sar1-Sec23-Sec24 complex, forming the outer coat of the COPII cage (Stagg et al, 2008). Assembled vesicles bud off from specific subdomains of the ER membrane, named ER-exit sites (ERES) (Barlowe et al, 1994), whose number and size vary among cell types and organisms, thus influencing their secretion rate. Several additional proteins assist the COPII-mediated transport and, as a result, the molecular structure of COPII-coated vesicles acquires specificity and selectivity in different tissues for diverse cargoes. The concerted action of multiple factors such as tethering factors GM130 and GRASP65 and soluble N-ethylmaleimide-sensitive factor adaptor protein receptors (SNAREs) mediates the transport of proteins. In particular, SNAREs including syntaxin-5 (STX5), GS27, BET1 and Sec22B (Adolf et al, 2016; Rowe et al, 1998) play a central role in the cargo delivery process, as their donor-acceptor pairing mediates the fusion between the donor vesicle and the membrane of the acceptor compartment. In mammals, fusion takes place in the ER-Golgi-intermediate compartment (ERGIC), a distinct organelle located between the ER and the Golgi (Brandizzi & Barlowe, 2013; Xu et al, 2000). Vesicles that reach the ERGIC are tethered by the interaction of Sec23 with the transport protein particle (TRAPP) tethering complex (Zhao et al, 2017). From here, a retrograde transport along microtubules is mediated by COPI composed of seven subunits, four constituting the inner layer of the coat and the other forming the outer shell (Waters et al, 1991). The membrane recruitment and assembly of COPI coated vesicles is initiated by the ADP-ribosylation factor 1 (Arf1) upon GTP binding (Orci et al, 1993). This retrograde pathway allows to retrieve and return to the ER both absconded ER resident proteins and cargo receptors for recycling and further transport. The KDEL motif is the best described ER-retention signal that is located in the C-terminus of most ER-resident proteins, whose interaction with its receptor KDELR constitutes the retrograde sorting signal, leading to the recruitment of soluble ER-resident proteins to the coat and their retrograde transfer to the ER (Szul & Sztul, 2011). The Golgi apparatus serves as a central platform connecting anterograde and retrograde protein transport.

2.2.3. Intra-Golgi traffic: the delivery among different sub-compartments

The Golgi apparatus is a structurally organized organelle where glycosylation of soluble cargoes, membrane proteins and lipids is concluded. This complex is composed of a series of stacked and fenestrated *cisternae*, differing in enzymatic content and activity, that are kept adjacent by structural proteins and are interconnected by tubules to form a Golgi ribbon. These cisternae are clustered in parallel and are functionally organized in three major sub-compartments, namely the *cis*, medial and *trans* regions, with the *cis* compartment facing the ER (Klumperman, 2011). Juxtaposed to the trans sub-compartment is the trans-Golgi network (TGN), a tubular-vesicular clathrin-coated sorting hub that directs proteins to their final destination (Griffiths & Simons, 1986). Several models have been proposed to explain the mechanism of secretory protein transport through the Golgi including the anterograde vesicular transport between stable compartments and the cisternal progression/maturation model. The first schematizes the anterograde vesicular transport between stable and biochemically different compartments, where secretory cargo is enclosed in vesicles that bud from one compartment and fuse with another in a COPI-mediated manner, excluding Golgi resident proteins (Glick & Luini, 2011). Nevertheless, this model applies only for small cargoes able to fit in COPI vesicles. The second model describes the cisternal progression and maturation and the transport of large cargoes. In this model, *cis*-cisternae are continuously formed via the fusion of COPII vesicles and maturation occurs in a COPI-mediated recycling way by receiving medial and then trans-Golgi proteins from older cisternae. In the final stage of maturation, the cisterna progresses through the stack that has become a TGN element and disintegrates into anterograde and retrograde transport carriers (Glick & Luini, 2011). The most prominent non-exclusive models have been combined in an integrative model of intra-Golgi transport unifying constitutive recycling pathways, maturation and diffusive anterograde and retrograde transports (Boncompain & Perez, 2013). Of note, COPI-mediated transport is known to be inhibited by several compounds, including brefeldin A (BFA), a fungal metabolite that inhibits the recruitment of the small GTPase Arf1, which is the first step in the generation of Golgi-originated COPI-coated vesicles (Beck et al, 2009). BFA leads to the collapse of ER export as the inactivation

of Arf1 induces the dissociation of COPI and other peripheral proteins from the Golgi (Klumperman, 2000; Ward et al, 2001). This leads to the disassembly of the Golgi structure and results in the reversible redistribution of Golgi-proteins to the ER and washout of BFA allows reformation of a functional Golgi and reinstatement of protein export from the ER (Donaldson et al, 1992). Furthermore, nocodazole is yet another inhibitor of ER-Golgi transport that acts by interfering with the microtubule dynamics thus causing the reversible redistribution of Golgi proteins to peripheral sites of the ER, where they assemble into Golgi ministacks (Storrie et al, 1998).

2.2.4. TGN exit: reaching the final destination

The TGN plays the role of sorting station as it directs different cargo proteins packed into distinct transport carriers to their vesicular transport pipelines in order to reach various final destinations, such as the plasma membrane (PM) or endosomes. Different adaptors, effector molecules and sorting signals characterize these diverse trafficking routes and mediate the sorting of cargo proteins. The most well-known and best-characterized adaptor in charge of sorting at the TGN is the adaptor protein complex-1 (AP-1), a heterotetrameric complex containing an ARF-binding domain that binds to cargo proteins and phospholipids (Guo et al, 2017). Once budding occurs, vesicles deliver the cargo via microtubules-associated motor proteins along a cytoskeletal track (Bard & Malhotra, 2006). Finally, secretory vesicles and secretory granules fuse with the PM via the exocyst complex, an evolutionarily conserved complex consisting of eight subunits that is located to the limiting regions of the PM (Heider & Munson, 2012). The fusion with the PM, and the consequent delivery of cargoes to the extracellular space, marks the end of the ER-to-Golgi, intra Golgi and Golgi-to-PM journey of secretory cargoes.

2.3. The unconventional pathway

A minority of proteins, both soluble and membrane-bound, are released from cells through alternative routes distinct from the canonical pathways. These processes are collectively named unconventional protein secretion (UPS), also known as non-classical or ER/Golgi-

independent protein secretion (**Figure 5**). More than 20 cytoplasmic and nuclear secretory proteins are described to be exported by these unconventional means.

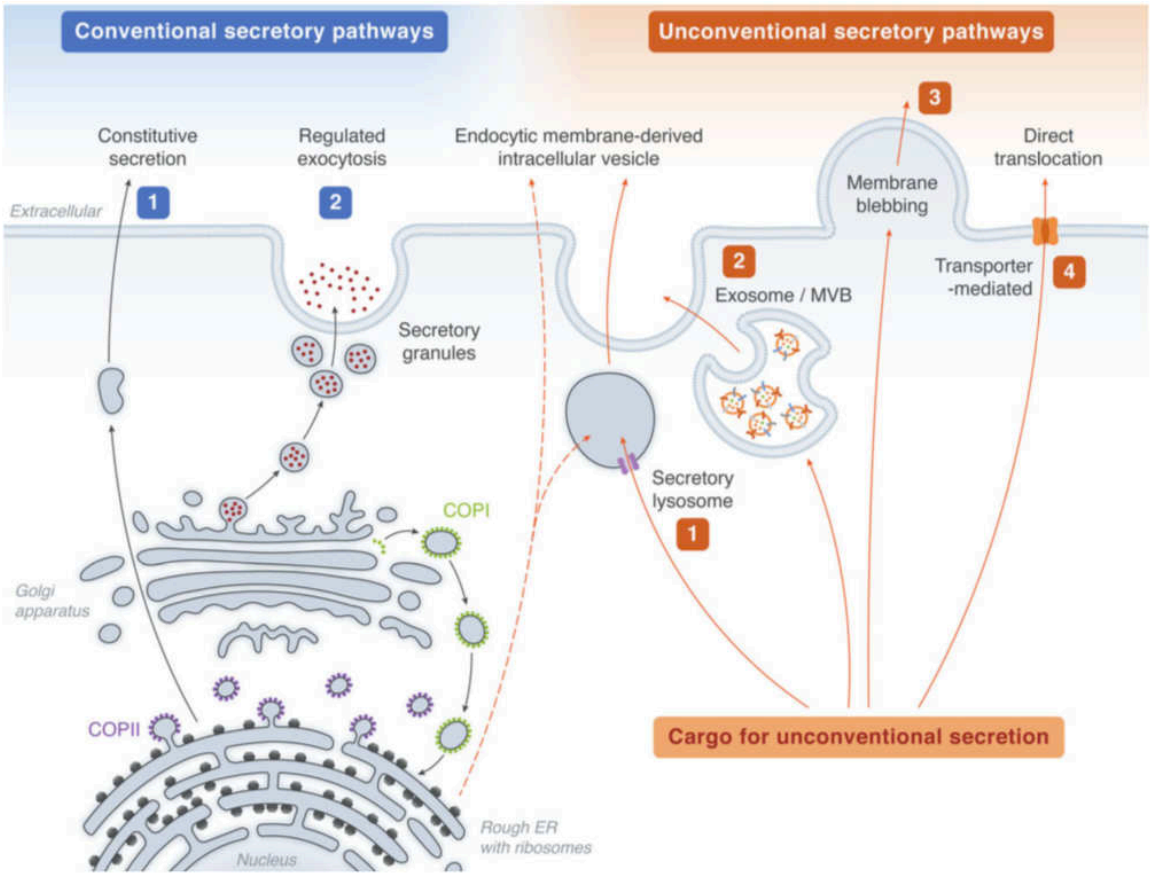

Figure 5. Secretory pathways (Bhattacharya et al, 2014). The conventional secretory pathway includes (1) constitutive secretion and (2) regulated exocytosis via secretory granules. The unconventional secretory pathway includes (1) secretion mediated by secretory lysosomes or (2) exosomes/multivesicular bodies, or direct translocation through (3) membrane blebbing or (4) through surface transporters. Abbreviations: ER, endoplasmic reticulum; COPII, coat protein complex II; COPI, coat protein complex I; MVB, multivesicular bodies.

The mechanisms and molecular components of this transport pathway are less well-characterized but certain details are beginning to emerge. Various proteins in charge of crucial extracellular functions such as regulation of immune responses or cell growth, that are lacking the N-terminal signal peptide, or even signal peptide-containing proteins, have been shown to be secreted in an COPII machinery-/Golgi-independent fashion (Ng & Tang, 2016). Among the earliest examples of unconventionally secreted proteins, are the fibroblast growth factor 2 (FGF2), secreted from a multitude of cell types during development, and interleukin 1β (IL-1β), an essential cytokine for acute inflammatory responses (Pallotta & Nickel, 2020). Other interesting and more recent examples are the *Dictyostelium discoideum* acyl-coenzyme A-binding protein (AcbA) (Duran et al, 2010) and the nuclear

protein high motility group box 1 protein (HMGB1) (Gardella et al, 2002), the latter actively released from a variety of immune cells, or passively released by dying cells stimulating further pro-inflammatory effects and recruiting diverse immune cells. Moreover, several proteins have been shown to be insensitive to the previously described effects of BFA, suggesting a bypass of the Golgi-mediated protein transport route. This is the case for a pool of CD45, the receptor protein Tyr phosphatase essential for T-cell development (Baldwin & Ostergaard, 2002) or for the antiviral protein ovine Mx1 (Toyokawa et al, 2007).

The UPS can follow four mechanistically distinct pathways, depending on the nature and cellular localization of the secretory cargo. The first type is the only non-vesicular UPS and it involves cytosolic proteins, such as FGF2, that are directly translocated from the cytoplasm to the PM (Schafer et al, 2004). In the remaining mechanisms, vesicular intermediates participate in the transport. Cytoplasmic proteins can be lodged into secretory lysosomes or lytic granules, even though the nature of these transporters remains elusive, yet displaying characteristics of both lysosomes and secretory granules (Holt et al, 2006). This has been documented for IL-1β (Andrei et al, 2004). Yet another type of UPS involves the shedding of microvesicles, also called ectosomes, from the PM to the extracellular space, where they circulate adjacent to the site of discharge before a rapid break down leads to the release of their content (Cocucci et al, 2009). Furthermore, the formation of exosomes in multivesicular bodies (MVB) by means of the endosomal sorting complexes required for transport (ESCRT) mediates the transport (Kowal et al, 2014), and these exosomes are released when the MVB move towards the cell periphery. Of note, some proteins possibly follow more than a single UPS route, as this is the case of IL-1β and some others can follow both canonical and unconventional pathways, such as the cystic fibrosis transmembrane conductor (CFTR). The reasons why cytoplasmic secretory proteins take advantage of the UPS instead of the classical pathways remains elusive, even some hypothetical causes have been proposed, such as the misfolding of certain proteins becoming not functional due to the oxidative environment in the lumen of the ER and the Golgi, or the binding to oligosaccharide species (Nickel & Rabouille, 2009). Despite the fact that several of UPS pathways are quite well characterized, others have been observed but yet lack mechanistic details, such as the autophagy-dependent protein secretion (Jiang et al, 2013).

2.4. Where do secretory and autophagy pathways meet?

Since its discovery, autophagy is predominantly known for its degradative lysosomal pathway. Interestingly, most (if not all) components of the autophagic molecular apparatus have been shown to mediate as well non-autophagic functions, mostly in the context of trafficking (Galluzzi & Green, 2019). Indeed, growing evidence points to functionally different terminations of this pathway impacting protein degradation and secretion. Autophagy facilitates secretion in both physiological and pathological conditions and the enhancement or attenuation of autophagy has been related to consequential alterations in secretion. How secretory autophagy diverges from degradative autophagy remains unclear. Nevertheless, changes in autophagy are demonstrated to modify the secretion of key signaling molecules and cytokines, as well as small molecular weight immune mediators (Kimura et al, 2017; Ma et al, 2013). The hypothesis that autophagy-relevant proteins could be involved in protein release irrespective of lysosomal degradation has first been formulated in the setting of the UPS (Rabouille, 2017). Multiple cargo types, mostly leaderless proteins lacking a secretion signal sequence that are unable to enter the conventional secretory pathway while playing extracellular functions, have been shown to undertake this autophagy machinery-dependent non-conventional *voyage* (Ponpuak et al, 2015), especially under conditions of stress. Indeed, stress may drive the cells to resort the UPS of cytosolic proteins in order to elicit a non-cell-autonomous signal. The stress-induced activation of the UPS may favor the disposal of accumulated unfolded proteins in the ER, in the context of ER stress, or alternative routes may be followed in order to allow some degree of secretion to occur in the case of trafficking defects in the canonical pathway. Release of IL-1β is an exquisite example of the implication of autophagy in secretion, as it depends on ATG genes including ATG5 and the sequestration membrane of the carriers have been shown to contain the autophagic marker LC3-II (Dupont et al, 2011). Acb1 secretion is also mediated by several autophagy-related proteins and its secretory pathway involves autophagosomes that evade fusion with the vacuole to prevent cargo degradation, but instead fuse with recycling endosomes for the transport to the PM and the release of their the cargo (Duran et al, 2010). Indeed, crucial autophagy components that drive the UPS are involved in the early stages of autophagosome formation but are not necessary for the final fusion with lysosomes. Autophagosomes can interact with

components of the endocytic pathway, fusing with endosomes or MVBs to form hybrid organelles termed amphisomes, that have been proposed as possible intermediates for the autophagy-mediated UPS (Fader & Colombo, 2009). Trafficking of autophagosomes has been shown to be dependent on proteins decorating the outer membrane: on the one side both degradative and secretory autophagy are labeled with LC3, while syntaxin-17 directs fusion of the degradative autophagosome with the lysosome, SEC22B and TRIM16 direct the autophagosome for secretion (New & Thomas, 2019). However, how these proteins are bypassing the lysosome and are secreted instead of being degraded remains unknown and more in general the understanding of the precise mechanistic of autophagy leading to UPS is relatively nascent and requires further investigations.

2.5. Techniques to monitor protein secretion

Given the previously discussed key role of secreted proteins as mediators of intercellular signaling, multiple methodologies have been developed to visualize and measure their secretion. The most commonly employed techniques are summarized in **Table 1**, together with their key features as well as their advantages and drawbacks.

Technique	Key feature	Advantages	Disadvantages	Ref.
Enzyme-linked immunosorbent assay (ELISA)	Antibody-mediated detection coupled with enzyme-substrate combinations	> Concentration of secreted protein in cell-free media > Easy to perform	> No clarification on specific secretory cellular population > Lack of secretion kinetics > No parallel detection of multiple proteins > Hardly applicable *in vivo* for proteins difficult to detect in serum due to their short-half life or rapid uptake	(Lequin, 2005; Shah & Maghsoudlou, 2016)
Enzyme-linked immunospot assay (ELISPOT)	ELISA working principle	> Monitoring of protein secretion frequency at single cell level > Possibility of simultaneously follow more than one protein > Highly efficient and fast assay with high specificity and sensitivity	> Lack of secretion kinetics >Impossibility to quantify the amount of secreted cytokine per cell >Relatively expensive >Ex vivo and in vitro applications only	(Ji & Forsthuber, 2016; Kalyuzhny, 2005)
Flow cytometry	Intracellular staining	> Protein expression at single-cell level > Simultaneous detection of multiple cytokines within a single cell > High throughput potential	> More focused on synthetization/storage than on secretion > Requirement of staining procedures	(Trautmann, 2013; Yin et al, 2015)
Temperature block assay	Synchronization of protein trafficking with temperature control	> Easy to perform and not expensive > Real-time observation	> Non physiological temperature > Temporary arrest of biosynthetic pathways > No *in vivo* applications	(Griffiths et al, 1985; Matlin & Simons, 1983)
Vesicular stomatitis virus G protein (VSVG) assay	Synchronization of protein trafficking with a thermosensitive viral glycoprotein	> Real-time observation > Kinetics information	> Temperature not within the physiological range > Not applicable *in vivo*	(Lafay, 1974)
Ultraviolet-B receptor (UVR-8) system	Light-mediated synchronization of protein trafficking	> Possibility of fusion with fluorescent and photoswitchable proteins > Potential *in vivo* applications	> Possible cellular damaging	(Chen et al, 2013b)
Retention using selective hooks (RUSH) system	Chemical-genetic strategy for reversible interaction between streptavidin and streptavidin-binding peptide (SBP), outcompeted by biotin	> Real time monitoring at single-cell level > High throughput potential > Physiological conditions > Versatility in secretory cargos and in retention localization > *In vivo* applications	> Two fusion proteins > Potential off-target effects	(Boncompain et al, 2012; Boncompain & Perez, 2014; Liu et al, 2020)

Table 1. Techniques for monitoring protein secretion. Key feature, advantages and disadvantages of the most commonly employed assays.

Depending on the protocol, these assays can be mostly classified into intermittent and continuous: successive but discontinuous snapshots or continuous measurements of protein secretion over time, respectively (Shirasaki & Ohara, 2018).

Cytokines are the best and well-characterized class of secreted proteins due to their important and tightly regulated role in orchestrating immune responses when cells encounter the invasion by a wide range of viral, fungal and bacterial pathogens (Lacy & Stow, 2011). Tumor necrosis factor (TNF), interferon gamma (IFN-γ), interleukins (IL) such as IL-1β and IL-6 are included in the array of soluble mediators secreted by different immune cells such as macrophages and dendritic cells. Newly synthesized or stored cytokines are released upon cellular stimulation and, as an example, the pathogenic stimulus lipopolysaccharide (LPS), major component of the membrane of Gram-negative bacteria, can potently trigger their release. Of note, the majority of cytokines in macrophages are processed and transported through the canonical pathway, yet less is known about the non-canonical transport of specific cytokines such as IL-1β (Murray & Stow, 2014). The concentration of secreted cytokines is typically measured with techniques taking advantage of antibody-mediated detection coupled with enzyme-substrate combinations, such as the enzyme-linked immunosorbent assay (ELISA) (Shah & Maghsoudlou, 2016). This technique allows to quantify the concentration of secreted proteins in cell-free media but without a clarification on the specific cellular population that contributed to that release. To overcome this disadvantage, the enzyme-linked immunospot (ELISPOT) assay was developed based on the ELISA working principle to enable the monitoring of protein secretion frequency at single-cell level, as it directly detects secreting cells (Kalyuzhny, 2005).

Flow cytometric assays offer the possibility to study cytokine production via intracellular staining, focusing more on storage then on secretion (Trautmann, 2013). This technique emerged for its capacity to study cytokine expression at the single-cell level and for the simultaneous detection of multiple cytokines within a single cell (Yin et al, 2015), even if not allowing for an absolute quantification.

One common bottleneck of the described assays is related to the necessity of cellular fixation and, along similar lines, to the analysis of a defined timepoint, lacking the possibility to follow the kinetics of the process. The technological progress in this field attracted lot of attention and the development of new and more performant assays monitoring protein secretion in

real-time has recently accelerated. Multiple modifications continuously improve sensitivity, quantitative accuracy and throughput. To cite a few examples, single-cell imaging of protein secretion in real-time became possible within a sophisticated assay platform with extremely high sensitivity (Shirasaki et al, 2014), as well as polymeric devices that have been developed to array different cell types in a defined space (Chiu et al, 2016), and microfluidic devices that precisely stimulate single cells and are able to quantify the rate and time of cytokine secretion under varying inputs (Junkin et al, 2016).

The easiest strategy to image protein secretion in a way that dissects the route of particular cargo proteins in real-time, is the synchronization of protein trafficking. One of the most commonly employed mechanisms to synchronize protein secretion involves temperature control. In the temperature block assay, proteins are retained within the ER at 15°C, arrested in the Golgi at 20°C and protein secretion is reinitiated with the temperature increasing to 37°C (Matlin & Simons, 1983; Saraste & Kuismanen, 1984), an efficient way to study protein secretion but causing a temporary arrest of most of biosynthetic pathways. An improvement of this assay takes advantage of a thermosensitive mutant of vesicular stomatitis virus-G glycoprotein (VSVG). VSVG is retained in the ER at 39.5°C, when the temperature is lowered to 32°C its conformational changes are compatible with its traffic through the Golgi apparatus towards the PM (Kreis & Lodish, 1986; Lafay, 1974). Nevertheless, the temperature that is applied is not within the physiological range which prevents this technique to be applied *in vivo*. Light-triggered protein secretion is a novel tool offering new perspectives for protein control, such as the plant photoreceptor protein ultraviolet-B receptor (UVR8)-system which can be used to conditionally sequester secretory cargo in the ER followed by a light-mediated release (Chen et al, 2013b). Chemical-inducible systems include assays where an engineered protein accumulates as aggregates in the ER and whose secretion is stimulated by a synthetic small-molecular drug that induces protein disaggregation (Rivera et al, 2000). To fulfill the need of a versatile trafficking assay where diverse cargos can be synchronized under physiological conditions and in a high throughput fashion, the retention using selective hooks (RUSH) system was developed. The RUSH technique (**Figure 6**) is the most relevant single-cell based assay at physiological temperature and offers the potential of analyzing different transport characteristics of a multitude of secretory cargos that follow

the ER-Golgi-PM trafficking route (Boncompain et al, 2012; Boncompain & Perez, 2014). In this assay that relies on the selective retention and release of cargo molecules from a subcellular localization, secretory trafficking can be synchronized from any part of the secretion pathway. The RUSH system is based on two fusion proteins: the hook, stably expressing core streptavidin (STR) together with a subcellular localization signal such as KDEL, CD74 for the ER or Golgin-84 for the Golgi apparatus, and the reporter, where the STR-binding peptide (SBP) is commonly fused to a fluorescence biosensor such as GFP, allowing for the real-time or end-point imaging. The core principle of this assay is the reversible interaction between SBP and STR, that at steady state are bound with high affinity but that can be outcompeted by biotin, a natural non-toxic vitamin that freely diffuse within the cell and has a higher affinity for STR than SBP (Bayer & Wilchek, 1990; Keefe et al, 2001). Hence, in the absence of biotin the reporter is anchored to the hook via the STR-SBP interaction and this can be observed in the donor compartment, when biotin is added to the system, it interacts with STR on the hook and this leads to the close-to-immediate release of the reporter that can freely resume its journey tracked by means of the fluorescent protein toward its final destination.

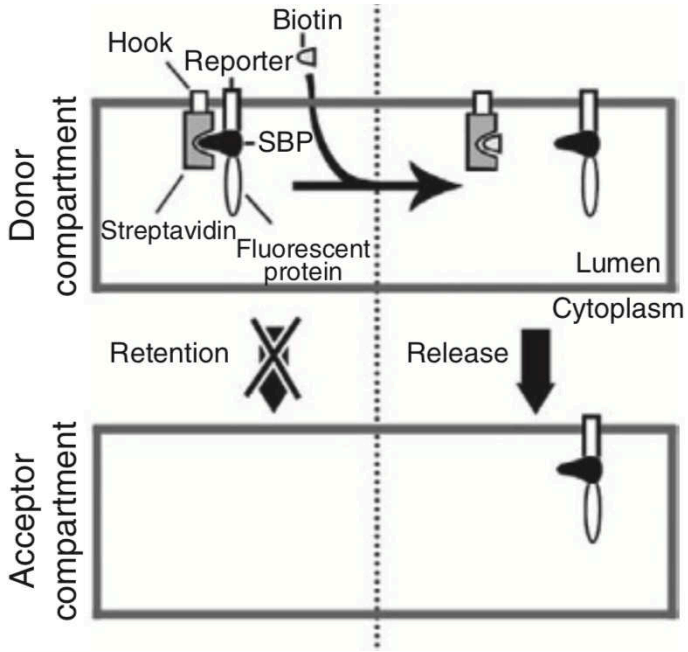

Figure 6. Principle of the RUSH system (Boncompain et al, 2012). The reporter is anchored in the donor compartment by means of its interaction with the hook mediated by the core streptavidin and the SBP. A fluorescent protein is attached to the hook allowing for monitoring. When biotin is added to the system it induces the release from the hook of the reporter that can traffic to its acceptor compartment. Abbreviations: SBP, streptavidin binding domain.

The high throughput potential of this system was employed to perform several phenotypic screens of compound libraries. A campaign conducted in the context of immunogenic cell death (ICD) was designed to identify pharmacological HMGB1 releasing agents by means of a RUSH system where HMGB1 was retained in the nucleus by streptavidin that was fused with several nuclear localization sequences (Liu et al, 2017).

Moreover, another RUSH system targeting the ER was employed to identify inhibitors of conventionally secreted proteins, showing a series of unrelated drugs to suppress protein synthesis compromising ER morphology and Golgi integrity, with a variable degree of reversibility, opening new horizons in the characterization of clinically used drugs' mode of action (Zhao et al, 2018).

Recently, the RUSH system was equipped with LC3 and SQSTM, two chimeric proteins involved in autophagy, whose retention both in the ER and in the Golgi failed to induce signs of autophagy. This system can be used as an additional assay to enforce the subcellular shuttling of functional LC3 and p62 (Loos et al, 2019).

More recently, the RUSH assay was used to monitor the trafficking of calreticulin (CALR), an ER-resident chaperone that translocated to the PM upon stress, playing the role of an "eat-me" signal for immune-mediated responses, and showed that mutations of CALR lead to its mis-localization outside of the ER, driving myeloproliferative disease (Liu et al, 2020).

To overcome the general pitfall of *in vitro* models, that while allowing the control of most experimental variables and permitting precise quantitative analysis, have reduced physiological relevance, our team recently developed *in vivo* version of the RUSH system designed to work in mice, aiming at broadening aspects of the physiological/organismal complexity. The hydrodynamic injection of vectors coding for the hook, the ER-localized STR targeting KDEL, together with the secretory tagged SBP as reporter, enabled the expression of these transgenes in the liver of mice. Despite the fact that introduction of these two vectors might have an impact on the hepatic metabolism and thus organismal physiology, this system endowed the consequent possibility to synchronize the trafficking from hepatocytes by means of intraperitoneal (*i.p.)* injections of biotin (Liu et al, 2020), thus opening new insights to explore protein secretion in more physiological settings.

3. Fatty acids

3.1 A variety of chemically different hydrocarbon chains

Lipids are a class of energy-yielding nutrients that tend to be hydrophobic, non-polar and primarily composed of carbon, hydrogen and oxygen atoms. In nature, fats (typically solid at 25°C) and oils (liquid at that temperature), also called triglycerides because of their glycerol skeleton coupled with three fatty acid tails, are the most abundant lipids and are present in food, such as dairy products, meat as well as baked goods. The nutritional and functional significance of fats and oils are deeply linked to their physical and chemical structure.

Fatty acids (FAs), both free and as part of complex lipids, have been shown to play a number of key and functional roles in cellular structure, metabolism, gene regulation and homeostasis. Thus, phospholipids, glycolipids and lipoprotein are involved in the structural composition of cellular membranes, they represent a source of energy stored in triacylglycerols and several lipid metabolites serve as intra- and extra-cellular mediators and hormones (Calder, 2015). Chemically, FAs are aliphatic carbon chains with a methyl group on one end of the molecule (designed as omega, ω) and a carboxylic group at the other end. FAs are highly diverse and more than 100 different natural FAs have been described thus far. FAs are classified depending on their chemical structure and subsequent biochemical properties, such as their saturation status (saturated or unsaturated FAs, *i.e.* absence or presence of double bonds between neighboring carbons, respectively), carbon number (even or odd number of carbon atoms), chain nature (straight, branched or cyclic), length (short or long) and geometry of the double bond (*cis* or *trans* isomer).

Saturated fatty acids are characterized by a mostly straight hydrocarbon backbone with an even number of carbon atoms, usually ranging from 12 to 22. Saturated fatty acids are enriched in meat, dairy products, palm and coconut oils. Palmitic acid (C16:0), also called palmitate in its ionized form, is the most widely occurring saturated FA, and lauric acid (C12:0), myristic acid (C14:0), and stearic acid (C18:0) also belong to this group. Conversely, unsaturated FAs whose primary sources are vegetables oils, nuts and fish, have a chain length in the range of 16-22 carbon atoms, and they contain one (monounsaturated FAs; MUFAs)

or more (polyunsaturated FAs, PUFAs) double bonds in varying positions of their structure. Depending on whether the hydrogen atoms are on the same side of the double bond or on opposite sides, the unsaturated FA is defined as a *cis*- or *trans*-isomer, respectively. Most naturally produced unsaturated FAs are in the *cis*-configuration and the *cis* double bond causes a bend or a kink in the FA structure, preventing it from packing tightly and resulting in their liquid form at room temperature. Conversely, *trans* isomers that result in a straight conformation are rare in nature, as they are only synthesized in small amount in the rumen of certain ruminants such as sheep and goat (Stender et al, 2008), and they may be produced during industrial processing by partial hydrogenation of unsaturated oils in order to obtain a desirable consistency as well as enhanced shelf life for many processed food products, such as margarine or some types of peanut butter (Craig-Schmidt, 2006). To a lesser extent, they may also form during heating and frying of oils at high temperature (Kadhum & Shamma, 2017).

The position of the first unsaturation with respect to the methyl end (ω) distinguishes between ω-3, ω-6 and ω-9 unsaturated FAs, where the first double bond exists as the third, the sixth or the ninth carbon-carbon bond from the terminal end ω, respectively.

A major nutritionally important ω-9 MUFAs is oleic acid (C18:1), from here onward called oleate (oleic acid anionic form), whose *trans* isomer is the elaidic acid, the major industrially produced *trans*-unsaturated FA in the food supply, while the PUFA family includes ω-3 PUFAs such as α-linoleic acid (C18:3), eicosapentaenoic acid (C20:5), docosahexaenoic acid (C22:6) and ω-6 PUFAs such as linoleic acid (C18:2), γ-linolenic acid (C18:3) and arachidonic acid (C20:4) (**Figure 7**) (Radzikowska et al, 2019).

In humans, FAs are ingested with foods and synthesized by cells, and certain among them are considered essential for adequate growth and reproduction. However, mammals are unable to synthesize FAs such as linoleic acid, also called linoleate, an ω-6 PUFA derived from meat or α-linoleic acid, also called linolenate, an ω-3 PUFA derived from vegetable oils, due to the lack of enzymes allowing the introduction of double bonds at carbon atoms beyond C-9 in their chain (Anez-Bustillos et al, 2018). To date, linoleic acid and α-linoleic acid, are acknowledged to play an essential role and need to be supplied by the diet as a starting point for the synthesis of other unsaturated FAs. Conditionally essential FAs, long

chain derivatives of those essential PUFAs, are sometimes called as such because they are highly necessary in various physiological functions and they are synthesized within the body, but they should also be delivered with foods.

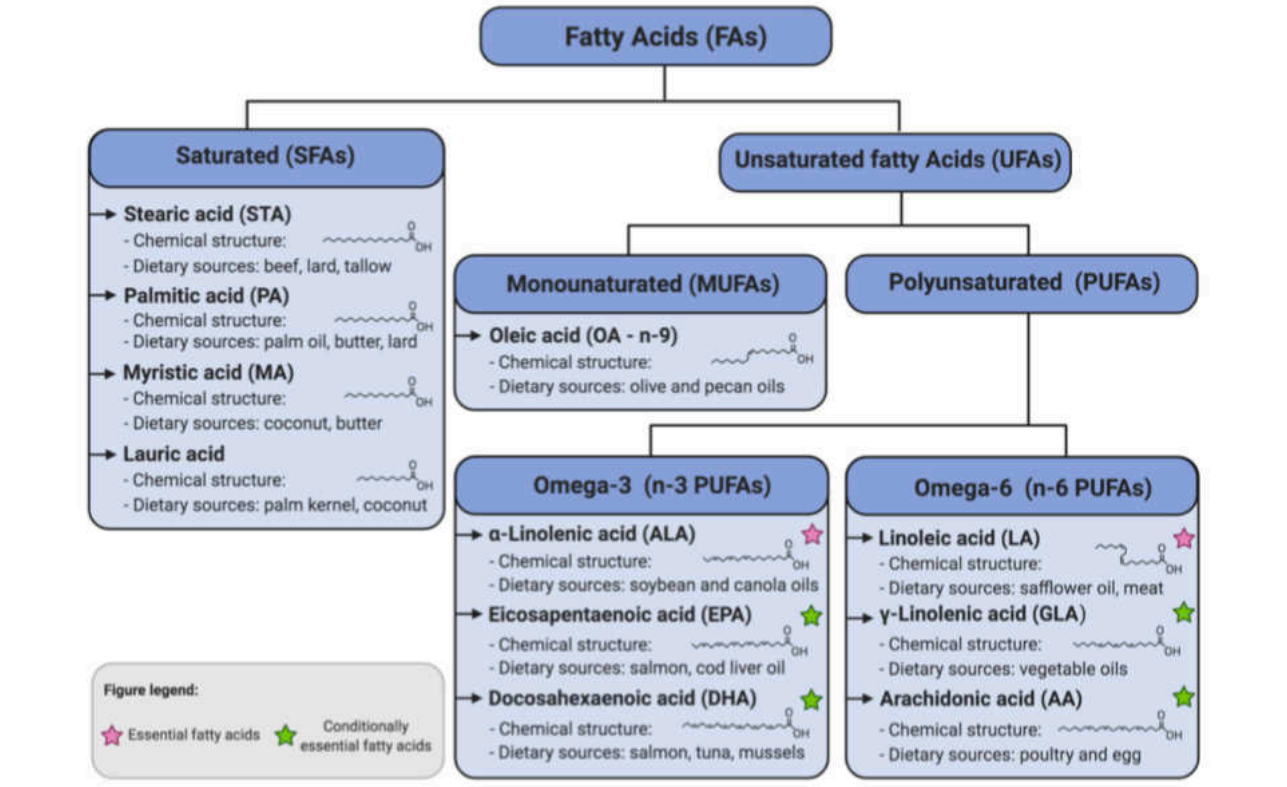

Figure 7. Classification of fatty acids (Radzikowska et al, 2019). Classification, chemical structure and primary dietary sources of the most common FAs.

3.2 Oleate: the most abundant *cis*-mono-unsaturated fatty acid

Oleate (C18:1), also called 9-octadecenoic acid, possesses an 18-carbons chain with a double bond in a *cis*-configuration located at carbons 9,10 from the methyl end and it is the most abundant *cis*-MUFA in our body, as well as in our diet. Its *trans* counterpart is elaidate is the mainly produced by industrial hydrogenation of edible oils (**Figure 8**). Indeed, numerous food sources naturally contain oleate, mainly edible oils, such as olive oil, sunflower oil, or canola oil, but it is also present in animal-derived fats such as lard and butter. Olive oil, the yellow-colored oil produced by mechanical and physical processes from *Olea Europaea,* a tree crop naturally growing in the Mediterranean area, plays a central role in the traditional

Mediterranean diet and it is an especially rich source of oleate. Despite the fact that the composition of olive oil may vary with the altitude, maturation stage, time of harvest or cultivated variety, the amount of oleate is up to 55-83%, followed by a variable but significant amount of saturated FAs including palmitic acid (up to 20%) and stearic acid (up to 4%), PUFA including linoleic acid (up to 6%), and some small amount of antioxidant micronutrients, namely polyphenols and squalene (Bester et al, 2010). The same holds true for sunflower oil and canola oil, where the amount of oleate is around 60%.

Oleate is considered as a non-essential FA since it can be *de novo* synthesized in humans by a Δ9-desaturation of stearic acid catalyzed by the enzyme Stearoyl-CoA desaturase 1, and many cell membrane phospholipids contain significant oleate proportions (Calder, 2015).

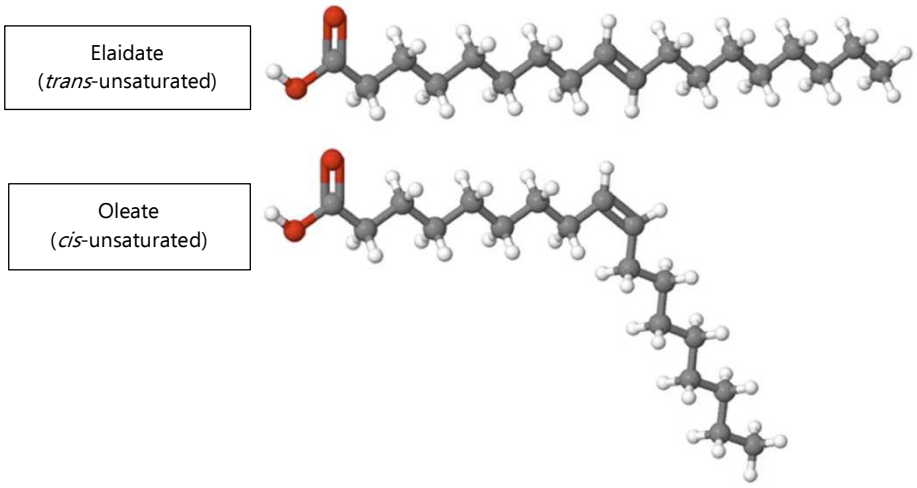

Figure 8. Chemical structure of oleate and elaidate. Oleate is a *cis*-monounsaturated FA presenting one double bond in its hydrocarbon chain located among carbons 9 and 10 and has a *cis*-configuration as hydrogens of its double bond are situated on the same side causing a "kink" in the chain. The *trans* isomer of oleate is elaidate, whose *trans*-unsaturation results in a straight structure.

3.3 Influence of fatty acids on health

It is nowadays evident that healthy dietary routines throughout the entire course of life are part of a wide range of habits allowing to promote and maintain good health and, in parallel, prevent developing risks of pathologies such as cardiovascular diseases (*e.g.* heart attacks), leading cause of death worldwide taking an estimated 31% of all mortalities, or diabetes, also positioned among the ten major causes of death (WHO, Retrieved 2021-24-01). FAs have a documented track record of type-dependent effects on organismal health. The World

Health Organization (WHO) recommends ranges of nutrient intake goals for multiple dietary factors, such as total fats that should not exceed 30% of total energy intake, the amount of saturated FAs intake to be less than 10% of the total and, in addition, industrially produced *trans*-unsaturated FAs should be less than 1% (FAO, 2010; WHO, 2003). In 2018 the WHO released the "REPLACE" action package, calling on governments to remove *trans*-unsaturated FAs from the global food chain by 2023 (Ghebreyesus & Frieden, 2018; Parziale & Ooms, 2019; WHO, 2018), as this is already the case for the US Federal Drug Administration (FDA) that in 2015 finalized its decision to ban all dietary sources of *trans*-unsaturated FAs (Brownell & Pomeranz, 2014).

Indeed, *trans*-unsaturated FAs are considered to negatively impact human health, especially at the cardiovascular level (Brouwer et al, 2013), and their nutritional uptake or plasma concentration are positively correlated with the severity of coronary arteriosclerosis (Hadj Ahmed et al, 2018) and inflammatory biomarkers (Mazidi et al, 2017) or leukocytes telomeres shortening (Mazidi et al, 2018), the latter related to aging. Accordingly, excessive intake of *trans*-unsaturated FAs was shown to contribute to the progression of cardiovascular disease also in animal models (Monguchi et al, 2017).

Because of their similar structure, *trans*-unsaturated FAs are claimed to act like saturated FAs, and they are both well known for their potential toxicity as well as to the induction of chronic inflammation that contributes to metabolic syndrome (Ralston et al, 2017). Metabolic studies have shown that at different extent, they both increase blood lipid levels, namely raising low-density lipoprotein (LDL)-cholesterol, which may account for the positive link between those types of FAs consumption and coronary artery disease (de Souza et al, 2015; Ginter & Simko, 2016; Siri-Tarino et al, 2010).

On the contrary, the beneficial impact of mono-*cis*-unsaturated FAs represented by oleate, associated with the Mediterranean diet, are nowadays well known, mostly when observing diets where saturated FAs were replaced by unsaturated FAs, and also when analyzing effects directly related to the presence of olive oil in the diet. Indeed, the beneficial effects of olive oil is stated to be a combinatory effect induced both by the oleate content but also by other minor components such as polyphenols (Mazzocchi et al, 2019; Sales-Campos et al, 2013; Santangelo et al, 2018), and both FDA and EFSA agencies established health claims stating

that these two components of olive oil contribute to the maintenance of normal blood cholesterol levels (EFSA, 2011; FDA, 2018). There is an abundance of literature providing insights into the role of oleate in health and disease. Indeed, olive oil was shown to impact the prevention of cardiovascular disorders (Bendinelli et al, 2011; Guasch-Ferre et al, 2014; Romani et al, 2019), with an improvement in the serum lipoprotein profile (Zambon et al, 2000), a decrease in inflammatory markers (Bogani et al, 2007) and a lowering effect on blood pressure levels (Bermudez et al, 2011; Ferrara et al, 2000). Furthermore, its consumption has also been related to a reduced gastric-duodenal ulcers risk (Bermudez et al, 2011).

3.3.1 Clinical trials involving oleate

In the last two decades, the role of oleate in human health and in disease prevention has been studied in various clinical trials, including few phase I, II and IV studies (**Table 2**). Most of them aim to investigate how the consumption of dietary oleate, mostly via olive oil-enriched meals, influence the body composition, a broad range of metabolic responses that are important in the development of cardiovascular diseases (CVD), inflammatory response and metabolic dysfunction in healthy subjects as well as obese or Type 2 diabetic patients. In addition, one clinical trial (NCT04373421) aims to evaluate the anti-inflammatory properties of oleate on the postoperative complications after removal of molars in oral/maxillofacial surgery via oleate mouthwashes.

It is has been conclusively demonstrated that olive oil plays a key role in the Mediterranean diet's cardio-protective effect, attributing its beneficial effects on many CVD risk factors, including blood pressure, lipid profiles, endothelial function, inflammation and thrombosis, and factors related to metabolic syndrome (Lopez-Miranda et al, 2010). Results show that olive-rich diets improve glucose metabolism, reduce body weight (Lasa et al, 2014) and constitute an alternative approach to low-fat diets for effective nutritional treatment of diabetes (Perez-Martinez et al, 2011).

Indication	Phase	Status	Reference	Notes	Title
Chronic kidney disease	NA	Completed	NCT02993380	Dietary supplement: stir-fried olive oil or natural olive oil	Effect of Olive Oil on Erythrocyte Membrane Fatty Acid Contents in Hemodialysis Patients
Hypertension and cardiovascular diseases	NA	Recruiting	NCT03820336	Dietary supplement: Extra Virgin Olive Oil	Cardiovascular Effects of EVOO in Healthy Reproductive-aged Women
Type 2 Diabetes Mellitus	NA	Recruiting	NCT03774095	Dietary supplement: Hydrolyzed pine nut oil and olive oil	Effects of Pine Nut and Olive Oil as FFA1/FFA4 and GPR119 Agonists on Glucose Tolerance in Healthy Overweight or Obese Subjects
Cardiovascular diseases	NA	Completed	NCT02802904	Dietary supplement: Virgin Olive Oil	Multicountry Studies on the Effect of Positional Distribution of Fatty Acids at Triglyceride Backbone on Serum Lipids, Lipoprotein(a) and LDL-subclasses in Healthy Malaysian Volunteers
Nutritional intervention	I&II	Completed	NCT03886597	Table Olives	Nutritional Intervention With Table Olives in Healthy Volunteers (BIOLIVA)
Type 2 Diabetes Mellitus	NA	Completed	NCT04077216	Dietary supplement: Extra Virgin Olive Oil (EVOO)	Effect of Extra Virgin Olive Oil on Postprandial Blood Glucose in Type 2 Diabetes Mellitus Patients
Post-operatory oral surgery	IV	Active, not recruiting	NCT04373421	Mouthwash	Effect of St. John's Wort and Olive Oils on the Postoperative Complications
Cardiovascular disease and metabolic syndrome	NA	Completed	NCT03054779	Dietary supplement: Regular canola oil or high oleic acid canola oil	Canola Oil Multi-center Intervention Trial II (COMIT II): Effects of Oleic Acid Enriched and Regular Canola Oil on Body Composition and Lipid Metabolism in Participants With Metabolic Syndrome Risk Factors
Cardiovascular disease and metabolic syndrome	NA	Completed	NCT02029833	Dietary supplement: Regular canola oil or high oleic acid canola oil	Canola Oil Multi-Centre Intervention Trial II (COMIT2): Effects of Oleic Acid Enriched and Regular Canola Oil on Body Composition and Lipid Metabolism in Participants With Metabolic Syndrome
Cardiovascular disease	NA	Completed	NCT02145936	Diet enriched in oleic acid	Effect of Dietary Fatty Acids on Cardiovascular Disease Risk Indicators and Inflammation
Metabolic syndrome	NA	Completed	NCT02061267	Dietary supplement: combined with Vitamin B3	Olive Oil and Nampt on Postprandial Inflammation and Atherosclerosis in the Setting of Metabolic Syndrome (OLNAMS)
Insulin resistance	NA	Completed	NCT01541592	Dietary fat via nasoduodenal tube	Does Class of Dietary Fat Affect Insulin Resistance?

Obesity	NA	Completed	NCT01612234	Dietary supplement: high oleate diet	Saturated Fat Versus Monounsaturated Fat and Insulin Action
Obesity	NA	Completed	NCT01066091	Dietary supplement: combined with mashed potatoes	Postprandial Inflammatory Response in Healthy Men: Effect of Dietary Fat Source, Obesity and Age
Cardiovascular disease	NA	Completed	NCT01233778	Dietary supplement: high oleic acid canola oil alone or combined with DHA canola oil	Canola Oil Multicentre Intervention Trial (COMIT): Canola and Flax Oils in Modulation of Vascular Function and Biomarkers of Cardiovascular Disease Risk
Metabolic syndrome	NA	Completed	NCT01351012	Dietary supplement: high oleic acid canola oil alone or combined with DHA canola oil	Canola Oil Multicentre Intervention Trial (COMIT): Canola and Flax Oils in Modulation of Vascular Function and Biomarkers of Cardiovascular Disease Risk
Inflammation and metabolism	NA	Completed	NCT00715312	Diet with Novel Olein	Effect of Oleic Acid on Inflammation Markers and Blood Lipid Metabolites
Cardiovascular disease	II	Completed	NCT00927199	Dietary supplement: high-oleic canola oil alone or combined with flaxseed oil blend	Efficacy of High-oleic Canola and Flaxseed Oils for Hypercholesterolemia and Cardiovascular Disease Risk Factors
Obesity	NA	Completed	NCT00059254	Dietary supplement: Oleic acid	Differential Metabolism of Dietary Fatty Acids
Nutritional intervention	NA	Completed	NCT01042340	Calogen® - an energy dense oleic acid-based formula	Energy Dense Oleic Acid Rich Formula to Newly Admitted Geriatric Patients
Lipid profile	NA	Completed	NCT01124487	Dietary Supplement: The acute effects of dietary fat on lipid profile, insulin sensitivity and inflammatory markers	The Acute Effects of Oleic Acid Enriched-diets on Lipids, Insulin Sensitivity and Serum Inflammatory Markers

Table 2. List of clinical trials involving oleate. Major oleate clinical trials in the last two decades.

3.4 Type-dependent biological effects of fatty acids

Given the previously discussed different roles played by FAs on health and the consideration that distinct FAs influence the composition of cellular membranes, multiple studies focused attention on the impact of distinct classes of FAs in model organisms or at the cellular level to provide mechanistic insights, both employing panels of FAs or using oleate, elaidate or palmitate as representants of *cis*-unsaturated, *trans*-unsaturated and saturated FAs, respectively. A more complete list of relevant fatty acids belonging to the class of saturated, *trans*-unsaturated only, *cis/trans* unsaturated and *cis*-unsaturated only is reported in **Table 3**, where the main characteristics of the molecules are indicated such as the raw formula, the localization(s) of unsaturation(s) in the carbon backbone, the resulting molecular configuration, the semi-structural formula as well as the LC3 lipidation effect extracted from (Sauvat et al, 2018).

Class	Acid name	Formula	Position of =	Configuration of =	LC3 lipidation	SSF
Saturated FA	Palmitic	C16H32O2	/	/	Yes	
	Stearic	C18H36O2	/	/	Yes	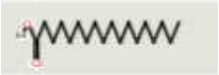
Trans-unsaturated FA	Elaidic	C18H34O2	9	Trans	No	
	Linoelaidic	C18H32O2	9,12	Trans, Trans	No	
	Palmitelaidic	C16H30O2	9	Trans	No	
	Trans-vaccenic	C18H34O2	11	Trans	No	
Trans/cis-unsaturated FA	α-calendic	C18H30O2	8,10,12	Trans, Trans, Cis	Yes	
	Rumenic	C18H32O2	9,11	Cis, Trans	Yes	
Cis-unsaturated FA	α-linolenic	C18H30O2	9,12,15	Cis, Cis, Cis	Yes	
	Arachidonic	C20H32O2	5,8,11,14	Cis, Cis, Cis, Cis	No	
	Eicosenoic	C20H38O2	11	Cis	No	
	Erucic	C22H42O2	9	Cis	No	
	γ-linolenic	C18H30O2	6,9,12	Cis, Cis, Cis, Cis	Yes	
	Linoleic	C18H32O2	9,12	Cis, Cis	No	
	Myristoleic	C14H26O2	9	Cis	Yes	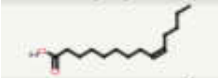
	Nervonic	C24H46O2	15	Cis	No	
	Oleic	C18H34O2	9	Cis	Yes	
	Palmitoleic	C16H30O2	9	Cis	Yes	
	Stearidonic	C18H28O2	6,9,12,15	Cis, Cis, Cis, Cis	Yes	
	Vaccenic	C18H34O2	11	Cis	Yes	

Table 3. Molecular properties of relevant FAs. FAs are divided in four groups depending on their main molecular characteristics: saturated FAs, *trans*-unsaturated FAs, *trans*/*cis*-unsaturated FAs and *cis*-unsaturated FAs. For each FA the raw formula (Formula), the unsaturation position (Position of =), the position(s) of the unsaturation(s) in the carbon backbone (Configuration of =), LC3 lipidation effect extracted from (Sauvat et al, 2018) and the semi-structural formula (SSF) is reported. Abbreviation: FA, fatty acid.

There are documented evidences of type-dependent biological effects, even if not always concordant, exerted by FAs on fundamental cellular processes and significant examples that constitute the basis of the research study are cited hereafter, mostly related to the aging process, cell stress pathways and autophagy. This differential impact is shown to be dictated by physicochemical molecular differences, such as the length of the carbon backbone or the saturation status (Sauvat et al, 2018). Nevertheless, despite the fact that *trans*-unsaturated FAs and saturated FAs are claimed to act similarly, to what extent they exert the same effect at the cellular level and share the same mechanism of action remains unclear.

The substantial spatial change of *trans*-unsaturated FAs molecules is the main reason for their capacity to distort cellular membranes. Indeed, membrane fluidity is a function of its FA content, and disorders in membrane phospholipids has a wide implication for the body systems and functions, as this determines the extent of signaling transport and transmission through the membrane (Ginter & Simko, 2016). In this context, a recent study on β–cells exposed to FAs showed changes in their membrane physicochemical properties decreasing membrane tension and thus increasing membrane fluidity, with stronger effects exhibited by oleate as compared to palmitate (Oberhauser et al, 2020).

FAs were shown by our team to have differential effects on the aging process. In mice, the metabolomic profile of the liver, heart and skeletal muscle revealed an oleate-selective increase of anti-aging related metabolites such as nicotinamide adenine dinucleotide and polyamines (Enot et al, 2015). Along similar lines, oleate, but not palmitate, was shown to increase the lifespan of different model organisms such as *Saccharomyces cerevisiae* and *Drosophila melanogaster* (Sauvat et al, 2018).

Differential impacts were also shown on the Golgi apparatus and the ER. Only *cis*- and *cis-trans*-unsaturated FAs have been shown to be highly efficient to perturbate Golgi morphology in U2OS cells (Sauvat et al, 2018). On the contrary, the accumulation of saturated FA in β–cells has been associated with significant impact on the ER function and morphology, resulting in the induction of the ER stress responses and in a swelling of the ER appearing as clefts that expand throughout the cytosol (Pineau et al, 2009). In this setting, oleate was shown to fail in inducing detectable signs of ER stress, while there is an overwhelming consensus that palmitate promotes this type of cellular response (Biden et al,

2014; Karaskov et al, 2006; Laybutt et al, 2007). More specifically, FAs impact on pancreatic β-cells was deepened due to their possible impairment on pancreatic functions, such as the compensation for insulin resistance, whose failure is documented in type 2 diabetes. Indeed, FAs deprivation causes a loss of insulin secretion, a process rapidly reversible by replacement with FAs while elevated FA supply augments the secretion. However, if chronically in excess, saturated FA can reduce insulin secretion (Prentki et al, 2002) and lead to cell apoptosis, while unsaturated FAs were foreseen as harmless or even protective to β-cells, not only protecting palmitate-treated cells from apoptosis by suppressing ER stress (Sommerweiss et al, 2013), but also improving insulin secretion (Sanjuan et al, 2007). The same was shown to hold also in stem cells, mesenchymal pre-adipocytes and exocrine pancreatic acinar cells, where palmitate increased the level of ER stress exerting a deleterious effect, poly-unsaturated FAs caused milder elevation of ER stress markers, while oleate attenuated the ER stress response (Danino et al, 2015). More recently, the combination of oleate and palmitate resulted in a significant reduction in palmitate-mediated toxicity to pancreatic acinar cells confirming the protective effect induced by oleate (Ben-Dror & Birk, 2019). In macrophages palmitate was shown to potently active the UPR and inflammatory gene expression, while elaidate and oleate were shown to have the opposite effect (Oteng et al, 2017), consistently with the evidence that saturated and *cis*-unsaturated FAs are pro- and anti-lipotoxic, respectively (L'Homme et al, 2013).

In U2OS cells, saturated, *cis*- and *cis*-*trans*-unsaturated FAs were shown to induce signs of ER stress, eliciting the activation of the two ER-stress linked transcription factors ATF4 and XBP1, while *trans*-unsaturated FAs failed to do so (Sauvat et al, 2018).

Last but not least, there is an increasing interest in autophagy regulation by FAs, as they are shown to differently modulate the autophagy machinery (Bankaitis, 2015; Niso-Santano et al, 2015a), and this point will be discussed in more details in **Paragraph 3.4.1**. Interestingly, systematic screens performed by our team showed that saturated and *cis*-unsaturated FAs do induce signs of autophagy, although via a canonical and a non-canonical pathway, respectively (Niso-Santano et al, 2015b; Sauvat et al, 2018), while *trans*-unsaturated FAs globally fail inducing autophagy and rather inhibit the conventional pathway induced by saturated FAs. Recent studies have shown that autophagy is essential for proper β-cells

function and survival, however, there is little consensus about the impact of FAs on autophagy in β-cells, as for example some reports suggest that palmitate induces autophagy, whereas others suggest that it impairs the autophagic flux to induce cell death (Assali et al, 2019; Las et al, 2011; Varshney et al, 2017) and similarly conflicting results are shown in hepatic tissue (Mei et al, 2011; Tu et al, 2014).

In the neuronal context, studies analyzed the FA-modulated autophagy in hypothalamic neurons and showed a differential regulation. Palmitate, but not oleate, nor palmitoleate, a shorter version of oleate, or arachidonate, a poly-cis-unsaturated FA, increased autophagy in hypothalamic neuronal cells (Park et al, 2019; Reginato et al, 2020).

These discrepancies underscore the complexity of lipid effects on cultured cells, potentially explained by variations in experimental conditions. Indeed, the final concentration of the FA, its solvent, the duration of the exposure and employed cultured cells can be interesting parameters to be taken into account when comparing different studies.

3.4.1 Oleate and autophagy: an intricate relationship

The relationship between oleate and autophagy is unusual and curious. Oleate was shown to induce signs of autophagy in different cell types while not having effects in others, underlying the controversial complexity of its effects and suggesting a tissue-dependent response to the FA. Major studies of the past decade on this subject are reported in **Table 4**, where oleate-modulatory effects on autophagy are documented providing details on study parameters and techniques. Results obtained in parallel by employing additional FAs are presented to compare effects of different FAs on the autophagic machinery in the same experimental model.

FA	LC3 lipidation	Technique	Results	Model	Ref
Oleate	Yes	IF	↑GFP-LC3 puncta, ↑siULK1, ↑siBECN1, ↑PIK3C3, ↑+3MA, ↑+Wort, no effect in siATG5, siATG7 ↑↑+E-64d+pepstatin No effect on FYVE dots	Human osteosarcoma U2OS	(Niso-Santano et al, 2015b)
		WB	↑LC3 lipidation, no effect in siATG5/siATG7 ↑↑+E-64d+pepstatin		
		Radiolabelling	↑Degradation of long-lived proteins, ↓+E-64d+pepstatin		
		TEM	↓distance GFP-LC3/p62, ↑LC3+ Golgi structures		
		WB	In heart, liver, muscle ↑LC3-II, ↓p-62, ↑p-AMPK In Becn1+/- liver and kidney ↑LC3-II, and ↑↑+leupeptin, ↓p-62	C57BL6 mice	
		IF	In WT and ∆atg6 ↑BODIPY+ lipid droplet	*Saccharomyces cerevisiae*	
		IF	In WT and BEC-1 ↑LGG-1+ puncta	*Caenorhabditis elegans*	
Palmitate	Yes	IF	↑GFP-LC3 puncta, no effect in siATG5, siATG7, siULK1, siBECN1, siPIK3C3, +3MA, +Wort ↑↑+E-64d+pepstatin ↑FYVE dots	Human osteosarcoma U2OS	
		WB	↑LC3 lipidation, no effect in siATG5/siATG7 ↑↑+E-64d+pepstatin		
		Radiolabelling	↑Degradation of long-lived proteins, ↓+E-64d+pepstatin		
		TEM	↓distance GFP-LC3/p62, ↑LC3+ fractures		
		WB	In heart, liver, muscle ↑LC3 lipidation, ↓p-62, ↑p-AMPK In Becn1+/- liver and kidney no effect	C57BL6 mice	
		IF	In WT ↑BODIPY+ lipid droplet, no effect in ∆atg6	*Saccharomyces cerevisiae*	
		IF	In WT ↑LGG-1+ puncta, no effect in BEC-1+/-	*Caenorhabditis elegans*	

Oleate	Yes	IF	↑GFP-LC3 puncta, no effect in ATG5 KO No effect on FYVE dots	Human osteosarcoma U2OS	(Sauvat et al, 2018)
		WB	↑LC3 lipidation, ↑↑+CQ		
Palmitate	Yes	IF	↑GFP-LC3 puncta, no effect in ATG5 KO, ↑FYVE dots		
		WB	↑LC3 lipidation, ↑↑+CQ		
Elaidate	No	IF	No effect on GFP-LC3, no effect in ATG5 KO ↑FYVE dots		
		WB	No effect on LC3 lipidation, ↑+CQ		
Palmitoleate	Yes	IF	↑GFP-LC3 puncta		
Oleate	Yes	IF	↑GFP-LC3 puncta, ↑↑+CQ ↓+3MA, ↓+NAC	HepG2 Primary mouse hepatocytes	(Mei et al, 2011)
		WB	↑LC3 lipidation, ↑↑+BAF, ↑↑+CQ No effect on 4EBP1 or p70S6K		
		TEM	↑Double membranes AP, ↑LD		
Palmitate	No	IF	No effect on GFP-LC3, ↑+CQ		
		WB	No effect on LC3 lipidation, ↑+CQ, ↑+BAF, ↓4EBP1		
		TEM	No effect on AP, slight ↑ LD		
Palmitoleate	Yes	IF	↑GFP-LC3 puncta		
		WB	↑LC3 lipidation		
Oleate	No	WB	No effect on LC3 lipidation	Human hepatoma SMCC-7721 and HepG2	(Tu et al, 2014)
		IF	No effect on GFP-LC3		
Palmitate	Yes	WB	↑LC3 lipidation, ↓p-62, no effect in +3MA, +NAC, +SP600125, siATG5, siBECN1		
		IF	↑ GFP-LC3 puncta, no effect +SP600125		
		TEM	↑ Autophagic vacuoles		

Oleate	Yes	WB	↑↑LC3 lipidation, ↑↑↑+CQ No effect on AMPK, no effect +Compound C No effect on mTOR or 4EBP No effect +NAC	MIN6 Mouse islets	(Chu et al, 2019)
		IF	↑↑ RFP in mRFP-GFP-LC3		
Palmitate	Yes	WB	↑LC3 lipidation, ↑↑+CQ		
		IF	↑ RFP in mRFP-GFP-LC3		
Palmitate	No	WB	↑LC3 lipidation	Pacreatic BRIN-BD11 and INS-1E cells Human islets	(Dhayal et al, 2019)
		IF	↑ yellow in mRFP-GFP-LC3		
Palmitoleate	No	WB	No LC3 lipidation		
		IF	No effect on mRFP-GFP-LC3		
Oleate	Yes	TEM	↑Autolysosomes	Tongue squamous cells carcinoma CAL27 and UM1	(Jiang et al, 2017)
		WB	↑LC3 lipidation, ↓p-62, ↑p-Akt, ↑mTOR		
Oleate	No	WB	No effect on LC3 lipidation, no effect +E-64d+pepstatin	Hypothalamic N41 cells	(Park et al, 2019)
Palmitate	Yes	WB	↑LC3 lipidation, ↑↑+E-64d+pepstatin		
Arachidonate	No	WB	No effect on LC3 lipidation, no effect +E-64d+pepstatin		

Table 4. Major studies on oleate-induced autophagy. Major oleate-related researches in the autophagy context of the last decade are listed. Abbreviations: IF, immunofluorescence; WB, western blot; TEM, transmission electron microscopy; Wort, wortmannin; 3MA, 3-methyladenine; KO, knock out; CQ, chloroquine; NAC, N-acetylcysteine; BAF, bafilomycin A1; AP, autophagosome; LD, lipid droplet.

Autophagy has been extensively studied in human osteosarcoma U2OS cells, where LC3 lipidation and p62 degradation induced by oleate was exacerbated by the addition of E-64 and pepstatin, two inhibitors of lysosomal proteases, and where it accelerated the degradation of long-lived proteins (Niso-Santano et al, 2015b), hallmarks of a functional autophagy. A screen conducted by our team on a panel of FAs in osteosarcoma U2OS cells revealed that both saturated and unsaturated FAs induce autophagy although by activating different molecular mechanisms: saturated FAs with 15-18 carbons such as palmitate trigger autophagy via the canonical pathway while unsaturated FAs such as oleate induce the redistribution of LC3 to Golgi-associated vesicles through a non-canonical pathway. Indeed, even if on one side its autophagy-stimulatory activity was shown to be dependent on the ATG12-ATG5 and ATG7-dependent conjugation system, it turned out to be independent on BECN1 and PIK3C3 (Niso-Santano et al, 2015b). BECN1-independency was shown also in *Saccharomyces cerevisiae* lacking atg6 (yeast ortholog of mammalian BECN1) as well as in the nematodes lacking BEC-1 (*Caenorhabditis elegans* ortholog of mammalian BECN1). Along similar lines, administration of oleate was shown not only to induce a rapid autophagic response in the heart, liver and skeletal muscle of wild-type (WT) C57BL/6 mice, but LC3 lipidation was induced also in livers of $Becn1^{+/-}$ mice (Niso-Santano et al, 2015b). Based on these findings, oleate is known to induce a "non-canonical" type of autophagy that requires further investigation.

In HepG2 cells and primary mouse hepatocytes, oleate but not palmitate was shown to induce autophagy (Mei et al, 2011), even though the oleate-induced response in hepatocytes remains controversial, as studies reported that only the presence of palmitate induces an autophagic response (Ning et al, 2019; Tu et al, 2014).

In pancreatic β-cells MIN6 and mouse islets as well as in aortic vascular smooth muscle VSMC cells, oleate was shown to be a more effective autophagy activator than palmitate (Cheng et al, 2017; Chu et al, 2019) and it exerts a pro-autophagic effect also in tongue squamous cell carcinomas (CAL27 and UM1 cells) (Jiang et al, 2017) and in retinal pigment epithelial ARPE-19 cells (Chang et al, 2020).

In hypothalamic neurons, palmitate was shown to induce an autophagic response (Park et al, 2019; Reginato et al, 2020) while oleate and arachidonate showed no effects.

The link between autophagy, that has recently been recognized as a major mechanism to counteract cardiovascular aging and diminishing arteriosclerosis (Ho et al, 2017; Torisu et al, 2016), and FAs, particularly when dealing with non-canonical autophagy elicited by oleate remains intriguing and needs to be further explored.

Aim of the work

The rationale beyond this study is the well-established differential impact of FAs on human health: *trans*-unsaturated FAs contained in industrially processed hydrogenated oils are known to have negative effects and to cause (a certain degree of) toxicity, while *cis*-unsaturated FAs present in specific plant oils such as olive oil, show health-promoting effects at multiple levels. The physicochemical properties of different classes of FAs, notably saturated versus *cis*- or *trans*-unsaturated hydrocarbon chains, have been shown to induce rather divergent and intriguing effects also at the cellular level, particularly when considering the activation of autophagy-related circuitries. Autophagy has recently been recognized as a major mechanism to counteract cardiovascular aging and to diminish arteriosclerosis and FAs have been shown to regulate autophagy in rather diverse manners. This link still remains elusive and mechanisms underlying the differential effects need further elucidation.

The present work focuses on oleate, the most abundant *cis*-unsaturated FA in our diet and organism, which has been shown to induce unconventional cellular stress possibly related to its beneficial effects on health. The aim is to obtain mechanistic insights into the complex network of oleate-induced cellular effects with a special focus on the aggregation of LC3 at sites of the morphologically altered Golgi apparatus. Given the peculiar phenotype of perinuclear LC3 aggregation, the presented work aimed to develop robust analysis workflows for the time-resolved study of LC3 distribution and dynamics. Furthermore, a genome-wide screen on human cells aimed at exploring the genetic basis of autophagy elicited both by oleate and palmitate, as representatives of the *cis*-unsaturated and saturated class of FAs, respectively. The identification of genes specifically involved in the oleate-induced effects allowed to study oleate specific cellular pathways, and to mechanistically characterize oleate-induced effects *in vitro* and *in vivo*.

To further explore the possibility that other chemical entities exert similar cellular effects, a screen on a chemical library mostly composed of FDA-approved drugs aimed at discovering "oleate mimetics", while investigations on molecular descriptors of a panel of FA by using a machine learning algorithm is meant to provide a deeper characterization of the molecular properties responsible for the oleate-like cellular effects.

1. Oleate-induced aggregation of LC3 at the trans-Golgi network is linked to a protein trafficking blockade

Oleate, the most abundant endogenous and dietary cis-unsaturated fatty acid, has the atypical property to cause the redistribution of microtubule-associated proteins 1A/1B light chain 3B (referred to as LC3) to the trans-Golgi network (TGN), as shown here. A genome-wide screen identified multiple, mostly Golgi transport-related genes specifically involved in the oleate-induced relocation of LC3 to the Golgi apparatus. Follow-up analyses revealed that oleate also caused the retention of secreted proteins in the TGN, as determined in two assays in which the secretion of proteins was synchronized, (i) an assay involving a thermosensitive vesicular stomatitis virus G (VSVG) protein that is retained in the endoplasmic reticulum (ER) until the temperature is lowered, and (ii) an isothermic assay involving the reversible retention of the protein of interest in the ER lumen and that was used both in vitro and in vivo. A pharmacological screen searching for agents that induce LC3 aggregation at the Golgi apparatus led to the identification of "oleate mimetics" that share the capacity to block conventional protein secretion. In conclusion, oleate represents a class of molecules that act on the Golgi apparatus to cause the recruitment of LC3 and to stall protein secretion.

Cell Death Differ. 2020 Dec 17. doi: 10.1038/s41418-020-00699-3. Online ahead of print.
PMID: 33335289

Cell Death & Differentiation
https://doi.org/10.1038/s41418-020-00699-3

Cell Death & Differentiation

ARTICLE

Oleate-induced aggregation of LC3 at the trans-Golgi network is linked to a protein trafficking blockade

Giulia Cerrato[1,2,3] · Marion Leduc[1,2] · Kevin Müller[1,2] · Peng Liu[1,2] · Liwei Zhao[1,2] · Juliette Humeau[1,2] · Wei Xie[1,2,3] · Shuai Zhang[1,2,3] · Oliver Kepp[1,2] · Allan Sauvat[1,2] · Guido Kroemer[1,2,4,5,6]

Received: 28 May 2020 / Revised: 20 November 2020 / Accepted: 25 November 2020

Abstract

Oleate, the most abundant endogenous and dietary *cis*-unsaturated fatty acid, has the atypical property to cause the redistribution of microtubule-associated proteins 1A/1B light chain 3B (referred to as LC3) to the trans-Golgi network (TGN), as shown here. A genome-wide screen identified multiple, mostly Golgi transport-related genes specifically involved in the oleate-induced relocation of LC3 to the Golgi apparatus. Follow-up analyses revealed that oleate also caused the retention of secreted proteins in the TGN, as determined in two assays in which the secretion of proteins was synchronized, (i) an assay involving a thermosensitive vesicular stomatitis virus G (VSVG) protein that is retained in the endoplasmic reticulum (ER) until the temperature is lowered, and (ii) an isothermic assay involving the reversible retention of the protein of interest in the ER lumen and that was used both in vitro and in vivo. A pharmacological screen searching for agents that induce LC3 aggregation at the Golgi apparatus led to the identification of "oleate mimetics" that share the capacity to block conventional protein secretion. In conclusion, oleate represents a class of molecules that act on the Golgi apparatus to cause the recruitment of LC3 and to stall protein secretion.

These authors contributed equally: Allan Sauvat, Guido Kroemer

Edited by M. Piacentini

Supplementary information The online version of this article (https://doi.org/10.1038/s41418-020-00699-3) contains supplementary material, which is available to authorized users.

✉ Oliver Kepp
captain.olsen@gmail.com

✉ Guido Kroemer
kroemer@orange.fr

[1] Equipe labellisée par la Ligue contre le cancer, Université de Paris, Sorbonne Université, INSERM UMR1138, Centre de Recherche des Cordeliers, Paris, France

[2] Metabolomics and Cell Biology Platforms, Gustave Roussy, Villejuif, France

[3] Université Paris Sud, Paris Saclay, Faculty of Medicine, Kremlin Bicêtre, France

[4] Pôle de Biologie, Hôpital Européen Georges Pompidou, AP-HP, Paris, France

[5] Suzhou Institute for Systems Medicine, Chinese Academy of Medical Sciences, Suzhou, China

[6] Department of Women's and Children's Health, Karolinska Institutet, Karolinska University Hospital, Stockholm, Sweden

Introduction

Autophagy is characterized by the redistribution of microtubule-associated proteins 1A/1B light chain 3B (hereafter referred to as LC3) from a diffuse cytosolic pattern towards the membranes of autophagosomes and autolysosomes [1–3]. This process can be monitored by measuring the lipidation of LC3 (i.e., its conjugation to phosphatidylethanolamine that increases its electrophoretic mobility in immunoblot experiments) or more conveniently by visualizing the redistribution of LC3 into cytoplasmic puncta that can be detected by immunofluorescence or by conjugation of LC3 to fluorescent proteins [4, 5]. A myriad of different endogenous and exogenous factors can stimulate or suppress autophagy, with important implications for cellular physiology and organismal health. As a general pattern, autophagy is required for maintenance of cellular homeostasis, meaning that its inhibition precipitates the manifestation of degenerative diseases, while its activation can delay the aging process [6–9].

Fatty acids have a profound effect on autophagy. Oleic acid (IUPAC name: *cis*-9-octadecenoic acid) is the most abundant mono-unsaturated fatty acid in our body, as well as in our diet [10, 11]. As other medium and long-chain

cis-unsaturated fatty acids, be they mono- or poly-unsaturated, oleate (the oleic acid anionic form) induces a non-canonical type of autophagy in which LC3 and other proteins from the LC3 family are conjugated to phosphatidylethanolamine and preferentially redistribute to the Golgi apparatus. This process is "non-canonical" in the sense that it does not require the activation of the Beclin-1 (BECN1)-phosphatidylinositol 3-kinase catalytic subunit type 3 (PIK3C3, best known as VPS34) complex [12]. In sharp contrast, saturated fatty acids, among which palmitic acid (IUPAC name: Hexadecanoic acid, the most abundant one), induce autophagy through a canonical pathway that requires both the ATG5/ATG7/ATG12 conjugation system (that conjugates LC3 to phosphatidylethanolamine) and the BECN1/PIK3C3 complex, resulting into the distribution of LC3 to cytoplasmic puncta without any preference for the Golgi apparatus [12]. Finally, *trans*-fatty acids such as elaidic acid (IUPAC name: *trans*-9-octadecenoic acid, an isomer of oleic acid) do not induce autophagy at all and rather inhibit the LC3 lipidation and redistribution induced by palmitic acid but not by oleic acid [13].

The aforementioned findings suggest that the physicochemical properties of different classes of fatty acids (saturated versus *cis*- or *trans*-unsaturated carbon chains) rather than their individual biochemical functions (e.g., in specific lipidation reactions) or their binding to specific G-protein-coupled receptor (which distinguish fatty acids of distinct lengths) [14–16] determine their effects on autophagy. Moreover, it is tempting to speculate that the well-described negative effects of *trans*-unsaturated fatty acids (contained in industrially processed hydrogenated oil) on human health are due to autophagy inhibition [16–18]. Similarly, the positive effect of *cis*-unsaturated fatty acids (contained in specific plant oils such as olive oil) [19] might be explained by the activation of autophagy-related circuitries [20].

Enticed by these perspectives, we decided to investigate the genetic basis of the oleate effect on human cells, starting with a genome-wide screen to identify the pathways that explain the specifics of autophagy induction by this mono-*cis*-unsaturated fatty acid.

Results

A genome-wide screen to explore oleate-induced LC3 puncta

Biosensor cell lines expressing a fusion protein composed by LC3 and green fluorescent protein (GFP) can be used to monitor autophagy-related processes [21]. Both oleate and palmitate induce GFP-LC3 puncta, though with different morphologies [12, 13], namely the formation of relatively few puncta, usually close to one pole of the nucleus, for oleate and a more speckled pattern in which multiple puncta distribute all over the cytoplasm for palmitate. To understand the genetic basis of the oleate-induced phenotype, we performed a robotized genome-wide small interfering (si)RNA-based phenotypic screen in which human osteosarcoma U2OS cells stably expressing GFP-LC3 were transfected with 18 120 distinct siRNAs targeting a majority of the known human mRNAs, then treated with either oleate or palmitate, and finally monitored to quantify cytoplasmic GFP-LC3 dots by automated high-content image analysis (Fig. 1a).

Most of the siRNAs had no effect on the formation of puncta in response to either oleate or palmitate, while some targeting the central autophagic protein conjugation system (*ATG5*, *ATG7*, *ATG12*) reduced GFP-LC3 dots induced by both fatty acids. Other siRNAs participating in the Beclin 1 complex (such as *ATG16L1* and *BECN1*) only interfered with palmitate, not oleate, -induced GFP-LC3 puncta, in accordance with a prior report [12]. In contrast, a small subset of semi-manually selected 85 genes appears to specifically interfere with the formation of puncta induced by oleate, but not palmitate (Fig. 1b). Among these siRNAs, two target subunits of the COPI complex (*COPB1*, *COPB2*) that is also targeted by brefeldin A, an inhibitor of ER-to-Golgi anterograde protein transport known to prevent oleate-induced relocation of GFP-LC3 to the Golgi apparatus without affecting palmitate-induced GFP-LC3 puncta [12]. Similarly, another protein involved in ER-to-Golgi transport, syntaxin-5 (STX5) [22], is required for the oleate, but not palmitate, -induced phenotype (Fig. 1a, b). Gene ontology (GO) analysis of the most prominent oleate-specific siRNAs revealed that most of the highly significant ($p < 0.001$) terms deal with Golgi-relevant transport processes (Fig. 1c), while the palmitate specific siRNAs did not relate to any significant biological process, even when including a wider set of genes.

A post-deconvolution bioinformatic STRING analysis that reconstructs documented protein-protein interactions among the oleate hits yielded a network of proteins involved in Golgi-related transport and ER stress with a central node that involves eukaryotic initiation factor 2α (EIF2A, best known as eIF2α) and several of its kinases (Fig. 1d) as part of the "integrated stress response" [23–26]. As a consequence, we decided to focus our study on these processes.

Validation of selected hits from the screen

In the next step, we retrieved all the siRNAs identified in the robotized screen as oleate-specific inhibitors of GFP-LC3 dots and tested them manually on U2OS cells co-expressing two fluorescent biosensors, namely a fusion protein composed by beta-1,4-galactosyltransferase 1 (GALT1) and

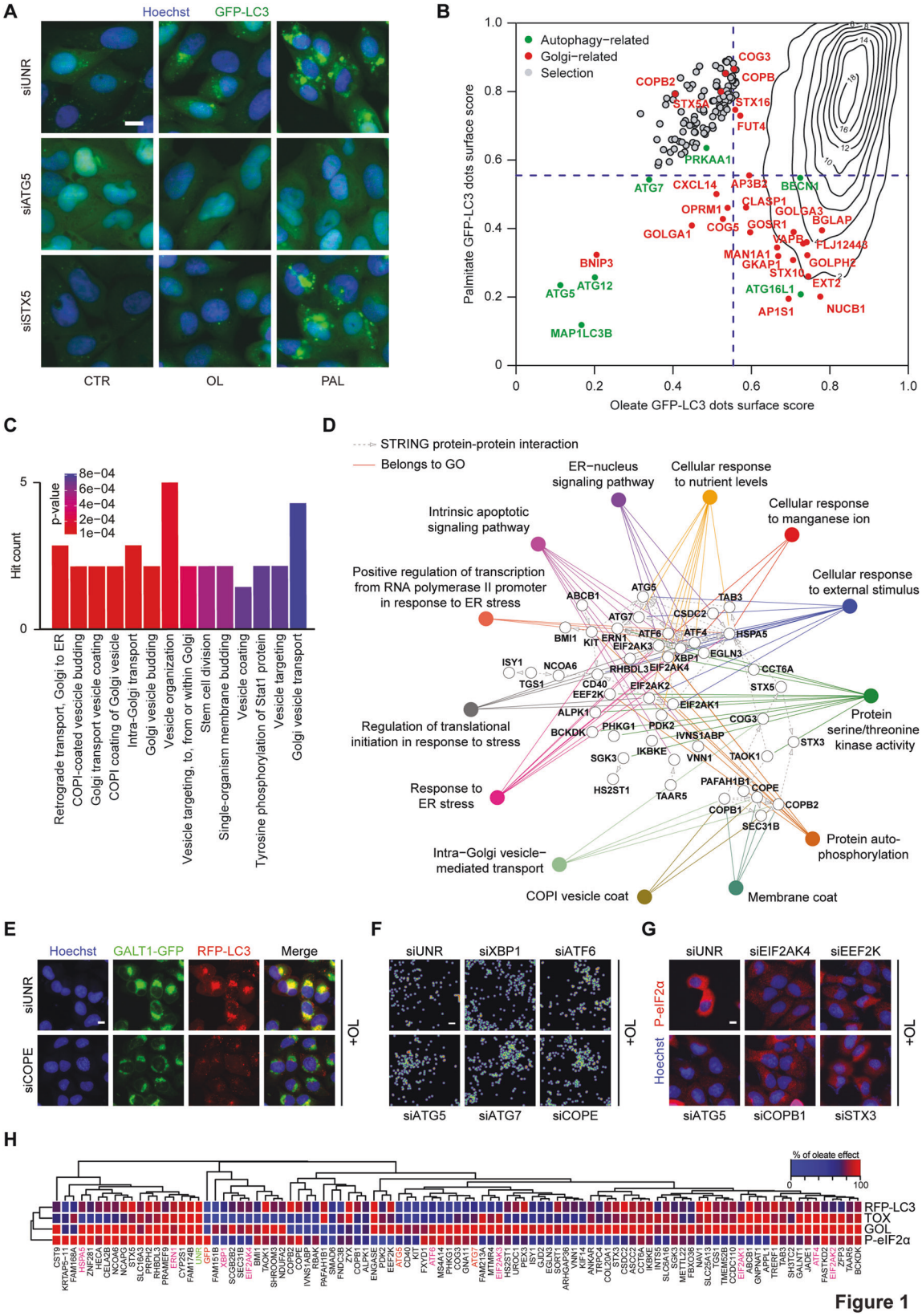
A
Hoechst
GFP-LC3
siUNR
siATG5
siSTX5
CTR
OL
PAL
B
Autophagy−related
Golgi−related
Selection
Palmitate GFP-LC3 dots surface score
Oleate GFP-LC3 dots surface score
COG3
COPB2
COPB
STX5A
STX16
FUT4
PRKAA1
ATG7
CXCL14
AP3B2
BECN1
CLASP1
OPRM1
GOLGA3
BGLAP
GOLGA1
COG5
GOSR1
VAPB
TLJ12443
MAN1A1
GKAP1
GOLPH2
STX10
EXT2
BNIP3
ATG12
ATG5
ATG16L1
AP1S1
NUCB1
MAP1LC3B
C
p-value
8e−04
6e−04
4e−04
2e−04
1e−04
Hit count
Retrograde transport, Golgi to ER
COPI-coated vesicle budding
Golgi transport vesicle coating
COPI coating of Golgi vesicle
Intra-Golgi transport
Golgi vesicle budding
Vesicle organization
Vesicle targeting, to, from or within Golgi
Stem cell division
Single-organism membrane budding
Vesicle coating
Tyrosine phosphorylation of Stat1 protein
Vesicle targeting
Golgi vesicle transport
D
STRING protein-protein interaction
Belongs to GO
ER−nucleus signaling pathway
Cellular response to nutrient levels
Intrinsic apoptotic signaling pathway
Cellular response to manganese ion
Positive regulation of transcription from RNA polymerase II promoter in response to ER stress
Cellular response to external stimulus
Regulation of translational initiation in response to stress
Protein serine/threonine kinase activity
Response to ER stress
Protein auto-phosphorylation
Intra−Golgi vesicle−mediated transport
COPI vesicle coat
Membrane coat
E
Hoechst
GALT1-GFP
RFP-LC3
Merge
siUNR
siCOPE
+OL
F
siUNR
siXBP1
siATF6
siATG5
siATG7
siCOPE
+OL
G
siUNR
siEIF2AK4
siEEF2K
P-eIF2α
Hoechst
siATG5
siCOPB1
siSTX3
+OL
H
% of oleate effect
RFP-LC3
TOX
GOL
P-eIF2α

Figure 1

◀ **Fig. 1 Identification of genes involved in oleate-induced LC3 puncta and target deconvolution. a–d** Human osteosarcoma U2OS cells stably expressing GFP-LC3 were transfected with 18 120 distinct small-interfering RNAs (siRNAs) for 24 h. After transfection, cells were left untreated or treated with either 500 µM oleate or 500 µM palmitate for 6 h, before fixation, nuclei counterstaining with Hoechst 33342 and image acquisition by fluorescence microscopy. LC3 aggregation was evaluated by assessing the formation of GFP-LC3 puncta by fluorescence microscopy. **a** Representative images of untreated cells (CTR), cells treated with oleate (OL) or palmitate (PAL) and transfected with either an unrelated siRNA (siUNR), siATG5 (used as a control of autophagy inhibition) or siSTX5 (Golgi-related gene of interest) are depicted. The scale bar equals 10 µm. **b** The average area of GFP-LC3 puncta per cell was quantified, and data were normalized between negative (cells left untreated and transfected with siUNR) and positive controls (cells treated with OL and transfected with siUNR) and scaled by calculating *Z*-scores. GFP-LC3 dots surface scores were then computed by performing a sigmoid transformation on *Z*-scores and reported in a bi-parametric plot, showing the comparison between oleate versus palmitate treatment. The gray dots represent one hundred primarily selected oleate-specific hits. Autophagy-related and Golgi-related genes are represented in green and red respectively, and all other genes are represented as isopleths in a contour map. **c** Gene ontology (GO) relevant terms (excluding shared hits between oleate and palmitate) were reported in a bar chart showing the number of hits in each category. Colors represent the *p* value for each GO term. **d** Results from STRING analysis are displayed as a network interaction map and relevant GO terms (including shared hits between oleate and palmitate) are indicated. **e–h** U2OS cells stably co-expressing GALT1-GFP and RFP-LC3 were transfected with the indicated siRNAs and then treated with 500 µM oleate (OL) for 6 h. Upon treatment, cells were fixed, their nuclei counterstained with Hoechst 33342 and the phosphorylation of eIF2α (P-eIF2α) was assessed by means of immunofluorescence staining using a phosphoneoepitope-specific antibody recognizing eIF2α phosphorylation on serine 51, via fluorescence microscopy. RFP-LC3 dot aggregation (RFP-LC3), cell loss due to toxicity (TOX), Golgi surface (GOL), and P-eIF2α were quantified. **e** Representative images of GOL and RFP-LC3 of cells transfected with siUNR and siCOPE are depicted. The scale bar equals 10 µm. **f** For TOX, maps representing the cellular density per well of cells transfected with siUNR, siXBP1, siATF6, siATG5, siATG7, siCOPE are displayed and the scale bar represents 20 µm. **g** Representative images of P-eIF2α of cells transfected with siUNR, siEIF2AK4, siEEF2K, siATG5, siCOPB1, and siSTX3 are depicted and the scale bar equals 10 µm. **h** Each parameter was normalized to the unrelated (UNR) siRNA control, so that each value falls between 0 and 100%, the last value corresponding to the original effect, and the first to the maximum possible inhibition of the phenotype. SiRNAs depicted in green and red correspond to negative and positive controls respectively, while manually added genes are marked in pink.

GFP (for assessing Golgi morphology) and another chimeric protein composed by red fluorescent protein (RFP) and LC3 (for assessing RFP-LC3 puncta) (Fig. 1e). In addition, we measured the overall density of cells as a surrogate marker of viability (Fig. 1f), as well as the phosphorylation of eIF2α (on serine 51) by immunofluorescence staining with a phospho-neoepitope-specific antibody (Fig. 1g). Oleate-induced eIF2α phosphorylation was confirmed by immunoblot (Fig. S1). Moreover, the ER chaperone calreticulin, which is induced in the context of unfolded protein response (UPR) [27], was upregulated in response to oleate (Fig. S2A, B) and these oleate-induced effects occurred in a dose-dependent fashion (Fig. S2A–H).

Since oleate was previously described as an inducer of the UPR [13], we decided to add siRNAs targeting several UPR-related genes (*ATF4*, *ATF6*, *XBP1*, *EIF2AK1 to 4*, *HSPA5*, *ERN1*) to the validation experiments. Of note, many of these siRNAs (with the notable exception of *ERN1*), modulated the oleate effect (Fig. 1h). At least half of the siRNAs were validated with respect to the inhibition of oleate-induced RFP-LC3 puncta (including 3 out of the 4 eIF2α kinases), a reduction of eIF2α phosphorylation (including *ATG5*; eIF2α kinase 4, *EIF2AK4*; eukaryotic elongation factor 2 kinase, *EEF2K*; *COPB1*; *XBP1*) and attenuated the cytotoxicity of oleate (including *ATG5*, *ATG7*, *EIF2AK4*, as well as other ER stress-relevant genes such as *ATF6* and *XBP1*; and 2 subunits of the COPI complex). A minority of the siRNAs also prevented the shrinkage of the Golgi apparatus induced by oleate (*EIF2AK4*; several COPI subunits) (Fig. 1h). These findings suggest an intimate link between the ATG5/7/12 protein conjugation system, ER stress, and COPI complex with respect to the oleate-triggered LC3 relocation to the Golgi apparatus.

To further explore this link, we used U2OS cells knockout for ATG5 confirming that oleate-induced GFP-LC3 dots entirely rely on this essential autophagy protein. Moreover, $ATG5^{-/-}$ cells showed a partial rescue from oleate cytotoxicity, a minor but significant reduction of eIF2α phosphorylation, but failure to interfere with Golgi shrinkage (which even was accentuated in the knockout cells) (Figs. 2a, b and S3A, C). A knock-in mutation by means of CRISPR/Cas9 technology on U2OS cells stably transduced with RFP-LC3 that renders eIF2α non phosphorylatable (by replacing serine 51 by an alanine residue: $eIF2\alpha^{S51A}$) [28] interfered with the induction of RFP-LC3 dots by oleate, enhanced oleate cell killing, yet again had no effects on the Golgi shrinkage (Figs. 2c, d and S3B, D). Similar results were obtained for mouse embryonic fibroblasts (MEF) subjected to a quadruple knockout ($eIF2\alpha^{4KO}$) to remove all four eIF2α kinases from the genome [29], showing that eIF2α phosphorylation is required for the formation of oleate-elicited RFP-LC3 puncta (Fig. S4A, B). These findings underscore the involvement of a complex cascade of molecular events that imply Golgi-related structural proteins, the COPI complex, and the "integrated stress response" for the oleate-induced phenotype.

Oleate stalls protein secretion at the level of the Golgi

Intrigued by the partial colocalization of oleate-induced GFP-LC3 puncta with the Golgi marker GALT1 (Fig. 1e), we sought to more precisely map their subcellular

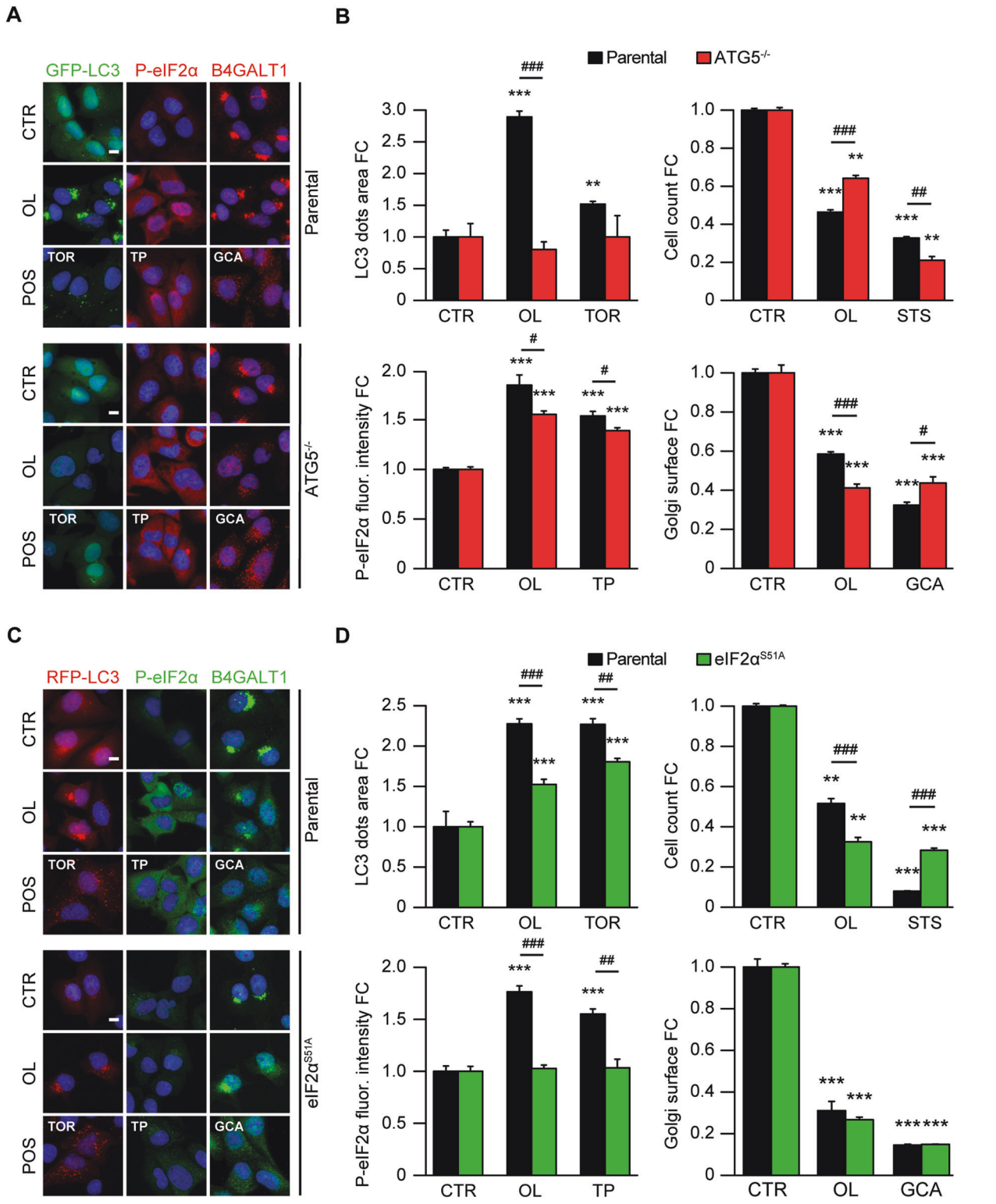

localization using a quantitative immunofluorescence staining approach at higher resolution. For this, we subjected U2OS cells stably expressing GFP-LC3 to the induction of puncta by oleate or palmitate and then stained the cells with antibodies specific for the ER protein calreticulin (CALR), ER-Golgi intermediate compartment-53 (ERGIC-53 encoded by the *LMAN1* gene), trans-Golgi network glycoprotein 46 (TGN46, official name: trans-Golgi network integral membrane protein 2, TGOLN2), 130 kDa *cis*-Golgi matrix protein (GM130, official name:

◀ **Fig. 2 Implication of ATG5 and the phosphorylation of eIF2α in oleate-induced LC3 aggregation.** Human osteosarcoma U2OS cells stably expressing GFP-LC3 that were either wild-type or knockout for ATG5 ($ATG5^{-/-}$), as well as U2OS cells expressing non phosphorylatable eIF2α ($eIF2\alpha^{S51A}$) and RFP-LC3 were left untreated (CTR) or were treated with 5 µg/mL golgicide A (GCA), 500 µM oleate (OL), 2 µM staurosporine (STS), 0.3 µM torin 1 (TOR) or 3 µM thapsigargin (TP) for 6 h. For viability studies, cells were treated for additional 6 h and further co-stained with propidium iodide and Hoechst 33342, followed by immediate live-cell acquisition. For all other conditions, cells were fixed, their nuclei counterstained with Hoechst 33342 and images were acquired by fluorescence microscopy. GFP- (or RFP-) LC3 dots area, eIF2α phosphorylation (P-eIF2α) (assessed by immunofluorescence staining with a phosphoneoepitope-specific eIF2α antibody), Golgi morphology (Golgi surface detected by immunofluorescence staining with anti-B4GALT1 antibody) and cell death (assessed by the cell count of cells with $Hoechst^{dim}$ and PI^- nuclei) were quantified. **a**, **c** Representative images of untreated cells (CTR), cells treated with OL or cells treated with the positive control for each assessed parameter (POS) (i.e., TOR for LC3 dots area, TP for P-eIF2α, GCA for Golgi disruption, and STS for cell death) are depicted for each knockout cell line ($ATG5^{-/-}$ and $eIF2\alpha^{S51A}$) together with the corresponding parental one (GFP-LC3 and RFP-LC3, respectively). Nuclei counterstained with Hoechst 33342 are represented in blue. The scale bar equals 10 µm. **b**, **d** For each assessed parameter and cell line, data were normalized to the untreated control, fold change (FC) means ±SD are reported in bar charts for one representative experiment depicting the oleate effect together with appropriate internal controls. Each condition was compared to the untreated control (*) and to the parental cell line ($^{\#}$) by means of a Welch's *t*-test ($^{\#}p < 0.05$, $^{**}/^{\#\#}p < 0.01$, $^{**}/^{\#\#\#}p < 0.001$).

Golgin subfamily A member 2, GOLGA2). Quantitative assessment of the colocalization of the fluorescent signals using a recently developed software [30] revealed that oleate (but not palmitate nor torin 1 and thapsigargin, which are "pure" activators of autophagy and ER stress, respectively) induced a selective and time-dependent colocalization of GFP-LC3 with the trans-Golgi marker TGN46, but not with the *cis*-Golgi network nor the ERGIC-53 or the ER (Figs. 3a-c and S5). This translocation of GFP-LC3 to the trans-Golgi was inhibited by brefeldin A and golgicide A (Fig. 3d–f).

Intrigued by these observations, we wondered whether oleate might interfere with protein secretion via the trans-Golgi network. To evaluate this conjecture, we took advantage of cells transiently expressing a thermosensitive mutant of vesicular stomatitis virus-G (VSVG) protein [31, 32] that is fused to yellow fluorescent protein (YFP). This protein is retained in the ER lumen at high temperature (40 °C), yet undergoes a conformational change compatible with its traffic through the secretory pathway, transiting through the Golgi apparatus towards the plasma membrane, once the temperature is lowered to a permissive level (32 °C) (Fig. 4a, b). While classical autophagy induction by means of the mechanistic target of rapamycin (mTOR) inhibitor torin 1 failed to interfere with the membrane translocation of VSVG-YFP although clearly stimulating the formation of RFP-LC3 puncta, oleate prevented VSVG-YFP to move beyond a structure that resembles the Golgi apparatus in close proximity or overlap with RFP-LC3 puncta, thus hindering it from reaching the plasma membrane (Fig. 4c–e). These time-dependent changes were quantified and subjected to statistical analysis to document the capacity of oleate to retain VSVG-YFP within the cell, to enhance the colocalization of VSVG-YFP and RFP-LC3 and to reduce the dispersion of RFP-LC3 dots (Fig. 4f–i). Hence, oleate interferes with conventional protein secretion at the level of the Golgi apparatus, likely at the level of the trans-Golgi network.

Confirmation of oleate-inhibited protein secretion with the RUSH system in vitro

To further explore the protein trafficking, we turned to yet another approach, the retention using selective hooks (RUSH) system [33], in which streptavidin was targeted to the ER surface (by fusing it to CD74 in the N-terminus), where it retains a GFP-LC3 chimera fused to streptavidin-binding domain (SBP, placed in the C-terminus), especially in the absence of free biotin (which can be quenched by the addition of avidin to the culture medium) [34]. Upon addition of a molar excess of biotin (which has a much higher affinity for streptavidin, in the range of 10^{-14} M, than SBP, outcompeting the latter), the SBP-GFP-LC3 fusion protein is released from the streptavidin "hook" and can rapidly redistribute to other locations (Fig. S6B, C). When biotin was combined with torin 1, SBP-GFP-LC3 was diffusely present in the cytoplasm, as determined by time-lapse microscopy. Conversely, when oleate was introduced into the system together with biotin, it inhibited the biotin-induced dispersion of SBP-GFP-LC3 (Fig. S6A, D), which however was efficiently released from streptavidin, as indicated by the loss of the co-staining of GFP and streptavidin (Fig. S6E, G) and colocalized with the trans-Golgi marker TGN46 (Fig. S6F, G). Interestingly, even when avidin was added to the system after oleate treatment, SBP-GFP-LC3 still colocalized with TGN46, probably showing an irreversible perturbation in the distribution of this protein by the fatty acid. These results, substantiated by quantitative image analysis, confirm that oleate deviates the intracellular voyage of GFP-LC3 towards the trans-Golgi network, even in conditions in which protein movements are synchronized by the RUSH system.

In another RUSH assay [35], streptavidin was targeted to the ER lumen (by means of the classical ER retention signal KDEL placed in the N-terminus), where it retains GFP fused to a streptavidin-binding domain (SBP, placed in the C-terminus). Upon addition of biotin, the SBP-GFP fusion protein can be secreted via the Golgi apparatus into the culture supernatant (Fig. 5a). We then determined the

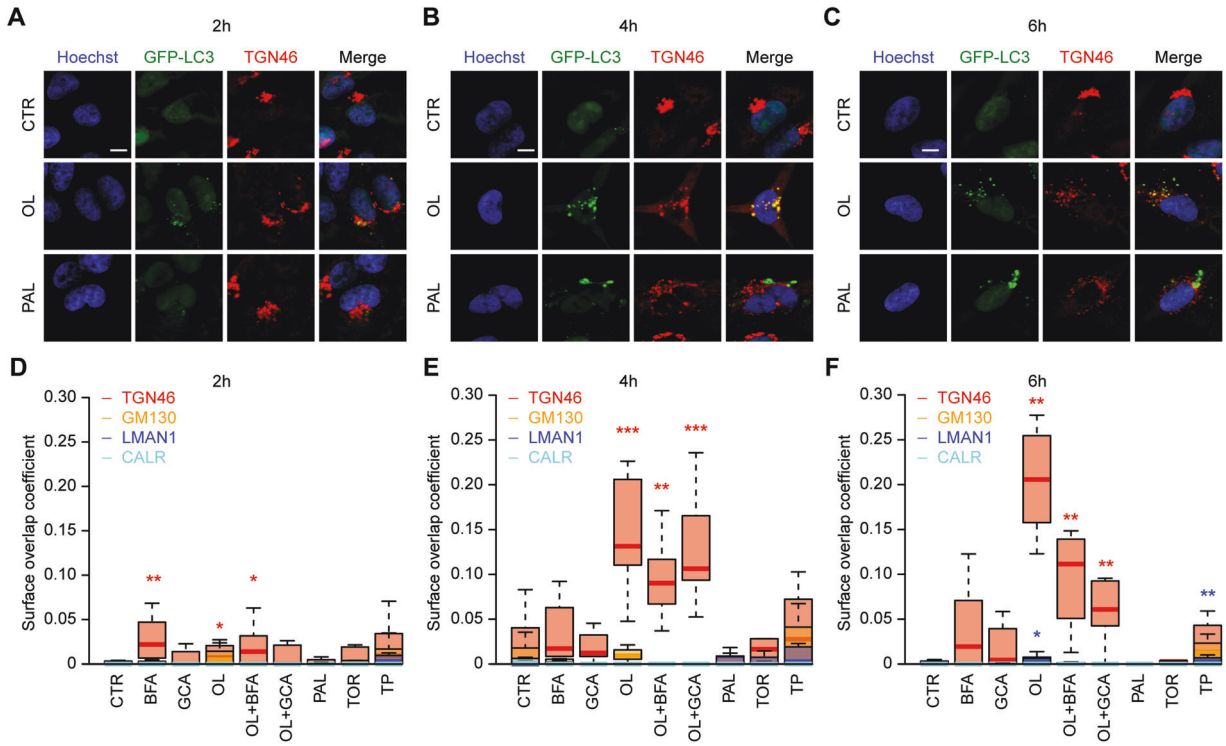

Fig. 3 Subcellular localization of LC3 after exposure to oleate. Human osteosarcoma U2OS cells stably expressing GFP-LC3 were left untreated (CTR) or treated with 5 µg/mL brefeldin A (BFA), 5 µg/mL golgicide A (GCA), 500 µM oleate (OL), 500 µM palmitate (PAL), 2 µM staurosporine (STS), 0.3 µM torin 1 (TOR), 3 µM thapsigargin (TP), or treated with a combination of OL with BFA or GCA for 2 h, 4 h or 6 h. After fixation, nuclear counterstaining with Hoechst 33342 and antibody-mediated staining of trans-Golgi network glycoprotein 46 (TGN46), 130 kDa *cis*-Golgi matrix protein (GM130), ER-Golgi intermediate compartment-53 (LMAN1) and endoplasmic reticulum calreticulin (CALR), the images at high-resolution were acquired by confocal microscopy at 60X and analyzed to determine the co-occurrence of the fluorescent signals. **a–c** For each timepoint, representative images of untreated cells (CTR), cells treated with OL or PAL and stained with anti-TGN46 antibody are depicted. The background of the images has been removed by subtracting the Gaussian blur of each channel from the original image. Scale bar = 10 µm. **d–f** For each timepoint, the average surface overlap coefficient (SOC) between GFP-LC3 puncta and the different subcellular compartment per cell was calculated from the cleaned images and data are shown as boxplots with *p* values calculated using a Mann–Whitney *U* test (*$p < 0.05$, **$p < 0.01$, ***$p < 0.001$).

effects of oleate on this protein release assay. As a positive control, brefeldin A caused full retention of SBP-GFP in the cell, in the proximity of the streptavidin hook, while the negative control torin 1 and palmitate failed to do so (Fig. 5b–f). Oleate caused a dose-dependent reduction in GFP secretion (Figs. 5b and S7A). In contrast, induction of the UPR by thapsigargin or tunicamycin failed to suppress GFP secretion in this system (Figs. 5b, c and S7A). Moreover, oleate did not affect protein synthesis (Fig. S7B, C), and inhibition of protein synthesis by cycloheximide did not interfere with the RUSH assay (Figs. 5b, c and S7B, C). Of note, instead of causing SBP-GFP to be withhold in the ER (as this would be observed with brefeldin A, Fig. 5d, e), oleate treatment led to a retention of GFP at the trans-Golgi network, as indicated by the colocalization of SBP-GFP and TGN46 (Fig. 5d, f).

In conclusion, oleate indeed blocks protein secretion at a step at which the protein of interest (here SBP-GFP) is trapped in the trans-Golgi network. Of note, the oleate-induced entrapment of SBP-GFP at the Golgi apparatus does not seem to require *ATG5* and *ATG7* (Fig. S8), meaning that LC3 translocation to the Golgi (which relies on *ATG5* and *ATG7*, see above in Fig. 1) might not be required for the blockade of protein secretion induced by oleate.

Identification of other compounds that induce an oleate-like inhibition of protein secretion

We wondered whether the oleate-induced alteration in protein trafficking is a unique feature or whether other chemical entities might exert similar cellular effects. For this, we exposed U2OS cells stably co-expressing GALT1-GFP and RFP-LC3 cells to 1 280 compounds from the Prestwick chemical library (mostly composed by FDA-approved drugs) to which we added oleate, as well as LTX-401, because we had noted in the past that this agent induces the redistribution of LC3 towards the Golgi [36]

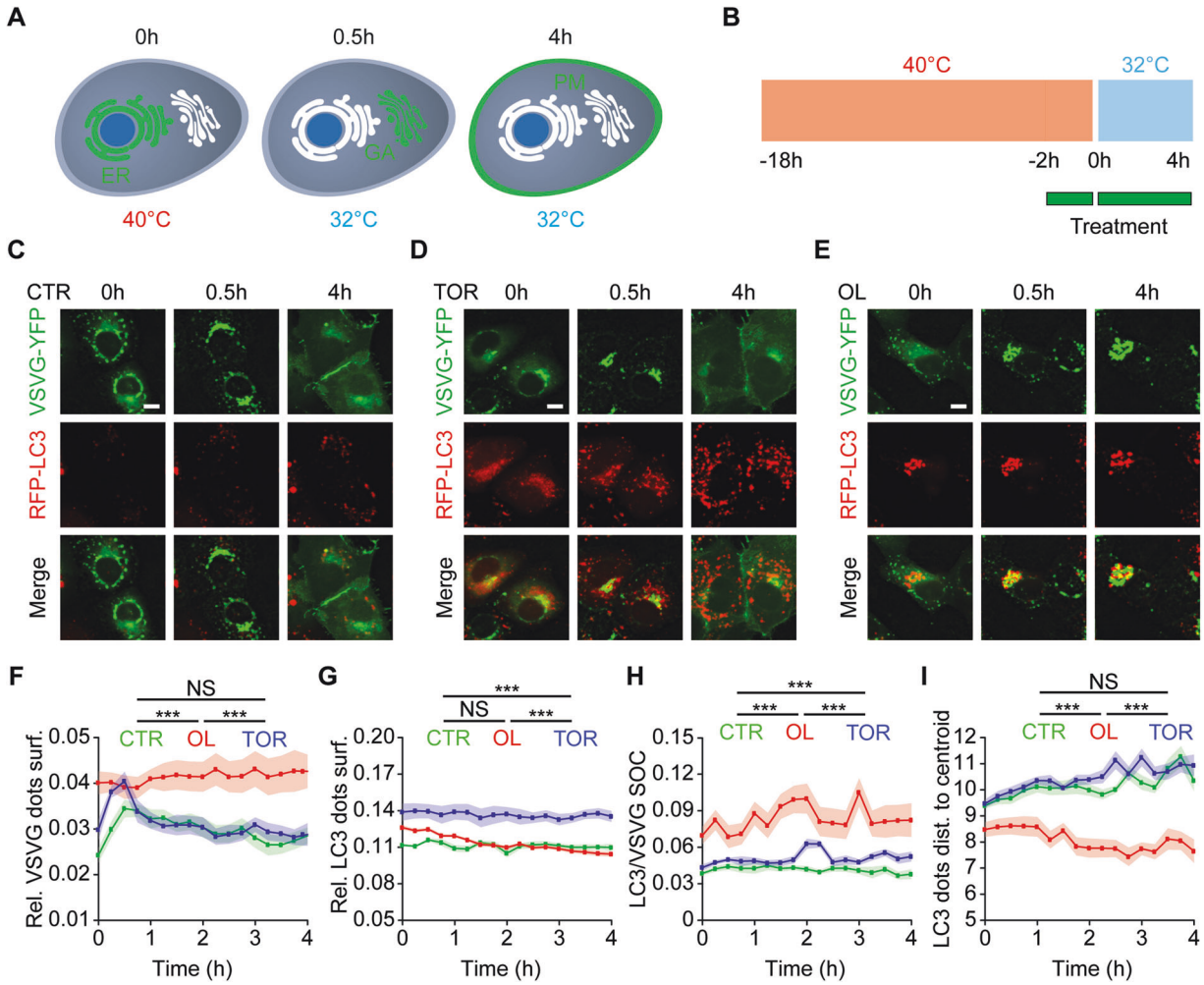

Fig. 4 Oleate blocks trans-Golgi network-to-plasma membrane protein trafficking. The oleate-induced inhibition of the trans-Golgi network (TGN)-to-plasma membrane (PM) protein trafficking was evaluated by means of a thermosensitive vesicular stomatitis virus G glycoprotein (VSVGtsO45) fused to yellow fluorescent protein (YFP) at its cytoplasmic tail (VSVG-YFP). **a** The principle of the VSVG-YFP assay is outlined. VSVG-YFP is retained in the endoplasmic reticulum (ER) at 40 °C and relocates from the ER, passing through the Golgi apparatus (GA) in ~0.5 h to the plasma membrane (PM) upon temperature reduction to 32 °C. **b** Human osteosarcoma U2OS cells stably expressing RFP-LC3 were transiently transfected with VSVG-YFP and were incubated at 40 °C for 16 h. Cells were left untreated (CTR) or treated with 0.3 µM torin 1 (TOR) or 500 µM oleate (OL) for 2 h at 40 °C, the temperature was then reduced to 32 °C followed by immediate live-cell acquisition with an image frequency acquisition of 10 min for 4 h. **c–e** Representative time-lapse images of VSVG-YFP and RFP-LC3 of untreated cells (CTR) and cells treated with TOR or OL are depicted. The scale bar corresponds to 10 µm. **f–i** Quantification of the relative VSVG-YFP dots surface, the relative RFP-LC3 surface, the surface overlap coefficient (SOC) between RFP-LC3 and VSVG-YFP, and the distance of LC3 dots to their centroid, is represented as means±SD throughout the time series for one representative experiment. The *p* value of each pairwise comparison was calculated using the Mann–Whitney *U* test (***$p < 0.001$, NS not significant).

and then measured RFP-LC3 puncta, shrinkage of the Golgi and effects on cellular viability. Hierarchical clustering yielded a series of oleate/LTX-401 "neighbors" that share similar cell biology effects, yet belong to rather different pharmacological classes including two anti-protozoal/antimalarial agents that target lysosomes (mefloquine and quinacrine), several serotonin reuptake inhibitors (paroxetine, sertraline, as well as indatraline that also acts on dopamine and norepinephrine reuptake), and the nonselective calcium channel blocker fendiline (Fig. 6a, b). Moreover, we performed a bioinformatic analysis of reported drug targets for these agents (extracted from the biochemical literature) to identify genes/proteins that interact with these "oleate mimetics", as defined above as well as in a previous work [13] (Fig. S9A). Of note, in the target database generated during the genome-wide search for modulators of the oleate-induced GFP-LC3 phenotype (see above, Fig. 1), such genes were relatively enriched as positive modulators/contributors (meaning that the siRNAs targeting them attenuated the phenotype), and

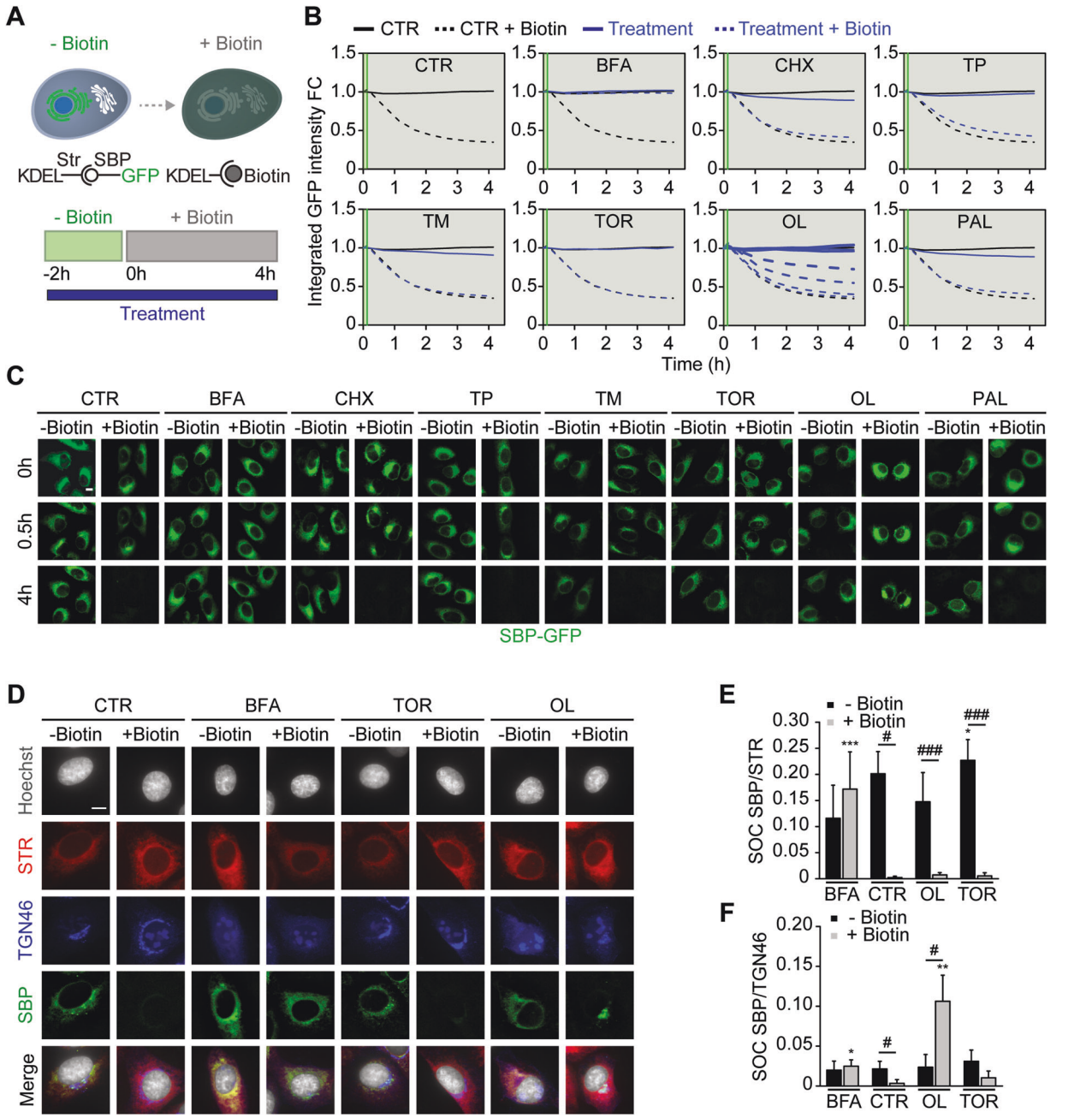

this tendency was borderline significant ($p = 0.072$, Kolmogorov–Smirnov test) (Fig. S9B, C). This suggests that the "oleate mimetics" act through a similar, at least partially overlapping, pathway to induce cytotoxicity and the GALT1-GFP/RFP-LC3 phenotype as oleate does.

Using a more direct approach, in another series of experiments, we confirmed that sertraline and fendiline acted similarly to oleate and LTX-401 to suppress protein secretion in the VSVG-YFP assay discussed above (Fig. 6c–i). Thus, pharmacological agents that induce alterations in Golgi morphology and the subcellular distribution of LC3 that resemble those induced by oleate are also inhibitors of conventional protein secretion.

Validation of inhibition of protein secretion by oleate in vitro and in vivo

To demonstrate that oleate can inhibit protein secretion in more physiological settings, we measured the release of tumor necrosis factor-α (TNF-α) from primary bone marrow-derived macrophages in response to bacterial lipopolysaccharide (LPS) in vitro (Fig. S10A). Like BFA,

◀ **Fig. 5 Oleate induces protein secretion blockade at the level of trans-Golgi network.** The retention using selective hooks (RUSH) assay was used to evaluate protein secretion from the endoplasmic reticulum (ER) in vitro. **a** The principle of the RUSH-secretion assay is schematized. Human osteosarcoma U2OS cells stably express a GFP reporter coupled to a streptavidin binding peptide (SBP) that in absence of biotin is retained by a streptavidin (Str) expressing hook targeting via KDEL to the ER. Upon biotin addition, the SBP-GFP reporter exits the ER due to the binding of biotin to streptavidin and it is secreted via exocytosis. U2OS cells stably co-expressing Str-KDEL and SBP-GFP were treated for 2 h in the absence of biotin. Biotin was added without removing the culture medium and live time-lapse images were acquired every 20 min for 4 h. **b** The integrated GFP fluorescence intensity was quantified at each time point and kinetics of protein secretion are represented as means in conditions without biotin (full line) and with biotin (dashed line) of cells left untreated (CTR), or treated with 5 µg/mL brefeldin A (BFA) as positive control for conventional secretion inhibition, 50 µM cycloheximide (CHX), 3 µM thapsigargin (TP), 3 µM tunicamycin (TM), 0.3 µM torin 1 (TOR) or 500 µM palmitate (PAL). For oleate (OL), cells were treated with a concentration range (125 µM, 250 µM, 375 µM and 500 µM) and data are displayed as lines with increasing thickness corresponding to increasing doses. **c** Representative time-lapse images of U2OS Str-KDEL-SBP-GFP untreated cells (CTR) and cells treated with BFA, CHX, TP, TM, TOR, OL, or PAL, in the presence (+) or absence (−) of biotin are displayed. The scale bar equals 10 µm. **d** Cells were fixed in the presence of Hoechst 33342 and antibody-mediated staining of trans-Golgi network glycoprotein 46 (TGN46) and streptavidin (STR) was performed. High-resolution images of untreated cells (CTR), and cells treated with BFA, TOR, and OL in presence (+) or absence (−) of biotin are depicted. The background of the images has been removed by subtracting the Gaussian blur of each channel to the original image. The scale bar indicates 10 µm. The colocalization of SBP-GFP/STR (**e**) and SBP-GFP/STR (**f**) was quantified by means of the surface overlap coefficient (SOC), and data are displayed as mean±SD for one representative experiment with p values calculated using a family-wise Welch's t-test against untreated control (fixed biotin treatment,*) or control without biotin (fixed drug, $^{\#}$) (*/$^{\#}p < 0.05$, **$p < 0.01$, ***/$^{\#\#\#}p < 0.001$).

oleate (but not palmitate, nor torin 1 or thapsigargin) inhibited the ELISA-detectable release of TNF-α into the supernatant (Fig. S10B), as it caused the retention of immunofluorescence detectable TNF-α in the cytoplasm of the macrophages (Fig. S10C, D). In addition, we tested the capacity of oleate to inhibit protein secretion in vivo, in mice. For this, we created a RUSH system in which the ER-sessile streptavidin hook retains an SBP-tagged *Gaussia* luciferase as a bate (Fig. 7a, b). Upon hydrodynamic injection of the two plasmids (the hook in threefold molar excess over the bate), this RUSH system is expressed in hepatocytes and responds to the intraperitoneal injection of biotin by a surge of luciferase in the blood plasma that can be easily quantified by means of a chemiluminescence assay (Fig. 7c, d). Pre-treatment of mice with oleate (but not palmitate) at doses that cause LC3 lipidation [12] 2 h before biotin injection induced a significant reduction in luciferase secretion in this system (Fig. 7e, f). These results demonstrate that oleate can cause a partial inhibition of protein secretion in vivo.

Discussion

Oleate, which is the most abundant endogenous and exogenous *cis*-unsaturated fatty acid, is clearly distinct from palmitate, the most abundant saturated fatty acid, with respect to its cellular effects, at multiple levels. Indeed, in contrast to palmitate, oleate activates a pathway that leads to the translocation of LC3 to, and its retention at, the trans-Golgi network. We have shown in the past that this oleate-induced process requires *ATG* genes involved in the conjugation of LC3 family proteins to phosphatidylethanolamine (such as *ATG5, ATG7,* and *ATG12*) but does not require a series of other *ATG* genes involved in phosphatidylinositol phosphorylation (such as *ATG14*, *BECN1,* and *PIK3C3/VPS34*) [12]. This led us to postulate that oleate induces a "non-canonical" pathway of autophagy. Here, we extend and refine this notion, based on a genome-wide screen for genes required for oleate to induce the redistribution of LC3 from a diffuse towards an oligo-punctiform pattern. Indeed, this screen led to the discovery that multiple genes involved in Golgi-related transport processes are specifically required for this LC3 relocation induced by oleate but not by palmitate.

Following up on this finding, we investigated the capacity of oleate to interfere with canonical (Golgi-dependent, brefeldin A-inhibitable) protein secretion, using two experimental systems in which the movement of proteins through the Golgi apparatus can be synchronized. The first (classical) system is based on a YFP-coupled thermosensitive VSVG protein that is retained in the ER until the temperature is switched to a low permissive range, while the second RUSH system is performed at isothermic conditions (excluding temperature effects on membrane fluidity) and involves the reversible (biotin-inhibitable) retention of GFP fused to SBP in the ER lumen by streptavidin. In both systems, oleate had similar effects. Oleate did not affect the rapid move of the protein of interest (VSVG-YFP or SBP-GFP) from the ER to the Golgi, yet caused its retention in the Golgi, in or at the same compartment that accumulates LC3, thus blocking protein secretion. Inhibition of protein secretion by oleate was also demonstrated in vitro, for LPS-inducible TNF-α release from macrophages, as well as in vivo, using a tailor-made RUSH system measuring the secretion of luciferase from hepatocytes. These findings suggest that oleate may influence protein secretion at physiologically relevant concentrations. Whether such levels of oleate may also be obtained by dietary ingestion of oleate-rich food items (such as olive oil) remains to be investigated.

Mechanistically, oleate acts differently from brefeldin A, which causes dispersion of the Golgi apparatus. Oleate caused partial shrinkage of the Golgi, while stimulating the retention of LC3 and secreted proteins at and within the

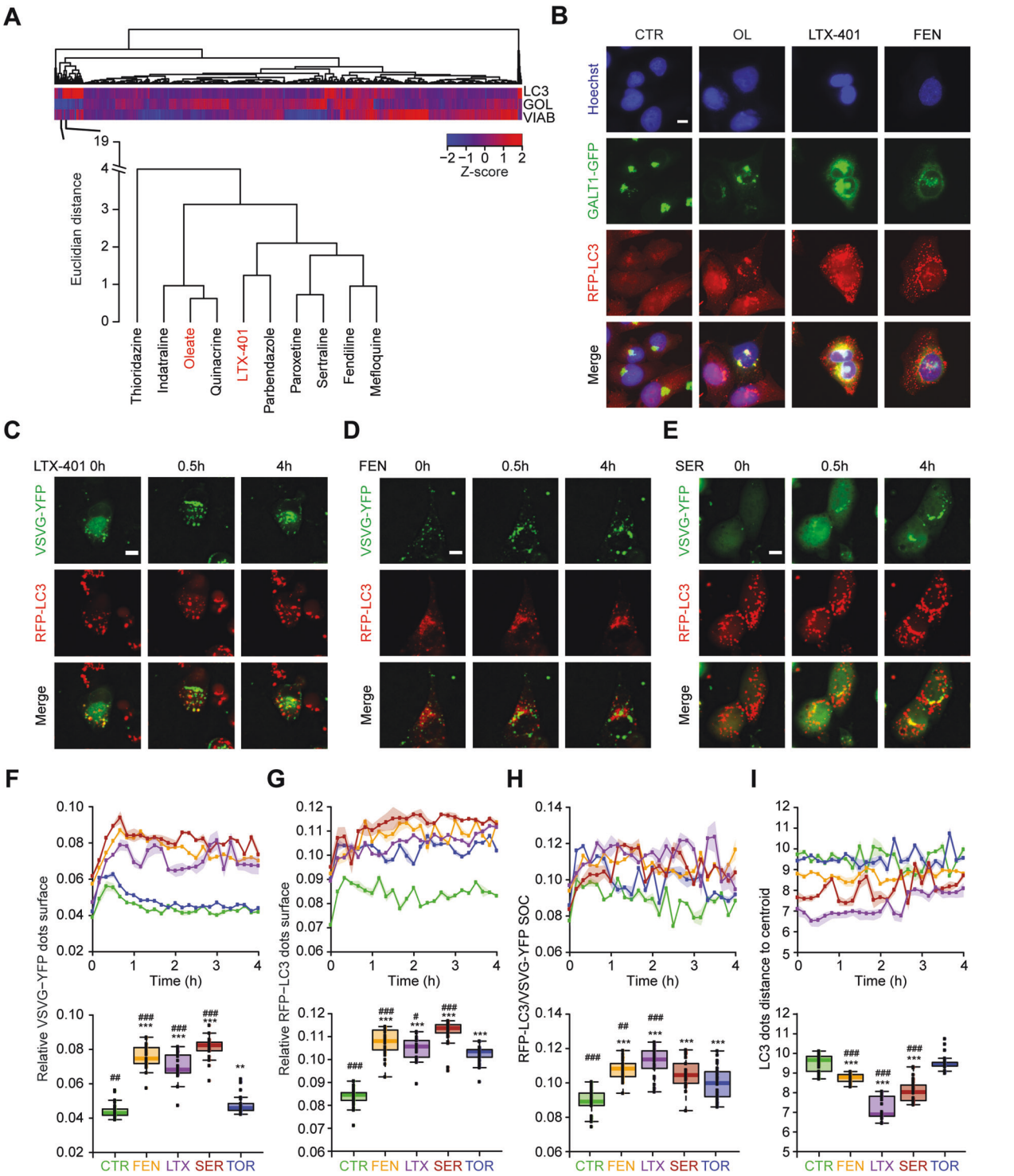

trans-Golgi compartment, respectively. Brefeldin A (or knockdown of subunits of the COPI complex, its pharmacological target) did not cause the redistribution of LC3 to puncta to the same extend as oleate but rather prevented the oleate-induced relocation of LC3 to the Golgi, supporting the contention that brefeldin A and oleate block protein secretion through rather distinct mechanisms. Of note, *ATG5* and *ATG7* were not required for the inhibition of protein secretion by oleate, supporting the idea that LC3 distribution to the Golgi (which relies on *ATG5* and *ATG7*) can be uncoupled from the effects of oleate on protein secretion. Similarly, it appears that the oleate-induced redistribution of LC3 to the Golgi requires inhibition of mTOR [12], but mTOR inhibition by torin 1 did not

◀ **Fig. 6 Identification of pharmacological oleate mimetics.** **a**, **b** Human osteosarcoma U2OS cells stably co-expressing RFP-LC3 and GALT1-GFP were left untreated (CTR), were treated with 500 µM oleate (OL), 5 µg/mL LTX-401 or were treated with the compounds from the Prestwick chemical library at 1 or 10 µM for 6 h. After fixation and nuclear counterstaining with Hoechst 33342, images were acquired by fluorescence microscopy and analyzed. **a** For RFP-LC3 dots surface (LC3), Golgi surface (GOL), and cell viability (VIAB), *Z*-scores were computed and reported in a hierarchically-ranked heatmap. Oleate neighboring is displayed as an expanded view below heatmap. **b** Representative images from the phenotypic screen of untreated cells (CTR) or cells treated with OL, LTX-401 as well as fendiline (FEN) are displayed. The scale bar represents 10 µm. **c–i** Human osteosarcoma U2OS cells stably expressing RFP-LC3 were transiently transfected with the thermosensitive vesicular stomatitis virus G glycoprotein (VSVGtsO45) fused to a fluorescent protein YFP at its cytoplasmic tail (VSVG-YFP) to evaluate the secretory pathway. Cells were left untreated (CTR) or treated with 5 µg/mL LTX-401, 10 µM FEN or 10 µM sertraline (SER), pharmacological compounds mimicking the phenotypic effect of oleate, as well as 0.3 µM torin 1 (TOR). **c–e** Representative time-lapse images of cells treated with LTX-401, FEN, and SER are depicted. The scale bar equals 10 µm. **f–i** The quantification of the relative VSVG-YFP dots surface, the relative RFP-LC3 dots surface, the surface overlap coefficient (SOC) between RFP-LC3 and VSVG-YFP and the RFP-LC3 dots distance to centroid are represented for the time series and in boxplots for each condition for one representative experiment. The *p* value of each pairwise comparison against control (CTR) (*) or torin 1 (TOR) (#) was calculated using a Mann–Whitney *U* test ($^{\#}p < 0.05$, $^{**/\#\#}p < 0.01$, $^{**/\#\#\#}p < 0.001$).

interfere with protein secretion, underscoring that both Golgi-related processes, LC3 aggregation and secreted protein retention, are separable from each other. Finally, oleate induced the phosphorylation of eIF2α (as do most autophagy inducers) [37–39] is a requirement for LC3 recruitment but not for Golgi shrinkage, again dissociating the two phenomena. At this point, it is not clear through which molecular mechanisms oleate affects the function of the trans-Golgi network. It can be speculated that oleate selectively affects the particular membrane properties of this Golgi compartment, which differs in its biochemical composition and biophysical features from other cellular endomembranes [40–42].

Of note, oleate is not unique in its capacity to induce the redistribution of LC3 to the Golgi and to simultaneously stall protein secretion at this level. Indeed, systematic screening of 1 280 pharmacological agents revealed the existence of other, chemically unrelated (though mostly lipophilic) compounds that induce the redistribution of LC3 towards the Golgi, as shown here, and that share with oleate the capacity to block protein secretion [35], stalling their transport at the trans-Golgi network. At this point, it is difficult to understand which might be the shared mode of action among these "oleate mimetics", although one common mode of action might be a perturbation of intracellular trafficking processes.

Mefloquine (an antimalarial agent) and quinacrine (an antiprotozoal and anthelmintic) share structural features, cause lysosomal alkalization [43, 44] and are both used for the treatment of systemic autoimmunity, especially in patients with cutaneous lupus erythematosus [45, 46]. It is possible, yet remains to be determined, that the inhibition of pro-inflammatory cytokine secretion by mefloquine or quinacrine in vivo [47, 48] is mediated by blocking protein secretion in the trans-Golgi compartment.

Several of the "oleate mimetics" act as reuptake inhibitors of neurotransmitters, as this applies to the antidepressants paroxetine, sertraline and indatraline [49, 50]. Such antidepressants are administered at a much lower dose (by one log) than mefloquine and quinacrine, suggesting that clinically useful concentrations will not lead to general protein secretion. However, it is possible that their accidental or intentional (suicidal) overdosing might induce such effects in vivo. Irrespective of these uncertainties, it appears that several pharmacological agents can affect cellular physiology in a similar fashion as oleate does.

In conclusion, oleate represents a class of molecules that cause the accumulation of LC3 at the Golgi apparatus as a sign of a local perturbation that culminates in the blockade of protein transport at the level of the trans-Golgi network.

Materials and methods

Cell lines

Human osteosarcoma U2OS wild-type (WT) cells were purchased from ATCC. U2OS cells stably expressing GFP-LC3, RFP-LC3, co-expressing RFP-LC3 and GALT1-GFP, co-expressing SBP-GFP and Str-KDEL, co-expressing SBP-GFP-LC3 and Str-CD74, U2OS ATG5 knockout ($ATG5^{-/-}$) expressing GFP-LC3 and U2OS bearing a mutant non phosphorylatable version of eIF2α (U2OS $eIF2\alpha^{S51A}$) and co-expressing RFP-LC3 were generated by our group in the past [28, 34–36, 38, 51, 52]. Mouse embryonic fibroblasts MEF WT and knockout (KO) for the four eIF2α kinases (MEF $eIF2\alpha^{4KO}$) were provided by Pr. Seeichi Oyadomari from Tokushima University, Tokushima, Japan. Both MEF WT RFP-LC3 and $eIF2\alpha^{4KO}$ RFP-LC3 were constructed from the aforementioned cell lines which were transduced using LentiBrite™ RFP-LC3 Lentiviral Biosensor viral particles (Merck Millipore, Burlington, MA, USA) according to the manufacturer's instructions [39].

Cell culture

Human osteosarcoma U2OS cells and mouse embryonic fibroblasts (MEF) were cultured in Dulbecco's Modified

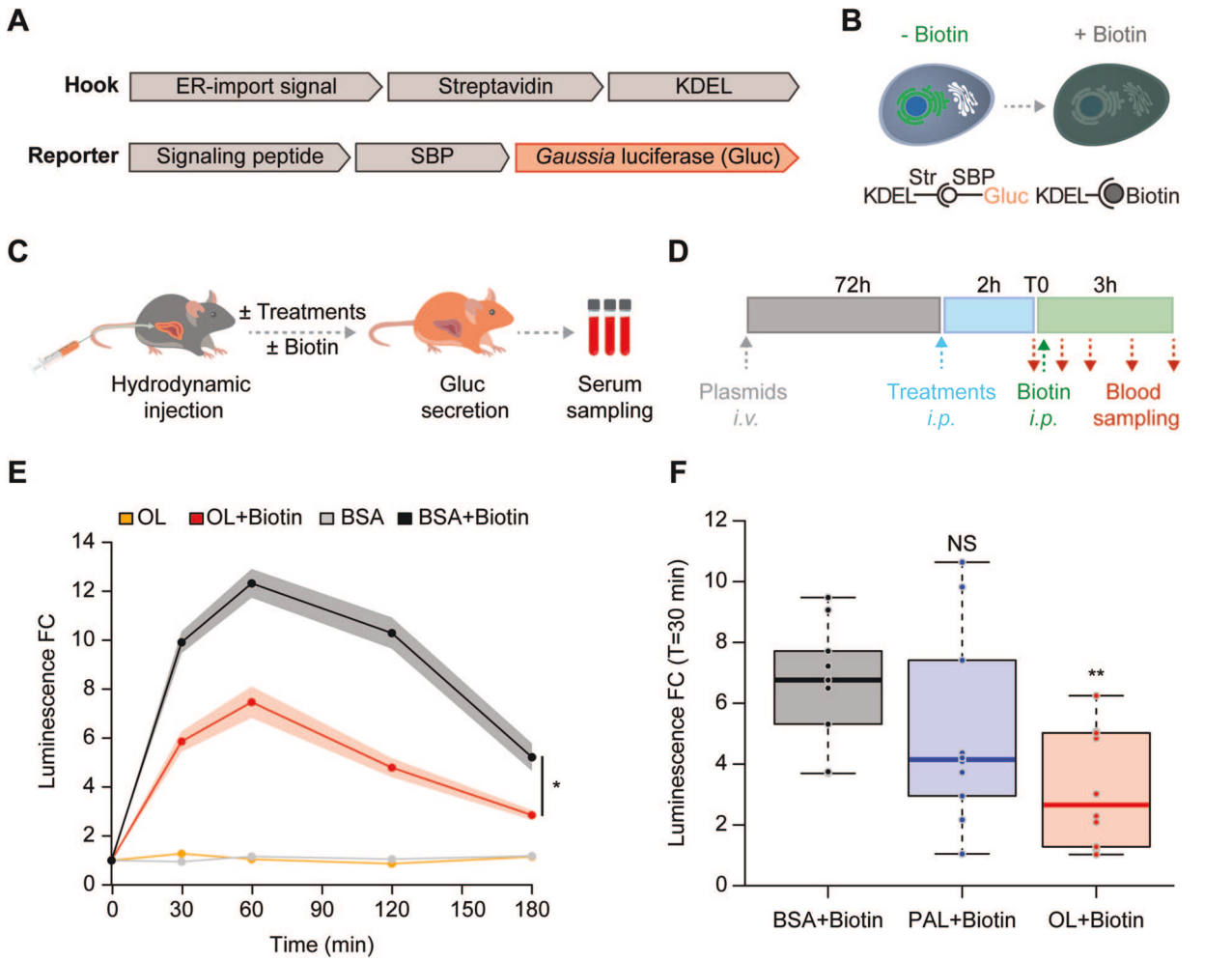

Fig. 7 Validation of oleate-induced protein secretion inhibition in vivo. The in vivo retention using selective hooks (RUSH) assay was employed to evaluate protein secretion in mice. **a** Vectors encoding the KDEL-Streptavidin hook and the secretory reporter streptavidin-binding peptide (SBP) coupled with the naturally secretable *Gaussia princeps* luciferase (Gluc) are displayed. **b** The principle of the RUSH-secretion assay is schematized. In presence of biotin, that outcompetes with streptavidin (Str), the SBP-Gluc bate is released from the Str-KDEL hook and secreted from the cell. **c**, **d** The hook and reporter vectors were co-expressed in hepatocytes by hydrodynamic intravenous (*i.v.*) injection through the tail vein. Seventy-two hours later, mice were treated by systemic (intraperitoneal, *i.p.*) injection for 2 h before *i.p.* injection of biotin (T0), causing the release of the Gluc into the circulation. Before biotin injection, and every 30/60 min, blood was sampled to assess the Gluc chemiluminescence activity. **e** Seventy-two hours after hydrodynamic *i.v.* injection of plasmids, mice were treated either with vehicle (10% BSA in endotoxin-free DPBS) or 100 mg/kg oleate (OL) for 2 h, followed by *i.p.* injection of biotin (+Biotin) or equivalent vehicle solution. Luciferase luminescence was assessed in serum samples and it was quantified throughout time, normalized to the control at the initial time and data are displayed as fold change (FC) mean±SEM (at least 6 mice per group are represented). **f** In an independent experiment, 72 h after hydrodynamic *i.v.* injection of plasmids, mice were treated either with vehicle (BSA), 100 mg/kg oleate (OL) or 100 mg/kg palmitate (PAL) for 2 h. Biotin was then injected *i.p.* and the luminescence FC 30 min after biotin injection is represented as boxplots with individual points. Outlier mice were excluded and p values were calculated using Mann–Whitney U test against the vehicle control (*$p < 0.05$, **$p < 0.01$, NS not significant).

Eagle Medium (Thermo Fisher Scientific, Carlsbad, CA, USA) supplemented with 10% fetal bovine serum (Gibco® Thermo Fisher Scientific), 1% nonessential amino acids (Thermo Fisher Scientific), 1% HEPES (Thermo Fisher Scientific) in a humidified incubator with 5% CO_2 at 37 °C. For U2OS cells co-expressing SBP-GFP and Str-KDEL, 0.25 mg/mL hygromycin (Invivogen, San Diego, CA, USA) and 0.5 mg/mL G418 (Invivogen) were added to the culture medium. For U2OS cells co-expressing SBP-GFP-LC3 and Str-CD74 culture medium was supplemented with 0.25 mg/mL hygromycin, 0.5 mg/mL G418, and 40 µM biotin (Sigma Aldrich, St Louis, MO, USA). Plastic supplies were purchased from Corning (Corning, NY, USA) and Greiner Bio-One (Kremsmünster, Austria).

Compounds and reagents

The Prestwick chemical library was obtained from Prestwick Chemical (Illkirch, France) and used at 1 and 10 µM. Fendiline and sertraline were aliquoted from the Prestwick

chemical library and both used at 10 µM. LTX-401 was provided by Lytix Biopharma (Tromsø, Norway) and used at 5 µg/mL. Avidin (A9275) used at 1 µM, biotin (B4501) used at 40 µM, brefeldin A (B6542) used at 5 µg/mL, staurosporine (S4400) used at 2 µM, thapsigargin (T9033) used at 3 µM, tunicamycin (T7765) used at 3 µM and cycloheximide (01810) used at 50 µM were purchased from Sigma-Aldrich (St Louis, MO, USA). Golgicide A (3584) used at 5 µg/mL and torin 1 (4247) used at 0.3 µM were purchased from Tocris Bioscience (Bristol, UK). Oleate (10-1801-13) and palmitate (10-1600-13), both used at 500 µM, were purchased from Larodan (Malmö, Sweden). Sodium oleate (O7501) and sodium palmitate (P9767) used at 100 mg/kg for in vivo experimentation were purchased from Sigma-Aldrich. Hoechst 33342 (H3570) and Lipofectamine® 2000 reagent were purchased from Thermo Fisher Scientific. Propidium iodide (P4864), formaldehyde (F8775), and Triton X-100 (T8787) were purchased from Sigma Aldrich (St. Louis, MO, USA).

Antibodies

Rabbit monoclonal antibodies against phospho-eIF2α (Ser51) (ab32157) used 1/500 for U2OS cells, LMAN1 (ab125006) used 1/150, GM130 (ab52649) used 1/300 and rabbit polyclonal antibody against calreticulin (ab2907) used 1/300 were purchased from Abcam (Cambridge, UK). Rabbit monoclonal antibody against phospho-eIF2α (Ser51) (119A11) used 1/500 for MEF cells was purchased from Cell Signaling Technology (Danvers, MA, USA). Rabbit polyclonal antibody against TGN46 (13573-1-AP) used 1/150 was purchased from Proteintech (Rosemont, IL, USA). Rabbit polyclonal antibody against B4GALT1 (PAB20512) used 1/500 was purchased from Abnova (Taipei, Taiwan). Mouse monoclonal antibody against streptavidin (sc52234) used 1/500 was purchased from Sant Cruz Biotechnology (Dallas, TX, USA). Anti-rabbit and anti-mouse AlexaFluor 488-, 568- and 647-labeled antibodies used 1/1000 were purchased from Thermo Fisher Scientific. For immunoblotting, LC3B (2775 S, Cell Signaling Technologies), PeIF2a (ab32157, Abcam), and eIF2α (9722 S, Cell Signaling Technologies) were used 1/1000, β-actin (ab6276, clone AC-15, Abcam) was diluted 1/10000.

Fluorescence microscopy, image acquisition and analysis

One day before treatment, U2OS WT or ATG5$^{-/-}$cells stably expressing GFP-LC3 or co-expressing RFP-LC3 and GALT1-GFP, U2OS eIF2α^{S51A} expressing RFP-LC3 and MEF or MEF eIF2α^{4KO} cells stably expressing RFP-LC3 were seeded in 384-well µClear imaging plates (Greiner Bio-One) and let adhere for 24 h. The next day, cells were treated to assess LC3 aggregation and Golgi morphology at 6 h, co-occurrence of LC3 puncta and subcellular structures at 2, 4, and 6 h, eIF2α phosphorylation (P-eIF2α) at 6 h and viability at 12 h. For viability studies, cells were further co-stained with 0.5 µg/mL propidium iodide and 2.5 µg/mL Hoechst 33342 for 20 min followed by immediate live-cell acquisition. For all other conditions, cells were fixed with 3.7% formaldehyde containing 1 µg/mL Hoechst 33342 for 1 h at room temperature. When measuring the formation of LC3 puncta and the morphology of the Golgi, the fixative was exchanged to PBS and the plates were analyzed by automated microscopy. To assess P-eIF2α and co-occurrence of LC3 puncta and subcellular structures, an additional immunostaining was performed. Cells were permeabilized with 0.1% Triton X-100 for 10 min (except for P-eIF2α in U2OS cells) and unspecific antibody binding was blocked by incubation with 2% BSA for 1 h at room temperature. After overnight incubation at 4 °C with the primary antibody, cells were repeatedly washed with PBS, stained with AlexaFluor-568 (or 488, or 647)-coupled secondary antibody for 2 h at room temperature and then washed with PBS before acquisition. For automated fluorescence microscopy, a robot-assisted Molecular Devices IXM XL BioImager and a Molecular Devices IXM-C (Molecular Devices, Sunnyvale, CA, USA) equipped with either a SpectraX or an Aura II light source (Lumencor, Beaverton, OR, USA), adequate excitation and emission filters (Semrock, Rochester, NY, USA) and a 16-bit monochromes sCMOS PCO.edge 5.5 camera (PCO Kelheim, Germany) or an Andor Zyla camera (Belfast, Northern Ireland) and a 20X or 60X PlanAPO objective (Nikon, Tokyo, Japan) were used to acquire a minimum of four view fields per well. For live cellular imaging, the atmospheric environment was controlled by means of an Ibidi gas mixer (Gräfelfing, Germany). The images were segmented and analyzed with the freely available software R (https://www.r-project.org), integrated with the *EBImage* package from the Bioconductor repository (https://www.bioconductor.org), the *MetaxpR* package (https://github.com/kroemerlab/MetaxpR), the *RBioFormats* package (https://github.com/aoles/RBioFormats), as well as the *MorphR* package (https://github.com/kroemerlab/MorphR). The primary region of interest (ROI) was defined by a polygon mask around the nucleus allowing for the enumeration of cells, the detection of morphological alterations of the nucleus and nuclear fluorescence intensity. Secondary cytoplasmic ROIs were used for the quantification of P-eIF2α intensity. To quantify GFP- (or RFP-) LC3 aggregation, a segmentation mask of high-intensity dots was generated in the cytoplasm of cells. For co-occurrence analysis, images were analyzed using the ColocalizR software [30] calculating the surface overlap coefficient (SOC) between fluorophores of interest. Golgi morphology was

evaluated by quantifying the Golgi surface. For viability studies, the number of nuclei was measured in fixed cells, while in live-imaged cells dead cells (PI^+) were quantified compared to live cells ($Hoechst^{dim}$ and PI^-). After exclusion of cellular debris and dead cells, parameters of interest were normalized, statistically evaluated, and graphically depicted by using R software. Images were extracted, pixel intensities scaled to be visible (in the same extent for all images of a given experiment) and the background of the images has been removed by subtracting the Gaussian blur of each channel to the original image.

High-throughput siRNA interference

U2OS cells stably expressing GFP-LC3 were seeded in 384-well μClear imaging plates and let adhere for 24 h. The day after, cells were transfected with the siGenome genome-wide small-interfering RNA (siRNA) library (Dharmacon, Lafayette, CO, USA) targeting 18 120 genes of the human genome (one gene represented as a SMARTpool of 4 individual siRNAs in one well) for 24 h at a final concentration of 30 nM by means of DharmaFECT™ transfection reagent (Dharmacon) according to the manufacturer's instructions. A siUNR (UAAGGCUAUGAAGAGAUAC) was used as a non-targeting control. Medium was discarded, cells let adapt for additional 24 h and then treated for 6 h with oleate or palmitate or left untreated as control prior to fixation and image acquisition as previously described. The average surface of GFP-LC3 puncta per cell was quantified. Before scaling data by calculating *Z*-scores, the data was normalized between negative (untreated cells and cells transfected with siUNR) and positive controls (cells treated with oleate and transfected with siUNR). A sigmoid transformation was performed on *Z*-scores to generate smoothened GFP-LC3 dots surface scores [53]. A bi-parametric plot was generated for the comparison of oleate- and palmitate-specific GFP-LC3 dots surface scores and 100 oleate-specific hits were semi-automatically determined and 15 non-expressed genes in the U2OS cell line were excluded. Briefly, 2 thresholds were defined by the 5% percentile of oleate and palmitate GFP-LC3 dots surface scores, thus defining a quadrant of oleate-specific hits, inside of which a manual gating was applied. Corresponding genes plus control siRNAs and manually added siRNAs were used to transfect U2OS cells stably expressing RFP-LC3 and GALT1-GFP for 24 h, the medium was then discarded, cells let adapt for additional 24 h before a 6 h treatment with oleate, fixation, and image acquisition as previously described. RFP-LC3 aggregation, toxicity, Golgi surface, and P-eIF2α intensity were measured as explained above. Each of the latter parameter was normalized to the unrelated (UNR) siRNA control and for plotting the heatmap, each value was ranged between 0 and 100% of oleate-induced effect, the first value corresponding to maximum inhibition of the phenotype and the last value corresponding to the original effect.

Bioinformatic analysis on oleate-specific hits

Genes modulating oleate-induced effects were subjected to Gene Ontology (GO) analysis by means of the *clusterProfiler* package (https://www.bioconductor.org). Relevant enriched terms from the "biological process" category were kept based on their associated p value (<0.1). In addition, proteins encoded by the identified target genes were further analyzed using the STRING tool (https://www.string-db.org), indicating confirmed and putative protein-protein interactions.

VSVG trafficking experiments

One day prior to transfection, U2OS cells stably expressing RFP-LC3 were seeded in 96-well μClear imaging plates (Greiner Bio-One) and let adhere for 24 h. The following day, transient transfection with ts045 VSVG-YFP plasmid was performed using Lipofectamine® 2000 according to the manufacturer's protocol (Thermo Fisher Scientific). The plasmid was a kind gift from Dr. Frank Perez from Institut Curie, Paris, France. On the next day, cells were incubated for 16 h at 40 °C to maintain VSVG-YFP in the endoplasmic reticulum. Cells were then treated or left untreated for 2 h at 40 °C. Upon temperature shift to 32 °C, cells were observed by live-cell microscopy for 4 h with a frequency of image acquisition of one image every 10 min. The images were segmented and analyzed with R using the *EBImage* package. The relative VSVG-YFP and RFP-LC3 dots surfaces, the surface overlap coefficient (SOC) between VSVG and LC3 and the LC3 average dots distance to centroid (indicating the degree of dots spread) were quantified throughout the time series.

Retention using selective hooks (RUSH) system to evaluate protein trafficking in vitro

U2OS cells stably co-expressing Str-KDEL and SBP-GFP or co-expressing Str-CD74 and SBP-GFP-LC3 were seeded in 384-well μClear imaging plates in the absence and presence of biotin respectively and let adapt for 24 h. U2OS Str-CD74-SBP-GFP-LC3 cells were incubated additional 12 h in the presence of avidin. Cells were then treated or left untreated in the absence of biotin and in the presence of avidin respectively for 2 h and observed by live-cell microscopy for 2 h with a frequency of image acquisition of one image every 30 min. Next, 40 μM biotin was added and images were acquired every 20 min for 4 h. For U2OS Str-KDEL-SBP-GFP, cell integrated cytoplasmic GFP

intensity was quantified in the entire image (after background correction by gaussian blur subtraction) for each timepoint. For U2OS Str-CD74-SBP-GFP-LC3, the dispersion of LC3 was quantified as dots distance to centroid. For both cell lines, co-occurrence between GFP and streptavidin, and between GFP and TGN46 was quantified using ColocalizR software. For siRNA interference, U2OS Str-KDEL-SBP-GFP were transfected for 24 h at a final concentration of 30 nM by means of DharmaFECT™ transfection reagent (Dharmacon) according to the manufacturer's instructions. Medium was discarded, cells let adapt for additional 48 h and then left untreated or treated in absence of biotin for 2 h prior to biotin addition and live imaging acquisition as previously described. Fluorescence loss was quantified on an image-basis, by calculating the sum of integrated intensities differences over time, divided by the initial value.

Phenotypic screen of oleate mimetics

U2OS cells stably expressing RFP-LC3 and GALT1-GFP were seeded in 384-well μClear imaging plates and let adhere for 24 h. The following day, cells were treated with compounds from the Prestwick chemical library, oleate, and LTX-401 for 6 h. Cells were fixed, imaged, segmented, and analyzed as previously described. Data were submitted to a min-max normalization using appropriate controls for each assessed parameter (untreated control/oleate for LC3 aggregation, untreated control/golgicide A for Golgi disruption, untreated control alone for cellular viability), and then scaled to unit variance. Thereafter, hierarchical clustering was performed on single drugs by selecting for each agent the concentration that induced maximal LC3 aggregation.

Statistical analysis

Statistics were performed using freely available software R. Unless mentioned, all depicted barcharts are showing mean ±SD from triplicate instances. Each experiment was conducted independently at least three times, with one being represented. Unless mentioned, significance levels were assessed by means of a Welch's *t*-test (when comparing means) or a Mann–Whitney *U* test (when comparing medians) against appropriate control ($*p < 0.05$, $**p < 0.01$, $***p < 0.001$).

Immunoblotting

After treatment, cells were washed with cold PBS, harvested with pre-warmed 0.25% trypsin/EDTA and lysed with RIPA buffer (89901, Thermo Fisher Scientific) supplemented with Pierce protease and phosphatase inhibitors (A32955 and A32957, Thermo Fisher Scientific) on ice. Samples were sonicated and centrifuged at 12000 g for 15 min at 4 °C, followed by the quantification of protein content by means of the Bio-Rad laboratory DC Protein Assay (500-0113, 500-0114, 500-0115, BioRad, CA, USA) following the manufacturer's instructions. Next, 20 μg of protein were dissolved in NuPAGE® LDS sample buffer 4X (NP0007, Invitrogen) and NuPAGE® sample reducing agent 10X (NP0009, Invitrogen) and denaturized at 100 °C for 10 min. Protein samples were separated on pre-cast 4-12% polyacrylamide NuPAGE™ Bis-Tris gels (NP0336, Thermo Fisher Scientific) in NuPAGE® MOPS SDS Running buffer (NP0001, Thermo Fisher Scientific) and electro-transferred to EtOH-activated PVDF membranes (88518, Thermo Fisher Scientific) in transfer buffer (25 mM Tris, 190 mM glycine, 20% ethanol in H_2O) (EU0550, Euromedex, Souffelweyersheim, France). Membranes were incubated in Tris-buffered saline with Tween®20 detergent (TBST, 20 mM Tris, pH7.5, 150 mM NaCL, 0.1% Tween®20 in H_2O) (P1379, Sigma Aldrich; ET220-B, Euromedex) supplemented with 5% BSA (04-100-812, Euromedex) for 1 h in order to saturate unspecific binding sites. Thereafter, membranes were probed with primary antibodies specific to LC3B, PeIF2a, and eIF2α, diluted 1/1000 in 5% BSA in TBST overnight at 4 °C on a rocking shaker. Equal loading was verified by means of β-actin diluted 1/10000 in 5% BSA in TBST. The day after, membranes were extensively washed with TBST and then incubated with goat anti-rabbit IgG(H + L) horseradish peroxidase (HRP)-labeled secondary antibody (4050-05, Southern Biotech, Birmingham, AL, USA) diluted 1/5000 in 5% BSA in TBST for 1 h at room temperature. Immunoreactive bands were visualized by means of the ECL™ Prime western blotting detection reagents (RPN2236, Cytiva, Marlborough, MA, USA) and chemiluminescence images were acquired with an ImageQuant LAS4000 digital imaging system (GE Healthcare, Little Chalfont, UK).

In silico gene target analysis of oleate-mimetics

Gene targets of oleate mimetics, enriched with neighbors stemming from a colocalization analysis performed in a previous work [30], were retrieved using the Power User Gateway interface of PubChem to query the BioAssay database [54], and relevant genes were kept when at least two drugs had associated records, with at least one of them described as active. The list of genes was further curated by excluding non-expressed genes in the U2OS cell line, as reported in the protein atlas (https://www.proteinatlas.org). An enrichment in low scores was investigated by comparing the distribution of the obtained targets versus whole-genome gene set LC3 aggregation scores by performing a Kolmogorov–Smirnov test.

AHA incorporation to assess translation

Translation was studied by evaluating the incorporation of L-azidohomoalanine (AHA), a labeled amino acid analog of methionine containing an azide moiety, by means of the Click-iT™ chemistry according to the manufacturer's instructions (C10289, Thermo Fisher Scientific). In short, U2OS wild-type cells were seeded in 384-well μClear imaging plates and let adapt for 24 h. The next day, cells were treated or left untreated in complete medium for 4 h and multiple PBS washing steps were performed. Cells were then treated 30 min in the presence of methionine-free medium (21013024, Thermo Fisher Scientific), followed by additional 1.5 h in methionine-free medium supplemented with 25 μM L-azidohomoalanine (AHA). Afterward, cells were fixed with 3.7% formaldehyde containing 1 μg/mL Hoechst 33342 for 1 h at room temperature, permeabilized with 0.1% Triton X-100 for 10 min and unspecific antibody binding was blocked by incubation with 2% BSA. After incubation with AlexaFluor 488-coupled azide for 2 h at room temperature, cells were imaged as previously described. The cytoplasmic GFP intensity (AHA) was quantified with the software R and data was normalized to the control.

In vivo experimentation

Wild-type C57BL/6 mice were purchased from Envigo (HARLAN FRANCE, Gannat, France) and were housed in the animal facility of the Gustave Roussy Cancer Campus with 12 h light and dark cycles, in a pathogen-free, temperature-controlled environment where they received water and food *ad libitum*. Animal experiments were conducted in compliance with the EU Directive 63/2010/EU from the European Parliament and were approved by the local Ethics Committee of the Gustave Roussy Cancer Campus (CEEA IRCIV/IGR no. 26, registered at the French Ministry of Research, with the protocol number 23146 / 2019112800493053). "BiostaTGV" software was used to calculate the number of animals to be included in each group in order to reach statistical significance, based on expected results.

In vivo RUSH assay

The RUSH plasmids pCDH-streptavidin (Str)-KDEL [35] and pCDH-ss-SBP-Gluc were injected into the tail vein of C57Bl/6 10 weeks old female mice via hydrodynamic injection as described previously [55]. pCDH-ss-SBP-Gluc was generated by replacing GFP in pCDH-ss-SBP-EGFP [35] with the coding sequence of secretable *Gaussia princeps* luciferase (Gluc) synthesized by Eurofins Genomics (Ebersberg, Germany). In short, mice were injected with 90 μg pCDH-streptavidin (Str)-KDEL plus 30 μg pCDH-ss-SBP-Gluc diluted in 37 °C pre-warmed sterile saline solution. DNA injection was performed with 5 mL BD Luer-Lok syringes (309646, BD Biosciences) equipped with 25 G needles. The entire volume was injected within 5-8 s under continuous pressure.

Seventy-two hours after plasmid delivery, mice were randomly treated via a single intraperitoneal injection (*i.p.*) of 100 mg/kg oleate or 100 mg/kg palmitate both diluted in endotoxin-free DPBS supplemented with 10% BSA or equivalent vehicle solution. Two hours later, mice were treated with 15 mg/kg biotin *i.p.* or equivalent vehicle solution for 3 h. Before biotin injection, 30 min and every hour after that, 10 μL of blood was withdrawn through the mandibular vein and immediately mixed with 2 μL of 50 mM EDTA anticoagulant, centrifuged at $6000 \times g$ for 2 min at 4 °C and plasma was frozen at −20 °C.

Bioluminescence was assessed with 100 μM coelenterazine (sc-205904, Santa Cruz Biotechonolgy) prior diluted in PBS supplemented with 5 mM NaCl, at pH 7.2 and stabilized at room temperature for 30 min. In short, 5 μL serum per sample were transferred into Nunc™ F96 MicroWell™ white polystyrene plates (236105, Thermo Fisher Scientific), 100 μL/well of 100 μM coelenterazine were added and the Gluc chemiluminescence activity was immediately measured using a FluorStar Optima Plate Reader. Data were analyzed using R as follows: first, each individual was normalized to its initial value after biotin injection, and outliers were excluded timewise when its absolute scaled value (to unit variance) was higher than 2. Means and SEM of at least six mice per group were thereafter computed for plotting purposes, and time series or endpoint groups were compared by means of a pairwise Mann–Whitney *U*-test.

Measurement of extracellular TNF-α by sandwich ELISA

The ELISA max™ Deluxe Set for mouse TNF-α (430904, BioLegend®) was employed to measure TNF-α released in cell culture supernatants. Bone marrow-derived macrophages (BMDM) were generated from femurs and tibias of dissected legs from 8 to 10-week-old C57Bl/6 mice. Bone marrow was extracted from bones by cutting joints with a scalpel and flushing the exposed bone marrow with a 10 mL syringe filled with 1% BSA in PBS. Clumps were dissociated by pipetting and red blood cells were lysed with cell lysis buffer (0.01 M Tris, 0.83% NH_4Cl in Milli-Q water). The cell suspension was passed through a 70 μm cell strainer and cells were seeded into 15 cm Petri-dishes in BMDM culture medium composed of RPMI 1640 medium supplemented with 10% FBS, 200 mM L-Glutamine (35050061, Thermo Fisher Scientific), 100 U/ml penicillin (15140122, Thermo Fisher Scientific), 1 M HEPES

(15630056, Thermo Fisher Scientific), 1% MEM Non-Essential Amino Acids Solutions (11140035, Thermo Fisher Scientific), and 50 µM β-mercaptoethanol (31350010, Thermo Fisher Scientific) supplemented with 50 ng/ml recombinant mouse M-CSF (416-ML-050, R&D Systems, MI, USA).

On day 3, the supernatant was removed and BMDM growth medium freshly supplemented with M-CSF was added. BMDM were harvested on day 6 and seeded in 24-well cell culture plates (3524, Corning) in BMDM growth medium freshly supplemented with M-CSF. The following day, BMDM were activated with 100 ng/mL lipopolysaccharide (LPS) (L4391, Sigma Aldrich) for 16 h. Next, BMDM were washed twice with PBS and treated for 2 h with selected compounds in combination or absence of LPS. Supernatant was collected and centrifuged. ELISA was performed as described in the provider's protocol. Briefly, high binding 96-well plates (3361, Corning) were coated with anti-TNF-α capture antibody overnight at 4 °C. After multiple washing with washing buffer, blocking buffer was added to block unspecific binding for 1 h at RT on a rocking shaker. 100 µL of standards and samples diluted in 1% BSA in PBS were added in each coated-well for 2 h at RT with shaking. After washing, the anti-TNF-α detection antibody was added for 1 h with shaking. Plates were then rinsed and incubated with avidin-HRP-conjugated secondary antibody. After extensive washing, 100 µL of TMB substrate solution (34029, Thermo Fisher Scientific) was added in all wells and incubated for 15 min at RT in the dark until colorizing. Immediately after, stop solution (2 M H_2SO_4) was added and the absorbance at 450 nm was assessed with a SpectraMax I3 multi-mode microplate reader (Molecular Devices). TNF-α concentration was quantified with software R by establishing an absorbance-concentration model using a mixed polynomial-exponential fit.

Assessment of intracellular TNF-α by flow cytometry

BMDM were collected, differentiated, activated, and treated as described above. Cells were detached with cell lifters, centrifuged, and washed twice with PBS. Firstly, BMDM were stained with LIVE/DEAD™ Fixable Yellow Dead Cell Stain Kit (L34968, Invitrogen) and incubated with purified anti-mouse CD16/32 antibody (101302, BioLegend®) to block Fc receptors and non-specific antibody binding for 20 min, at 4 °C. BMDM were then stained with F4/80 monoclonal antibody (BM8) coupled to AlexaFluor 488 (53-4801-82, Invitrogen) at 1 µg/mL in 1% BSA in PBS for 30 min at 4 °C covered in foil. Fixation and permeabilization for intracellular staining were performed by means of the Cyto-Fast™ Fix/Perm Buffer Set (426803, BioLegend®) according to manufacturer's protocol. BMDM were then stained with 0.125 µg of anti-mouse TNF-α monoclonal antibody (MP6-XT22) coupled to APC (17-7321-82, Invitrogen). In control samples, the isotype control antibody rat IgG1 kappa isotype control (eBRG1) coupled to APC (17-4301-82, Invitrogen) was included. After multiple washes, samples were run on a BD LSR Fortessa flow cytometer, and data were acquired using BD FACS Diva software (BD Biosciences). Intracellular TNF-α was assessed by quantifying the ratio of live $F4/80^+$ APC^+ BMDM among the total amount of live $F4/80^+$ BMDM using R software, combined with the *flowCore* package (available on https://www.bioconductor.org/ repository).

Acknowledgements GC is supported by a scholarship of the Fondation pour la Recherche Médicale (FRM FDT202001011060). GK is supported by the Ligue contre le Cancer (équipe labellisée); Agence National de la Recherche (ANR)—Projets blancs; ANR under the frame of E-Rare-2, the ERA-Net for Research on Rare Diseases; Association pour la recherche sur le cancer (ARC); Cancéropôle Ile-de-France; Chancellerie des universités de Paris (Legs Poix), Fondation pour la Recherche Médicale (FRM); a donation by Elior; European Research Area Network on Cardiovascular Diseases (ERA-CVD, MINOTAUR); Gustave Roussy Odyssea, the European Union Horizon 2020 Project Oncobiome; Fondation Carrefour; High-end Foreign Expert Program in China (GDW20171100085 and GDW20181100051), Institut National du Cancer (INCa); Inserm (HTE); Institut Universitaire de France; LeDucq Foundation; the LabEx Immuno-Oncology; the RHU Torino Lumière; the Seerave Foundation; the SIRIC Stratified Oncology Cell DNA Repair and Tumor Immune Elimination (SOCRATE); and the SIRIC Cancer Research and Personalized Medicine (CARPEM).

Author contributions Conceptualization, GK, AS, and GC; Methodology, GK, AS, GC, JH, ML, and PL; Investigation, GC, KM, PL, LZ, WX, and SZ; Formal analysis, AS, GC, and ML; Writing—Original Draft, GK, GC, and AS; Writing—Review & Editing, GK, GC, OK, and JH; Funding acquisition, GK; Supervision, OK and GK.

Compliance with ethical standards

Conflict of interest GK and OK are cofounders of Samsara Therapeutics. GK is a founder of everImmune and Therafast Bio.

Ethics Animal experiments were conducted in compliance with the EU Directive 63/2010/EU from the European Parliament and were approved by the local Ethics Committee of the Gustave Roussy Cancer Campus (CEEA IRCIV/IGR no. 26, registered at the French Ministry of Research.

References

1. Kabeya Y, Mizushima N, Ueno T, Yamamoto A, Kirisako T, Noda T, et al. LC3, a mammalian homologue of yeast Apg8p, is localized in autophagosome membranes after processing. EMBO J. 2000;19:5720–8.

2. Galluzzi L, Baehrecke EH, Ballabio A, Boya P, Bravo-San Pedro JM, Cecconi F, et al. Molecular definitions of autophagy and related processes. The EMBO journal. 2017;36:1811–36.
3. Mizushima N. The ATG conjugation systems in autophagy. Current Opinion Cell Biol. 2019;63:1–10.
4. Mizushima N, Yoshimori T, Levine B. Methods in mammalian autophagy research. Cell. 2010;140:313–26.
5. Klionsky DJ, Abdelmohsen K, Abe A, Abedin MJ, Abeliovich H, Acevedo Arozena A, et al. Guidelines for the use and interpretation of assays for monitoring autophagy (3rd edition). Autophagy. 2016;12:1–222.
6. Galluzzi L, Pietrocola F, Bravo-San Pedro JM, Amaravadi RK, Baehrecke EH, Cecconi F, et al. Autophagy in malignant transformation and cancer progression. EMBO J. 2015;34:856–80.
7. Hansen M, Rubinsztein DC, Walker DW. Autophagy as a promoter of longevity: insights from model organisms. Nat Rev Mol Cell Biol. 2018;19:579–93.
8. Levine B, Kroemer G. Biological functions of autophagy genes: a disease perspective. Cell. 2019;176:11–42.
9. Morishita H, Mizushima N. Diverse cellular roles of autophagy. Annual Rev Cell Dev Biol. 2019;35:453–75.
10. Sales-Campos H, Souza PR, Peghini BC, da Silva JS, Cardoso CR. An overview of the modulatory effects of oleic acid in health and disease. Mini Rev Med Chem. 2013;13:201–10.
11. Widmer RJ, Flammer AJ, Lerman LO, Lerman A. The Mediterranean diet, its components, and cardiovascular disease. Am J Med. 2015;128:229–38.
12. Niso-Santano M, Malik SA, Pietrocola F, Bravo-San Pedro JM, Marino G, Cianfanelli V, et al. Unsaturated fatty acids induce non-canonical autophagy. EMBO J. 2015;34:1025–41.
13. Sauvat A, Chen G, Muller K, Tong M, Aprahamian F, Durand S, et al. Trans-fats inhibit autophagy induced by saturated fatty acids. EBioMed. 2018;30:261–72.
14. Sundqvist M, Christenson K, Holdfeldt A, Gabl M, Martensson J, Bjorkman L, et al. Similarities and differences between the responses induced in human phagocytes through activation of the medium chain fatty acid receptor GPR84 and the short chain fatty acid receptor FFA2R. Biochim et biophys acta Mol Cell Res. 2018;1865:695–708.
15. Bolognini D, Barki N, Butcher AJ, Hudson BD, Sergeev E, Molloy C, et al. Chemogenetics defines receptor-mediated functions of short chain free fatty acids. Nat Chem Biol. 2019;15:489–98.
16. Luckmann M, Trauelsen M, Frimurer TM, Schwartz TW. Structural basis for GPCR signaling by small polar versus large lipid metabolites-discovery of non-metabolite ligands. Current Opinion Cell Biol. 2020;63:38–48.
17. de Souza RJ, Mente A, Maroleanu A, Cozma AI, Ha V, Kishibe T, et al. Intake of saturated and trans unsaturated fatty acids and risk of all cause mortality, cardiovascular disease, and type 2 diabetes: systematic review and meta-analysis of observational studies. Bmj. 2015;351:h3978.
18. Wang DD, Hu FB. Dietary fat and risk of cardiovascular disease: recent controversies and advances. Annual Rev Nutr. 2017;37:423–46.
19. Corella D, Coltell O, Macian F, Ordovas JM. Advances in understanding the molecular basis of the mediterranean diet effect. Annual Rev Food Sci Techn. 2018;9:227–49.
20. Enot DP, Niso-Santano M, Durand S, Chery A, Pietrocola F, Vacchelli E, et al. Metabolomic analyses reveal that anti-aging metabolites are depleted by palmitate but increased by oleate in vivo. Cell Cycle. 2015;14:2399–407.
21. Bravo-San Pedro JM, Pietrocola F, Sica V, Izzo V, Sauvat A, Kepp O, et al. High-throughput quantification of GFP-LC3(+) dots by automated fluorescence microscopy. Methods in enzymology. 2017;587:71–86.
22. Linders PT, Horst CV, Beest MT, van den Bogaart G. Stx5-Mediated ER-Golgi transport in mammals and yeast. Cells. 2019;8.
23. Harding HP, Zhang Y, Zeng H, Novoa I, Lu PD, Calfon M, et al. An integrated stress response regulates amino acid metabolism and resistance to oxidative stress. Mol Cell. 2003;11:619–33.
24. Lu PD, Jousse C, Marciniak SJ, Zhang Y, Novoa I, Scheuner D, et al. Cytoprotection by pre-emptive conditional phosphorylation of translation initiation factor 2. EMBO J. 2004;23:169–79.
25. Kroemer G, Marino G, Levine B. Autophagy and the integrated stress response. Mol cell. 2010;40:280–93.
26. Pakos-Zebrucka K, Koryga I, Mnich K, Ljujic M, Samali A, Gorman AM. The integrated stress response. EMBO Rep. 2016;17:1374–95.
27. Heal R, McGivan J. Induction of calreticulin expression in response to amino acid deprivation in Chinese hamster ovary cells. Biochem J. 1998;329(Pt 2):389–94.
28. Humeau J, Sauvat A, Cerrato G, Xie W, Loos F, Iannantuoni F, et al. Inhibition of transcription by dactinomycin reveals a new characteristic of immunogenic cell stress. EMBO Mol Med. 2020;12:e11622.
29. Taniuchi S, Miyake M, Tsugawa K, Oyadomari M, Oyadomari S. Integrated stress response of vertebrates is regulated by four eIF2alpha kinases. Sci Rep. 2016;6:32886.
30. Sauvat A, Leduc M, Muller K, Kepp O, Kroemer G. ColocalizR: An open-source application for cell-based high-throughput colocalization analysis. Comp Biol Med. 2019;107:227–34.
31. Lafay F. Envelope proteins of vesicular stomatitis virus: effect of temperature-sensitive mutations in complementation groups III and V. J Virol. 1974;14:1220–8.
32. Coria AS, Masseroni ML, Diaz, Anel AM. Regulation of PKD1-mediated Golgi to cell surface trafficking by Galphaq subunits. Biol Cell. 2014;106:30–43.
33. Boncompain G, Divoux S, Gareil N, de Forges H, Lescure A, Latreche L, et al. Synchronization of secretory protein traffic in populations of cells. Nat Meth. 2012;9:493–8.
34. Loos F, Xie W, Sica V, Bravo-San Pedro JM, Souquere S, Pierron G, et al. Artificial tethering of LC3 or p62 to organelles is not sufficient to trigger autophagy. Cell Death Dis. 2019;10:771.
35. Zhao L, Liu P, Boncompain G, Loos F, Lachkar S, Bezu L, et al. Identification of pharmacological inhibitors of conventional protein secretion. Sci Rep. 2018;8:14966.
36. Zhou H, Sauvat A, Gomes-da-Silva LC, Durand S, Forveille S, Iribarren K, et al. The oncolytic compound LTX-401 targets the Golgi apparatus. Cell Death Differ. 2018;25:227–8.
37. Talloczy Z, Jiang W, Virgin HWt, Leib DA, Scheuner D, Kaufman RJ, et al. Regulation of starvation- and virus-induced autophagy by the eIF2alpha kinase signaling pathway. Proc Nat Acad Sci USA. 2002;99:190–5.
38. Shen S, Niso-Santano M, Adjemian S, Takehara T, Malik SA, Minoux H, et al. Cytoplasmic STAT3 represses autophagy by inhibiting PKR activity. Mol Cell. 2012;48:667–80.
39. Humeau J, Leduc M, Cerrato G, Loos F, Kepp O, Kroemer G. Phosphorylation of eukaryotic initiation factor-2α (eIF2α) in autophagy. 2020;11:433.
40. Geatti O, Shapiro B, Barillari B. Scintigraphic depiction of an insulinoma by I-131 metaiodobenzylguanidine. Clinical nuclear medicine. 1989;14:903–5.
41. Ha KD, Clarke BA, Brown WJ. Regulation of the Golgi complex by phospholipid remodeling enzymes. Biochimica et biophysica acta. 2012;1821:1078–88.
42. Casares D, Escriba PV, Rossello CA. Membrane lipid composition: effect on membrane and organelle structure, function and compartmentalization and therapeutic avenues. Int J Mol Sci. 2019;20.

43. Glaumann H, Motakefi AM, Jansson H. Intracellular distribution and effect of the antimalarial drug mefloquine on lysosomes of rat liver. Liver. 1992;12(4 Pt 1):183–90.
44. Parks A, Charest-Morin X, Boivin-Welch M, Bouthillier J, Marceau F. Autophagic flux inhibition and lysosomogenesis ensuing cellular capture and retention of the cationic drug quinacrine in murine models. PeerJ. 2015;3:e1314.
45. Hamaguchi M, Suzuki K, Fujita H, Uzuka T, Matsuda H, Shishido-Hara Y, et al. Successful treatment of non-HIV progressive multifocal leukoencephalopathy: case report and literature review. J Neurol. 2020;267:731–8.
46. Ugarte A, Danza A, Ruiz-Irastorza G. Glucocorticoids and antimalarials in systemic lupus erythematosus: an update and future directions. Current Opinion Rheumatol. 2018;30:482–9.
47. Ram A, Mabalirajan U, Singh SK, Singh VP, Ghosh B. Mepacrine alleviates airway hyperresponsiveness and airway inflammation in a mouse model of asthma. Int Immunopharmacol. 2008;8:893–9.
48. Alves P, Bashir MM, Wysocka M, Zeidi M, Feng R, Werth VP. Quinacrine suppresses tumor necrosis factor-alpha and IFN-alpha in Dermatomyositis and cutaneous lupus erythematosus. J Invest Dermatol Symp Proc. 2017;18:S57–S63.
49. Thase ME, Denko T. Pharmacotherapy of mood disorders. Annual Rev Clin Psych. 2008;4:53–91.
50. Cipriani A, Furukawa TA, Salanti G, Chaimani A, Atkinson LZ, Ogawa Y, et al. Comparative efficacy and acceptability of 21 antidepressant drugs for the acute treatment of adults with major depressive disorder: a systematic review and network meta-analysis. Lancet. 2018;391:1357–66.
51. Martins I, Kepp O, Schlemmer F, Adjemian S, Tailler M, Shen S, et al. Restoration of the immunogenicity of cisplatin-induced cancer cell death by endoplasmic reticulum stress. Oncogene. 2011;30:1147–58.
52. Chen G, Xie W, Nah J, Sauvat A, Liu P, Pietrocola F, et al. 3,4-Dimethoxychalcone induces autophagy through activation of the transcription factors TFE3 and TFEB. EMBO Mol Med. 2019;11:e10469.
53. Sauvat A, Cerrato G. Whole Genome Screenings results. figshare. Dataset. 2020. https://doi.org/10.6084/m9.figshare.13227686.
54. Wang Y, Xiao J, Suzek TO, Zhang J, Wang J, Zhou Z, et al. PubChem's BioAssay Database. Nucleic Acids Res. 2012;40:D400–12.
55. Liu P, Zhao L, Loos F, Marty C, Xie W, Martins I, et al. Immunosuppression by mutated calreticulin released from malignant cells. Mol Cell. 2020;77:748–60 e9.

Supplemental Figures and Legends

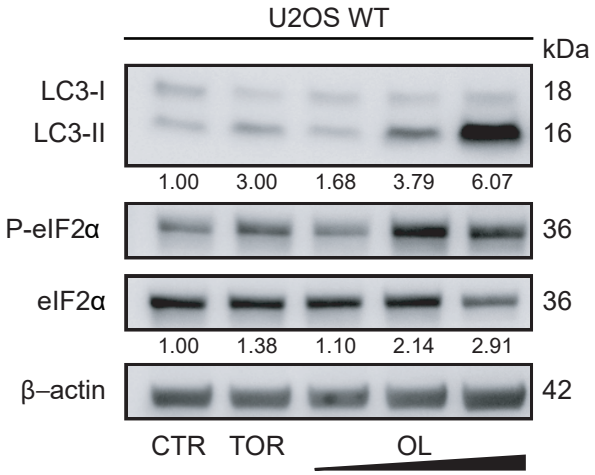

Figure S1

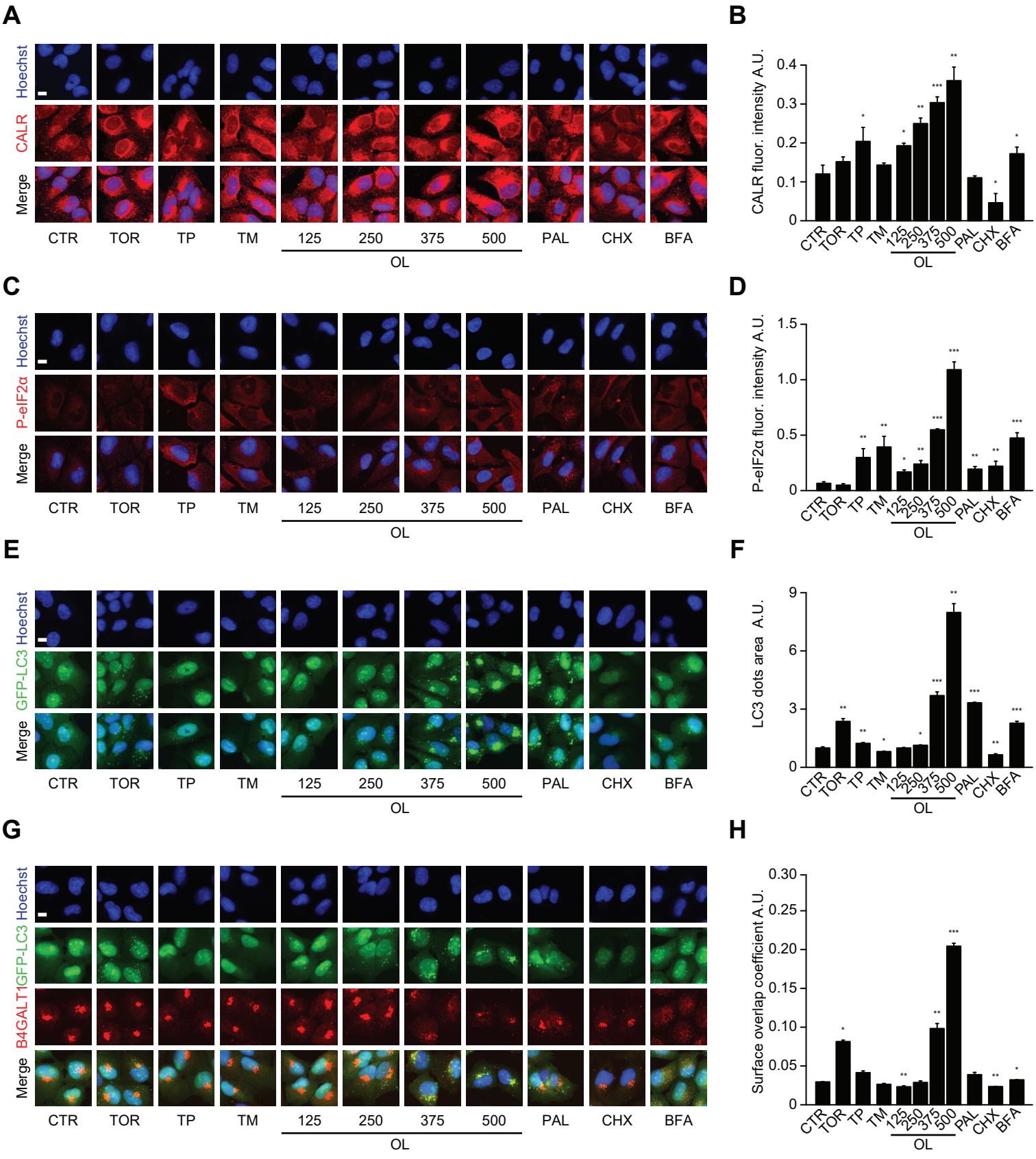
A
Hoechst
CALR
Merge
CTR
TOR
TP
TM
125
250
375
500
OL
PAL
CHX
BFA
B
CALR fluor. intensity A.U.
0.4
0.3
0.2
0.1
0
C
P-eIF2α
D
P-eIF2α fluor. intensity A.U.
1.5
1.0
0.5
E
GFP-LC3
F
LC3 dots area A.U.
9
6
3
G
B4GALT1GFP-LC3
H
Surface overlap coefficient A.U.
0.30
0.25
0.20
0.15
0.10
0.05

Figure S2

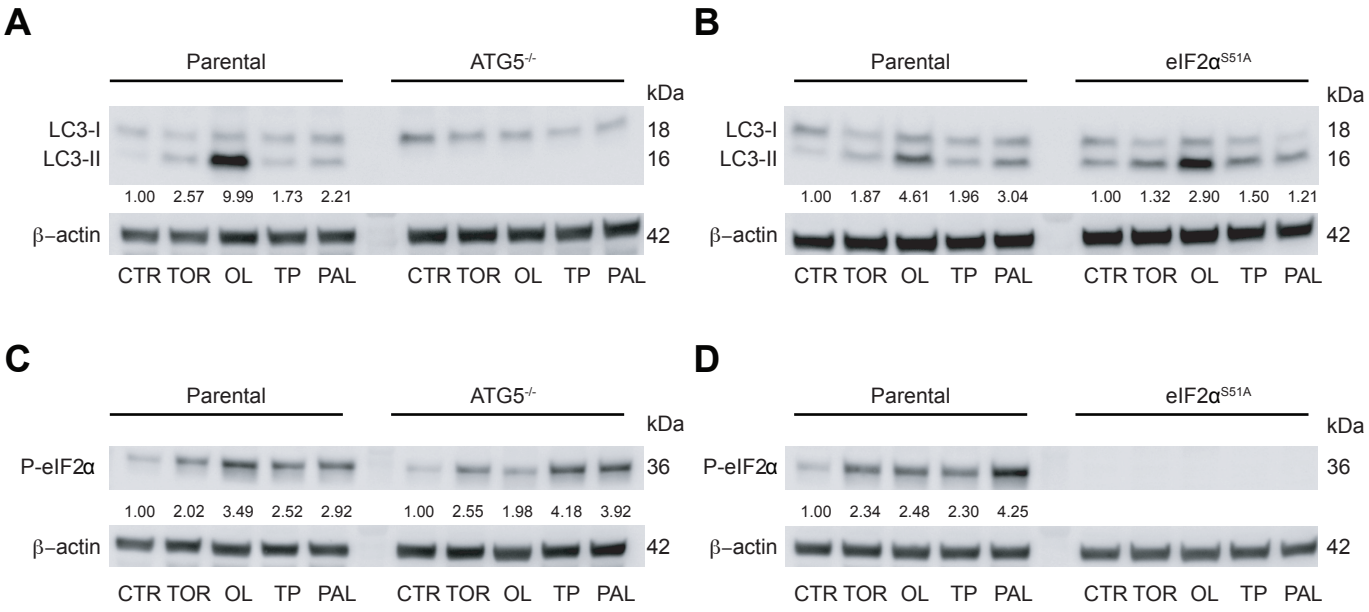
A
Parental
ATG5-/-
kDa
LC3-I
LC3-II
18
16
1.00 2.57 9.99 1.73 2.21
β–actin
42
CTR TOR OL TP PAL CTR TOR OL TP PAL
B
Parental
eIF2αS51A
kDa
LC3-I
LC3-II
18
16
1.00 1.87 4.61 1.96 3.04
1.00 1.32 2.90 1.50 1.21
β–actin
42
CTR TOR OL TP PAL CTR TOR OL TP PAL
C
Parental
ATG5-/-
kDa
P-eIF2α
36
1.00 2.02 3.49 2.52 2.92
1.00 2.55 1.98 4.18 3.92
β–actin
42
CTR TOR OL TP PAL CTR TOR OL TP PAL
D
Parental
eIF2αS51A
kDa
P-eIF2α
36
1.00 2.34 2.48 2.30 4.25
β–actin
42
CTR TOR OL TP PAL CTR TOR OL TP PAL

Figure S3

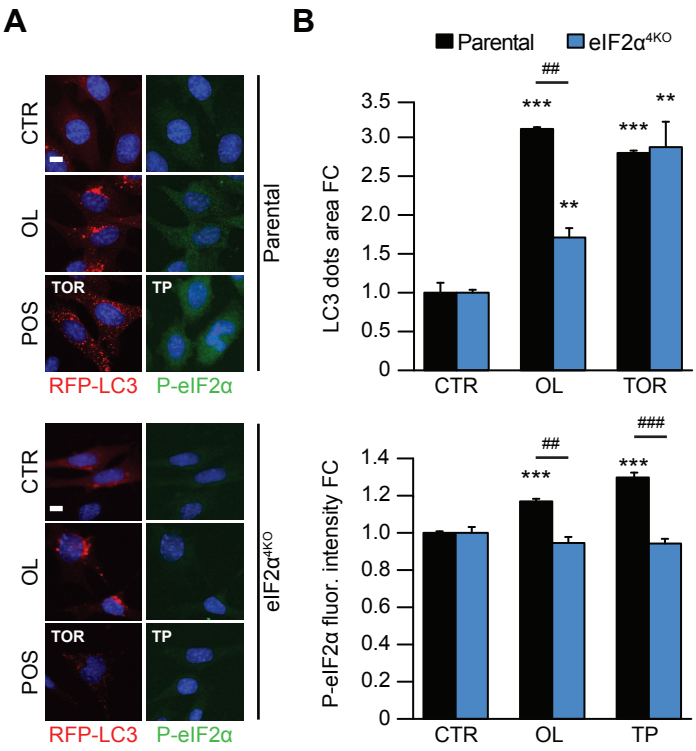
A
B
CTR
OL
POS
TOR
TP
RFP-LC3
P-eIF2α
Parental
eIF2α4KO
Parental
eIF2α4KO
LC3 dots area FC
P-eIF2α fluor. intensity FC
CTR
OL
TOR
TP
##
###
***
**

Figure S4

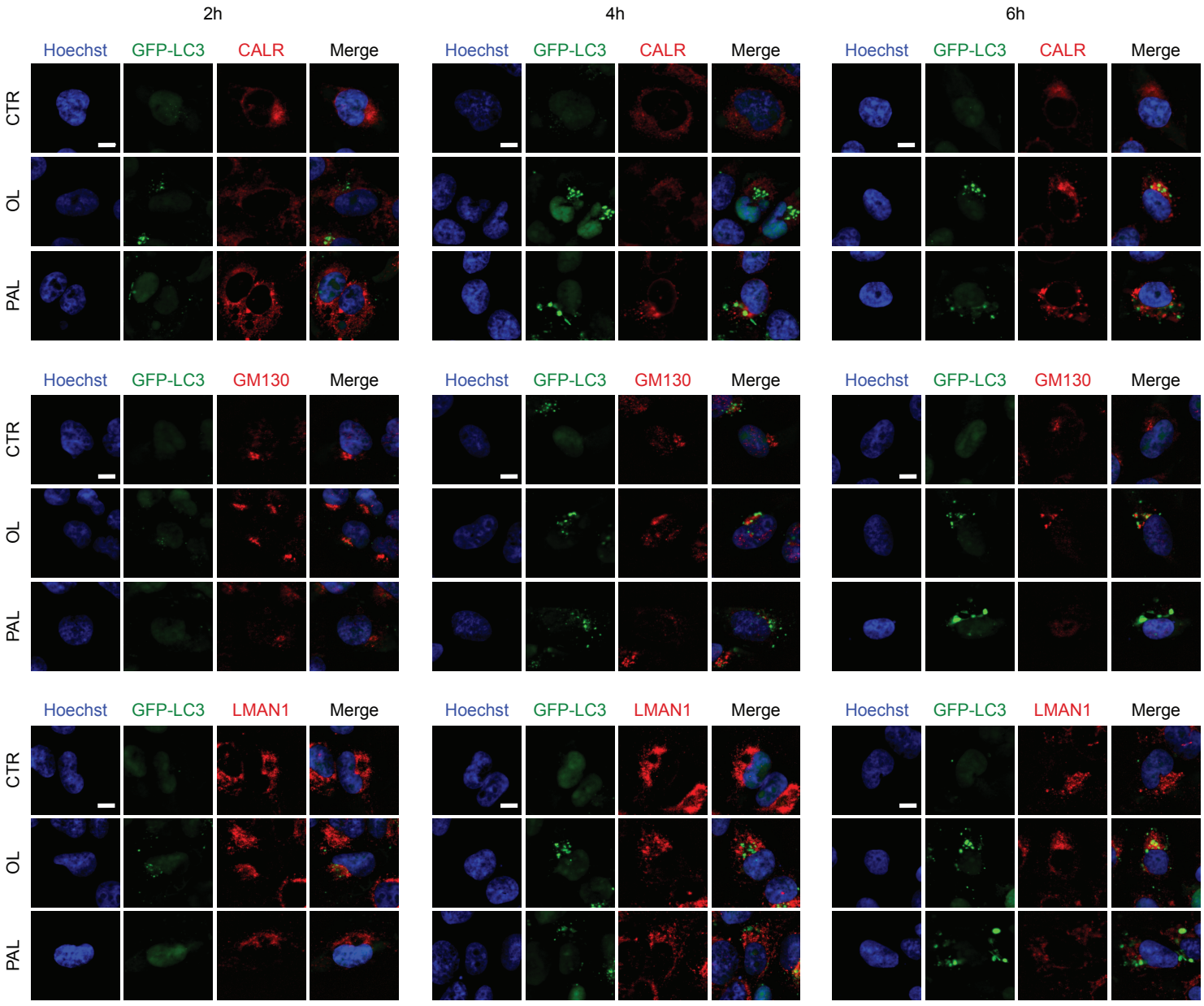

Figure S5

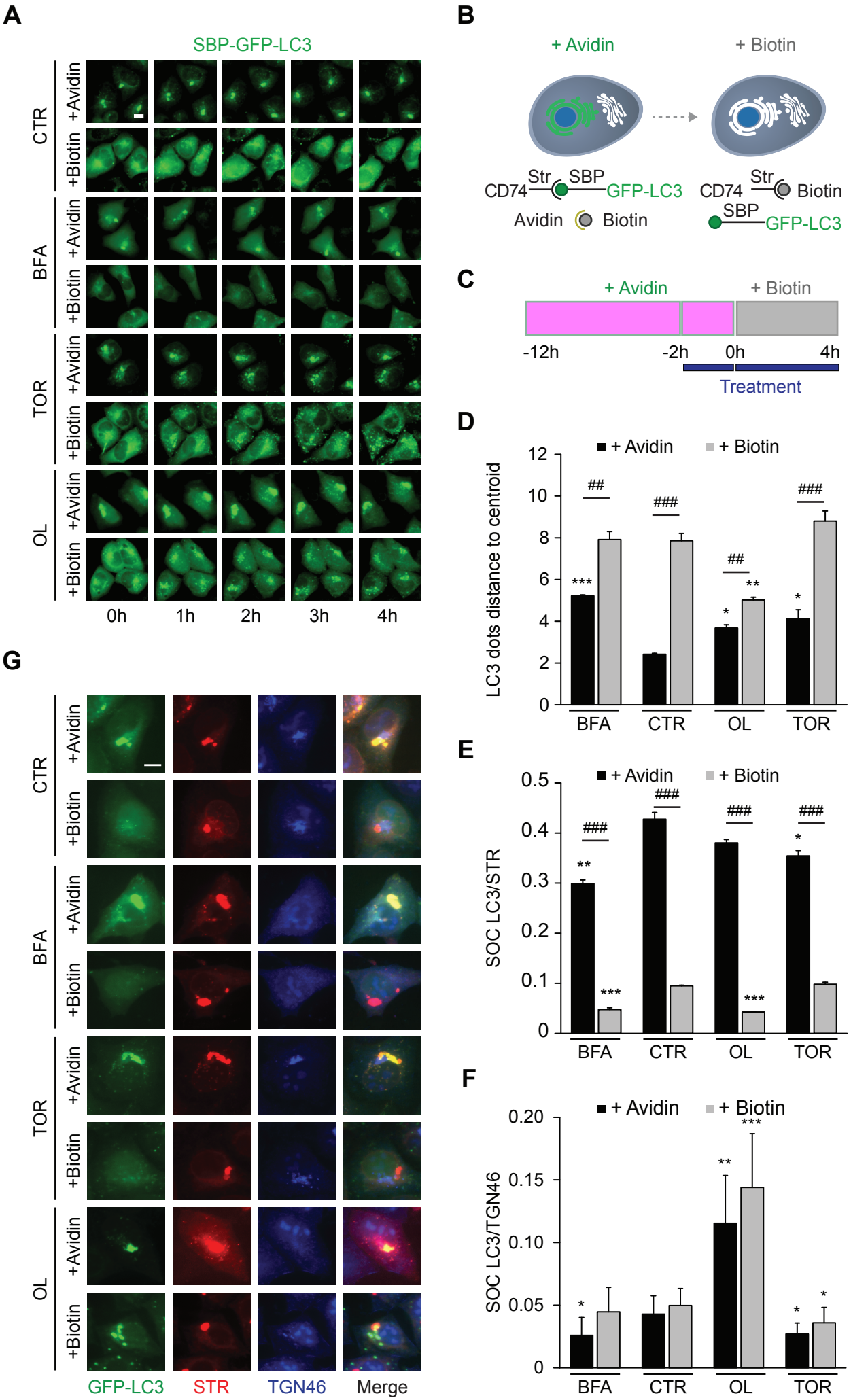
A
SBP-GFP-LC3
CTR
BFA
TOR
OL
+Avidin
+Biotin
0h
1h
2h
3h
4h
B
+ Avidin
+ Biotin
CD74
Str
SBP
GFP-LC3
Avidin
Biotin
C
+ Avidin
+ Biotin
-12h
-2h
0h
4h
Treatment
D
+ Avidin
+ Biotin
LC3 dots distance to centroid
BFA
CTR
OL
TOR
E
SOC LC3/STR
F
SOC LC3/TGN46
G
GFP-LC3
STR
TGN46
Merge

Figure S6

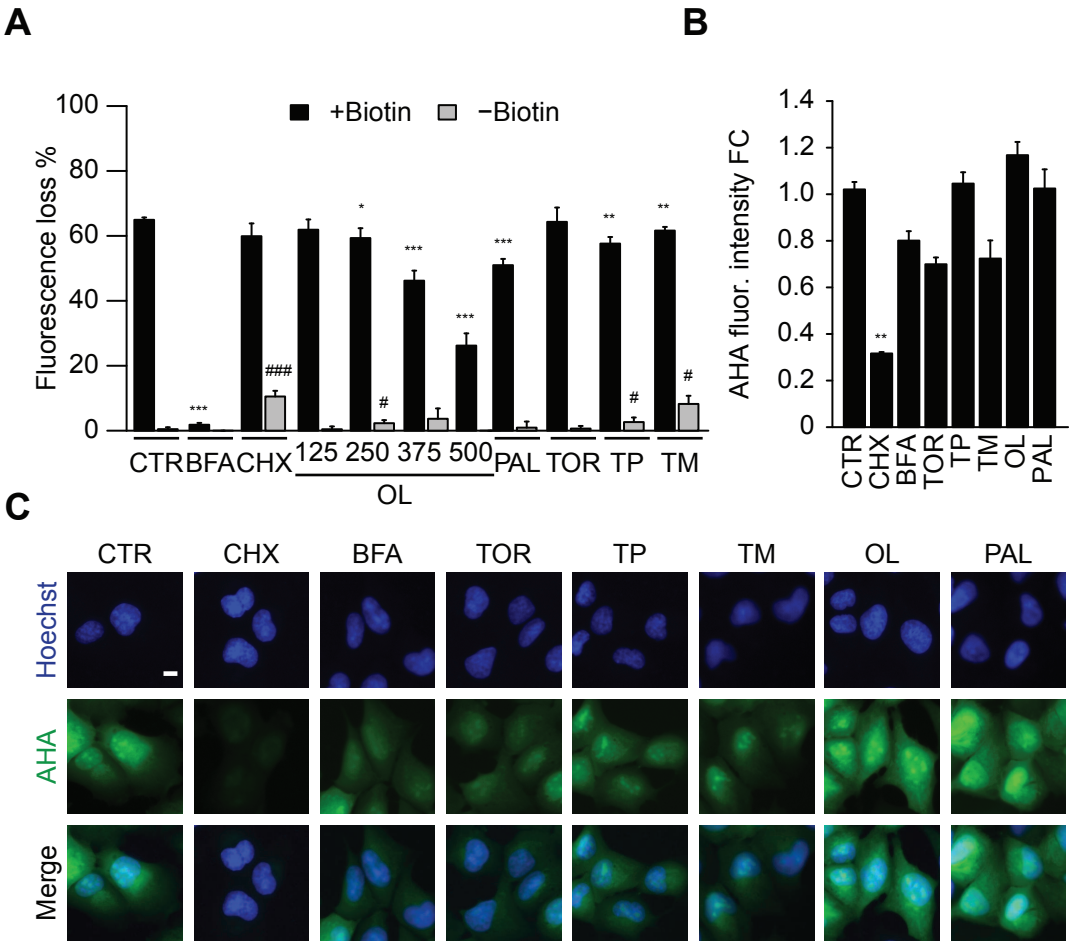
A
B
C
+Biotin
−Biotin
Fluorescence loss %
100
80
60
40
20
0
CTR
BFA
CHX
125 250 375 500
OL
PAL
TOR
TP
TM
AHA fluor. intensity FC
1.4
1.2
1.0
0.8
0.6
0.4
0.2
0
CTR
CHX
BFA
TOR
TP
TM
OL
PAL
Hoechst
AHA
Merge

Figure S7

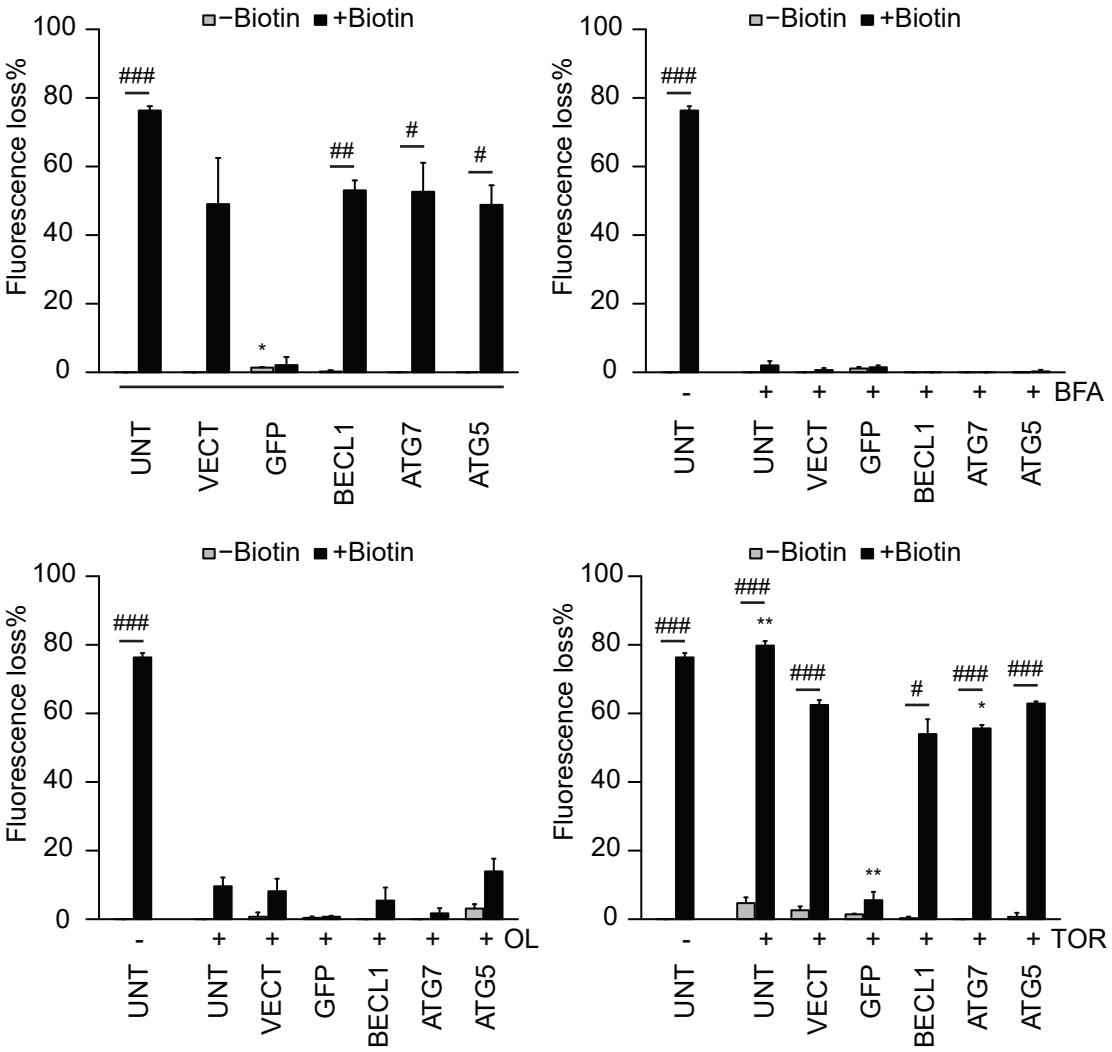
−Biotin
+Biotin
Fluorescence loss%
100
80
60
40
20
0
###
##
#
*
UNT
VECT
GFP
BECL1
ATG7
ATG5
BFA
OL
TOR
**

Figure S8

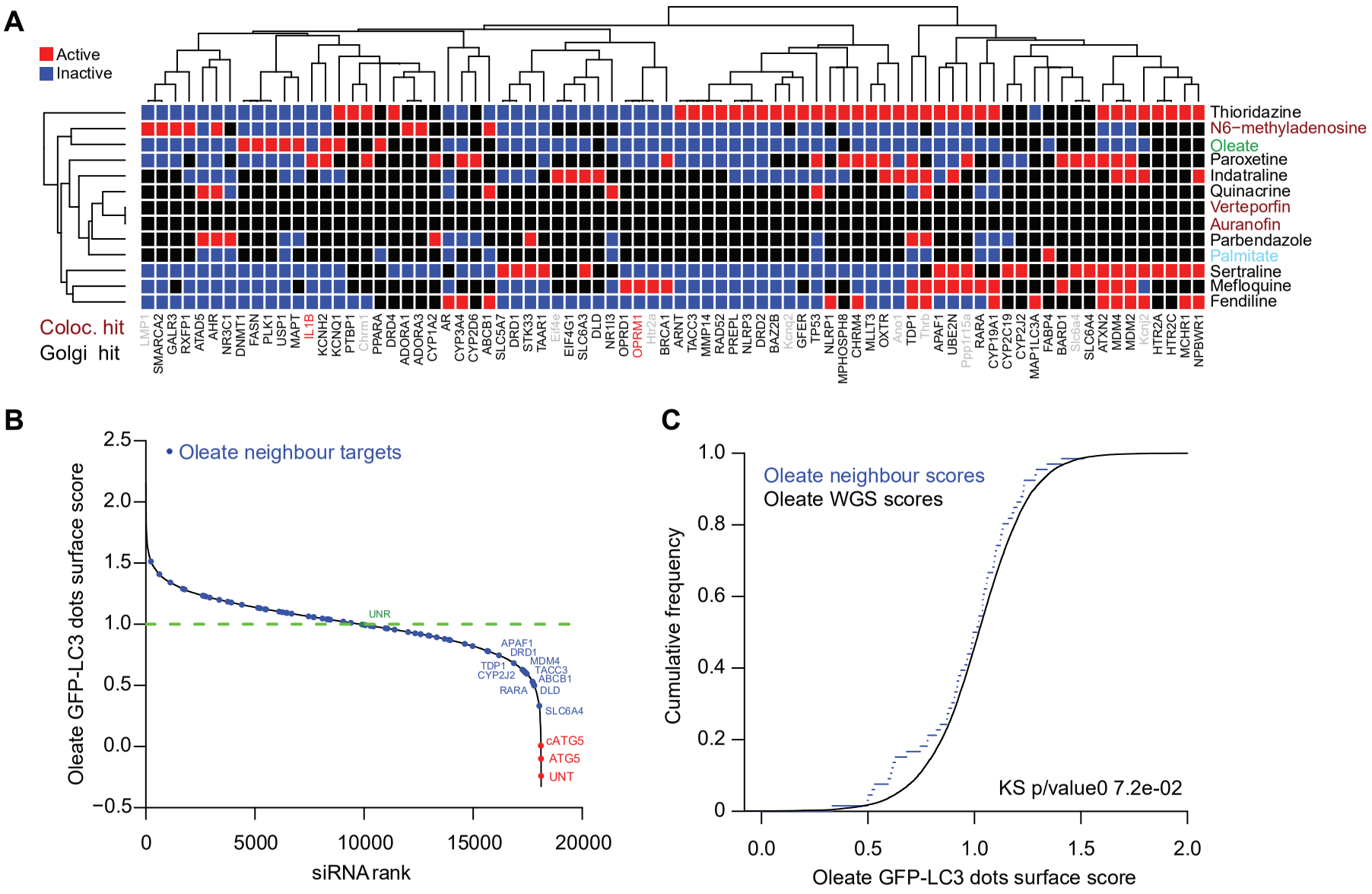
A
Active
Inactive
Thioridazine
N6−methyladenosine
Oleate
Paroxetine
Indatraline
Quinacrine
Verteporfin
Auranofin
Parbendazole
Palmitate
Sertraline
Mefloquine
Fendiline
Coloc. hit
Golgi hit
LMP1 SMARCA2 GALR3 RXFP1 ATAD5 AHR NR3C1 DNMT1 FASN PLK1 USP1 MAPT IL1B KCNH2 KCNQ1 PTBP1 Chrm1 PPARA DRD4 ADORA1 ADORA3 CYP1A2 AR CYP3A4 CYP2D6 ABCB1 SLC5A7 DRD1 STK33 TAAR1 Eif4e EIF4G1 SLC6A3 DLD NR1I3 OPRD1 OPRM1 Htr2a BRCA1 ARNT TACC3 MMP14 RAD52 PREPL NLRP3 DRD2 BAZ2B Kcnq2 GFER TP53 NLRP1 MPHOSPH8 CHRM4 MLLT3 OXTR Ano1 TDP1 Thrb APAF1 UBE2N Ppp1r15a RARA CYP19A1 CYP2C19 CYP2J2 MAP1LC3A FABP4 BARD1 Slc6a4 SLC6A4 ATXN2 MDM4 MDM2 Kcnj2 HTR2A HTR2C MCHR1 NPBWR1
B
• Oleate neighbour targets
Oleate GFP-LC3 dots surface score
siRNA rank
UNR
APAF1
DRD1
MDM4
TACC3
ABCB1
DLD
SLC6A4
TDP1
CYP2J2
RARA
cATG5
ATG5
UNT
C
Oleate neighbour scores
Oleate WGS scores
Cumulative frequency
Oleate GFP-LC3 dots surface score
KS p/value0 7.2e-02

Figure S9

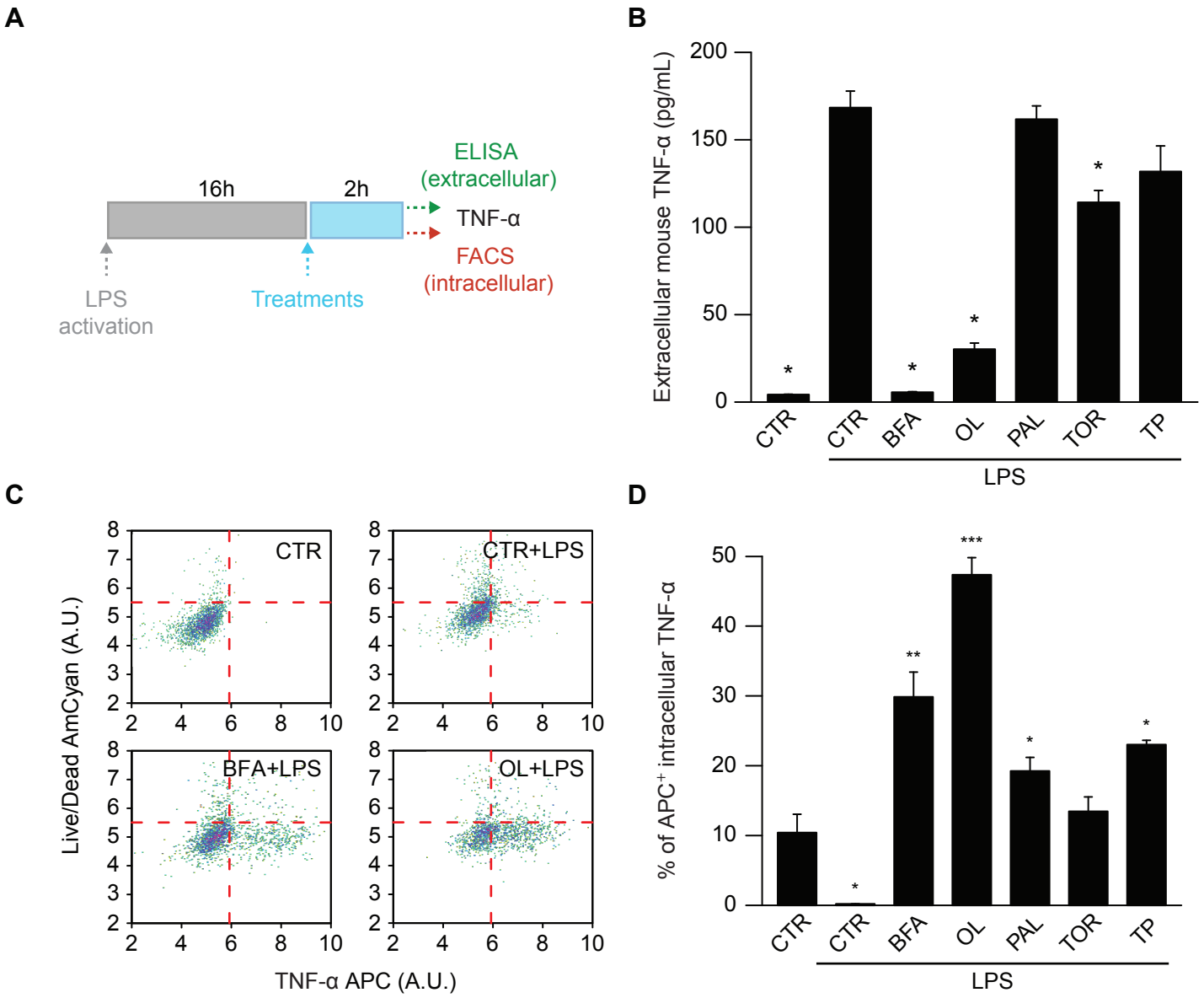
A
16h
2h
ELISA
(extracellular)
TNF-α
FACS
(intracellular)
LPS
activation
Treatments
B
Extracellular mouse TNF-α (pg/mL)
200
150
100
50
0
CTR
CTR
BFA
OL
PAL
TOR
TP
LPS
C
CTR
CTR+LPS
BFA+LPS
OL+LPS
Live/Dead AmCyan (A.U.)
TNF-α APC (A.U.)
D
% of APC+ intracellular TNF-α
50
40
30
20
10
0
CTR
CTR
BFA
OL
PAL
TOR
TP
LPS

Figure S10

Legends to supplemental figures

Figure S1. Oleate-induced effects occur in a dose-dependent fashion in immunoblotting. Human osteosarcoma U2OS wild-type (WT) cells were left untreated (CTR), treated with 0.3 μM torin 1 (TOR), or with a dose-range of OL (125 μM, 250 μM and 375 μM) for 6 h. Cells were harvested and proteins were separated by SDS-polyacrylamide gel electrophoresis and they were then detected by immunoblot. Representative immunoblots are depicted. β-actin levels were monitored to ensure equal loading of lanes, and densitometry was employed to quantify the abundance of lipidated LC3 (LC3-II), normalized to β-actin levels, and phosphorylation of eIF2α (P-eIF2α), normalized to eIF2α levels for one representative experiment.

Figure S2. Oleate-induced effects occur in a dose-dependent fashion in immunofluorescence. (A-H) Human osteosarcoma U2OS cells stably expressing GFP-LC3 were left untreated (CTR), treated with 0.3 μM torin 1 (TOR), 3 μM thapsigargin (TP), 3 μM tunicamycin (TM), a dose-range of OL (125 μM, 250 μM, 375 μM, 500 μM), 500 μM palmitate (PAL), 50 μM cycloheximide (CHX), or 5 μg/mL brefeldin A (BFA) for 6 h and cells were then fixed, their nuclei counterstained with Hoechst 33342 and images were acquired by fluorescence microscopy. The expression of calreticulin (CALR) **(A, B)**, the phosphorylation of eIF2α (P-eIF2α) **(C, D),** LC3 aggregation **(E, F)** and the colocalization between GFP-LC3 and the Golgi marker B4GALT1 **(G, H)** was assessed by fluorescence microscopy. **(A, C, E, G)** Representative images of each assessed parameter are depicted. Scale bar equals 10 μm. **(B, D, F, H)** Quantification of each parameter is represented as means ± SD for one representative experiment, baselines levels were subtracted from data and each condition was compared to the untreated control (*) by means of a Welch's t-test (*$p<0.05$, **$p<0.01$, ***$p<0.001$).

Figure S3. Validation of oleate-induced effect by immunoblot. (A, C) Human osteosarcoma U2OS cells stably expressing GFP-LC3 that were either wild-type or knockout for ATG5 (ATG5$^{-/-}$), **(B, D)** as well as U2OS cells expressing non-phosphorylatable eIF2α (eIF2α^{S51A}) and RFP-LC3 were left untreated (CTR) or were treated with 0.3 μM torin 1 (TOR), 500 μM oleate (OL), 3 μM thapsigargin (TP) or 500 μM palmitate for 6 h. Cells were harvested and proteins were separated by SDS-polyacrylamide gel electrophoresis and they were then detected by immunoblot. Representative immunoblots from one representative experiment are depicted. β-actin levels were monitored to ensure equal loading of lanes, and densitometry was employed to quantify the abundance of lipidated LC3 (LC3-II) and phosphorylation of eIF2α (P-eIF2α), both normalized to β-actin levels.

Figure S4. Implication of eIF2α kinases phosphorylation in the formation of oleate-induced RFP-LC3 puncta. Mouse embryonic fibroblasts (MEF) stably expressing RFP-LC3 either wild-type or knockout for the four eIF2α kinases (eIF2α^{4KO}) were left untreated (CTR) or treated with 500 μM oleate (OL), 0.3 μM torin 1 (TOR) or 3 μM thapsigargin (TP) for 6 h. Cells were fixed, their nuclei counterstained with Hoechst 33342 and images were acquired by fluorescence microscopy. RFP-LC3 dots area, eIF2α phosphorylation (P-eIF2α) (assessed by means of immunofluorescence staining with a phosphoneoepitope-specific eIF2α antibody) and Golgi disruption (evaluating the Golgi surface by means of immunofluorescence staining with anti-B4GALT1 antibody) were quantified. **(A)** Representative images of untreated cells (CTR), cells treated with OL or cells treated with the positive control for each parameter (POS) (*i.e.* TOR for LC3 dots area and TP for P-eIF2α) are depicted. Nuclei marked with Hoechst 33342 are displayed in blue. Scale bar equals 10 μm. **(B)** For each assessed parameter and cell line, data were normalized to the untreated control, fold change (FC) means ± SD for one representative experiment are reported in barcharts depicting the oleate effect together with

appropriate internal controls. Each condition was compared to the untreated control (*) and to the parental cell line (#) by means of a Welch's t-test (*/#$p<0.05$, **/##$p<0.01$, ***/###$p<0.001$).

Figure S5. Subcellular localization of LC3 after exposure to oleate. Human osteosarcoma U2OS cells stably expressing GFP-LC3 were left untreated (CTR) or treated with 5 μg/mL brefeldin A (BFA), 5 μg/mL golgicide A (GCA), 500 μM oleate (OL), 500 μM palmitate (PAL), 2 μM staurosporine (STS), 0.3 μM torin 1 (TOR), 3 μM thapsigargin (TP), or treated with a combination of OL with BFA or GCA for 2 h, 4 h or 6 h. After fixation, nuclear counterstaining with Hoechst 33342 and antibody-mediated staining of trans-Golgi network glycoprotein 46 (TGN46), 130 kDa cis-Golgi matrix protein (GM130), ER-Golgi intermediate compartment-53 (LMAN1) and endoplasmic reticulum calreticulin (CALR), the images at high-resolution were acquired by confocal microscopy at 60X and analyzed to determine the co-occurence of the fluorescent signals. Representative images of untreated cells (CTR), cells treated with OL or PAL and stained with anti-CALR, anti-GM130 and anti-LMAN1 antibody are depicted for each time point for one representative experiment. The background of the images has been removed by subtracting the Gaussian blur of each channel from the original image. Scale bar equals 10 μm.

Figure S6. Oleate induces protein trafficking blockade at the level of *trans*-Golgi network. The retention using selective hooks (RUSH) assay was used to evaluate LC3 voyage from the endoplasmic reticulum (ER). **(A)** Representative time lapse images of untreated cells (CTR) and cells treated with 5 μg/mL brefeldin A (BFA) as positive control for conventional secretion inhibition, 3 μM torin 1 (TOR) and 500 μM oleate (OL) in the presence of avidin (+ Avidin) or biotin (+ Biotin) are depicted. Scale bar equals 10 μm. **(B)** Principle of the RUSH system.

Human osteosarcoma U2OS cells stably expressing a streptavidin binding peptide (SBP) coupled to a GFP-LC3 reporter, that in presence of avidin is retained by a streptavidin (Str) expressing hook targeting via CD74 to the ER. Upon biotin addition, avidin is titrated out and SBP-GFP-LC3 exits the ER due to the binding of biotin to Str. **(C)** U2OS cells co-expressing Str-CD74 and SBP-GFP-LC3 were incubated in the presence of avidin for 12 h, cells were then treated for 2 h in the presence of avidin, live time lapse images were acquired every 30 min for 2 h. Upon biotin addition, images were further acquired every 20 min for 4 h. Cells were then fixed in the presence of Hoechst 33342 and antibody-mediated staining of trans-Golgi network glycoprotein 46 (TGN46) and streptavidin (STR) was performed. **(D)** The dispersion of LC3 was quantified as the dots distance to centroid. The colocalization of LC3/STR **(E)** and LC3/TGN46 **(F)** was quantified by means of the surface overlap coefficient (SOC) and data are displayed as mean ± SD for one representative experiment with p-values calculated using a family-wise Welch's t-test against untreated control (fixed avidin/biotin-treatment,*) or avidin control (fixed drug,#) (*/#$p<0.05$, **/##$p<0.01$, ***/###$p<0.001$). **(G)** Representative high-resolution images of untreated cells (CTR), and cells treated with BFA, TOR and OL are depicted. The background of the images has been removed by subtracting the Gaussian blur of each channel to the original image. Scale bar equals 10 µm.

Figure S7. Evaluation of protein secretion and protein translation. (A) The retention using selective hooks (RUSH) assay was used to evaluate protein secretion from the endoplasmic reticulum (ER). U2OS cells stably co-expressing Str-KDEL and SBP-GFP were left untreated (CTR), or treated with 5 µg/mL brefeldin A (BFA) as positive control for conventional secretion inhibition, 50 µM cycloheximide (CHX), a concentration range (125 µM, 250 µM, 375 µM and 500 µM) of oleate (OL), 500 µM palmitate (PAL), 0.3 µM torin 1 (TOR), 3 µM thapsigargin (TP) or 3 µM tunicamycin (TM) for 2 h in the absence of biotin. Biotin was added without

removing the culture medium and in the end of the live time lapse imaging, cells were fixed in the presence of Hoechst 33342 and the percentage of the fluorescence loss compared to the initial time-point was quantified. Data were displayed as mean ± SD for one representative experiment with p-values calculated using a family-wise Welch's t-test against untreated control (fixed biotin treatment,*) or control without biotin (fixed drug, #) (*/#$p<0.05$, **/##$p<0.01$, ***/###$p<0.001$). **(B, C)** Translation was evaluated by assessing the incorporation of L-azidohomoalanine (AHA) by means of Click-iT® chemistry. Human osteosarcoma U2OS cells were left untreated (CTR) or pre-treated with 50 µM cycloheximide (CHX), 5 µg/mL brefeldin A (BFA), 0.3 µM torin 1 (TOR), 3 µM thapsigargin (TP), 3 µM tunicamycin (TM), 500 µM oleate (OL) or 500 µM palmitate (PAL) in complete medium for 4 h followed by washout. The treatments pursued in methionine-free medium for 30 min and continued for additional 1.5 h in methionine-free medium supplemented with 25 µM L-azidohomoalanine (AHA). After fixation, nuclear counterstaining with Hoechst 33342 and addition of an Alexa Fluor-488-coupled azide, AHA incorporation was assessed by fluorescence microscopy. **(B)** The cytoplasmic AHA intensity was quantified and data were normalized to the untreated control, fold-change means ± SD are reported for one representative experiment. Each condition was compared to the untreated control by means of a Welch's t-test (*$p<0.05$, **$p<0.01$, ***$p<0.001$). **(C)** Representative images of cells treated with the aforementioned compounds are depicted. Scale bar equals 10 µm.

Figure S8. Perturbation of oleate-induced trafficking blockade by gene knockdown. Human osteosarcoma U2OS cells co-expressing streptavidin-KDEL and SBP-GFP were transfected with GFP, BECL1, ATG7, ATG5 siRNAs or VECT (Vector) for 24 h, let adapt for 48 h and then left untreated (CTR) or treated with 5 µg/mL brefeldin A (BFA) as positive control for conventional secretion inhibition, 0.3 µM torin 1 (TOR) or 500 µM oleate (OL) for

2 h in the absence of biotin. Without removing the medium, biotin was added and live time lapse images were acquired every 20 min for 4 h by fluorescence microscopy. The percentage of fluorescence loss compared to the initial time-point was quantified and data were displayed as mean ± SD for one representative experiment with p-values calculated using a family-wise Welch's t-test against vector control (fixed biotin-treatment,*) or control without biotin (fixed siRNA transfection,#) (*/#$p<0.05$, **/##$p<0.01$, ***/###$p<0.001$).

Figure S9. Oleate-mimetics *in silico* gene target analysis. *In silico* analysis of oleate neighbors (reported in black) enriched with neighbors found from a previous work (reported in dark red) gene targets retrieved from the BioAssay database. **(A)** Genetic targets were retained when at least two oleate-neighbors had associated records with at least one of them described as active and gene ontology was performed on selected genes. All the targets are reported in a heatmap and the color code indicates for which drugs a given gene is targeted. Genes reported in red are not expressed in human osteosarcoma U2OS cells and genes reported in grey are not expressed in human. **(B)** Identified genetic targets (reported in blue) were ranked within whole-genome screen results, showing shared hits between the *in silico* and the *in vitro* analyses. UNT represents the untreated control, cATG5 represent an oleate treatment with ATG5 control siRNA, ATG5 represents an oleate treatment with ATG5 siRNA from the whole- genome library and UNR represents an oleate treatment with unrelated control siRNA. **(C)** A Kolmogorov-Smirnov test was performed to compare genetic targets GFP-LC3 dots surface score distribution with the whole genome dataset. Empiric cumulative distributions of mentioned scores are depicted.

Figure S10. Validation of oleate-induced blockade of protein secretion on bone-marrow derived macrophages. (A) Bone marrow-derived macrophages (BMDM) were cultured in

presence of 50 ng/mL M-CSF for 7 days. BMDM were activated with 100 ng/mL lipopolysaccharide (LPS) for 16 h and following left untreated (CTR) or treated in combination with LPS and 5 μg/mL brefeldin A (BFA), 500 μM oleate (OL), 500 μM palmitate (PAL), 0.3 μM torin 1 (TOR) or 3 μM thapsigargin (TP) for 2 h. Cell supernatant was collected to measure the presence of extracellular TNF-α by means of sandwich ELISA and cells were harvested to assess intracellular TNF-α by flow cytometry. **(B)** Quantification of extracellular TNF-α is reported as bar charts with data represented as means ± SD for one representative experiment. Each condition was compared to the untreated control by means of a Welch's t-test (*$p<0.05$, **$p<0.01$, ***$p<0.001$). **(C)** Representative bi-parametric plots of $F4/80^+$ BMDM comparing mean fluorescence intensity of TNF-α APC and LiveDead AmCyan of a set number of events are displayed. **(D)** Quantification of the intracellular TNF-α APC, represented by the percentage of APC^+ among living $F4/80^+$ macrophages, is displayed as bar charts where data are represented as means ± SD for one representative experiment. Each condition was compared to the untreated control by means of a Welch's t-test (*$p<0.05$, **$p<0.01$, ***$p<0.001$).

2. A genome-wide RNA interference screen disentangles the Golgi tropism of LC3

Oleate, the most abundantly occurring cis-unsaturated fatty acid, has the particularity to induce the accumulation of MAP1LC3B/LC3 (microtubule associated protein 1 light chain 3 beta) at the trans-Golgi apparatus. A genome-wide RNA interference screen designed to identify the mechanisms of this LC3 redistribution led to the identification of a BECN1-PIK3C3-independent pathway that, however, requires the ATG12–ATG5 and ATG7-dependent conjugation system, and several genes/proteins involved in endoplasmic reticulum (ER)-to-Golgi anterograde protein transport, as well as the unfolded protein response, including the integrated stress response that results in the phosphorylation of EIF2A/eIF2α (eukaryotic translation initiation factor 2A). Functional experiments revealed that oleate blocks conventional protein secretion, stalling the process at the level of the trans-Golgi network. Oleate-induced blockade of protein secretion occurred even after depletion of ATG5, suggesting that it does not rely on the recruitment of LC3 to the Golgi apparatus (which does require ATG5). Rather, it appears that oleate and other pharmacological inhibitors of protein secretion with a similar mode of action provoke a perturbation of the trans-Golgi compartment that secondarily results in the local enrichment of LC3.

Autophagy. 2021 Mar;17(3):820-822. doi: 10.1080/15548627.2020.1861836. Epub 2020 Dec 23. PMID: 33300447

Autophagy

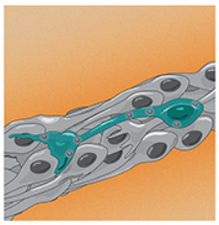

Autophagy

ISSN: (Print) (Online) Journal homepage: https://www.tandfonline.com/loi/kaup20

A genome-wide RNA interference screen disentangles the Golgi tropism of LC3

Giulia Cerrato, Oliver Kepp, Allan Sauvat & Guido Kroemer

To cite this article: Giulia Cerrato, Oliver Kepp, Allan Sauvat & Guido Kroemer (2021) A genome-wide RNA interference screen disentangles the Golgi tropism of LC3, Autophagy, 17:3, 820-822, DOI: 10.1080/15548627.2020.1861836

To link to this article: https://doi.org/10.1080/15548627.2020.1861836

AUTOPHAGY
2021, VOL. 17, NO. 3, 820–822
https://doi.org/10.1080/15548627.2020.1861836

Taylor & Francis
Taylor & Francis Group

AUTOPHAGIC PUNCTUM

A genome-wide RNA interference screen disentangles the Golgi tropism of LC3

Giulia Cerrato[a,b,c], Oliver Kepp [a,b], Allan Sauvat [a,b], and Guido Kroemer [a,b,d,e,f]

[a]Equipe labellisée par la Ligue contre le cancer, Université de Paris, Sorbonne Université, INSERM UMR1138, Centre de Recherche des Cordeliers, Paris, France; [b]Metabolomics and Cell Biology Platforms, Gustave Roussy, Villejuif, France; [c]Faculty of Medicine, Université Paris Sud, Paris Saclay, Kremlin Bicêtre, France; [d]Pôle de Biologie, Hôpital Européen Georges Pompidou, AP-HP, Paris, France; [e]Suzhou Institute for Systems Medicine, Chinese Academy of Medical Sciences, Suzhou, China; [f]Karolinska Institute, Department of Women's and Children's Health, Karolinska University Hospital, Stockholm, Sweden

ABSTRACT

Oleate, the most abundantly occurring *cis*-unsaturated fatty acid, has the particularity to induce the accumulation of MAP1LC3B/LC3 (microtubule associated protein 1 light chain 3 beta) at the *trans*-Golgi apparatus. A genome-wide RNA interference screen designed to identify the mechanisms of this LC3 redistribution led to the identification of a BECN1-PIK3C3-independent pathway that, however, requires the ATG12–ATG5 and ATG7-dependent conjugation system, and several genes/proteins involved in endoplasmic reticulum (ER)-to-Golgi anterograde protein transport, as well as the unfolded protein response, including the integrated stress response that results in the phosphorylation of EIF2A/eIF2α (eukaryotic translation initiation factor 2A). Functional experiments revealed that oleate blocks conventional protein secretion, stalling the process at the level of the *trans*-Golgi network. Oleate-induced blockade of protein secretion occurred even after depletion of ATG5, suggesting that it does not rely on the recruitment of LC3 to the Golgi apparatus (which does require ATG5). Rather, it appears that oleate and other pharmacological inhibitors of protein secretion with a similar mode of action provoke a perturbation of the *trans*-Golgi compartment that secondarily results in the local enrichment of LC3.

ARTICLE HISTORY
Received 23 November 2020
Revised 30 November 2020
Accepted 4 December 2020

KEYWORDS
Autophagy; fatty acids; oleate; protein secretion; unfolded protein response

There are fundamental differences with respect to the effects of distinct classes of fatty acids on cellular and organismal physiology. Saturated fatty acids represented by palmitate, the most abundant endogenous or food-born molecule of this class, induce cellular stress including macroautophagy/autophagy through a canonical pathway that involves the ATG12–ATG5 and ATG7-dependent conjugation system, as well as the BECN1-PIK3C3-dependent pathway. Dietary *cis*-unsaturated fatty acids represented by oleate, the most abundant naturally occurring molecule of this category, induce signs of autophagy such as the redistribution of LC3 to cytoplasmic puncta. Intriguingly, such puncta arise in a BECN1-PIK3C3-independent (non-canonical) fashion, colocalize with the *trans*-Golgi network, and rarely involve two membranes. *Trans*-unsaturated fatty acids such as elaidate (the *trans*-isomer of oleate), which are particularly generated during industrial food processing, induce neither conventional autophagy nor non-conventional LC3 puncta, but rather inhibit the conventional pathway induced by saturated fatty acids, with no effect on non-conventional autophagy triggered by *cis*-unsaturated fatty acids.

Intrigued by these observations, which might be related to the health-improving effects of *cis*-unsaturated fatty acids (and the notorious toxicity of trans-unsaturated fatty acids), we decided to explore the mechanisms causing the oleate-induced relocation of LC3 to the Golgi apparatus [1]. For this, we transfected human osteosarcoma U2OS cells equipped with a green fluorescent protein (GFP)-LC3 biosensor with more than 18,000 distinct siRNAs targeting the majority of the known human mRNAs, and determined their effect on the formation of GFP-LC3 puncta elicited by either oleate or palmitate. The results of this genome-wide screen together with the post-deconvolutional validation, indicate that a series of proteins localized at the Golgi apparatus are indeed selectively required for the oleate-induced accumulation of LC3 at this organelle. These components include several structural Golgi proteins, proteins required for endoplasmic reticulum (ER)-to-Golgi anterograde protein transport (such as COPB1, COPB2 and STX5 [syntaxin 5]), as well as multiple genes associated with ER stress, including genes involved in the integrated stress response (IRS) such as EIF2A/eIF2α (eukaryotic translation initiation factor 2A) and several of its kinases. These findings were validated by using chemical inhibitors of the ER-to-Golgi protein transport (such a brefeldin A or golgicide A) and genetic systems to abolish the IRS (namely, a knockin mutation of *EIF2A* to render it non-phosphorylable, or the knockout of the four known *EIF2A* kinase genes).

We found that oleate affects the subcellular morphology of the Golgi apparatus, correlating with a blockade of conventional (Golgi-dependent) protein secretion that causes secretory cargo to be stalled at the level of the *trans*-Golgi network. This oleate-induced blockade of protein secretion was observed using several different experimental systems including (i) an assay involving a thermosensitive vesicular stomatitis virus G (VSVG) protein that is retained in the ER until the temperature is

CONTACT Oliver Kepp captain.olsen@gmail.com; Guido Kroemer kroemer@orange.fr Equipe labellisée par la Ligue contre le cancer, Université de Paris, Sorbonne Université, INSERM UMR1138, Centre de Recherche des Cordeliers, 15 Rue de l'École de Médecine, 75006 Paris, France

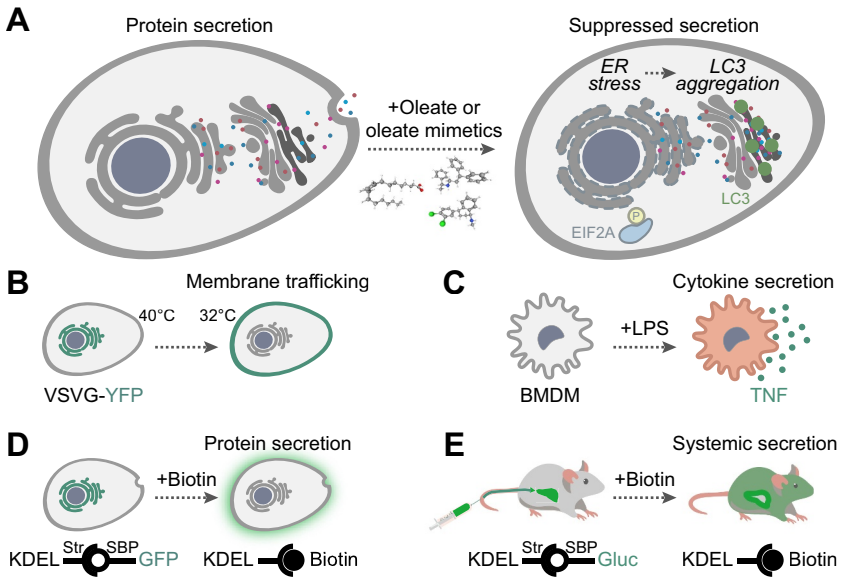

Figure 1. Oleate stalls Golgi-mediated protein secretion. (A) Oleate and its functional analogs, the "oleate mimetics", perturb the Golgi morphology and function downstream of the integrated stress response, secondarily causing the redistribution of LC3 to this organelle. (B-E) Different experimental systems employed to monitor protein secretion. (B) The thermosensitive vesicular stomatitis virus G (VSVG) protein is retained in the endoplasmic reticulum (ER) at 40°C and traffics toward the plasma membrane upon temperature shift to 32°C. (C) TNF (tumor necrosis factor) secretion by bone marrow-derived macrophages (BMDM) is induced by lipopolysaccharide (LPS). (D) The retention using selective hooks (RUSH) technique is employed to sequester in the ER a GFP reporter that can be released with biotin *in vitro*, (E) or a *Gaussia* luciferase (Gluc)-reporter that is expressed in mouse hepatocytes through hydrodynamic injection and can be systemically released with biotin *in vivo*.

lowered, (ii) the lipopolysaccharide-inducible release of TNF/TNFα from activated macrophages, and (iii) a retention using selective hooks (RUSH) system involving, on the one hand, streptavidin (the hook) targeted to the ER lumen and, on the other hand, as a "bait", GFP fused to a streptavidin-binding peptide (SBP) that can be released from streptavidin by adding biotin. This latter system was also introduced into mice after replacing GFP by *Gaussia* luciferase (Gluc). Hydrodynamic injection was used to simultaneously introduce the 2 plasmids into mouse hepatocytes, one coding for an ER-lumenal streptavidin (the hook, in molar excess) and the other coding for the SBP-luciferase fusion protein (the reporter). In this *in vivo* system, protein secretion is orchestrated by biotin (which liberates the SBP-luciferase chimera from its streptavidin hook), and the intraperitoneal administration of oleate (but not palmitate) ahead of biotin, significantly reduces protein secretion.

We next asked whether the blockade of protein secretion by oleate requires the presence of LC3 at the *trans*-Golgi network. However, knockout of *Atg5* abolishes the oleate-induced relocation of LC3 to the Golgi apparatus without restoring protein secretion. This result suggests that an oleate-induced perturbation of the Golgi apparatus causes the relocation of LC3 to this organelle, whereas LC3 is not required for this disturbance to occur. In line with this interpretation, we have found in the past that enforced recruitment of LC3 or SQSTM1 (sequestosome 1) to the Golgi apparatus (induced by means of a chemogenetic system) does not affect the integrity of this organelle. However, we could use the phenotypic alterations induced by oleate with respect to the redistribution of LC3 (fused to red fluorescent protein, RFP) and the Golgi-associated B4GALT1 (beta-1,4-galactosyltransferase 1; fused to GFP) to screen a compound library and to identify pharmacological agents that mimic the cellular alterations induced by oleate. This screen led to the identification of several compounds including two antiprotozoal/antimalarial agents (mefloquine and quinacrine), several serotonin reuptake inhibitors (paroxetine, sertraline, as well as indatraline that also acts on dopamine and norepinephrine reuptake) and the nonselective calcium channel blocker fendiline as "oleate neighbors". These "oleate mimetics" also inhibited conventional protein secretion, supporting the notion that this pathway of Golgi perturbation is indeed of pharmacological relevance (Figure 1).

Disclosure statement

OK and GK are scientific cofounders of Samsara Therapeutics. GK is a scientific cofounder of Therafast Bio.

Funding

GC is supported by a scholarship of the Fondation pour la Recherche Médicale. GK is supported by the Ligue contre le Cancer (équipe labellisée); Agence National de la Recherche (ANR) – Projets blancs; ANR under the frame of E-Rare-2, the ERA-Net for Research on Rare Diseases; AMMICa US23/CNRS UMS3655; Association pour la recherche sur le cancer (ARC); Association "Le Cancer du Sein, Parlons-en!"; Cancéropôle Ile-de-France; Chancelerie des universités de Paris (Legs Poix), Fondation pour la Recherche Médicale (FRM); a donation by Elior; European Research Area Network on Cardiovascular Diseases (ERA-CVD, MINOTAUR); Gustave Roussy Odyssea, the European Union Horizon 2020 Project Oncobiome; Fondation Carrefour; High-end Foreign Expert Program in China [GDW20171100085 and GDW20181100051], Institut National du Cancer (INCa); Inserm (HTE); Institut Universitaire de France; LeDucq Foundation; the LabEx Immuno-Oncology [ANR-18-IDEX-0001]; the RHU Torino Lumière; the Seerave Foundation; the SIRIC Stratified Oncology Cell DNA Repair and Tumor Immune Elimination (SOCRATE); and the SIRIC Cancer Research and Personalized Medicine (CARPEM).

ORCID

Oliver Kepp http://orcid.org/0000-0002-6081-9558
Allan Sauvat http://orcid.org/0000-0001-7076-8638
Guido Kroemer http://orcid.org/0000-0002-9334-4405

Reference

[1] Cerrato G, Leduc M, Müller K, et al. Oleate-induced aggregation of LC3 at the trans-Golgi network is linked to a protein trafficking blockade. Cell Death Differ. in press

3. Live cell imaging of LC3 dynamics

Macroautophagy (hereafter referred to as autophagy) serves the liberation of energy resources through the degradation of cellular components and is characterized by the formation of double-membraned vesicle, commonly referred to as autophagosome. Microtubule-associated proteins 1A/1B light chain 3B (hereafter referred to as LC3) plays a crucial role during autophagosome formation, as cleavage of its immature form and subsequent conjugation to phosphatidylethanolamine facilitates autophagosomal membrane biogenesis. Indeed, the redistribution of green fluorescent protein (GFP)-conjugated LC3 from a diffuse cytosolic pattern into forming autophagosomes constitutes a morphological phenotype (commonly referred to as LC3 *puncta*) applicable to phenotypic analysis. The quantification of LC3 *puncta* in end-point assays has extensively been used in the past, allowing for the identification of autophagy modulators. Here we describe a robust method employing automated confocal live cell imaging for the study of time-resolved LC3 dynamics. Furthermore, this method can be used to differentiate between different phenotypes such as the homogeneous distribution of LC3 *puncta* in the cytoplasm, and the aggregation of LC3 clusters juxtaposed to the nucleus thus allowing for functional predictions.

Methods in Cell Biology. doi.org/10.1016/bs.mcb.2020.10.003. Epub 2021 Mar 1. In press.

Live cell imaging of LC3 dynamics

Giulia Cerrato[1-3], Allan Sauvat[1,2], Oliver Kepp[#1,2], Guido Kroemer[#1,2,4-6]

[1]Equipe labellisée par la Ligue contre le cancer, Université de Paris, Sorbonne Université, INSERM UMR1138, Centre de Recherche des Cordeliers, Paris, France; [2]Metabolomics and Cell Biology Platforms, Gustave Roussy, Villejuif, France; [3]Université Paris Sud, Paris Saclay, Faculty of Medicine, Kremlin Bicêtre, France; [4]Pôle de Biologie, Hôpital Européen Georges Pompidou, AP-HP, Paris, France; [5]Suzhou Institute for Systems Medicine, Chinese Academy of Medical Sciences, Suzhou, China; [6]Karolinska Institutet, Department of Women's and Children's Health, Karolinska University Hospital, Stockholm, Sweden

Correspondence to: **Oliver Kepp** (captain.olsen@gmail.com)
Gustave Roussy Cancer Campus
39, rue Camille Desmoulins
94800 - Villejuif
+33(0)1 42 11 45 16

or Guido Kroemer (kroemer@orange.fr)
Centre de Recherche des Cordeliers
15, rue de l'École de Médecine
75006 - Paris
+33(0) 1 44 27 76 67

Key words: Autophagy, fatty acids, image analysis, LC3 aggregation

Running title: Monitoring autophagy

Conflict of Interest: G.K. and O.K are cofounders of Samsara Therapeutics. G.K. is a founder of everImmune and Therafast Bio

Abstract

Macroautophagy (hereafter referred to as autophagy) serves the liberation of energy resources through the degradation of cellular components and is characterized by the formation of double-membraned vesicle, commonly referred to as autophagosome. Microtubule-associated proteins 1A/1B light chain 3B (hereafter referred to as LC3) plays a crucial role during autophagosome formation, as cleavage of its immature form and subsequent conjugation to phosphatidylethanolamine facilitates autophagosomal membrane biogenesis. Indeed, the redistribution of green fluorescent protein (GFP)-conjugated LC3 from a diffuse cytosolic pattern into forming autophagosomes constitutes a morphological phenotype (commonly referred to as LC3 *puncta*) applicable to phenotypic analysis. The quantification of LC3 *puncta* in end-point assays has extensively been used in the past, allowing for the identification of autophagy modulators. Here we describe a robust method employing automated confocal live cell imaging for the study of time-resolved LC3 dynamics. Furthermore, this method can be used to differentiate between different phenotypes such as the homogeneous distribution of LC3 *puncta* in the cytoplasm, and the aggregation of LC3 clusters juxtaposed to the nucleus thus allowing for functional predictions.

1. Introduction

Autophagy is a cellular mechanism that is evolutionary conserved from yeast to mammals. It is precisely orchestrated by a set of autophagy related genes (ATG) and serves two fundamental purposes. First, autophagy sequesters potentially harmful endogenous and exogenous matter for lysosomal degradation (Galluzzi et al, 2017) thus acting as a clearance mechanism facilitating the reestablishment of homeostasis. Second, autophagy liberates energy resources by the catabolic processing of cellular components in conditions of demand. During this process the autophagic cargo is sequestered by characteristic double-membraned vesicles, referred to as autophagosomes, which eventually fuse with lysosomes, generating so-called autolysosomes (Reggiori & Ungermann, 2017). The process culminates in the degradation of the autophagosomal content by lysosomal hydrolyses, allowing the maintenance or reestablishment of cellular and organismal homeostasis, counteracting the accumulation of detrimental cellular content (such as long-lived, aggregated or misfolded proteins, as well as damaged organelles), regulating cellular growth and providing constituents to sustain anabolic reactions and cellular repair processes (Hansen et al, 2018; Yang & Klionsky, 2010a).

Monitoring the morphological phenotypes of autophagy allowed to characterize the autophagic machinery in its molecular details and, unquestionably, the most widely employed marker for the assessment of autophagy is microtubule-associated proteins 1A/1B light chain 3B (MAP1LC3B), best known as LC3 (Kabeya et al, 2000). Indeed, LC3 plays a crucial role in the autophagic cascade during the elongation and closure of the autophagosomal membrane precursor, the phagophore (also called isolation membrane) (Axe et al, 2008). The coordinated action of a subset of ATG proteins allows the cytosolic cleavage of LC3 precursor (pro-LC3) into its mature form LC3-I that lipidates (i.e. the conjugation to phosphatidylethanolamine) into the forming phagophore and is further converted into the autophagosomal membrane-associated form LC3-II (Yang & Klionsky, 2010b).

Various physiological and pathological states can induce autophagy, and this can be reproduced and studied *in vitro* by monitoring the lipidation of LC3 employing protein chromatography and immunoblot (taking advantage of the 2 kDa difference in the molecular weight of LC3-I and its cleaved form LC3-II, resulting in the higher electrophoretic motility of the latter) (Klionsky et al, 2012) or immunofluorescence microscopy combined with a green fluorescent protein (GFP)-LC3 protein chimera (Bravo-San Pedro et al, 2017; Klionsky et al, 2012).

During the past decade several GFP-LC3-based high throughput screens were conducted and facilitated the identification of novel autophagy activating and inhibiting drugs from large chemical libraries (Hale et al, 2016; Orvedahl et al, 2011; Zhang et al, 2007). Nevertheless, these end-point assays lack the possibility to monitor the evolution of LC3 lipidation over time. Compared to the

study of fixed cells, live cell imaging where an environmental controlled chamber enables the regulation of temperature, humidity and gas composition, is less prone to false negative results as the induction of autophagy can be measured at multiple time points for an extended duration, even if caution needs to be taken to avoid cellular injury due to repetitive imaging. The live observation of LC3 lipidation enriches the understanding of the autophagic process by adding information on its dynamics. In addition, it is interesting to note that during the induction of autophagy LC3 *puncta* form in rather distinct ways, with peculiar phenotypes varying from a diffuse cytoplasmic distribution of small bright dots, to a perinuclear aggregation of LC3 (Niso-Santano et al, 2015).

Here, we describe a detailed workflow for the acquisition and analysis of GFP-LC3 *puncta* formation in human cancer cell lines stably expressing GFP-LC3 by live cell confocal microscopy.

2. Material

2.1 Disposables

1. Polystyrene flasks (75 cm^2) for cell culture
2. 96-well cell imaging plates with clear bottom for cell culture (*e.g.* 96-well µClear imaging plates, Greiner Bio-One, Kremsmünster, Austria)
3. 96-well conical bottom plates
4. Conical polypropylene centrifuge tube (15 mL)
5. Pipet-aid and serological pipettes (5 and 10 mL)
6. Aspiration pipettes (2 mL)
7. Micropipettes (0.2-2 µL, 1-20 µL, 20-200 µL, 200-1000 µL), multichannel pipet (20-200 µL) and corresponding sterile tips
8. Sterile and disposable pipetting reservoirs (25 mL)
9. Cell counting slides

2.2 Equipment

1. Humidified cell culture incubator allowing for standard cell culture conditions (37°C, 5% CO_2)
2. Standard bench top centrifuge
3. Cell culture laminar flow hood
4. Hemocytometer
5. Automated high-content confocal microscope (*e.g.* robot-assisted Molecular Devices IXM-C running MetaXpress® software, Molecular Devices, Sunnyvale, CA, USA) equipped with a 20 x PlanAPO objective (*e.g.* Nikon, Tokyo, Japan) with the appropriate filter set (*e.g.* FITC)
6. Environmental controller for live cell imaging (*e.g.* Ibidi gas mixer, Gräfelfing, Germany) and environmental heater
7. R software (freely available at https://www.r-project.org/) for image segmentation and data analysis

2.3 Reagents

1. Culture medium adequate for the cell type containing serum (*e.g.* 10% fetal bovine serum) and enriched with required supplements such as 1% non-essential amino acids, 1 mM sodium pyruvate, 10 mM 2-[4-(2- hydroxyethyl)piperazin-1-yl]ethanesulfonic acid (HEPES) buffer
2. 0.25% Trypsin solution with EDTA (0.05%)

3. 0.4% Trypan blue solution
4. Chemical compounds to test properly diluted (*e.g*. torin 1, #4247, Sigma-Aldrich, St Louis, MO, USA; bafilomycin A1, #1334, Tocris Bioscience (Bristol, UK); oleate and palmitate, Larodan, Malmö, Sweden)

3. Methods

3.1 Cell culture routine

1. Human osteosarcoma U2OS cells stably expressing GFP-LC3 (see *Note 1*) are routinely maintained in a humidified cell culture incubator in standard culture conditions (at 37°C, under 5% CO_2) and cultured in Dulbecco's modified Eagle's medium (DMEM) medium enriched with 10% fetal bovine serum (FBS), 1 mM sodium pyruvate and 10 mM HEPES buffer (see *Note 2*).
2. After thawing, a one-week recovery time is needed for cells to readapt to standard culture conditions and for allowing them to re-establish normal cell cycles.
3. 75-80% confluence is the optimal limit condition for maintenance culture (see *Note 3*). Cell culture routine requires to discard exhausted culture medium by vacuum aspiration and detach the cell monolayer with 2 mL of pre-warmed 0.25% trypsin/EDTA (see *Notes 4-6*).
4. Once detached, a twofold-volume of pre-warmed culture medium is added to the flask in order to stop enzymatic activity of trypsin and cell suspension is collected into a 15 mL centrifuge tube.
5. Centrifugation at 400 g at room temperature for 5 minutes allows cell pellet formation and consequent medium/trypsin removal. Cells are then suspended in culture medium, diluted and reseeded in a new flask for cell culture (see *Note 7*). This procedure allows to properly maintain cells in culture as well as to prepare cells for experimental procedures (see *Notes 8-9*).

3.2 Cell seeding

1. Density of GFP-LC3 U2OS cells (whose suspension is prepared as described in paragraph 3.1.5), is evaluated by trypan blue staining (1:1 trypan blue – cell suspension ratio) in a hemocytometer using a light microscope, allowing for the exclusion of dead cells in the counting step (see *Note 10*).
2. Cell suspension is adjusted in order to seed 1.2 x 10^4 cells in 200 μL of culture medium per well in 96-well imaging plates and then poured in a 25 mL disposable reservoir allowing for cell seeding by multichannel pipet (see *Notes 11-13*).

3. Cells are incubated at 37°C, under 5% CO_2 in a humidified incubator for at least 12 h to let them adapt and adhere (see *Note 14*).

3.3 Cell treatment

1. Cellular confluence needs to be checked via light microscopy to assure that it is suitable for treatment (see *Note 15*).
2. The batch of compounds to be tested (*e.g*. 0.3 µM torin 1, 500 µM oleate, 500 µM palmitate, 0.1 µM bafilomycin A1) are diluted to their final concentration in complete culture medium and vortexed to assure proper homogeneity (see *Notes 16-17*).
3. To allow a convenient workflow, diluted compounds can be arrayed in a 96-well plate with conical bottom and directly pipetted from there (see *Note 18*).

3.4 Live cell imaging

1. Immediately after treatment, the plate is placed in an automated confocal microscope and the acquisition is launched by the MetaXpress® software. In the microscope chamber, the atmospheric environment is controlled by means of a gas mixer (for humidity and to maintain 5% CO_2), as well as a heater to allow for 37°C culture condition (see *Notes 19-20*).
2. A minimum of 4 fields of view per well is acquired with a 20X objective using a GFP filter set (see *Note 21*). The time of exposure is adjusted according to fluorescence intensity, Z-stacks are defined (*e.g* 5 plans with a z-step of 1.5µm, then projected using a best-focus algorithm) and the time-lapse interval is configured (*e.g*. one image every 30 minutes for a 6 h duration) (see *Notes 22-23*).

3.5 Image analysis and features extraction

1. Images are analyzed with the freely available software R (https://www.r-project.org), integrated with the *MetaxpR package* (https://github.com/kroemerlab/MetaxpR) for the collection of data generated by the Molecular Devices MetaXpress® software and the *EBImage package* (see *Note 24*) from the Bioconductor repository (https://www.bioconductor.org), as well as the *RBioFormats* and the *MorphR* packages (https://github.com/aoles/RBioFormats, https://github.com/kroemerlab/MorphR) for image processing. A customized image segmentation algorithm (https://github.com/kroemerlab/NNRS) was developed to compute the features of interest. The principal steps of the segmentation workflow are listed below.

a. For the detection of cells the primary region of interest (ROI) is defined by a polygon mask contouring cellular dimension. To this aim images are transformed and processed by a normalization step where pixel intensities are scaled between 0 and 1, corrected by histogram scaling according to control conditions (based on image percentiles) for each timepoint, thereafter cleaned from bright structures by top hat-filtering, and finally enhanced by a sigmoidal transformation to increase the signal to noise ratio. Automated image thresholding for binarization is ultimately applied using the Otsu's method (see *Note 25*).
b. Cellular objects are separated by black top hat filtering to detect elements that are smaller than the structuring element (circular, 5 pixel radius) and darker than their surrounding. The obtained image is then subjected to a sigmoidal normalization, binarized by the Otsu's method, and filtered for elements larger than 100 pixels. The resulting mask is removed from the previously obtained cell mask, enabling the detection of cellular borders by means of a watershed transformation, thus separating adjacent cells and generating one mask per cell (see *Note 26*).
c. Dots are detected by white top-hat filtering allowing to select elements that are smaller than the structuring element and brighter than their surroundings (see *Note 27*). In order to include differently sized dots, a set of different kernel values is applied. As described above, sigmoidal normalization, followed by the Otsu's thresholding method, enables the detection of bright fluorescent dots, generating a supplemental dots mask within the cellular mask.

2. After exclusion of cellular debris and dead cells (see *Note 28*), the area (dots surface) and number (dots count) of GFP-LC3 *puncta* (**Fig. 1A,B**) are computed within each cellular mask and is then graphically depicted on a time scale. In addition, the centroid of the GFP-LC3 dots in each cell is computed (see *Note 29*), and the distance of each dot to this centroid (dots distance to centroid) is calculated (**Fig. 1C**). In order to balance values from less bright dots with brighter ones, a pondered mean of dots distances by dots integrated intensities is applied.

3.6 Data interpretation

The live monitoring of LC3 lipidation allows to characterize two relevant features. First, the LC3 dot aggregation dynamics can be resolved in time allowing to discriminate a slowly evolving aggregation and a rapid induction of GFP-LC3 *puncta*. Second, GFP-LC3 *puncta* can be dispersed in the cytoplasm or aggregate in clusters. A high number of bright fluorescent *puncta* (dots count), coupled with a low dots surface can be interpreted as a spread phenotype, such as it is the case after treatment with torin 1 (**Fig. 1D**). This holds true also in the presence of bafilomycin A1, a potent V-ATPase

inhibitor commonly used to determine the lysosome-dependent degradation (**Fig. 1D**). Conversely, the aggregation of GFP-LC3 *puncta* in clusters results in an increase in dots surface such as it can be observed after palmitate treatment (**Fig. 1D**). In addition, the "Dots distance to centroid" is yet another parameter that can be used to identify the aggregation of GFP-LC3 *puncta* as it is the case for example after oleate treatment (**Fig. 1D**). This parameter yields in higher values when *puncta* are spread and lower values for their aggregation.

4. Concluding Remarks

One of the most widely used technique to monitor autophagy is to follow by fluorescence microscopy the relocation of fluorescent protein-tagged LC3 (such as GFP-LC3) from the cytoplasm to a punctiform localization during its lipidation into autophagosomal membranes. The aggregation of GFP-LC3 in cytoplasmic *puncta* can be interpreted as an induction of autophagy yet autophagic flux needs to be confirmed with additional assays (Klionsky et al, 2012). The method described here provides a reliable approach to monitor LC3 lipidation in live cell confocal microscopy, documenting the dynamics of the phenomenon. Furthermore, the analysis of number and appearance of GFP-LC3 *puncta* together with their mean distance to centroid allows to distinguish among rather different phenotypes of LC3 aggregation, hence opening new approaches for the characterization, and classification, of distinct compounds that might yield insights into their distinct mode of action.

Acknowledgments: GK is supported by the Ligue contre le Cancer (équipe labellisée); Agence National de la Recherche (ANR) – Projets blancs; ANR under the frame of E-Rare-2, the ERA-Net for Research on Rare Diseases; Association pour la recherche sur le cancer (ARC); Cancéropôle Ile-de-France; Chancellerie des universités de Paris (Legs Poix), Fondation pour la Recherche Médicale (FRM); a donation by Elior; European Research Area Network on Cardiovascular Diseases (ERA-CVD, MINOTAUR); Gustave Roussy Odyssea, the European Union Horizon 2020 Project Oncobiome; Fondation Carrefour; High-end Foreign Expert Program in China (GDW20171100085 and GDW20181100051), Institut National du Cancer (INCa); Inserm (HTE); Institut Universitaire de France; LeDucq Foundation; the LabEx Immuno-Oncology; the RHU Torino Lumière; the Seerave Foundation; the SIRIC Stratified Oncology Cell DNA Repair and Tumor Immune Elimination (SOCRATE); and the SIRIC Cancer Research and Personalized Medicine (CARPEM).

Notes

1. A detailed method on how to efficiently transfect U2OS cells with the GFP-LC3 chimera is described in (Bravo-San Pedro et al, 2017). Any other cell line expressing a fluorescent tagged-LC3 can be used.
2. Culture medium and supplements should be adapted according to cell type following the official recommendations of the America Type Culture Collection (ATCC, Manassas, VA, USA) and stored at 4°C. Antibiotics such as 100 U/mL penicillin or 100 µg/mL streptomycin can be added during cell culture routine.
3. If cells are too confluent, signaling networks are altered and this can potentially lead to metabolic perturbations in cells and cause cell death. For the U2OS cell line, it is recommended to pass cells at 1:10 ratio twice per week, and this should be adapted in function of each specific cell line doubling time. Conversely, if the desired confluence is not reached, cells should not be detached but medium should be renewed until proper confluence is achieved.
4. All reagents used for cell culture need to be pre-warmed at 37°C. Furthermore, optimal activity of trypsin is achieved at 37°C, hence pre-warmed trypsin expedites cell detachment.
5. It is preferable to use commercially available trypsin products such as TrypLE™ Express (Gibco®, Thermo Fisher Scientific, Carlsbad, CA, USA), as self-prepared solutions could possibly be less efficient and less stable.
6. Trypsin incubation time can vary depending on the cell type. For U2OS cells 3 minutes are enough to obtain a complete cell detachment. Long term incubation with trypsin (>10 minutes), needs to be avoided as it stripes cell surface proteins and lead to cell death.
7. Cell passage number is an important parameter to be aware of and should not exceed 20, as random mutations can accumulate the longer cells are in culture, cell signaling and proliferation rates may change and these stresses can cause the expression of aberrant phenotypes.
8. Culture medium for experimental procedures must be antibiotics-free to avoid any possible risk of chemical interference.
9. A fluorescence loss can be observed in successive cell passages, it is thus recommended to periodically restart cell culture from early passage stocks.
10. Alternative to automated counting, reusable cell counting slides can be used.
11. Culture medium without phenol red should be preferred, as this will reduce background during image acquisition.
12. 96-well plates are preferable for experiments with extended duration as the high volume of liquid allows minimizing effects caused by evaporation, but 384-well plates can be employed for short time courses.

13. In order to homogeneously seed cells, the cell suspension in the reservoir needs to be well mixed during the seeding operation.
14. Cellular adhesion time can vary depending on the cell type. Incomplete adhesion may result in increased sensitivity of cells to experimental interventions.
15. Cellular confluence needs to be optimized in function of the doubling time of the selected cell line, as confluence in untreated controls should not exceed 80% at the end time-point of the assay. Furthermore, confluence needs to be the same in every experimental repetition, as this influences cellular interaction as well as drug availability. Variations may have opposing impacts on cells, hence leading to unreproducible or misleading results.
16. Torin 1 is diluted in DMSO at 0.3 mM and aliquots in 0.5 mL Eppendorf tubes are stocked at -20°C. Freeze-thaw cycles need to be limited to not alter the physicochemical properties of the molecule.
17. Oleate and palmitate are diluted in ethanol at 100 mM and stocked at 4°C. More generally, if fatty acids diluted in ethanol are used, special care needs to be taken for their correct dilution in cell culture medium. Both fatty acid and culture medium need to be pre-warmed at 37°C. The solution needs to be repeatedly mixed by shaking the tubes or by up-and-down movements with a pipette. The 1x solution needs to be maintained at 37°C at all times and used immediately after preparation.
18. Soluble compounds can be prepared at a 2x concentration in complete medium in a 96-well with conical bottom. The cell monolayer can be firstly filled with 100 µL of complete medium, and 100 µL of compound solution at 2x concentration can be added. This procedure prevents cells from drying and hence it allows avoiding undesirable cellular stress.
19. Environmental conditions need to be set in advance in order to ensure their correct stabilization within the microscope.
20. If massive evaporation occurs, the addition of mineral oil on top of the culture medium can limit the phenomenon, without compromising gas exchanges.
21. The acquisition of 4 fields of view allows to analyze a representative number of cells.
22. The distance among different planes needs to be adjusted according to cellular morphology and plate dimensions. Acquire Z-stacks allows to obtain a composite image, corresponding to a projection (maximal or searching for the best focus) of multiple images acquired at different Z positions. The resulting composite image has a greater depth of field compared to any of the individual images.
23. Timepoints and duration of the acquisition can be set according to the dynamics of the phenomenon under study. For faster aggregations, it is preferable to set shorter timepoints.

24. The *EBImage library* contains built-in functions for image processing and analysis, especially in the context of high throughput microscopy-based cellular assays.
25. The Otsu's method is a binarization algorithm that in image analysis is employed to perform automatic image thresholding. It returns an intensity threshold that separates pixels in two classes by maximizing the intra-class variance. The pixels whose gray level is less than this computed threshold will be assigned to the background, else to the foreground.
26. In this setting, a nuclear staining as a seed to propagate the mask is not required.
27. The structuring element need to be carefully selected, as its choice will influence which elements are extracted, i.e. the bigger the kernel, the larger will be the extracted elements.
28. Debris, and dead cells (detected by their increased fluorescence intensity coupled with a decreased area) need to be removed from the data set as these can interfere with the results.
29. The centroid is defined as the average position of all points of an object, also called barycenter of a shape. In this setting, all detected dots within a single cellular mask are accounted to find their internal centroid.

Legends to Figure

Figure 1. Quantification of LC3 lipidation. Human osteosarcoma U2OS cells stably expressing GFP-LC3 were seeded into 96-well plates and allowed to adhere. The day after, cells were left untreated (CTR) or treated with 0.3 μM torin 1 (TOR), 500 μM oleate (OL), 500 μM palmitate (PAL), and 0.1 μM bafilomycin a1 (BAF). Immediately after treatment, cells were subjected to live cell imaging for 6 h at 30 minutes intervals, inside a chamber of an automated confocal microscope under environmental controlled conditions. For each timepoint, dots surface **(A)**, dots count **(B)** and dots distance to centroid **(C)** were quantified and the mean ± standard deviation is displayed over time for each treatment condition. **(D)** Representative time lapse images of untreated cells (CTR) and cells treated with TOR, OL, PAL and BAF are depicted. The scale bar corresponds to 10 μm.

References

Axe EL, Walker SA, Manifava M, Chandra P, Roderick HL, Habermann A, Griffiths G, Ktistakis NT (2008) Autophagosome formation from membrane compartments enriched in phosphatidylinositol 3-phosphate and dynamically connected to the endoplasmic reticulum. *The Journal of cell biology* **182:** 685-701

Bravo-San Pedro JM, Pietrocola F, Sica V, Izzo V, Sauvat A, Kepp O, Maiuri MC, Kroemer G, Galluzzi L (2017) High-Throughput Quantification of GFP-LC3(+) Dots by Automated Fluorescence Microscopy. *Methods in enzymology* **587:** 71-86

Galluzzi L, Baehrecke EH, Ballabio A, Boya P, Bravo-San Pedro JM, Cecconi F, Choi AM, Chu CT, Codogno P, Colombo MI, Cuervo AM, Debnath J, Deretic V, Dikic I, Eskelinen EL, Fimia GM, Fulda S, Gewirtz DA, Green DR, Hansen M et al (2017) Molecular definitions of autophagy and related processes. *The EMBO journal* **36:** 1811-1836

Hale CM, Cheng Q, Ortuno D, Huang M, Nojima D, Kassner PD, Wang S, Ollmann MM, Carlisle HJ (2016) Identification of modulators of autophagic flux in an image-based high content siRNA screen. *Autophagy* **12:** 713-726

Hansen M, Rubinsztein DC, Walker DW (2018) Autophagy as a promoter of longevity: insights from model organisms. *Nature reviews Molecular cell biology* **19:** 579-593

Kabeya Y, Mizushima N, Ueno T, Yamamoto A, Kirisako T, Noda T, Kominami E, Ohsumi Y, Yoshimori T (2000) LC3, a mammalian homologue of yeast Apg8p, is localized in autophagosome membranes after processing. *The EMBO journal* **19:** 5720-5728

Klionsky DJ, Abdalla FC, Abeliovich H, Abraham RT, Acevedo-Arozena A, Adeli K, Agholme L, Agnello M, Agostinis P, Aguirre-Ghiso JA, Ahn HJ, Ait-Mohamed O, Ait-Si-Ali S, Akematsu T, Akira S, Al-Younes HM, Al-Zeer MA, Albert ML, Albin RL, Alegre-Abarrategui J et al (2012) Guidelines for the use and interpretation of assays for monitoring autophagy. *Autophagy* **8:** 445-544

Niso-Santano M, Malik SA, Pietrocola F, Bravo-San Pedro JM, Marino G, Cianfanelli V, Ben-Younes A, Troncoso R, Markaki M, Sica V, Izzo V, Chaba K, Bauvy C, Dupont N, Kepp O, Rockenfeller P, Wolinski H, Madeo F, Lavandero S, Codogno P et al (2015) Unsaturated fatty acids induce non-canonical autophagy. *The EMBO journal* **34:** 1025-1041

Orvedahl A, Sumpter R, Jr., Xiao G, Ng A, Zou Z, Tang Y, Narimatsu M, Gilpin C, Sun Q, Roth M, Forst CV, Wrana JL, Zhang YE, Luby-Phelps K, Xavier RJ, Xie Y, Levine B (2011) Image-based genome-wide siRNA screen identifies selective autophagy factors. *Nature* **480:** 113-117

Reggiori F, Ungermann C (2017) Autophagosome Maturation and Fusion. *Journal of molecular biology* **429:** 486-496

Yang Z, Klionsky DJ (2010a) Eaten alive: a history of macroautophagy. *Nature cell biology* **12:** 814-822

Yang Z, Klionsky DJ (2010b) Mammalian autophagy: core molecular machinery and signaling regulation. *Current opinion in cell biology* **22:** 124-131

Zhang L, Yu J, Pan H, Hu P, Hao Y, Cai W, Zhu H, Yu AD, Xie X, Ma D, Yuan J (2007) Small molecule regulators of autophagy identified by an image-based high-throughput screen. *Proceedings of the National Academy of Sciences of the United States of America* **104:** 19023-19028

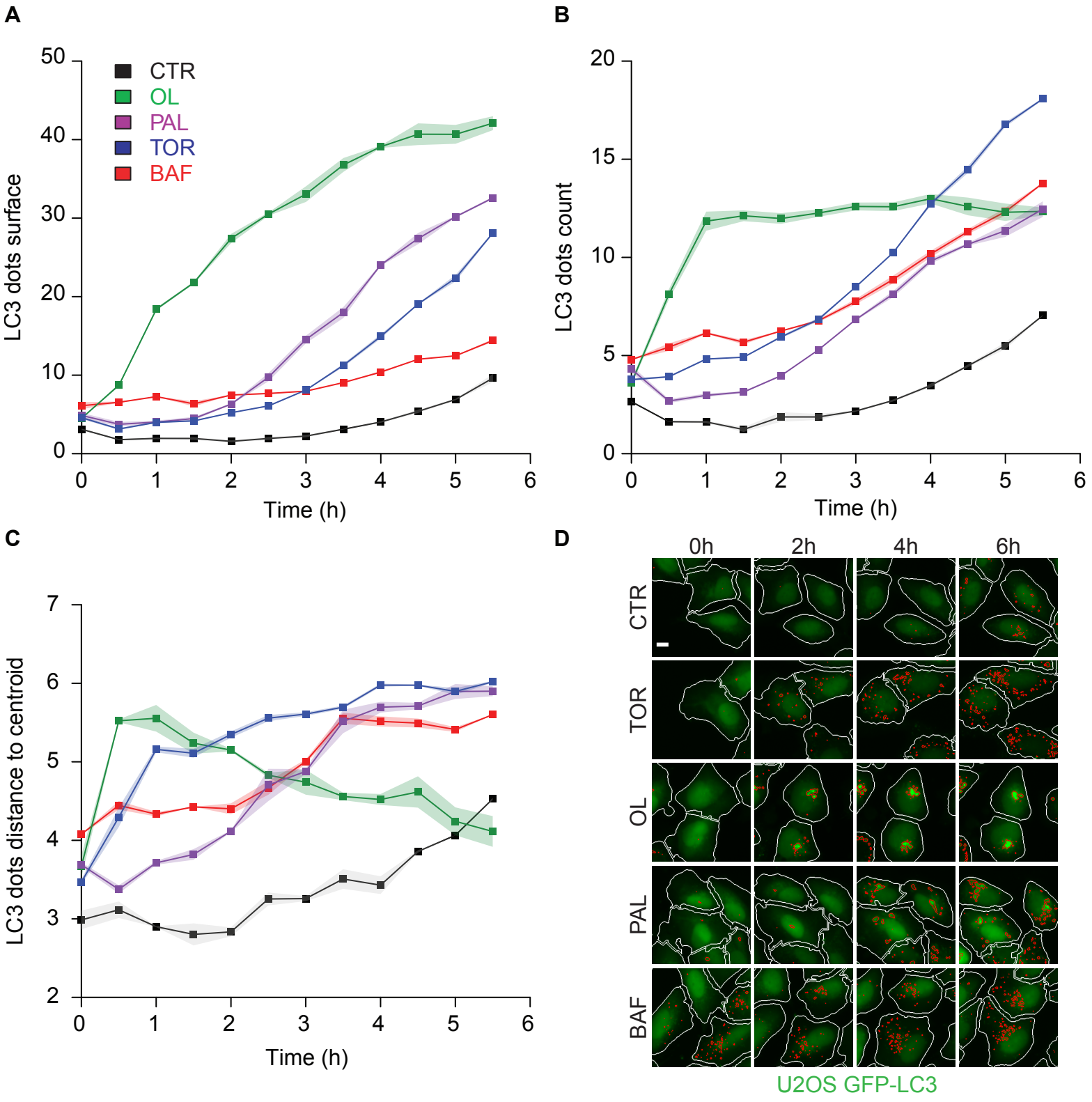
A
B
C
D
CTR
OL
PAL
TOR
BAF
LC3 dots surface
LC3 dots count
LC3 dots distance to centroid
Time (h)
0h
2h
4h
6h
U2OS GFP-LC3

Figure 1

Discussion

Saturated and unsaturated FAs exhibit a fundamental and significant degree of variation with respect to their effects at the cellular level as well as on the physiology of the organism. Notorious negative effects of *trans*-unsaturated/saturated FAs and the well-known health-promoting effects of *cis*-unsaturated FAs open interesting challenges in deepening the knowledge about their differential mechanistic at multiple levels, with the aim to potentially relate beneficial or toxic effects to specific pathways. Despite some inconsistencies among studies, potentially explained by variations in experimental conditions, such as cell type, final concentration of FA, its solvent and the duration of the exposure, it is clear that there is a profound relationship among different classes of FAs with the induction of autophagy. It is paramount to deepen this link, notably as autophagy has recently been recognized as the principal mechanism preventing cardiovascular aging.

In particular, LC3 lipidation induced by FAs follows rather divergent molecular pathways (Bankaitis, 2015). Palmitate, the major FA in the saturated class, induces autophagy via the classical pathway involving all conjugation systems, while *trans*-unsaturated FAs such as elaidate, the *trans* isomer of oleate, induce neither conventional nor non-canonical autophagy, but rather exert an inhibitory effect on autophagy activated by saturated FA (Sauvat et al, 2018). In contrast, oleate, the most abundant endogenous and dietary *cis*-unsaturated FA, displays clearly different cellular effects from other FAs at multiple levels. Our team postulated that oleate induces a form of autophagy that bypasses the classical machinery, naming it as a non-canonical pathway where only a subset of ATG genes is required (Niso-Santano et al, 2015a). On the one hand, the ATG genes involved in the conjugation of LC3 to PE such as ATG5, ATG7 and ATG12 are involved in the process, while a series of genes related to phosphatidylinositol phosphorylation such as ATG14, BECN1 and PIK3C3 are not required.

In this research study, the short-term exposure to oleate was shown to be an exquisite trigger of an atypical aggregation of LC3 at the level of the trans-Golgi network (TGN), as demonstrated by colocalization assessments at high-resolution. Furthermore, a genome-wide screen performed on human osteosarcoma cells allowed to extend and refine the notion of non-canonical autophagy by pointing out specific genes selectively required for

oleate, but not for palmitate, to induce the peculiar redistribution of LC3 at the TGN. Among those, a key role is played by genes involved in Golgi-related transport processes, including several structural Golgi proteins and proteins required for Golgi budding / vesicular trafficking, as well as genes associated with the UPR. These findings opened insights to further explore the capacity of oleate to interfere with canonical protein secretion and to induce signs of ER stress. For the first, multiple experimental systems validated the ability of oleate to block conventional and Golgi-dependent protein secretion, causing secretory cargo to be stalled within the TGN, while palmitate did not show remarkable impacts. This effect was observed using a classical assay involving a YFP-coupled VSVG protein that is retained in the ER until the temperature is lowered, despite its non-physiological temperature. The same was confirmed when protein traffic was synchronized in the RUSH assay via the reversible retention of an ER-streptavidin-fused hook with a SBP-GFP-coupled reporter, whose travel toward the extracellular space is engaged only when biotin is added to the system. Oleate-induced effect on both these systems was comparable: it did not affect the movement of the protein of interest from the ER to the Golgi, but caused a protein secretion blockade at the level of the Golgi, yet in the same compartment that accumulates LC3. In more physiological settings, oleate-induced inhibition of protein secretion was confirmed with the reduced release, accompanied with an intracellular increase, of TNF-α production triggered by LPS in macrophages. One further development that could be done is to administrate oleate and LPS to mice and measure the cytokines content in the plasma. To obtain insights at the organismal level, we designed and applied the RUSH system *in vivo*. The tailor-made *in vivo* RUSH system validated the differential impact of oleate and palmitate when measuring the secretion of luciferase from hepatocytes, where only oleate induced a significant decreasing effect. This underscores that oleate, but not palmitate, influences protein secretion at physiologically relevant concentrations, nevertheless it remains unclear and to be demonstrated whether the dietary ingestion of oleate- or palmitate-rich food exerts the same effects. From a mechanistic point of view, oleate blockade of protein secretion follows a different mechanism than BFA, a fungal metabolite known to dissociate the COPI complex and other peripheral proteins from the Golgi causing a disassembly of the Golgi structure. Indeed, oleate causes a partial shrinkage of the

organelle with a parallel accumulation of proteins, (including LC3) in its inside, while BFA or the knockdown of subunits of the COPI complex, its pharmacological target, prevents the oleate-induced LC3 relocation. A clear proof of these diverse phenomena is shown here by means of the RUSH system, in which BFA induced secretory cargo to be stacked at the level of the ER, while oleate blockade happened in the TGN, supporting the assumption that these secretion inhibitory effects differently impact the secretory route.

In the context of UPR, oleate, as most autophagy activating agents do, induced the phosphorylation of eIF2α and this was shown not be a requirement for the Golgi morphology perturbation but only for LC3 aggregation, as demonstrated in cells carrying a non-phosphorylable mutant of eIF2α (S51A), as well as in cells subjected to a quadruple knockout of the four eIF2α kinases. As the biochemical composition as well as the biophysical properties of cellular endomembranes differ from one to another, some insights about the targeted effect of oleate on the TGN could be related to its particular membrane properties. With the current data, it is difficult to unravel the cause effect relationship between LC3 aggregation and the observed inhibition of protein secretion blockade. To gain further insights, the mechanistic exploration could be deepened by simultaneously monitoring LC3 and secretory proteins in a dual RUSH-system where trafficking kinetics could be followed at high resolution.

Since oleate is located at the crossroads of various metabolic pathways, we conducted a screen on a chemical library that allowed the identification of pharmacological agents which that affect cellular physiology similarly to oleate, named “oleate mimetics”. Indeed, these chemically unrelated agents induce the redistribution of LC3 to the Golgi and simultaneously stall protein secretion at that level, as validated by another independent screen. Among those, there is for example the anti-malarian agent mefloquine and the anti-protozoal quinacrine, both causing lysosomal alkalization, displaying similar structural features and employed in the treatment of systemic autoimmunity. It can be speculated that the inhibition of pro-inflammatory cytokine secretion is mediated by a blockade in the Golgi compartment. Following the same logics, several oleate mimetics such as the antidepressant patoxetine, sertraline and indatraline block the reuptake of neurotransmitters at the presynaptic neuronal membrane, thereby increasing the available extracellular concentration of

neurotransmitters and improving the signaling transmission among cells. Nevertheless, this was shown to exert an effect on pancreatic cells resulting in insulin secretion inhibition whereas oleate was shown to exert a pro-secretion effect on this population of cells. While a clear link between the 'oleate-phenotype' and protein secretion modulation can be postulated, it is however delicate to exert a structure/function relationship, as the sole shared molecular feature of "oleate mimetics" is their lipophilicity.

Another systematic screen conducted on a library composed of the most common FAs aimed to compare the cellular effects of the different classes of FAs, showed that *cis*- and *trans*-unsaturated FAs exerted different effects in the context of autophagy, UPR and Golgi perturbation, with *trans*-unsaturated FAs shown to be less active in eliciting cellular stress than the other two categories (Sauvat et al, 2018).

In this context, a first attempt to link multiple cellular parameters related to those processes and the properties of FA molecules including the length of their carbon chain, as well as the presence of *cis*- or *trans*-unsaturations, led to a pattern of differences. Systemic analysis underscored that the number of cis-unsaturated bonds (NCU) present in the molecule strongly correlated with its biological activity, thus indicating that the geometry of the molecule plays a crucial role in the observed cellular effects (Sauvat et al, 2018). To go further with this characterization and get more detailed molecular insights, here a dual machine learning approach was used to (1) identify FAs presenting a cellular phenotype close to the one triggered by oleate, by means of convolutional neural network applied on GFP-LC3/RFP-GALT1 micrographs and (2) retrieve relevant molecular descriptors that explained such a classification, using random forest algorithm (data not shown). The parameters that impacted the classification most, turned out to be two descriptors related to the spatial 3D "density" (i.e. the distribution of Euclidian distances between atom pairs) of the molecule. Even if it remains to be shown, one could speculate that such molecular specificity would be linked, at least partially, to the NCU. In an attempt to classify FAs based on these two parameters, three separated classes were identified: one including oleate and other *cis*-unsaturated FAs, another one including saturated and *trans*-unsaturated FAs and a third group which seem to be composed of FA exerting an over killing effect such as α-linolenic acid and linoleic acid. Thus, the deeper investigation of properties influencing cellular effects

showed that those are not dependent on the *cis*- and *trans*- configuration only but rely on deeper molecular characteristics.

At this point, it appears difficult to draw conclusions on the precise mechanism of action of the different FAs, as well as of the unrelated agents exerting similar cellular effects, even if perturbation of protein secretion turned out to be a common point. The potential specific molecular mechanisms behind the harmful effects of *trans*-unsaturated FAs and the positive effects elicited by *cis*-unsaturated FAs are still obscure, even though an interesting step forward in their characterization has been made.

With the aim to extend the research on autophagy even further, we are now developing a label-free phenotypical analysis that relies on brightfield imaging combined with an analysis using a deep convolutional neural network, a branch of machine learning that permits to assess and interpret features in complex images.

Finally, it remains an attractive challenge and it requires further mechanistic studies to fully clarify the exact role of FAs dictating peculiar cellular pathways and untangle the complex network of cellular events. In addition, further studies are needed also to clarify the contribution of edible oils on human health. Indeed, gaining a deeper understanding on FAs mechanistic may create new therapeutic windows for cardiovascular health, as well as for the treatment of diseases characterized by disrupted lipid metabolism or deregulated protein trafficking.

Collaborations

In addition to this project, I have participated to other research works, method protocol writings and reviews which led to the following publications:

- Sauvat A, Chen G, Muller K, Tong M, Aprahamian F, Durand S, Cerrato G, Bezu L, Leduc M, Franz J, Rockenfeller P, Sadoshima J, Madeo F, Kepp O, Kroemer G. **Trans-fats inhibit autophagy induced by saturated fatty acids**. *EBioMedicine*. 2018. 30:261-272

- Sauvat A, Cerrato G, Humeau J, Leduc M, Kepp O, Kroemer G. **High-throughput label-free detection of inhibited DNA-to-RNA transcription using brightfield microscopy and deep neural networks**. *Comput Biol Med*. In press

- Humeau J, Sauvat A, Cerrato G, Xie W, Loos F, Iannantuoni F, Bezu L, Lévesque S, Paillet J, Pol J, Leduc M, Zitvogel L, de Thé H, Kepp O, Kroemer G. **Inhibition of transcription by dactinomycin reveals a new characteristic of immunogenic cell stress**. *EMBO Mol Med*. 2020. 12(5):e11622

- Cerrato G, Humeau J, Sauvat A, Kepp O, Kroemer G. **Assessment of transcription inhibition as a stress pathway characteristic of immunogenic cell death**. *Methods Cell Biol*. 2021. Accepted for publication

- Cerrato G, Liu P, Martins I, Kepp O, Kroemer G. **Quantitative determination of phagocytosis by bone marrow-derived dendritic cells via imaging flow cytometry**. *Methods Enzymol*. 2020. 632:27-37

- Humeau J, Leduc M, Cerrato G, Loos F, Kepp O, Kroemer G. **Phosphorylation of eukaryotic initiation factor-2α (eIF2α) in autophagy**. *Cell Death Dis*. 2020. 11(6):433

- Bezu L, Kepp O, Cerrato G, Pol J, Fucikova J, Spisek R, Zitvogel L, Kroemer G, Galluzzi L. **Trial watch: Peptide-based vaccines in anticancer therapy**. *Oncoimmunology*. 2018. 7(12):e1511506

- Forveille S, Leduc M, Sauvat A, Cerrato G, Kroemer G, Kepp O. **High throughput screening for autophagy.** Methods Cell Biol. 2021. Online ahead of print

- Le Naour J, Liu P, Zhao L, Adjemian S, Sztupinszki Z, Taieb J, Mulot C, Silvin A, Dutertre CA, Ginhoux F, Sauvat A, Cerrato G, Castoldi F, Martins I, Stoll G, Paillet J, Mangane K, Richter C, Kepp O, Maiuri MC, Pietrocola F, Vandenabeele P, André F, Delaloge S, Szallasi Z, Laurent-Puig P, Zucman-Rossi J, Zitvogel L, Pol JG, Vacchelli E, Kroemer G. **A TLR3 ligand reestablishes chemotherapeutic responses in the context of FPR1 deficiency**. *Cancer Discov*. 2020. Online ahead of print

Bibliography

Adolf F, Rhiel M, Reckmann I, Wieland FT (2016) Sec24C/D-isoform-specific sorting of the preassembled ER-Golgi Q-SNARE complex. *Molecular biology of the cell* **27:** 2697-2707

Alers S, Loffler AS, Wesselborg S, Stork B (2012) Role of AMPK-mTOR-Ulk1/2 in the regulation of autophagy: cross talk, shortcuts, and feedbacks. *Molecular and cellular biology* **32:** 2-11

Andrei C, Margiocco P, Poggi A, Lotti LV, Torrisi MR, Rubartelli A (2004) Phospholipases C and A2 control lysosome-mediated IL-1 beta secretion: Implications for inflammatory processes. *Proceedings of the National Academy of Sciences of the United States of America* **101:** 9745-9750

Anez-Bustillos L, Dao DT, Fell GL, Baker MA, Gura KM, Bistrian BR, Puder M (2018) Redefining essential fatty acids in the era of novel intravenous lipid emulsions. *Clinical nutrition* **37:** 784-789

Arsov I, Adebayo A, Kucerova-Levisohn M, Haye J, MacNeil M, Papavasiliou FN, Yue Z, Ortiz BD (2011) A role for autophagic protein beclin 1 early in lymphocyte development. *Journal of immunology* **186:** 2201-2209

Assali EA, Shlomo D, Zeng J, Taddeo EP, Trudeau KM, Erion KA, Colby AH, Grinstaff MW, Liesa M, Las G, Shirihai OS (2019) Nanoparticle-mediated lysosomal reacidification restores mitochondrial turnover and function in beta cells under lipotoxicity. *FASEB journal : official publication of the Federation of American Societies for Experimental Biology* **33:** 4154-4165

Axe EL, Walker SA, Manifava M, Chandra P, Roderick HL, Habermann A, Griffiths G, Ktistakis NT (2008) Autophagosome formation from membrane compartments enriched in phosphatidylinositol 3-phosphate and dynamically connected to the endoplasmic reticulum. *The Journal of cell biology* **182:** 685-701

Baldwin TA, Ostergaard HL (2002) The protein-tyrosine phosphatase CD45 reaches the cell surface via golgi-dependent and -independent pathways. *The Journal of biological chemistry* **277:** 50333-50340

Bankaitis VA (2015) Unsaturated fatty acid-induced non-canonical autophagy: unusual? Or unappreciated? *The EMBO journal* **34:** 978-980

Bard F, Malhotra V (2006) The formation of TGN-to-plasma-membrane transport carriers. *Annual review of cell and developmental biology* **22:** 439-455

Barlowe C, Orci L, Yeung T, Hosobuchi M, Hamamoto S, Salama N, Rexach MF, Ravazzola M, Amherdt M, Schekman R (1994) COPII: a membrane coat formed by Sec proteins that drive vesicle budding from the endoplasmic reticulum. *Cell* **77:** 895-907

Barlowe C, Schekman R (1993) SEC12 encodes a guanine-nucleotide-exchange factor essential for transport vesicle budding from the ER. *Nature* **365:** 347-349

Bayer EA, Wilchek M (1990) Biotin-binding proteins: overview and prospects. *Methods in enzymology* **184:** 49-51

Beck R, Rawet M, Wieland FT, Cassel D (2009) The COPI system: molecular mechanisms and function. *FEBS letters* **583:** 2701-2709

Ben-Dror K, Birk R (2019) Oleic acid ameliorates palmitic acid-induced ER stress and inflammation markers in naive and cerulein-treated exocrine pancreas cells. *Bioscience reports* **39**

Bendinelli B, Masala G, Saieva C, Salvini S, Calonico C, Sacerdote C, Agnoli C, Grioni S, Frasca G, Mattiello A, Chiodini P, Tumino R, Vineis P, Palli D, Panico S (2011) Fruit, vegetables, and olive oil and risk of coronary heart disease in Italian women: the EPICOR Study. *The American journal of clinical nutrition* **93:** 275-283

Bermudez B, Lopez S, Ortega A, Varela LM, Pacheco YM, Abia R, Muriana FJ (2011) Oleic acid in olive oil: from a metabolic framework toward a clinical perspective. *Current pharmaceutical design* **17:** 831-843

Berryman S, Brooks E, Burman A, Hawes P, Roberts R, Netherton C, Monaghan P, Whelband M, Cottam E, Elazar Z, Jackson T, Wileman T (2012) Foot-and-mouth disease virus induces autophagosomes during cell entry via a class III phosphatidylinositol 3-kinase-independent pathway. *Journal of virology* **86:** 12940-12953

Bester D, Esterhuyse AJ, Truter EJ, van Rooyen J (2010) Cardiovascular effects of edible oils: a comparison between four popular edible oils. *Nutrition research reviews* **23:** 334-348

Bhattacharya A, Prakash YS, Eissa NT (2014) Secretory function of autophagy in innate immune cells. *Cellular microbiology* **16:** 1637-1645

Biden TJ, Boslem E, Chu KY, Sue N (2014) Lipotoxic endoplasmic reticulum stress, beta cell failure, and type 2 diabetes mellitus. *Trends in endocrinology and metabolism: TEM* **25:** 389-398

Bogani P, Galli C, Villa M, Visioli F (2007) Postprandial anti-inflammatory and antioxidant effects of extra virgin olive oil. *Atherosclerosis* **190:** 181-186

Boncompain G, Divoux S, Gareil N, de Forges H, Lescure A, Latreche L, Mercanti V, Jollivet F, Raposo G, Perez F (2012) Synchronization of secretory protein traffic in populations of cells. *Nature methods* **9:** 493-498

Boncompain G, Perez F (2013) The many routes of Golgi-dependent trafficking. *Histochemistry and cell biology* **140:** 251-260

Boncompain G, Perez F (2014) Synchronization of secretory cargos trafficking in populations of cells. *Methods in molecular biology* **1174:** 211-223

Bonifacino JS, Glick BS (2004) The mechanisms of vesicle budding and fusion. *Cell* **116:** 153-166

Brandizzi F, Barlowe C (2013) Organization of the ER-Golgi interface for membrane traffic control. *Nature reviews Molecular cell biology* **14:** 382-392

Bravo-San Pedro JM, Pietrocola F, Sica V, Izzo V, Sauvat A, Kepp O, Maiuri MC, Kroemer G, Galluzzi L (2017) High-Throughput Quantification of GFP-LC3(+) Dots by Automated Fluorescence Microscopy. *Methods in enzymology* **587:** 71-86

Brouwer IA, Wanders AJ, Katan MB (2013) Trans fatty acids and cardiovascular health: research completed? *European journal of clinical nutrition* **67:** 541-547

Brownell KD, Pomeranz JL (2014) The trans-fat ban--food regulation and long-term health. *The New England journal of medicine* **370:** 1773-1775

Buchberger A, Bukau B, Sommer T (2010) Protein quality control in the cytosol and the endoplasmic reticulum: brothers in arms. *Molecular cell* **40:** 238-252

Bugliani M, Mossuto S, Grano F, Suleiman M, Marselli L, Boggi U, De Simone P, Eizirik DL, Cnop M, Marchetti P, De Tata V (2019) Modulation of Autophagy Influences the Function and Survival of Human Pancreatic Beta Cells Under Endoplasmic Reticulum Stress Conditions and in Type 2 Diabetes. *Frontiers in endocrinology* **10:** 52

Calder PC (2015) Functional Roles of Fatty Acids and Their Effects on Human Health. *JPEN Journal of parenteral and enteral nutrition* **39:** 18S-32S

Chang YC, Lin CW, Chang YS, Chen PH, Li CY, Wu WC, Kao YH (2020) Monounsaturated oleic acid modulates autophagy flux and upregulates angiogenic factor production in human retinal pigment epithelial ARPE-19 cells. *Life sciences* **259:** 118391

Chen D, Chen X, Li M, Zhang H, Ding WX, Yin XM (2013a) CCCP-Induced LC3 lipidation depends on Atg9 whereas FIP200/Atg13 and Beclin 1/Atg14 are dispensable. *Biochemical and biophysical research communications* **432:** 226-230

Chen D, Gibson ES, Kennedy MJ (2013b) A light-triggered protein secretion system. *The Journal of cell biology* **201:** 631-640

Cheng CI, Lee YH, Chen PH, Lin YC, Chou MH, Kao YH (2017) Free Fatty Acids Induce Autophagy and LOX-1 Upregulation in Cultured Aortic Vascular Smooth Muscle Cells. *Journal of cellular biochemistry* **118:** 1249-1261

Cheong H, Lindsten T, Wu J, Lu C, Thompson CB (2011) Ammonia-induced autophagy is independent of ULK1/ULK2 kinases. *Proceedings of the National Academy of Sciences of the United States of America* **108:** 11121-11126

Chiu YJ, Cai W, Shih YR, Lian I, Lo YH (2016) A Single-Cell Assay for Time Lapse Studies of Exosome Secretion and Cell Behaviors. *Small* **12:** 3658-3666

Choi AM, Ryter SW, Levine B (2013) Autophagy in human health and disease. *The New England journal of medicine* **368:** 651-662

Chu KY, O'Reilly L, Mellet N, Meikle PJ, Bartley C, Biden TJ (2019) Oleate disrupts cAMP signaling, contributing to potent stimulation of pancreatic beta-cell autophagy. *The Journal of biological chemistry* **294:** 1218-1229

Cocucci E, Racchetti G, Meldolesi J (2009) Shedding microvesicles: artefacts no more. *Trends in cell biology* **19:** 43-51

Codogno P, Mehrpour M, Proikas-Cezanne T (2011) Canonical and non-canonical autophagy: variations on a common theme of self-eating? *Nature reviews Molecular cell biology* **13:** 7-12

Craig-Schmidt MC (2006) World-wide consumption of trans fatty acids. *Atherosclerosis Supplements* **7:** 1-4

Cuervo AM, Dice JF (1996) A receptor for the selective uptake and degradation of proteins by lysosomes. *Science* **273:** 501-503

Danino H, Ben-Dror K, Birk R (2015) Exocrine pancreas ER stress is differentially induced by different fatty acids. *Experimental cell research* **339:** 397-406

de Souza RJ, Mente A, Maroleanu A, Cozma AI, Ha V, Kishibe T, Uleryk E, Budylowski P, Schunemann H, Beyene J, Anand SS (2015) Intake of saturated and trans unsaturated fatty acids and risk of all cause mortality, cardiovascular disease, and type 2 diabetes: systematic review and meta-analysis of observational studies. *Bmj* **351:** h3978

Demirtas L, Guclu A, Erdur FM, Akbas EM, Ozcicek A, Onk D, Turkmen K (2016) Apoptosis, autophagy & endoplasmic reticulum stress in diabetes mellitus. *The Indian journal of medical research* **144:** 515-524

Dhayal S, Zummo FP, Anderson MW, Thomas P, Welters HJ, Arden C, Morgan NG (2019) Differential effects of saturated and unsaturated fatty acids on autophagy in pancreatic beta-cells. *Journal of molecular endocrinology* **63:** 285-296

Donaldson JG, Cassel D, Kahn RA, Klausner RD (1992) ADP-ribosylation factor, a small GTP-binding protein, is required for binding of the coatomer protein beta-COP to Golgi membranes. *Proceedings of the National Academy of Sciences of the United States of America* **89:** 6408-6412

Dupont N, Jiang S, Pilli M, Ornatowski W, Bhattacharya D, Deretic V (2011) Autophagy-based unconventional secretory pathway for extracellular delivery of IL-1beta. *The EMBO journal* **30:** 4701-4711

Duran JM, Anjard C, Stefan C, Loomis WF, Malhotra V (2010) Unconventional secretion of Acb1 is mediated by autophagosomes. *The Journal of cell biology* **188:** 527-536

Efeyan A, Sabatini DM (2010) mTOR and cancer: many loops in one pathway. *Current opinion in cell biology* **22:** 169-176

EFSA (2011) EFSA Panel on Dietetic Products, Nutrition and Allergies (NDA). Scientific Opinion on the substantiation of health claims related to polyphenols in olive and protection of LDL particles from oxidative damage (ID 1333, 1638, 1639, 1696, 2865), maintenance of normal blood HDL cholesterol concentrations (ID 1639). *EFSA Journal* **9(4):2033**

Enot DP, Niso-Santano M, Durand S, Chery A, Pietrocola F, Vacchelli E, Madeo F, Galluzzi L, Kroemer G (2015) Metabolomic analyses reveal that anti-aging metabolites are depleted by palmitate but increased by oleate in vivo. *Cell cycle* **14:** 2399-2407

Fader CM, Colombo MI (2009) Autophagy and multivesicular bodies: two closely related partners. *Cell death and differentiation* **16:** 70-78

FAO (2010) Fats and fatty acids in human nutrition. Report of an expert consultation. *FAO food and nutrition paper* **91:** 1-166

FDA (2018) FDA Completes Review of Qualified Health Claim Petition for Oleic Acid and the Risk of Coronary Heart Diseas.

Ferrara LA, Raimondi AS, d'Episcopo L, Guida L, Dello Russo A, Marotta T (2000) Olive oil and reduced need for antihypertensive medications. *Archives of internal medicine* **160:** 837-842

Florey O, Gammoh N, Kim SE, Jiang X, Overholtzer M (2015) V-ATPase and osmotic imbalances activate endolysosomal LC3 lipidation. *Autophagy* **11:** 88-99

Galluzzi L, Baehrecke EH, Ballabio A, Boya P, Bravo-San Pedro JM, Cecconi F, Choi AM, Chu CT, Codogno P, Colombo MI, Cuervo AM, Debnath J, Deretic V, Dikic I, Eskelinen EL, Fimia GM, Fulda S, Gewirtz DA, Green DR, Hansen M et al (2017) Molecular definitions of autophagy and related processes. *The EMBO journal* **36:** 1811-1836

Galluzzi L, Green DR (2019) Autophagy-Independent Functions of the Autophagy Machinery. *Cell* **177:** 1682-1699

Galluzzi L, Pietrocola F, Levine B, Kroemer G (2014) Metabolic control of autophagy. *Cell* **159:** 1263-1276

Gao P, Bauvy C, Souquere S, Tonelli G, Liu L, Zhu Y, Qiao Z, Bakula D, Proikas-Cezanne T, Pierron G, Codogno P, Chen Q, Mehrpour M (2010) The Bcl-2 homology domain 3 mimetic gossypol induces both Beclin 1-dependent and Beclin 1-independent cytoprotective autophagy in cancer cells. *The Journal of biological chemistry* **285:** 25570-25581

Gardella S, Andrei C, Ferrera D, Lotti LV, Torrisi MR, Bianchi ME, Rubartelli A (2002) The nuclear protein HMGB1 is secreted by monocytes via a non-classical, vesicle-mediated secretory pathway. *EMBO reports* **3:** 995-1001

Ge L, Melville D, Zhang M, Schekman R (2013) The ER-Golgi intermediate compartment is a key membrane source for the LC3 lipidation step of autophagosome biogenesis. *eLife* **2:** e00947

Ghebreyesus TA, Frieden TR (2018) REPLACE: a roadmap to make the world trans fat free by 2023. *Lancet* **391:** 1978-1980

Ginter E, Simko V (2016) New data on harmful effects of trans-fatty acids. *Bratislavske lekarske listy* **117:** 251-253

Glick BS, Luini A (2011) Models for Golgi traffic: a critical assessment. *Cold Spring Harbor perspectives in biology* **3:** a005215

Gorlich D, Rapoport TA (1993) Protein translocation into proteoliposomes reconstituted from purified components of the endoplasmic reticulum membrane. *Cell* **75:** 615-630

Griffiths G, Pfeiffer S, Simons K, Matlin K (1985) Exit of newly synthesized membrane proteins from the trans cisterna of the Golgi complex to the plasma membrane. *The Journal of cell biology* **101:** 949-964

Griffiths G, Simons K (1986) The trans Golgi network: sorting at the exit site of the Golgi complex. *Science* **234:** 438-443

Grishchuk Y, Ginet V, Truttmann AC, Clarke PG, Puyal J (2011) Beclin 1-independent autophagy contributes to apoptosis in cortical neurons. *Autophagy* **7:** 1115-1131

Grotemeier A, Alers S, Pfisterer SG, Paasch F, Daubrawa M, Dieterle A, Viollet B, Wesselborg S, Proikas-Cezanne T, Stork B (2010) AMPK-independent induction of autophagy by cytosolic Ca2+ increase. *Cellular signalling* **22:** 914-925

Guasch-Ferre M, Hu FB, Martinez-Gonzalez MA, Fito M, Bullo M, Estruch R, Ros E, Corella D, Recondo J, Gomez-Gracia E, Fiol M, Lapetra J, Serra-Majem L, Munoz MA, Pinto X, Lamuela-Raventos RM, Basora J, Buil-Cosiales P, Sorli JV, Ruiz-Gutierrez V et al (2014) Olive oil intake and risk of cardiovascular disease and mortality in the PREDIMED Study. *BMC medicine* **12:** 78

Guo Y, Yang F, Tang X (2017) An Overview of Protein Secretion in Yeast and Animal Cells. *Methods in molecular biology* **1662:** 1-17

Hadj Ahmed S, Kharroubi W, Kaoubaa N, Zarrouk A, Batbout F, Gamra H, Najjar MF, Lizard G, Hininger-Favier I, Hammami M (2018) Correlation of trans fatty acids with the severity of coronary artery disease lesions. *Lipids in health and disease* **17:** 52

Hale CM, Cheng Q, Ortuno D, Huang M, Nojima D, Kassner PD, Wang S, Ollmann MM, Carlisle HJ (2016) Identification of modulators of autophagic flux in an image-based high content siRNA screen. *Autophagy* **12:** 713-726

Hansen M, Rubinsztein DC, Walker DW (2018) Autophagy as a promoter of longevity: insights from model organisms. *Nature reviews Molecular cell biology* **19:** 579-593

Harding HP, Zhang Y, Zeng H, Novoa I, Lu PD, Calfon M, Sadri N, Yun C, Popko B, Paules R, Stojdl DF, Bell JC, Hettmann T, Leiden JM, Ron D (2003) An integrated stress response regulates amino acid metabolism and resistance to oxidative stress. *Molecular cell* **11:** 619-633

Hayashi-Nishino M, Fujita N, Noda T, Yamaguchi A, Yoshimori T, Yamamoto A (2009) A subdomain of the endoplasmic reticulum forms a cradle for autophagosome formation. *Nature cell biology* **11:** 1433-1437

He C, Klionsky DJ (2009) Regulation mechanisms and signaling pathways of autophagy. *Annual review of genetics* **43:** 67-93

Heckmann BL, Green DR (2019) LC3-associated phagocytosis at a glance. *Journal of cell science* **132**

Heider MR, Munson M (2012) Exorcising the exocyst complex. *Traffic* **13:** 898-907

Hetz C (2012) The unfolded protein response: controlling cell fate decisions under ER stress and beyond. *Nature reviews Molecular cell biology* **13:** 89-102

Ho TT, Warr MR, Adelman ER, Lansinger OM, Flach J, Verovskaya EV, Figueroa ME, Passegue E (2017) Autophagy maintains the metabolism and function of young and old stem cells. *Nature* **543:** 205-210

Holt OJ, Gallo F, Griffiths GM (2006) Regulating secretory lysosomes. *Journal of biochemistry* **140:** 7-12

Hotamisligil GS (2010) Endoplasmic reticulum stress and the inflammatory basis of metabolic disease. *Cell* **140:** 900-917

Humeau J, Leduc M, Cerrato G, Loos F, Kepp O, Kroemer G (2020) Phosphorylation of eukaryotic initiation factor-2alpha (eIF2alpha) in autophagy. *Cell death & disease* **11:** 433

Jacquin E, Leclerc-Mercier S, Judon C, Blanchard E, Fraitag S, Florey O (2017) Pharmacological modulators of autophagy activate a parallel noncanonical pathway driving unconventional LC3 lipidation. *Autophagy* **13:** 854-867

Jager S, Bucci C, Tanida I, Ueno T, Kominami E, Saftig P, Eskelinen EL (2004) Role for Rab7 in maturation of late autophagic vacuoles. *Journal of cell science* **117:** 4837-4848

Ji N, Forsthuber TG (2016) ELISPOT Techniques. *Methods in molecular biology* **1304:** 63-71

Jiang L, Wang W, He Q, Wu Y, Lu Z, Sun J, Liu Z, Shao Y, Wang A (2017) Oleic acid induces apoptosis and autophagy in the treatment of Tongue Squamous cell carcinomas. *Scientific reports* **7:** 11277

Jiang S, Dupont N, Castillo EF, Deretic V (2013) Secretory versus degradative autophagy: unconventional secretion of inflammatory mediators. *Journal of innate immunity* **5:** 471-479

Junkin M, Kaestli AJ, Cheng Z, Jordi C, Albayrak C, Hoffmann A, Tay S (2016) High-Content Quantification of Single-Cell Immune Dynamics. *Cell reports* **15:** 411-422

Kadhum AA, Shamma MN (2017) Edible lipids modification processes: A review. *Critical reviews in food science and nutrition* **57:** 48-58

Kalyuzhny AE (2005) Chemistry and biology of the ELISPOT assay. *Methods in molecular biology* **302:** 15-31

Karaskov E, Scott C, Zhang L, Teodoro T, Ravazzola M, Volchuk A (2006) Chronic palmitate but not oleate exposure induces endoplasmic reticulum stress, which may contribute to INS-1 pancreatic beta-cell apoptosis. *Endocrinology* **147:** 3398-3407

Kato H, Nishitoh H (2015) Stress responses from the endoplasmic reticulum in cancer. *Frontiers in oncology* **5:** 93

Kaushik S, Cuervo AM (2018) The coming of age of chaperone-mediated autophagy. *Nature reviews Molecular cell biology* **19:** 365-381

Keefe AD, Wilson DS, Seelig B, Szostak JW (2001) One-step purification of recombinant proteins using a nanomolar-affinity streptavidin-binding peptide, the SBP-Tag. *Protein expression and purification* **23:** 440-446

Kelly RB (1985) Pathways of protein secretion in eukaryotes. *Science* **230:** 25-32

Kim YC, Guan KL (2015) mTOR: a pharmacologic target for autophagy regulation. *The Journal of clinical investigation* **125:** 25-32

Kimura S, Noda T, Yoshimori T (2007) Dissection of the autophagosome maturation process by a novel reporter protein, tandem fluorescent-tagged LC3. *Autophagy* **3:** 452-460

Kimura T, Jia J, Kumar S, Choi SW, Gu Y, Mudd M, Dupont N, Jiang S, Peters R, Farzam F, Jain A, Lidke KA, Adams CM, Johansen T, Deretic V (2017) Dedicated SNAREs and specialized TRIM cargo receptors mediate secretory autophagy. *The EMBO journal* **36:** 42-60

Kirkin V, McEwan DG, Novak I, Dikic I (2009) A role for ubiquitin in selective autophagy. *Molecular cell* **34:** 259-269

Klionsky DJ, Abdelmohsen K, Abe A, Abedin MJ, Abeliovich H, Acevedo Arozena A, Adachi H, Adams CM, Adams PD, Adeli K, Adhihetty PJ, Adler SG, Agam G, Agarwal R, Aghi MK, Agnello M, Agostinis P, Aguilar PV, Aguirre-Ghiso J, Airoldi EM et al (2016) Guidelines for the use and interpretation of assays for monitoring autophagy (3rd edition). *Autophagy* **12:** 1-222

Klumperman J (2000) The growing Golgi: in search of its independence. *Nature cell biology* **2:** E217-219

Klumperman J (2011) Architecture of the mammalian Golgi. *Cold Spring Harbor perspectives in biology* **3**

Kouroku Y, Fujita E, Tanida I, Ueno T, Isoai A, Kumagai H, Ogawa S, Kaufman RJ, Kominami E, Momoi T (2007) ER stress (PERK/eIF2alpha phosphorylation) mediates the polyglutamine-induced LC3 conversion, an essential step for autophagy formation. *Cell death and differentiation* **14:** 230-239

Kowal J, Tkach M, Thery C (2014) Biogenesis and secretion of exosomes. *Current opinion in cell biology* **29:** 116-125

Kreis TE, Lodish HF (1986) Oligomerization is essential for transport of vesicular stomatitis viral glycoprotein to the cell surface. *Cell* **46:** 929-937

Kroemer G, Marino G, Levine B (2010) Autophagy and the integrated stress response. *Molecular cell* **40:** 280-293

L'Homme L, Esser N, Riva L, Scheen A, Paquot N, Piette J, Legrand-Poels S (2013) Unsaturated fatty acids prevent activation of NLRP3 inflammasome in human monocytes/macrophages. *Journal of lipid research* **54:** 2998-3008

Lacy P, Stow JL (2011) Cytokine release from innate immune cells: association with diverse membrane trafficking pathways. *Blood* **118:** 9-18

Lafay F (1974) Envelope proteins of vesicular stomatitis virus: effect of temperature-sensitive mutations in complementation groups III and V. *Journal of virology* **14:** 1220-1228

Lamb CA, Yoshimori T, Tooze SA (2013) The autophagosome: origins unknown, biogenesis complex. *Nature reviews Molecular cell biology* **14:** 759-774

Las G, Serada SB, Wikstrom JD, Twig G, Shirihai OS (2011) Fatty acids suppress autophagic turnover in beta-cells. *The Journal of biological chemistry* **286:** 42534-42544

Lasa A, Miranda J, Bullo M, Casas R, Salas-Salvado J, Larretxi I, Estruch R, Ruiz-Gutierrez V, Portillo MP (2014) Comparative effect of two Mediterranean diets versus a low-fat diet on glycaemic control in individuals with type 2 diabetes. *European journal of clinical nutrition* **68:** 767-772

Laybutt DR, Preston AM, Akerfeldt MC, Kench JG, Busch AK, Biankin AV, Biden TJ (2007) Endoplasmic reticulum stress contributes to beta cell apoptosis in type 2 diabetes. *Diabetologia* **50:** 752-763

Lemasters JJ (2014) Variants of mitochondrial autophagy: Types 1 and 2 mitophagy and micromitophagy (Type 3). *Redox biology* **2:** 749-754

Lequin RM (2005) Enzyme immunoassay (EIA)/enzyme-linked immunosorbent assay (ELISA). *Clinical chemistry* **51:** 2415-2418

Liu P, Zhao L, Loos F, Iribarren K, Lachkar S, Zhou H, Gomes-da-Silva LC, Chen G, Bezu L, Boncompain G, Perez F, Zitvogel L, Kepp O, Kroemer G (2017) Identification of pharmacological agents that induce HMGB1 release. *Scientific reports* **7:** 14915

Liu P, Zhao L, Loos F, Marty C, Xie W, Martins I, Lachkar S, Qu B, Waeckel-Enee E, Plo I, Vainchenker W, Perez F, Rodriguez D, Lopez-Otin C, van Endert P, Zitvogel L, Kepp O, Kroemer G (2020) Immunosuppression by Mutated Calreticulin Released from Malignant Cells. *Molecular cell* **77:** 748-760 e749

Loos F, Xie W, Sica V, Bravo-San Pedro JM, Souquere S, Pierron G, Lachkar S, Sauvat A, Petrazzuolo A, Jimenez AJ, Perez F, Maiuri MC, Kepp O, Kroemer G (2019) Artificial tethering of LC3 or p62 to organelles is not sufficient to trigger autophagy. *Cell death & disease* **10:** 771

Lopez-Miranda J, Perez-Jimenez F, Ros E, De Caterina R, Badimon L, Covas MI, Escrich E, Ordovas JM, Soriguer F, Abia R, de la Lastra CA, Battino M, Corella D, Chamorro-Quiros J, Delgado-Lista J, Giugliano D, Esposito K, Estruch R, Fernandez-Real JM, Gaforio JJ et al (2010) Olive oil and health: summary of the II international conference on olive oil and health consensus report, Jaen and Cordoba (Spain) 2008. *Nutrition, metabolism, and cardiovascular diseases : NMCD* **20:** 284-294

Ma Y, Galluzzi L, Zitvogel L, Kroemer G (2013) Autophagy and cellular immune responses. *Immunity* **39:** 211-227

Martinez J, Almendinger J, Oberst A, Ness R, Dillon CP, Fitzgerald P, Hengartner MO, Green DR (2011) Microtubule-associated protein 1 light chain 3 alpha (LC3)-associated phagocytosis is required for the efficient clearance of dead cells. *Proceedings of the National Academy of Sciences of the United States of America* **108:** 17396-17401

Martinez J, Cunha LD, Park S, Yang M, Lu Q, Orchard R, Li QZ, Yan M, Janke L, Guy C, Linkermann A, Virgin HW, Green DR (2016) Noncanonical autophagy inhibits the autoinflammatory, lupus-like response to dying cells. *Nature* **533:** 115-119

Mathur A, Hayward JA, Man SM (2018) Molecular mechanisms of inflammasome signaling. *Journal of leukocyte biology* **103:** 233-257

Matlin KS, Simons K (1983) Reduced temperature prevents transfer of a membrane glycoprotein to the cell surface but does not prevent terminal glycosylation. *Cell* **34:** 233-243

Matsunaga K, Morita E, Saitoh T, Akira S, Ktistakis NT, Izumi T, Noda T, Yoshimori T (2010) Autophagy requires endoplasmic reticulum targeting of the PI3-kinase complex via Atg14L. *The Journal of cell biology* **190:** 511-521

Mazidi M, Banach M, Kengne AP (2018) Association between plasma trans fatty acids concentrations and leucocyte telomere length in US adults. *European journal of clinical nutrition* **72:** 581-586

Mazidi M, Gao HK, Kengne AP (2017) Inflammatory Markers Are Positively Associated with Serum trans-Fatty Acids in an Adult American Population. *Journal of nutrition and metabolism* **2017:** 3848201

Mazzocchi A, Leone L, Agostoni C, Pali-Scholl I (2019) The Secrets of the Mediterranean Diet. Does [Only] Olive Oil Matter? *Nutrients* **11**

Mei S, Ni HM, Manley S, Bockus A, Kassel KM, Luyendyk JP, Copple BL, Ding WX (2011) Differential roles of unsaturated and saturated fatty acids on autophagy and apoptosis in hepatocytes. *The Journal of pharmacology and experimental therapeutics* **339:** 487-498

Mestre MB, Fader CM, Sola C, Colombo MI (2010) Alpha-hemolysin is required for the activation of the autophagic pathway in Staphylococcus aureus-infected cells. *Autophagy* **6:** 110-125

Mizushima N (2007) Autophagy: process and function. *Genes & development* **21:** 2861-2873

Mizushima N (2010) The role of the Atg1/ULK1 complex in autophagy regulation. *Current opinion in cell biology* **22:** 132-139

Mizushima N, Yamamoto A, Matsui M, Yoshimori T, Ohsumi Y (2004) In vivo analysis of autophagy in response to nutrient starvation using transgenic mice expressing a fluorescent autophagosome marker. *Molecular biology of the cell* **15:** 1101-1111

Mizushima N, Yoshimori T, Ohsumi Y (2011) The role of Atg proteins in autophagosome formation. *Annual review of cell and developmental biology* **27:** 107-132

Monguchi T, Hara T, Hasokawa M, Nakajima H, Mori K, Toh R, Irino Y, Ishida T, Hirata KI, Shinohara M (2017) Excessive intake of trans fatty acid accelerates atherosclerosis through promoting inflammation and oxidative stress in a mouse model of hyperlipidemia. *Journal of cardiology* **70:** 121-127

Murray RZ, Stow JL (2014) Cytokine Secretion in Macrophages: SNAREs, Rabs, and Membrane Trafficking. *Frontiers in immunology* **5:** 538

Nakano A, Muramatsu M (1989) A novel GTP-binding protein, Sar1p, is involved in transport from the endoplasmic reticulum to the Golgi apparatus. *The Journal of cell biology* **109:** 2677-2691

Nemazanyy I, Blaauw B, Paolini C, Caillaud C, Protasi F, Mueller A, Proikas-Cezanne T, Russell RC, Guan KL, Nishino I, Sandri M, Pende M, Panasyuk G (2013) Defects of Vps15 in skeletal muscles lead to autophagic vacuolar myopathy and lysosomal disease. *EMBO molecular medicine* **5:** 870-890

Neufeld TP (2010) TOR-dependent control of autophagy: biting the hand that feeds. *Current opinion in cell biology* **22:** 157-168

New J, Thomas SM (2019) Autophagy-dependent secretion: mechanism, factors secreted, and disease implications. *Autophagy* **15:** 1682-1693

Ng F, Tang BL (2016) Unconventional Protein Secretion in Animal Cells. *Methods in molecular biology* **1459:** 31-46

Nickel W, Rabouille C (2009) Mechanisms of regulated unconventional protein secretion. *Nature reviews Molecular cell biology* **10:** 148-155

Ning J, Zhao C, Chen JX, Liao DF (2019) Oleate inhibits hepatic autophagy through p38 mitogen-activated protein kinase (MAPK). *Biochemical and biophysical research communications* **514:** 92-97

Nishida Y, Arakawa S, Fujitani K, Yamaguchi H, Mizuta T, Kanaseki T, Komatsu M, Otsu K, Tsujimoto Y, Shimizu S (2009) Discovery of Atg5/Atg7-independent alternative macroautophagy. *Nature* **461:** 654-658

Niso-Santano M, Bravo-San Pedro JM, Maiuri MC, Tavernarakis N, Cecconi F, Madeo F, Codogno P, Galluzzi L, Kroemer G (2015a) Novel inducers of BECN1-independent autophagy: cis-unsaturated fatty acids. *Autophagy* **11:** 575-577

Niso-Santano M, Malik SA, Pietrocola F, Bravo-San Pedro JM, Marino G, Cianfanelli V, Ben-Younes A, Troncoso R, Markaki M, Sica V, Izzo V, Chaba K, Bauvy C, Dupont N, Kepp O, Rockenfeller P, Wolinski H, Madeo F, Lavandero S, Codogno P et al (2015b) Unsaturated fatty acids induce non-canonical autophagy. *The EMBO journal* **34:** 1025-1041

Oberhauser L, Granziera S, Colom A, Goujon A, Lavallard V, Matile S, Roux A, Brun T, Maechler P (2020) Palmitate and oleate modify membrane fluidity and kinase activities of INS-1E beta-cells alongside altered metabolism-secretion coupling. *Biochimica et biophysica acta Molecular cell research* **1867:** 118619

Orci L, Palmer DJ, Ravazzola M, Perrelet A, Amherdt M, Rothman JE (1993) Budding from Golgi membranes requires the coatomer complex of non-clathrin coat proteins. *Nature* **362:** 648-652

Orvedahl A, Sumpter R, Jr., Xiao G, Ng A, Zou Z, Tang Y, Narimatsu M, Gilpin C, Sun Q, Roth M, Forst CV, Wrana JL, Zhang YE, Luby-Phelps K, Xavier RJ, Xie Y, Levine B (2011) Image-based genome-wide siRNA screen identifies selective autophagy factors. *Nature* **480:** 113-117

Oteng AB, Bhattacharya A, Brodesser S, Qi L, Tan NS, Kersten S (2017) Feeding Angptl4(-/-) mice trans fat promotes foam cell formation in mesenteric lymph nodes without leading to ascites. *Journal of lipid research* **58:** 1100-1113

Pallotta MT, Nickel W (2020) FGF2 and IL-1beta - explorers of unconventional secretory pathways at a glance. *Journal of cell science* **133**

Park S, Oh TS, Kim S, Kim EK (2019) Palmitate-induced autophagy liberates monounsaturated fatty acids and increases Agrp expression in hypothalamic cells. *Animal cells and systems* **23:** 384-391

Parziale A, Ooms G (2019) The global fight against trans-fat: the potential role of international trade and law. *Globalization and health* **15:** 46

Perez-Martinez P, Garcia-Rios A, Delgado-Lista J, Perez-Jimenez F, Lopez-Miranda J (2011) Mediterranean diet rich in olive oil and obesity, metabolic syndrome and diabetes mellitus. *Current pharmaceutical design* **17:** 769-777

Pineau L, Colas J, Dupont S, Beney L, Fleurat-Lessard P, Berjeaud JM, Berges T, Ferreira T (2009) Lipid-induced ER stress: synergistic effects of sterols and saturated fatty acids. *Traffic* **10:** 673-690

Ponpuak M, Mandell MA, Kimura T, Chauhan S, Cleyrat C, Deretic V (2015) Secretory autophagy. *Current opinion in cell biology* **35:** 106-116

Prentki M, Joly E, El-Assaad W, Roduit R (2002) Malonyl-CoA signaling, lipid partitioning, and glucolipotoxicity: role in beta-cell adaptation and failure in the etiology of diabetes. *Diabetes* **51 Suppl 3:** S405-413

Proikas-Cezanne T, Takacs Z, Donnes P, Kohlbacher O (2015) WIPI proteins: essential PtdIns3P effectors at the nascent autophagosome. *Journal of cell science* **128:** 207-217

Puri C, Renna M, Bento CF, Moreau K, Rubinsztein DC (2013) Diverse autophagosome membrane sources coalesce in recycling endosomes. *Cell* **154:** 1285-1299

Rabanal-Ruiz Y, Otten EG, Korolchuk VI (2017) mTORC1 as the main gateway to autophagy. *Essays in biochemistry* **61:** 565-584

Rabouille C (2017) Pathways of Unconventional Protein Secretion. *Trends in cell biology* **27:** 230-240

Radzikowska U, Rinaldi AO, Celebi Sozener Z, Karaguzel D, Wojcik M, Cypryk K, Akdis M, Akdis CA, Sokolowska M (2019) The Influence of Dietary Fatty Acids on Immune Responses. *Nutrients* **11**

Ralston JC, Lyons CL, Kennedy EB, Kirwan AM, Roche HM (2017) Fatty Acids and NLRP3 Inflammasome-Mediated Inflammation in Metabolic Tissues. *Annual review of nutrition* **37:** 77-102

Reginato A, Siqueira BP, Miyamoto JE, Portovedo M, Costa SO, de Fante T, Rodrigues HG, Ignacio-Souza LM, Torsoni MA, Torsoni AS, Le Stunff H, Belsham DD, Milanski M (2020) Acute effects of fatty acids on autophagy in NPY neurones. *Journal of neuroendocrinology* **32:** e12900

Rivera VM, Wang X, Wardwell S, Courage NL, Volchuk A, Keenan T, Holt DA, Gilman M, Orci L, Cerasoli F, Jr., Rothman JE, Clackson T (2000) Regulation of protein secretion through controlled aggregation in the endoplasmic reticulum. *Science* **287:** 826-830

Romani A, Ieri F, Urciuoli S, Noce A, Marrone G, Nediani C, Bernini R (2019) Health Effects of Phenolic Compounds Found in Extra-Virgin Olive Oil, By-Products, and Leaf of Olea europaea L. *Nutrients* **11**

Romao S, Gasser N, Becker AC, Guhl B, Bajagic M, Vanoaica D, Ziegler U, Roesler J, Dengjel J, Reichenbach J, Munz C (2013) Autophagy proteins stabilize pathogen-containing phagosomes for prolonged MHC II antigen processing. *The Journal of cell biology* **203:** 757-766

Rouschop KM, van den Beucken T, Dubois L, Niessen H, Bussink J, Savelkouls K, Keulers T, Mujcic H, Landuyt W, Voncken JW, Lambin P, van der Kogel AJ, Koritzinsky M, Wouters BG (2010) The unfolded protein response protects human tumor cells during hypoxia through regulation of the autophagy genes MAP1LC3B and ATG5. *The Journal of clinical investigation* **120:** 127-141

Rowe T, Dascher C, Bannykh S, Plutner H, Balch WE (1998) Role of vesicle-associated syntaxin 5 in the assembly of pre-Golgi intermediates. *Science* **279:** 696-700

Russell RC, Tian Y, Yuan H, Park HW, Chang YY, Kim J, Kim H, Neufeld TP, Dillin A, Guan KL (2013) ULK1 induces autophagy by phosphorylating Beclin-1 and activating VPS34 lipid kinase. *Nature cell biology* **15:** 741-750

Sales-Campos H, Souza PR, Peghini BC, da Silva JS, Cardoso CR (2013) An overview of the modulatory effects of oleic acid in health and disease. *Mini reviews in medicinal chemistry* **13:** 201-210

Sanjuan MA, Dillon CP, Tait SW, Moshiach S, Dorsey F, Connell S, Komatsu M, Tanaka K, Cleveland JL, Withoff S, Green DR (2007) Toll-like receptor signalling in macrophages links the autophagy pathway to phagocytosis. *Nature* **450:** 1253-1257

Santangelo C, Vari R, Scazzocchio B, De Sanctis P, Giovannini C, D'Archivio M, Masella R (2018) Anti-inflammatory Activity of Extra Virgin Olive Oil Polyphenols: Which Role in the Prevention and Treatment of Immune-Mediated Inflammatory Diseases? *Endocrine, metabolic & immune disorders drug targets* **18:** 36-50

Saraste J, Kuismanen E (1984) Pre- and post-Golgi vacuoles operate in the transport of Semliki Forest virus membrane glycoproteins to the cell surface. *Cell* **38:** 535-549

Sauvat A, Chen G, Muller K, Tong M, Aprahamian F, Durand S, Cerrato G, Bezu L, Leduc M, Franz J, Rockenfeller P, Sadoshima J, Madeo F, Kepp O, Kroemer G (2018) Trans-Fats Inhibit Autophagy Induced by Saturated Fatty Acids. *EBioMedicine* **30:** 261-272

Scarlatti F, Maffei R, Beau I, Codogno P, Ghidoni R (2008) Role of non-canonical Beclin 1-independent autophagy in cell death induced by resveratrol in human breast cancer cells. *Cell death and differentiation* **15:** 1318-1329

Schafer T, Zentgraf H, Zehe C, Brugger B, Bernhagen J, Nickel W (2004) Unconventional secretion of fibroblast growth factor 2 is mediated by direct translocation across the plasma membrane of mammalian cells. *The Journal of biological chemistry* **279:** 6244-6251

Seo AY, Lau PW, Feliciano D, Sengupta P, Gros MAL, Cinquin B, Larabell CA, Lippincott-Schwartz J (2017) AMPK and vacuole-associated Atg14p orchestrate mu-lipophagy for energy production and long-term survival under glucose starvation. *eLife* **6**

Settembre C, Zoncu R, Medina DL, Vetrini F, Erdin S, Erdin S, Huynh T, Ferron M, Karsenty G, Vellard MC, Facchinetti V, Sabatini DM, Ballabio A (2012) A lysosome-to-nucleus signalling mechanism senses and regulates the lysosome via mTOR and TFEB. *The EMBO journal* **31:** 1095-1108

Shah K, Maghsoudlou P (2016) Enzyme-linked immunosorbent assay (ELISA): the basics. *British journal of hospital medicine* **77:** C98-101

Shibutani ST, Yoshimori T (2014) A current perspective of autophagosome biogenesis. *Cell research* **24:** 58-68

Shirasaki Y, Ohara O (2018) Challenges in Developing Protein Secretion Assays at a Single-Cell Level. *Methods in molecular biology* **1808:** 1-7

Shirasaki Y, Yamagishi M, Suzuki N, Izawa K, Nakahara A, Mizuno J, Shoji S, Heike T, Harada Y, Nishikomori R, Ohara O (2014) Real-time single-cell imaging of protein secretion. *Scientific reports* **4:** 4736

Siri-Tarino PW, Sun Q, Hu FB, Krauss RM (2010) Saturated fatty acids and risk of coronary heart disease: modulation by replacement nutrients. *Current atherosclerosis reports* **12:** 384-390

Smith DM, Patel S, Raffoul F, Haller E, Mills GB, Nanjundan M (2010) Arsenic trioxide induces a beclin-1-independent autophagic pathway via modulation of SnoN/SkiL expression in ovarian carcinoma cells. *Cell death and differentiation* **17:** 1867-1881

Sommerweiss D, Gorski T, Richter S, Garten A, Kiess W (2013) Oleate rescues INS-1E beta-cells from palmitate-induced apoptosis by preventing activation of the unfolded protein response. *Biochemical and biophysical research communications* **441:** 770-776

Stagg SM, LaPointe P, Razvi A, Gurkan C, Potter CS, Carragher B, Balch WE (2008) Structural basis for cargo regulation of COPII coat assembly. *Cell* **134:** 474-484

Stender S, Astrup A, Dyerberg J (2008) Ruminant and industrially produced trans fatty acids: health aspects. *Food & nutrition research* **52**

Storrie B, White J, Rottger S, Stelzer EH, Suganuma T, Nilsson T (1998) Recycling of golgi-resident glycosyltransferases through the ER reveals a novel pathway and provides an explanation for nocodazole-induced Golgi scattering. *The Journal of cell biology* **143:** 1505-1521

Szul T, Sztul E (2011) COPII and COPI traffic at the ER-Golgi interface. *Physiology* **26:** 348-364

Talloczy Z, Jiang W, Virgin HWt, Leib DA, Scheuner D, Kaufman RJ, Eskelinen EL, Levine B (2002) Regulation of starvation- and virus-induced autophagy by the eIF2alpha kinase signaling pathway. *Proceedings of the National Academy of Sciences of the United States of America* **99:** 190-195

Tian S, Lin J, Jun Zhou J, Wang X, Li Y, Ren X, Yu W, Zhong W, Xiao J, Sheng F, Chen Y, Jin C, Li S, Zheng Z, Xia B (2010) Beclin 1-independent autophagy induced by a Bcl-XL/Bcl-2 targeting compound, Z18. *Autophagy* **6:** 1032-1041

Tooze SA, Martens GJ, Huttner WB (2001) Secretory granule biogenesis: rafting to the SNARE. *Trends in cell biology* **11:** 116-122

Torisu K, Singh KK, Torisu T, Lovren F, Liu J, Pan Y, Quan A, Ramadan A, Al-Omran M, Pankova N, Boyd SR, Verma S, Finkel T (2016) Intact endothelial autophagy is required to maintain vascular lipid homeostasis. *Aging cell* **15:** 187-191

Toyokawa K, Carling SJ, Ott TL (2007) Cellular localization and function of the antiviral protein, ovine Mx1 (oMx1): I. Ovine Mx1 is secreted by endometrial epithelial cells via an 'unconventional' secretory pathway. *American journal of reproductive immunology* **57:** 13-22

Trautmann L (2013) Beyond surface markers with a universal cell secretion assay. *Cytometry Part A : the journal of the International Society for Analytical Cytology* **83:** 177-178

Tu QQ, Zheng RY, Li J, Hu L, Chang YX, Li L, Li MH, Wang RY, Huang DD, Wu MC, Hu HP, Chen L, Wang HY (2014) Palmitic acid induces autophagy in hepatocytes via JNK2 activation. *Acta pharmacologica Sinica* **35:** 504-512

Uytterhoeven V, Lauwers E, Maes I, Miskiewicz K, Melo MN, Swerts J, Kuenen S, Wittocx R, Corthout N, Marrink SJ, Munck S, Verstreken P (2015) Hsc70-4 Deforms Membranes to Promote Synaptic Protein Turnover by Endosomal Microautophagy. *Neuron* **88:** 735-748

Varshney R, Gupta S, Roy P (2017) Cytoprotective effect of kaempferol against palmitic acid-induced pancreatic beta-cell death through modulation of autophagy via AMPK/mTOR signaling pathway. *Molecular and cellular endocrinology* **448:** 1-20

Viotti C (2016) ER to Golgi-Dependent Protein Secretion: The Conventional Pathway. *Methods in molecular biology* **1459:** 3-29

Walter P, Ron D (2011) The unfolded protein response: from stress pathway to homeostatic regulation. *Science* **334:** 1081-1086

Ward TH, Polishchuk RS, Caplan S, Hirschberg K, Lippincott-Schwartz J (2001) Maintenance of Golgi structure and function depends on the integrity of ER export. *The Journal of cell biology* **155:** 557-570

Waters MG, Serafini T, Rothman JE (1991) 'Coatomer': a cytosolic protein complex containing subunits of non-clathrin-coated Golgi transport vesicles. *Nature* **349:** 248-251

WHO (2003) Diet, nutrition and the prevention of chronic diseases. *World Health Organization technical report series* **916:** i-viii, 1-149, backcover

WHO (2018) REPLACE Trans-fat. An Action Package to Eliminate Industrially- produced Trans-fatty Acids.

WHO (Retrieved 2021-24-01)

Xu D, Joglekar AP, Williams AL, Hay JC (2000) Subunit structure of a mammalian ER/Golgi SNARE complex. *The Journal of biological chemistry* **275:** 39631-39639

Yamamoto A, Cremona ML, Rothman JE (2006) Autophagy-mediated clearance of huntingtin aggregates triggered by the insulin-signaling pathway. *The Journal of cell biology* **172:** 719-731

Yang Z, Klionsky DJ (2010a) Eaten alive: a history of macroautophagy. *Nature cell biology* **12:** 814-822

Yang Z, Klionsky DJ (2010b) Mammalian autophagy: core molecular machinery and signaling regulation. *Current opinion in cell biology* **22:** 124-131

Yin Y, Mitson-Salazar A, Prussin C (2015) Detection of Intracellular Cytokines by Flow Cytometry. *Current protocols in immunology* **110:** 6 24 21-26 24 18

Zachari M, Ganley IG (2017) The mammalian ULK1 complex and autophagy initiation. *Essays in biochemistry* **61:** 585-596

Zambon D, Sabate J, Munoz S, Campero B, Casals E, Merlos M, Laguna JC, Ros E (2000) Substituting walnuts for monounsaturated fat improves the serum lipid profile of hypercholesterolemic men and women. A randomized crossover trial. *Annals of internal medicine* **132:** 538-546

Zhang L, Yu J, Pan H, Hu P, Hao Y, Cai W, Zhu H, Yu AD, Xie X, Ma D, Yuan J (2007) Small molecule regulators of autophagy identified by an image-based high-throughput screen. *Proceedings of the National Academy of Sciences of the United States of America* **104:** 19023-19028

Zhao L, Liu P, Boncompain G, Loos F, Lachkar S, Bezu L, Chen G, Zhou H, Perez F, Kepp O, Kroemer G (2018) Identification of pharmacological inhibitors of conventional protein secretion. *Scientific reports* **8:** 14966

Zhao S, Li CM, Luo XM, Siu GK, Gan WJ, Zhang L, Wu WK, Chan HC, Yu S (2017) Mammalian TRAPPIII Complex positively modulates the recruitment of Sec13/31 onto COPII vesicles. *Scientific reports* **7:** 43207

Zhou X, Wang L, Hasegawa H, Amin P, Han BX, Kaneko S, He Y, Wang F (2010) Deletion of PIK3C3/Vps34 in sensory neurons causes rapid neurodegeneration by disrupting the endosomal but not the autophagic pathway. *Proceedings of the National Academy of Sciences of the United States of America* **107:** 9424-9429

Zhu JH, Horbinski C, Guo F, Watkins S, Uchiyama Y, Chu CT (2007) Regulation of autophagy by extracellular signal-regulated protein kinases during 1-methyl-4-phenylpyridinium-induced cell death. *The American journal of pathology* **170:** 75-86

Summary in French

Il a été récemment montré que les acides gras naturellement présents dans l'alimentation présentent divers effets biologiques. L'acide gras naturel insaturé (i.e. possédant une double liaison carbone-carbone dans sa chaîne aliphatique) le plus abondant, l'oléate, le principal composant de l'huile d'olive, a été montré comme augmentant la longévité des organismes étudiés, diminuant les risques des maladies cardiovasculaires et de l'arthrite rhumatoïde ainsi que prévenant l'inflammation induite par les acides gras saturés. Les acides gras insaturés contenus dans les végétaux et dans les tissus humains sont principalement des cis-isomères (ayant les atomes d'hydrogène du même côté de la chaîne carbonée), dont l'insaturation cause un "coude" dans la chaîne carbonée. Les trans-isomères, surtout générés au cours des procédés de transformation des aliments, comme l'hydrogénation partielle des graisses, ont des propriétés physicochimiques différentes. L'elaidate est notamment le trans-isomère de l'oléate, dont la production dérive de l'hydrogénation partielle d'huiles végétales, comme le palmitelaidate résulte de l'isomérisation de son précurseur naturel, le palmitoleate, alors que le linoelaidate, un acide gras polyinsaturé, provient de l'isomérisation du linoléate. Malgré leur origine, les acides gras trans-insaturés sont considérés comme ayant un effet défavorable sur la santé, spécialement concernant les risques de maladie cardiovasculaire. En effet, l'assimilation nutritionnelle ou la concentration dans le plasma des acides gras trans-insaturés est positivement corrélée avec la sévérité de l'artériosclérose coronaire, les biomarqueurs inflammatoires et le raccourcissement des télomères dans les leucocytes circulants, signe d'un vieillissement accéléré. Sur la base des études épidémiologiques, la US Federal Drug Administration a recommandé l'interdiction des sources des trans-acides gras dans l'alimentation. De la même façon, les acides gras saturés comme le palmitate sont notamment connus pour leur toxicité, un phénomène qui peut potentiellement contribuer à la pathogenèse de maladies lipotoxiques, ainsi qu'à l'induction d'inflammation chronique qui contribue à des syndromes métaboliques.

Motivés par le fait que les acides gras naturellement présents dans l'alimentation influencent la composition des membranes cellulaires et impactent la santé à long terme de façons différentes, notre équipe a approfondi la connaissance des effets biologiques des divers types d'acides gras. En particulier, l'étude des acides gras sur la régulation de l'autophagie,

mécanisme de recyclage et de réponse au stress cellulaire qui permet le recyclage d'éléments cellulaires grâce à la séquestration de la «cargaison» cytoplasmique dans les autophagosomes afin de réguler l'homéostasie cellulaire, a montré que les acides gras saturés et insaturés induisent l'autophagie via des mécanismes moléculaires différents. Nous avons pu démontrer que certains effets biologiques (notamment les réponses au stress cellulaire) sont différents en fonction de la longueur de la chaîne carbonée et de l'état de saturation, entre les isomères cis- et trans-. De plus, nous avons pu prouver via des analyses métaboliques que contrairement au traitement palmitate, les métabolites « antivieillissement » augmentent *in vivo* après le traitement oléate.

Ces constats ont été les moteurs pour une étude approfondie des mécanismes de stress cellulaire induits par les différents acides gras afin d'étudier la base génétique des effets induits par l'oléate, permettant de comprendre les voies spécifiquement activées par ce dernier et les relier à l'impact bénéfique qu'il présente sur la longévité et la santé. Grâce à l'utilisation de technologies robotisées haut-débit, un criblage du génome humain entier par ARNs interférents réalisé sur 18000 cibles génétiques identifiées dans le génome, a montré que la formation des agrégats de la protéine LC3 (dont la conjugaison à la phosphatidyléthanolamine est essentielle pour la génération de la membrane autophagosomale dans le processus de l'autophagie) typiquement induite par l'oléate implique une cascade complexe d'évènements moléculaires impliquant les protéines structurales constituant l'appareil de Golgi, ainsi que la réponse au stress du réticulum endoplasmique. Nous avons ainsi démontré par plusieurs études des réponses cellulaires systématiques au niveau moléculaire ainsi qu'au niveau des divers organelles cellulaires, que cette agrégation de LC3 spécifiquement induite par l'oléate a lieu dans le trans-Golgi d'une façon sélective et dépendante du temps. De façon intéressante, nous avons montré que l'oléate bloque même spécifiquement à plus grande échelle le trafic protéique au niveau de ce compartiment dans différents systèmes in vitro, comprenant des lignées d'ostéosarcome humain et des macrophages murins. Pour transposer les résultats obtenus in vitro dans un organisme plus proche de celui de l'homme, nous avons étudié in vivo la sécrétion d'une enzyme protéique, la Gaussia luciferase, dans la circulation de la souris et observé une diminution de sécrétion dans ce model expérimental aussi.

De plus, un criblage visant à rechercher des agents chimiques capables d'induire les mêmes effets cellulaires que l'oléate, a permis d'identifier plusieurs composés appartenant à diverses classes pharmacologiques. De la même manière que l'oléate ces composés induisent un blocage de la sécrétion protéique conventionnelle, renforçant l'idée que cette voie de perturbation du Golgi joue un rôle pharmacologique important.

En conclusion, ces résultats montrent que l'oléate représente une classe de molécules agissant sur l'appareil de Golgi pour y induire l'agrégation de LC3, tout en bloquant en même temps la sécrétion protéique.

université PARIS-SACLAY | ÉCOLE DOCTORALE Cancérologie : biologie - médecine - santé (CBMS)

Titre : Oléate: un inducteur atypique de stress cellulaire qui bloque la sécrétion protéique

Mots clés : Acides gras, autophagie, sécrétion protéique, criblage à haut débit, oléate, stress du réticulum endoplasmique

Résumé : Les diverses classes d'acides gras (chaines carbonées saturées ou *cis*-/*trans*- insaturées) influencent la physiologie au niveau de la cellule et de l'organisme de façon différente. Curieusement, ces catégories distinctes ont un effet important (mais différent) sur l'autophagie, le mécanisme intracellulaire de dégradation qui maintient l'homéostasie énergétique et protège les cellules contre le stress. L'oléate, l'acide gras *cis*-insaturé endogène et alimentaire le plus abondant, possède la propriété atypique d'induire une redistribution de la protéine LC3 (signe particulier d'autophagie) de manière non-canonique et préférentiellement dans l'appareil de Golgi. Puisqu'il a été montré que, d'une part, les acides gras *cis*-insaturés présentent des effets bénéfiques pour la santé et que, d'autre part, les acides gras *trans*-insaturés et saturés induisent des effets toxiques, nous avons décidé d'explorer les mécanismes à la base de la redistribution de LC3 au niveau de l'appareil de Golgi induite par l'oléate. Cette analyse pourrait nous éclairer sur l'origine des différents effets des acides gras sur la santé. Pour cela, un criblage robotisé du génome entier par ARNs interférents a permis d'identifier plusieurs gènes impliqués dans le transport des protéines lié à l'appareil de Golgi, et également dans la réponse intégrée au stress.
Des expériences supplémentaires ont montré que l'oléate impacte la morphologie subcellulaire de l'appareil de Golgi, en corrélation avec le blocage de la sécrétion protéique conventionnelle (dépendante du Golgi) lorsque que la cargaison est bloquée au niveau du réseau trans-golgien. L'inhibition de la sécrétion protéique a été observée dans plusieurs systèmes expérimentaux, tant *in vitro* qu'*in vivo*. De plus, un criblage visant à rechercher des agents chimiques capables d'induire les mêmes effets cellulaires que l'oléate, a permis d'identifier plusieurs composés appartenant à diverses classes pharmacologiques. De la même manière que l'oléate ces composés induisent un blocage de la sécrétion protéique conventionnelle, renforçant l'idée que cette voie de perturbation du Golgi joue un rôle pharmacologique important. En conclusion, ces résultats montrent que l'oléate représente une classe de molécules agissant sur l'appareil de Golgi pour y induire l'agrégation de LC3, tout en bloquant en même temps la sécrétion protéique.

Title : Oleate: an atypical cellular stress inducer that stalls protein secretion

Keywords : Fatty acids, autophagy, protein secretion, high-throughput screening, oleate, endoplasmic reticulum stress

Abstract : Distinct classes of fatty acids (FAs) (saturated or *cis*-/*trans*-unsaturated carbon chains) impact on cellular and organismal physiology in a different manner. Interestingly, these diverse categories have a profound (but different) effect on autophagy, the conserved intracellular degradation mechanism that maintains energy homeostasis and protects cells against stress. Oleate, the most abundant endogenous and dietary *cis*-unsaturated FA, has the atypical property to induce the redistribution of the LC3 protein (peculiar sign of autophagy) in a non-canonical fashion and preferentially to the Golgi apparatus. Intrigued by these observations, which might be related to the health-improving effects of *cis*-unsaturated FAs (and the notorious toxicity of *trans*-unsaturated and saturated FAs), we decided to explore the mechanisms causing the oleate-induced relocation of LC3 to the Golgi apparatus. To achieve this goal, a robotized RNA interference genome-wide screen led to the identification of multiple genes involved in the Golgi-related protein transport, as well as in the integrated stress response. Follow-up experiments revealed that oleate affected the subcellular morphology of the Golgi apparatus, correlating with a blockade of conventional (Golgi-dependent) protein secretion that caused secretory cargo to be stalled at the level of the trans-Golgi network. The inhibition of protein secretion was observed using several experimental systems, both *in vitro* and *in vivo*. Moreover, a systematic screen searching for other chemical entities that mimic the oleate-induced cellular effects led to the identification of several compounds belonging to rather different pharmacological classes. These "oleate mimetics" also shared with oleate the capacity to block conventional protein secretion, supporting the notion that this pathway of Golgi perturbation is indeed of pharmacological relevance. In conclusion, this research work shows that oleate represents a class of molecules that act on the Golgi apparatus to cause the recruitment of LC3 and to stall protein secretion.